A Gas Sensor for the Selective Detection of Volatile Organic Compounds

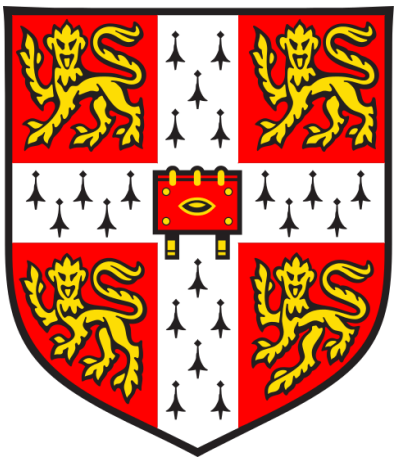

Andrew John Stretton

This dissertation is submitted for the degree of

Doctor of Philosophy

Girton College

January 2020

Declaration

This thesis is the result of my own work and includes nothing which is the outcome of work done in collaboration. It is not substantially the same as any work that has already been submitted before for any degree or other qualification. This thesis contains fewer than 65,000 words including appendices, bibliography, footnotes, tables and equations and has fewer than 150 figures.

Andrew Stretton

Acknowledgements

I would like to thank Lisa Hall for her patient supervision and valuable feedback on this thesis. This project was made possible with the funding and support of the EPSRC and the Centre for Doctoral Training in Sensing Technologies and Applications. Many thanks to Alphasense (in particular John Saffell and Wah On Ho) for lending equipment and supplying Photoionisation Detectors. From the workshop at CEB, I would like to thank Jon Summerfield and Gary Chapman for their assistance in the design and production of the adsorbent chip. Thank you to Chris Valentine for assistance in collecting nitrogen isotherm data.

Thank you to my friends at Cambridge and beyond who have been there for me during good times and bad. Special mentions to Bag End, The Norms, Champions of the Thames, Boys Boys Boys, The Quartermen, Team Tenby (& TWAGs), Goldney Blues and Tuesday Easy Run Club. For always being able to tell me what I needed to hear, and for being herself, thank you Naiara. Attempting a PhD is a luxury made available to me by generations of my family, who were never afforded the same opportunities they have continually provided for me. Thank you all, for now and for always.

Abstract

Volatile Organic Compounds (VOCs) are an important class of air pollutant because many of them are harmful to human health. VOCs are typically present at very low concentrations – parts-per-billion (ppb) and lower – which makes their detection a significant challenge. Standard measurement techniques, such as Gas Chromatography (GC), are typically sensitive and selective, but are limited by their large size, high cost and complexity to operate. Such factors restrict deployment for practical applications, including measurement across air quality networks. In contrast, gas sensors are typically small, inexpensive and easily deployed, but are limited by poor selectivity.

This work aims to establish the extent to which gas sensors can be used to achieve sensitive and selective detection of VOCs. Based on the processes of adsorption and desorption, it examines how temperature control of functionalised silica adsorbents can be used to produce discriminable signals of VOCs. In this context, the VOCs of interest were benzene, toluene, ethyl benzene, para-xylene (BTEX), due to their proven toxicity and prevalence in human environments. With the aim of producing a potentially deployable device, a novel sensing platform was designed and constructed. The main features of this Adsorption Device were an aluminium channel, a peltier module heating unit, flow path control and photoionisation detector (PID). In addition to unmodified silica, this thesis presents six modified silica adsorbents with amino, chloro, (n8) alkyl, fluoroalkyl, phenyl and chlorophenyl functionality.

Analysis of BTEX vapours with the seven silica adsorbents indicated adsorption was physical (physisorption) and desorption was readily reversible between 25 and 100 °C. Adsorption was influenced by the strength of adsorbent-vapour interaction, which could be increased by introducing delocalised electron density (phenyl and chlorophenyl silica), but modification could not compensate for any significant loss of surface area and pore volume that occurred. PID responses during adsorption and desorption were found to be discriminable from each other. Vapour desorption was examined with different heating profiles, which were found to initiate distinct response patterns. Principle Component Analysis (PCA) of Adsorption Device data indicated that the responses were sufficiently discriminable that they could be offer a means of vapour selectivity. Tests of the Adsorption Device indicate that selective detection of individual and dual component BTEX vapours is achievable in the ppb concentration range and with a cycle time of 10 minutes. Classification algorithms based on the Adsorption Device output were found to be at least as accurate as previously published research. This work presents significant progress towards to the development of a selective and practical sensor for air quality applications.

Contents

Abbreviations

2D	2 Dimensional
3D	3 Dimensional
ADC	Analog-to-Digital Converter
APTES	(3-Aminopropyl)triethoxysilane
BET	Brunauer, Emmett and Teller
BJH	Barrett-Joyner-Halenda
BTEX	Benzene, Toluene, Ethylbenzene & Xylene
C8TES	n-Octyltriethoxysilane
CLTES	(3-Chloropropyl)triethoxysilane
CNC	Computer Numerical Control
CNT	Carbon Nanotubes
DC	Direct Current
DEFRA	Department for Environment, Food and Rural Affairs
EPA	(United States) Environmental Protection Agency
EU	European Union
FID	Flame Ionisation Detector
FTIR	Fourier-Transform Infrared
IARC	International Agency for Research on Cancer
IR	Infrared
IUAPC	International Union of Pure and Applied Chemistry
GC	Gas Chromatography
kNN	k-Nearest Neighbours
LED	Light Emitting Diode
LDA	Linear Discriminant Analysis
LoD	Limit of Detection

MEK	Methyl Ethyl Ketone (2-butanone)
MOF	Metal Organic Framework
MOX	Metal Oxide
MS	Mass Spectrometry
PC	Personal Computer
PEG	Polyethylene glycol
PCA	Principal Component Analysis
PCTES	1-chloro-4-triethoxysilylbenzene
PDMS	Polydimethylsiloxane
PhTES	Triethoxyphenylsilane
$PM_{2.5}$	Particulate Matter (2.5 micrometres)
ppb	parts-per-billion
ppm	parts-per-million
ppt	parts-per-trillion
PID	Photoionisation Detector
p-i-d	Proportional-Integral-Derivative
POTES	1H,1H,2H,2H-Perfluorooctyltriethoxysilane
PTFE	Polytetrafluoroethylene (Teflon™)
PTR-MS	Proton-Transfer-Reaction Mass Spectrometry
QCM	Quartz Crystal Microbalance
RF	Random Forest
SAW	Surface Acoustic Wave
SIM	Selected Son Monitoring
SOA	Secondary Organic Aerosols
SVM	Support Vector Machine
STP	Standard Temperature and Pressure
TCD	Thermal Conductivity Detector

TGA	Thermal Gravimetric Analysis
txt	text (file type)
UK	United Kingdom
USB	Universal Serial Bus
UV	Ultraviolet
VOC	Volatile Organic Compound
WHO	World Health Organisation
xlsx	Excel Microsoft Office Open XML Format Spreadsheet (file type)
μGC	Micro Gas Chromatography

Nomenclature

A_0	Theoretical area under the PID output for a process with no adsorption
A_{obs}	Actual area observed under the PID output for a process with adsorption
A_{SD}	Baseline adjusted area of the sensor response during spontaneous desorption
A_{TD}	Baseline adjusted area of the sensor response during thermal desorption
C_e	Concentration at equilibrium
c_{VOC}	VOC concentration
G	Gas-phase species
GS	Surface adsorbed species (i.e. adsorbate)
K_{eq}	Equilibrium constant,
q_e	Equilibrium quantity adsorbed
q_m	Monolayer quantity adsorbed
ln	Natural logarithm
m_{ad}	Mass adsorbed (i.e. the adsorbate), during the sampling phase
m_{inj}	Mass 'injected' during sampling
m_{SD}	Mass spontaneously desorbed
m_{TD}	Mass thermally desorbed
p_{ad}	Proportion of VOC adsorbed
r	Baseline adjusted sensor response
r_{eq}	Sensor response at equilibrium
R	Ideal gas constant
R_f	Flow rate of sample stream
S	Adsorption sites on the solid adsorbent surface
S_l	Slope of the calibration curve

t_1	Start time of the sampling phase
t_2	End time of the sampling phase
t_{sam}	Sampling time
$\Delta H^{\emptyset}$	Standard enthalpy change
$\Delta G^{\emptyset}$	Standard Gibbs energy
$\Delta S^{\emptyset}$	Standard entropy
θ_m	Fraction of filled monolayer adsorption sites
σ	Molecular cross sectional area
σ_r	Standard deviation of the blank response

List of Tables

List of Figures

Chapter 1 Introduction

1.1 Volatile Organic Compounds

Volatile organic compounds (VOCs) are organic chemicals that have a high vapour pressure under normal indoor atmospheric conditions. The European Union (EU) defines VOCs as *'any organic compound having an initial boiling point less than or equal to 250 °C measured at a standard atmospheric pressure of 101.3 kPa'*,[1] although definitions can vary.[i] The volatility of a compound generally increases as boiling point decreases. Both benzene and formaldehyde are examples of VOCs and, according to their boiling points, formaldehyde (–19 °C) is more volatile than benzene (80 °C).[2]

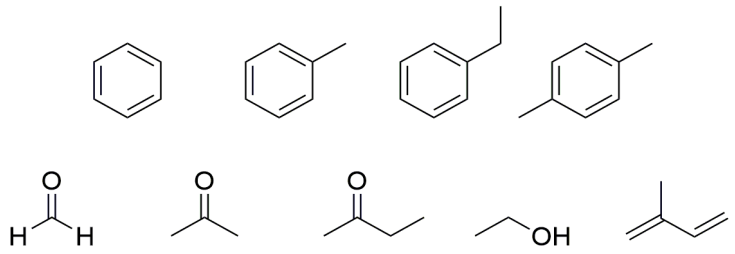

Figure 1.1. Chemical structures of common VOCs. *Top* (left to right): benzene, toluene, ethylbenzene, (para) xylene. *Bottom* (left to right): formaldehyde, acetone, methyl ethyl ketone (MEK, also known as 2-butanone), ethanol and isoprene.

1.1.1 Primary Sources

VOCs are ubiquitous throughout indoor, urban and natural environments, and result from a wide range of anthropogenic (originating in human activity) and other biological sources.[3,4] Biological sources include animals, plants and microbes living in terrestrial ecosystems and oceans. VOCs enter the atmosphere through processes associated with growth, maintenance and decay. They can function as

[i] The United States Environment Protection Agency (EPA) defines VOCs as *'any compound of carbon, excluding carbon monoxide, carbon dioxide, carbonic acid, metallic carbides or carbonates and ammonium carbonate, which participates in atmospheric photochemical reactions, except those designated by the EPA as having negligible photochemical reactivity'*.[2]

hormones, for signalling and defence, or as metabolic waste products.[5] Excluding methane, biological sources emit an estimated 1,150 million tonnes of carbon per year in the form of VOCs, of which approximately 500-600 million tonnes are isoprene.[5,6] Emission of isoprene is a mechanism used by plants to combat abiotic stress, such as heat stress caused by large fluctuations in temperature.[7] The remaining biological emissions are made up of hundreds of different VOCs from a variety of sources performing different functions including insect communication, fungal or microbial resistances, and the release of sex pheromones.[4]

Anthropogenic sources emit about 140 million tonnes of carbon per year in the form of VOCs.[5] Most emissions form a range of alkanes, alkenes, alkynes, aromatics, halocarbons, and compounds containing oxygen sulphur and nitrogen.[8] Compounds emitted are typically dependent on the industry. These include:

- **Petroleum Refining**. Producing a range of fuels, oils, waxes and additives from crude oil refining. During their production, VOCs are normally emitted from process waste streams, but can also be emitted during refining or leakage.[9]
- **Combustion processes.** Burning fossil fuels for transport, heat and energy,[10] or biomass, such clearing forest for agricultural land or the removal of agricultural waste.[11]
- **Manufacturing Industry**. VOCs are emitted during the production of a range of materials, including: chemicals from the polymer, fine chemical, and solvent industries; synthetic resins; packaging; leathers; pharmaceuticals; pesticides; coatings, inks and adhesives; electronic equipment, in particular semiconductors and integrated circuits, flat panel displays, printed circuit boards and terminal products.[8]
- **Coating and painting**. A range of VOCs are released during the coating and/or painting of products or materials such as vehicles, furniture, cables and household appliances.
- **Printing**, i.e. printing on materials such as paper, plastics, and textiles (including dyeing).
- **Household products,** such as cleaning agents, perfumes, air fresheners and adhesives.[12,13]

In the United Kingdom (UK), the leading sources of VOCs are industrial processes (22% of emissions), household products (18%), agriculture (14%), domestic burning (5%) and transport (5%).[14]

1.1.2 VOCs in the Atmosphere

In the atmosphere, VOCs act as fuel for photochemical reactions and precursors for secondary pollutants, including near-surface ozone (O_3) and secondary organic aerosols (SOAs).[15] Ozone production is determined by VOC concentration, and the magnitude produced varies between different classes of VOCs.[10] VOCs play a significant role in the production of photochemical smog, which commonly occurs above cities (Figure 1.2). It arises when VOCs and nitrogen oxides (NO_x), primarily from liquid fuel combustion, are oxidised by sunlight to produce near-surface ozone and airborne particles.[16] The identification of specific VOCs and their emission sources has been highlighted as important for the implementation of effective ozone control strategies.[10] SOAs form a large proportion of atmospheric fine particulate matter ($PM_{2.5}$), and are created by repeated oxidation of organic molecules.[17] In addition, chlorinated VOCs from anthropogenic sources react with sunlight in the stratosphere and are converted into active chlorine species that reduce the ozone layer.[18]

Figure 1.2. Photochemical smog over London (Credit: BBC News).

1.1.3 VOC Biomarkers

Hundreds of VOCs are emitted from humans, including in exhaled breath, from skin, urine, saliva, breast milk, blood and faeces.[19] Although many compounds may originate from previous environmental exposure,[20] the presence and concentration of VOCs endogenously produced by the body can be used as diagnostic biomarkers. The World Health Organisation (WHO) defines biomarkers as "*any substance, structure, or process that can be measured in the body or its products and influences or predicts the incidence of outcome or disease*".[21] For this reason, VOCs are suitable as non-invasive biomarkers.[22]

Breath analysis as a diagnostic method for diseases is a rapidly growing research and development field. Due to the non-invasive nature of breath analysis, it has emerged as a candidate for the early detection of diseases such as lung cancer.[23] It has been shown that screening for the early detection of cancer favourably influences the survival of cancer patients. For example, the five-year survival rate of stage I and stage III lung cancer patients improved by 70% and 20%, respectively, by early detection and treatment.[24] Despite this, a distributable and effective lung cancer screening practice is currently unavailable. Existing diagnostic methods, such as chest radiography or computed tomography (CT) scans have intrinsic health impacts themselves, and are incompatible with population-level screening.[25] Other techniques, such as gas chromatography-mass spectrometry (GC-MS), are limited for this function by their expense, bulkiness and complexity. Although most research has focussed on lung cancer, significant attention has also been given to other cancers, diabetes, asthma, chronic obstructive pulmonary disease, cystic fibrosis and tuberculosis.[26–31]

1.2 Impacts of VOCs on Human Health

In recent times, exposure to VOCs has become a prominent issue for human health. It has been shown that, even at trace level, chronic exposure can result in serious health effects, including disorders of the nervous system, diseases of vital organs, and an elevated risk of cancer.[3,32] The large number of VOCs is reflected in the wide range of possible health impacts caused by individual compounds. Given their low boiling points and high vapour pressures, the main exposure route to most VOCs is via inhalation.[33] Some VOCs are relatively harmless and have no known health effects, whereas other compounds are highly toxic. VOCs with reported chronic health impacts can be broadly classified as carcinogenic or non-carcinogenic (i.e. cancer causing or not cancer causing).[33] Non-carcinogenic effects include irritation, sensory effects, damage to the liver, kidneys and central nervous system and respiratory effects such as asthma.[34] The main carcinogenic effects are cancers of the lung, liver, kidney, biliary tract and blood (leukaemia and non-Hodgkin lymphoma).[35] Due to their developing physiology, children are more susceptible to pollutant exposure than adults.[36] For example, children exposed to a median level of 20 $\mu g/m^3$ (6.3 parts-per-billion, ppb) or more of benzene in their homes were 8 times more likely to have asthma than children living in homes with lower levels.[34]

The WHO International Agency for Research on Cancer (IARC) classifies 120 VOCs as carcinogenic to humans (Group 1), including benzene and formaldehyde.[37] Other VOCs display some carcinogenic activity, either as probably carcinogenic (Group 2A, IARC) such as styrene or dichloromethane, or as possibly carcinogenic (Group 2B, IARC) including ethylbenzene or chloroform. Other VOCs, such as toluene or xylene, are currently not classifiable as carcinogenic to humans (Group 3, IARC) due to inadequate evidence. In addition to the direct health impacts of VOC exposure, there are health impacts associated with secondary pollutants. It has been shown that exposure to ambient aerosols (including SOAs) can cause damage to respiratory and cardiovascular systems.[38] Beyond various health impacts, VOCs are often the cause of odour complaints, such as those associated with industrial activity. Even in cases where there are no confirmed health effects from a pollutant, exposure to odours can cause quality of life issues and stress-related physical disorders.[39]

1.2.1 Indoor Air Quality (IAQ)

On average, humans spend 90% of their time indoors, where concentrations of pollutants tend to be higher.[40] Consequently, indoor environments are considered a leading source of VOC exposure.[33] The most common indoor VOC emission sources include building materials such as carpets, insulation and paint; combustion processes such as smoking, cooking and heating; consumer products such as cleaning

products and air fresheners; dry-cleaned clothing; tap water; and personal care products.[41] One of the main sources of indoor VOCs is the infiltration of outdoor pollution into buildings.[40]

1.2.2 Regulation

In response to the adverse health effects of many VOCs, many compounds have been regulated by national and international organisations and governments. In 1999, the EU introduced the VOC Solvents Emission Directive (1999/13/EC), which sought to prevent or reduce the direct and indirect effects of emissions of VOCs into the environment and the potential risks to human health.[42,43] It covers a wide range of solvent using activities, e.g. printing, surface cleaning, vehicle coating, dry cleaning and manufacture of footwear and pharmaceutical products. The Directive requires relevant producers to comply either with the emission limits or with a reduction scheme, such as substituting products for low-solvent or solvent-free versions. EU Member States are obliged to report on the implementation of the Directive to the European Commission every three years.

The EU's 2008 Air Quality Directive (2008/50/EC) made the monitoring of benzene in ambient air mandatory.[44] It states that uncertainty of benzene measurement (in ambient air) is 25% and sets a limit value of 5 $\mu g/m^3$. In addition to benzene, the directive also obliges member states to have at least one monitoring site to measure VOC ozone precursors. These include toluene, ethylbenzene, xylenes and formaldehyde, in addition to a selection of alkanes, alkenes and alkyl-functionalised benzenes.[ii] In 2010, the WHO Air Quality Guidelines for Europe established exposure guidelines for a range of VOCs, including benzene, toluene and formaldehyde.[35] The guidelines state that ambient air concentrations of benzene above 17 $\mu g/m^3$ (5.2 ppb) are associated with an excess lifetime risk of 1/10,000.[iii] The exposure values for toluene and formaldehyde are 260 $\mu g/m^3$ (70 ppb) over one week and 100 $\mu g/m^3$ (80 ppb) over 30 min, respectively.

In the UK, responsibility for meeting air quality limit values is devolved to the national administrations in Wales, Scotland and Northern Ireland. The Secretary of State for Environment, Food and Rural Affairs has responsibility for meeting the limit values in England and the Department for Environment, Food and Rural Affairs (DEFRA) co-ordinates assessment and air quality plans for the UK as a whole. Under the Environment Act of 1995, the UK Government and the devolved administrations are required to produce a national air quality strategy, which defines the UK's air quality objectives. The most recent strategy, the Clean Air Strategy, was released in January 2019.[14] The strategy sets targets for the national

[ii] for the full list, see Annex X of the Air Quality Directive[44]

[iii] i.e. if 10,000 are exposed to benzene at a concentration of 17 $\mu g/m^3$ (5.2 ppb) then one cancer occurrence above the background chance may appear in those 10,000 persons from that particular exposure

reduction of emissions of five types of air pollution: fine particulate matter ($PM_{2.5}$); ammonia (NH_3), nitrogen oxides (NOx); sulphur dioxide (SO_2); and VOCs.[iv] The targets for VOC emissions are reductions of 32% by 2020 and 39% by 2030, compared to the 2005 baseline (1,042 kilotons).

[iv] Note that the Clean Air Strategy refers to VOCs as NMVOCs (non-methane volatile organic compounds)

1.3 VOC Measurement Methods

1.3.1 Laboratory Based Methods

In ambient air, VOCs are typically present in the parts-per-billion (ppb) or lower concentration ranges. As a result, discriminating between different VOCs is a significant challenge. Given the low concentrations of these analytes, sophisticated equipment is required for sensitive and selective detection.

Chromatographic Methods

The most common technique for selectively measuring VOCs is gas chromatography, often in combination with a detection method such as mass spectrometry (GC-MS).[45] The mobile phase is a carrier gas, usually an inert gas such as helium or an unreactive gas such as nitrogen. GC relies on separating components of a gaseous mixture based on their different chemical properties, primarily polarity and hydrophobicity. A typical gas chromatograph consists of a sample injector, a heated column and an elution detector (Figure 1.3).

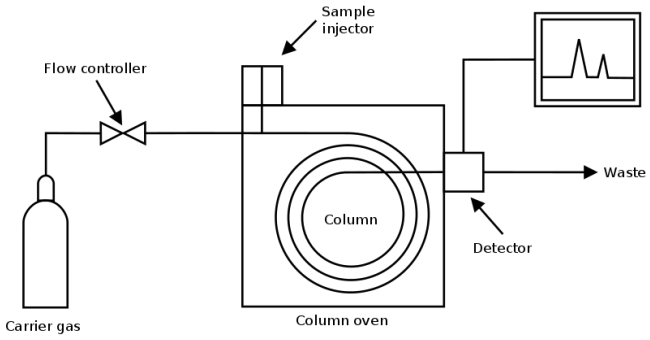

Figure 1.3. Diagram of a typical gas chromatograph (Image: Creative Commons License)

The stationary phase is a microscopic layer of liquid or polymer on an inert solid support, where the support can either be the column/channel itself, or a separate packed material. Gaseous compounds interact with the walls of the column, or, in the case of packed columns, the coating on the packing material (and/or the packing material itself). This causes each compound to elute at a different time, known as the retention time. Interactions between stationary phases and gaseous analytes are typically

dispersive, and such attractions increase with compound size.[v] Dipole, pi-pi and/or acid-base interactions may also occur, and separations are determined by differences in the overall effects of all interactions. Polarity is the most important characteristic for a given GC stationary phase, with selectivity based on the chemical principle of "likes dissolves like." For example, highly polar vapours will have stronger interactions with a polar surface than weakly polar vapours. Therefore a polar compound will take longer to elute from a polar chromatography column than a non-polar compound.[46] Non-polar phase materials are generally composed only of carbon and hydrogen atoms and contain carbon-carbon single bonds, whereas polar phase materials may also contain one or more atoms of bromine, chlorine, fluorine, nitrogen, oxygen, phosphorus, or sulfur.[47] Stationary phases are primarily silicone-based oils that have high temperature stability (Figure 1.4). These range in polarity from non-polar 100% polydimethylsiloxane (PDMS), 5% phenyl polysiloxane 95% PDMS, to mid-polar 6% cyanopropyl-phenyl polysiloxane, 94% PDMS, and polar polyethylene glycol (PEG). PEG-based phases are less common than siloxane phases due to their tendency to degrade and a relatively low thermal limit (approximately 280 °C, compared to over 300 °C for polysiloxane materials).[48] PDMS is a common GC stationary phase used for general applications, and has been used to separate benzene, toluene, ethyl benzene, xylene (BTEX), hydrocarbons and substituted aromatics.[49] Phase polarity can be increased by introducing higher monomer fractions of materials such as (phenyl)-methylpolysiloxane or (cyanopropylphenyl)-methylpolysiloxane.[48]

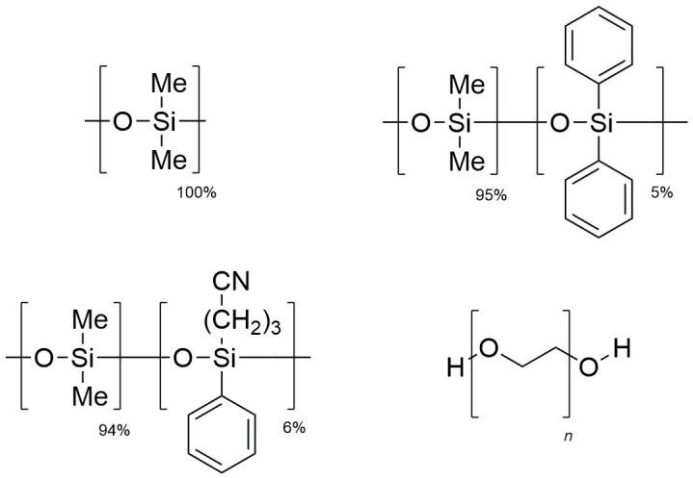

Figure 1.4. Structures of common stationary phase materials. *Top* – 100% PDMS (left) and 95% PDMS, 5% phenyl polysiloxane (right). *Bottom* – 94% PDMS 6% cyanopropyl-phenyl polysiloxane (left), polyethylene glycol (PEG, right).

[v] I.e. larger compounds with higher boiling points have longer retention.

To be adsorbed, an adsorbate molecule needs to reach the adsorbent particle surface by convection and diffusion. It then must diffuse along the length of a pore until it reaches a vacant adsorption site, where it can then adsorb onto the solid surface. These mass-transfer steps are driven by deviation from equilibrium. In an adsorbent bed, assuming a clean adsorbent, mass transfer begins upon introduction of the sample. The concentration of the (initial) adsorbate decreases immediately upon entering the column, until it reaches zero. As new adsorbate enters the column, the section of the column that the sample initially contacts is exposed to the adsorbate at the feed concentration. Eventually, the beginning of the column reaches equilibrium with the feed and no additional net mass transfer occurs. When the sample reaches a section of the column that has yet to reach equilibrium, mass transfer resumes, such that the adsorbate concentration decreases until it reaches nearly zero. The length where the concentration changes is named the mass-transfer zone. As this process continues, more adsorbent establishes equilibrium with the adsorbate, such that the sample must go further through the column to encounter column adsorbent that is not at equilibrium. Once the mass transfer zone reaches the end of the column, adsorbate starts to leave the column, which is called breakthrough. Eventually, the concentration of adsorbate in the effluent is the same as the concentration of the input sample concentration, at which point the entire column bed is in equilibrium with the sample.

GC has been used with a range of detectors for VOC measurement. These include flame ionization detectors (FID),[49,50] photo ionization detectors (PID),[50] thermal conductivity detectors (TCD), or mass spectrometers (MS).[49–51] Many standard GC-based methods are able to offer ppb or lower detection limits with both high selectivity and high accuracy.[52] Despite this, such methods cannot be used for real-time field monitoring due to large size, heavy weight, special carrier gases requirement and high maintenance. GC-MS has emerged as the gold standard for VOC measurements.[27,53–55] Whereas MS is limited by the requirement of high purity samples, standard GC detectors cannot distinguish multiple molecules that elute from the column at the same time. Therefore, GC and MS methods conveniently address the fundamental weakness of the other. When used in combination, GC and MS components can achieve better substance identification than either component used individually, as it is extremely unlikely that two molecules will have both the same elution time (from the GC) *and* the same mass spectrum (from the MS). Detection limits for VOC measurement with GC are typically in the ppb to ppt (parts-per-trillion) range. For example, a study that measured ambient VOCs reported a limit of detection for benzene was 0.08 ppb in full scan mode and 0.01 ppb in selected ion monitoring (SIM) mode. In this example, the total analysis time was ~60 minutes using a 100% PDMS stationary phase,[49] which provides high resolution but at the cost of long separation times. Separation times can be reduced by using more phases, such as 94% PDMS 6% cyanopropyl-phenyl polysiloxane.[56]

Given the low concentrations of VOCs in ambient air, sample preconcentration is usually required prior to analysis. A common technique is active sampling, which involves collecting samples through trap based systems, such as sorbent tubes or canisters, which are then manually analysed in a laboratory by trained technicians.[45] This approach is the stated reference method by the European Commission's Air Quality Directive,[44] although with additional equipment it is possible to automate the collection and analysis of ambient air samples (online analysis).[49] Post-collection laboratory analysis increases total analysis time and the risk of sample degradation during storage or transport.[56] In addition, off-line analyses do not provide concentration-time profiles since each measurement represents an average value of pollutant concentration over the selected sampling time.[56]

Frontal chromatography is a process that separates compounds based on differential retention factors on the stationary phase.[57] Mixtures are continuously fed into the column under conditions that are preferential towards one (or more) components in the mixture. Purified components are obtained at the outlet of the column, until the dynamic capacity of the stationary phase is exhausted and other sample components are eluted. This method is commonly used for purification of biological materials, such as proteins and antibody aggregates.[58–60]

Spectroscopic Methods

Infrared (IR) spectroscopy is a common and versatile analytical technique that can provide molecular specific information with minimal or no sample preparation.[61] A significant limitation of IR spectroscopy for use in ambient gas analysis is the strong absorption of water, which leads to poor limits of detection (LoD). The LoD can be improved by combining IR spectroscopy with specially designed sensing elements. For example, it has been reported that zinc oxide sensing elements can be used to detect polar VOCs including acetone and ethanol.[62] Despite this, the limit of detection was above 2 ppm and the spectrometer used is bulky benchtop equipment (Avatar 370 FTIR). Although possible to reach the ppb-range, this typically requires extensive equipment, such as telescope beam projection between buildings and detection components cooled with liquid nitrogen.[63,64] Ultraviolet (UV) spectroscopy has much weaker absorption bands for water and are typically more sensitive than IR methods.[65] Differential Optical Absorption Spectroscopy, a subtype of UV spectroscopy, has been shown to be able to detect BTEX compounds in the sub-ppb range, although the technique is limited by long acquisition times (up to 30 minutes) and attenuation of UV light though oxygen and ozone absorption.[65,66]

Limitations of Laboratory Based Methods

Most laboratory based methods require the use of passive samplers and successive offline analysis, which are time consuming, expensive and require skilled personnel to perform complex tasks.[67] The

equipment itself is also large, generally importable and expensive to purchase and maintain. These disadvantages mean that these offline methods are not compatible for in-field VOC measurement or automated VOC monitoring over dense spatial networks. As offline sampling requires manual intervention and multiple steps including sampling, storage, and shipping before analysis, it is susceptible to higher losses and has longer measurement cycles.[45] The requirement for better special and temporal coverage can only be met by reducing the size and costs of monitoring devices. Generally, there are two approaches to achieving this: 1) miniaturising existing technology, or 2) using low-cost and portable sensors.

1.3.2 Portable Systems

Miniaturised Gas Chromatography

Portable systems are typically derived from laboratory instrumentation and include modifications to reduce size, weight, and power consumption. Miniaturised chromatographs therefore maintain the principle features of standard GC instruments, such as a heated column, a detection component and a dedicated carrier gas, but are also small and more easily transported (Figure 1.5). A range of instruments used to measure VOCs have been reported in the literature,[56,68–73] which all incorporate at least one column ranging in size from 0.5 m to 20 m, and a variety of polymer stationary phases. At least four instruments have been reported to have a 1 ppb or lower Limit of Detection (LoD) for benzene,[56,69,70] with the lowest reported as 0.02 ppb.[70] Most systems use helium, nitrogen or hydrogen as the carrier gas, while three systems used filtered and cleaned air.[68,70,73]

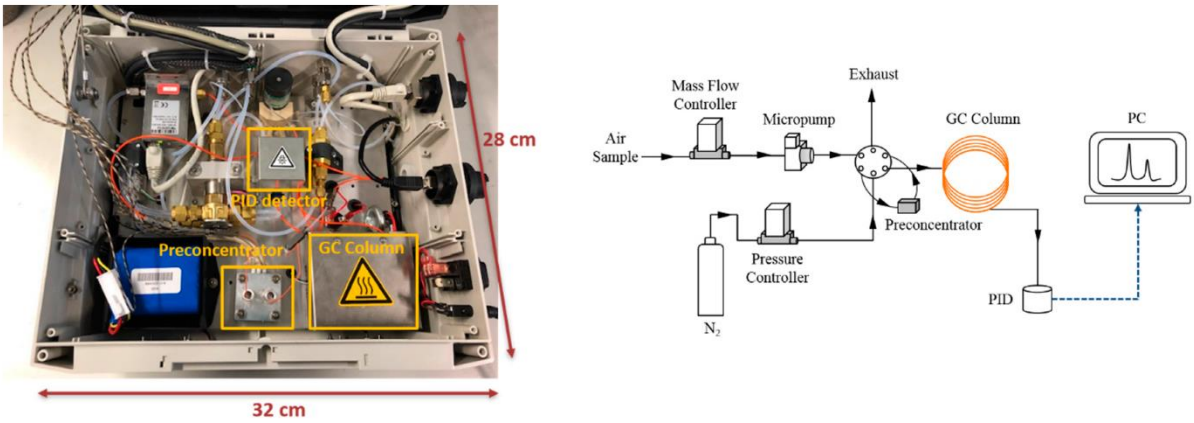

Figure 1.5. Example of a miniaturised gas chromatograph system. *Left* – photograph of the GC system. The column stationary phase was moderately polar Rxi-624 (94% PDMS 6% cyanopropyl-phenyl polysiloxane). *Right* – schematic view of the device. Figure adapted from reference (Creative Commons Attribution License).[56]

In addition to the instruments developed by research groups, many field portable GC instruments are commercially available.[74–82] The detection limits for these instruments fall within sub-ppb,[74–77] single to double figure ppb[78–80] or ppm ranges.[81,82] Many are battery powered, offering battery life between 3 and 9 hours.[74,75,78,80,82] Most systems use gas canisters (helium, nitrogen or hydrogen), with only one of the referenced instruments using cleaned ambient air.[81]

Some portable GCs incorporate detectors specifically developed for portable devices. These include mini PIDs, micro FIDs, quartz crystal microbalance (QCM), surface acoustic wave (SAW) arrays and metal oxide (MOX) sensors.[52,83–85] Although reliable VOC analyses are possible with miniaturised gas chromatographs, the relatively large size, high cost and high power demands impede long-term deployment of sensors for use in air quality networks (especially those that are battery powered).[86]

Micro Gas Chromatography (μGC)

In response to the limitations of bench-scale and miniaturised GC systems, many micro gas chromatography (μGC) instruments have been developed.[45,86,95–98,87–94] These instruments typically use microfabricated components including adsorbent preconcentrators[45,91,95,96] and etched microchannels, either coated[45,86–88,92–97] or packed[89–91,98] with an adsorbent stationary phase. As with miniaturised GC instruments, the carrier gas for μGC systems is either helium, nitrogen or hydrogen gas, although some systems have used air.[88,90,91,98] Although much smaller than conventional GC columns – typically with dimensions in the centimetre range (Figure 1.6) – μGC columns use the same range of stationary phase materials. The majority of reported systems used non-polar 100% PDMS,[45,86–89,92,95–97] although a few used polar materials such as Carbowax.[90,91,98] The lowest reported LoD for a BTEX compound (benzene) is 0.1 ppb,[91] although a LoD of 0.0165 ppb has been reported for formaldehyde.[95] Despite the potential of microfabrication to significant reductions in size and weight, the overall power demands for μGC systems remain high and represent a limiting factor in simultaneously meeting goals of high performance, miniaturization, and long-term battery operation.[86] In addition, they are expensive and complex enough to prevent their use in sensor network applications.[50]

Figure 1.6. Example of a μGC device. A: Silicon micromachined separation (left) and pre-concentration (right) columns, together with the micromachined filters (insets). B: complete packaged prototype. Figure adapted from reference (with permission).[99]

Portable Mass Spectrometry

Proton-transfer-reaction mass spectrometry (PTR-MS) allows real-time measurements of multiple volatile organic compounds (VOCs) in air with a high sensitivity (10-100 ppt) and a fast time response (1-10 seconds).[11] The sample air is continuously pumped through a drift tube reactor (as shown in Figure 1.7), where a fraction of the VOCs in the sample are ionised via a proton transfer reaction with hydronium ions (H_3O^+). This is a 'soft' ionisation method that prevents the fragmentation of product ions. Therefore the mass of the product ions equate to the individual compound mass plus one. At the end of the drift tube, the reagent and product ions are measured by a quadrupole mass spectrometer, and the product ion signal is proportional to the VOC mixing ratio.[11]

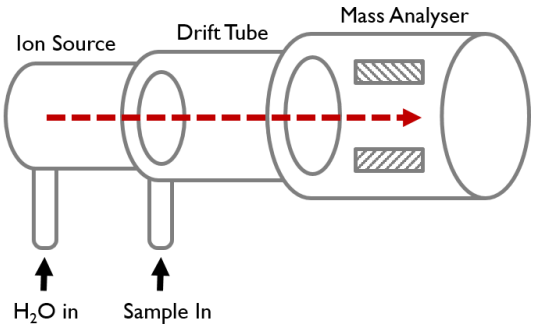

Figure 1.7. Diagram of a proton-transfer-reaction mass spectrometer, with a quadrupole mass analyser. The Ion Source ionises water vapour into hydronium ions (H_3O^+), which in turn ionise analytes in the sample gas. Ions are then separated according to their mass-to-charge ratio, and detected by a mass analyser.

PTR-MS doesn't require sample treatment, such as drying or pre-concentration, and can therefore be used to measure oxygenated VOCs, unlike methods which use off-line sampling with canisters. PTR-MS has been used to study a range topics including urban plumes; biomass burning plumes; and atmospheric measurements on aircraft, ships and vehicles.[11,100] It is possible to use the method in transport, but this requires significant equipment such as specially adapted aeroplanes.[101] A significant drawback of PTR-MS is that the mass of product ions is not a selective indicator of a given VOC, especially for isomers. In addition, the technique cannot detect light VOCs with proton affinities that are low, or close to water (such as formaldehyde).[102]

Limitations of Portable Systems

Although portable systems go some way to address the size and usability limitations of conventional laboratory based instruments, they are still largely impractical for many practical applications, such as monitoring air quality networks. Most systems tend to address only one limitation, such as size, but disregard others, such as using canister carrier gases that need regular replacement. In addition, few of the systems described in this section are scalable, hence placing a limit of the size area of a network that could be practically covered.

1.3.3 VOC Sensors

Requirements for mobile applications and improved spatial air quality measurements can only be satisfied through size and cost reductions of monitoring devices. It has been argued that in the future, air quality assessment should use exposure based monitoring of air pollutants with higher spatial resolution.[103] Commercial low-cost sensors represent an opportunity to develop networks of VOC measurement across large areas with higher spatial resolution at a lower cost than standard reference measurements methods.[44,104] Unlike methods that rely on gas sampling and lab-based analyses, gas sensors can provide near real time air pollution measurements electronically.[105] This simplifies both the reporting of air quality to the internet (Article 26 of the EU Air Quality Directive[44] and Article 23 of the INSPIRE Directive[106]) and means it is possible to assess the effect of short term action plans (as stated in Article 24 of the Air Quality Directive). A wide range of sensor technologies have been developed, which can be broadly divided in to the following categories of VOC sensor: photoionization detectors (PID), flame ionisation detectors (FID), electrochemical sensors, metal oxide (MOX) sensors, optical sensors, and sensor arrays.[105]

Photoionization Detector (PID)

PIDs use UV light to ionise gas molecules in sample vapour (Figure 1.8). The resulting ions produce an electric current that is proportional to the signal output of the detector. PIDs are not considered selective because *all* gas molecules with an ionization energies below that of the UV light are ionised. Xenon lamps have an ionization potential of 9.6 eV, but this is not low enough to distinguish many air pollutants. For example, it would be impossible to differentiate benzene, toluene and xylene as they all have ionization potentials below 9.6 eV. Additionally, PIDs are not suitable for measuring chlorofluorocarbons (CFCs).[105] PIDs are used as the detection component for a gas chromatographs, liquid chromatographs and mass spectrometers.[45,56,69,71,107,108] Many commercially available VOC analysers use PID technology.[76,77,80]

Recent attempts to improve upon the broadband nature of PID measurement have been achieved by incorporating additional sensing dimensions. In 2018, a portable and low cost PID was reported that provided two outputs: 1) a UV lamp to provide a broadband measure of total VOC concentration; 2) a variable electric field to deflect ions (produced by the UV lamp) towards an electrode detector.[109] The magnitude of deflection is dependent on ion compounds, and the sensor was shown to discriminate between 2-hexanone, isobutylene, propanol, 2-pentanone, 2-octanone and 2-heptanone vapours in the 2-10 ppm range. Another novel PID sensor, developed in 2019, used microfabricated electrodes coated with either silver nanowire or carbon nanotubes.[110] The sensor could detect toluene down to 500 ppb.

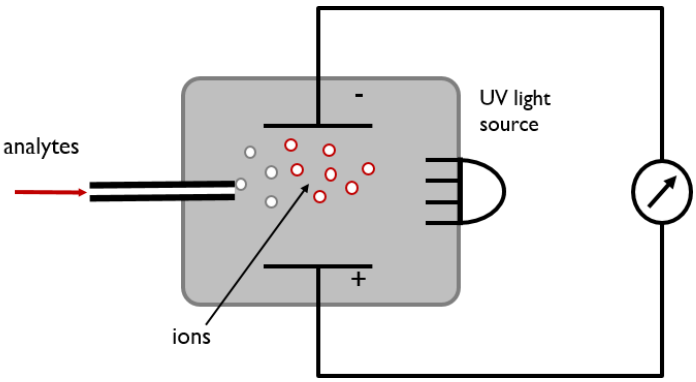

Figure 1.8. Principle of operation of a typical photoionization detector (PID).

Flame Ionisation Detector (FID)

Flame ionisation detectors (FID) measure analytes in gas streams, and are commonly used as the detector in both micro[86,88,89,92–94,97] and laboratory-scale GCs.[111] FIDs detect ions formed during the combustion of VOCs in a hydrogen flame, where the concentration of ions is proportional to the concentration of the VOCs in the sample. Like PIDs, FIDs are broadband sensors, meaning that they are not selective to different VOCs. FIDs are able to measure very low concentrations (ppt) and relatively inexpensive to purchase and maintain. Their disadvantages include requiring a supply of hydrogen and an inability to measure highly oxygenated species, as is possible with IR technology. In addition, the flame in FIDs oxidises all compounds that pass through, such that all VOCs are removed from the analyses stream, unlike non-destructive techniques such as PIDs.

Amperometric Sensors

Amperometric sensors require at least two electrodes, but may include three: measuring, counter and reference. Sample gas species diffuse through a gas permeable membrane to the measuring electrode, where an electron transfer occurs to produce an internal current that is proportional to the sample VOC concentration.[112] In general, amperometric sensors are low cost, low power and can be small sized (less than 20 mm x 20 mm).[105] Unlike PIDs and FIDs, it is possible to 'tune' these sensors selectivity for a given target. This can be achieved through a range of modifications, such as: targeting specific electrochemical reactions that are selective towards given species; changing the physical properties of the membrane, such as pore size; adjusting the bias voltages; or changing electrode materials themselves.[105] Such modifications have led to selective electrochemical sensors for gases including ozone (O_3),[113] ammonia (NH_3),[114] nitrogen dioxide (NO_2)[115] and nitric oxide (NO).[116] Electrochemical sensors for the detection of

these, and other gases, are commercially available from a range of manufacturers, including City Technology, Alphasense, Membrapor AG and SGX Sensortech. While there are currently no commercially available amperometric sensors for selective VOC detection, some have been reported in the academic literature.[117–125] Amperometric sensors typically have a low electrical consumption due to the low electrical current signal generated, with most power used to amplify the very low-level signal required to read the measurement.[105] Recent developments have led to the lowering of the limit of detection. For example, gold has been used to modify the platinum working electrode of an oxygen sensor and detect (but not differentiate) acetic acid, methyl ethyl ketone (MEK), ethanol, benzene, toluene and xylene in the 500-1000 ppb range.[122,123] More recently, a VOC LoD of 109 ppb was achieved by illuminating the sensing electrode with UV light.[124] Despite such modifications, the LoD for most VOC electrochemical sensors remains in the 100s of ppb range. A rare exception to this is the detection of formaldehyde. For example, Knake et al developed a sensor with a calculated a LoD of 13 ppb, although the sensor had cross sensitivity for many gases such as NO, NO_2 and SO_2.[125] Most commercially available sensors of this type are designed to give an averaged reading over 1-5 mins, so are not typically suitable for handling faster changes.

Resistive Metal Oxide Sensors

The resistance and conductivity of metal oxide (MOX) materials change in response to different ambient gases.[126] When MOX materials are heated in the presence of air at temperatures up to approximately 400 °C, oxygen is adsorbed on the oxide surface (Figure 1.9).[127] This traps electrons from the bulk of the material and, depending on the type of material, the resistance of the MOX will either increase (n-type) or decrease (p-type).[128] Further changes in resistance occur when other species, such as VOCs, present in the atmosphere react with the adsorbed oxygen (or directly with the MOX). The change in MOX resistance, or conductivity, then relates to a sensor signal which correlates to the concentration of the target gas. Although MOX sensors are normally compact and low cost, they are limited by their power consumption.[105] They tend to be smaller than electrochemical sensors but consume more power than PIDs.[105] In addition, they are cross sensitive to inorganic gases, meaning that their use for measuring VOCs is limited when gases such as NO, NO_2 or CO are also present in higher concentrations.[105] There are many manufacturers that make MOX sensors for VOC detection, including AMS, Unitec, UST, SGX SensorTech, Figaro, FIS, Synkera Technologies and Alphasense. Of the sensors produced by these manufacturers, Unitec SENS3000 has the best detection capability, able to produce responses that correlate with reference values for benzene at 25 ppb and below.[129]

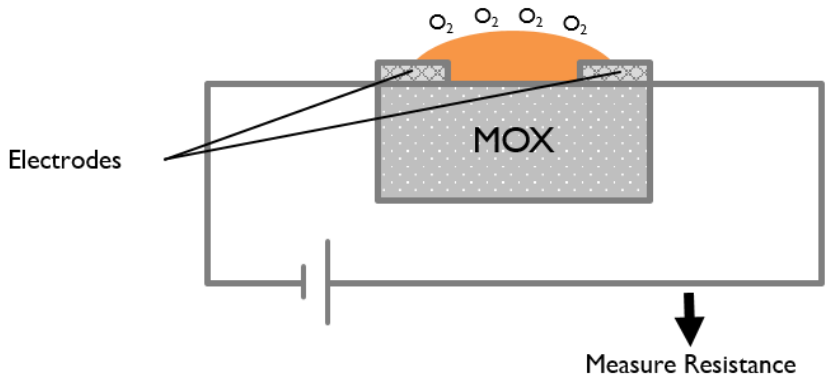

Figure 1.9. Typical metal oxide (MOX) gas sensor setup.

Many VOC MOX sensors have been reported in the academic literature, but there are relatively few that report a LoD of 1 ppm or lower.[130–136] At least three groups have reported the detection of BTEX compounds in the range of 100 to 200 ppb.[130–132] WO_3 films have been used to detect benzene at 200 ppb[132] and toluene, ethyl benzene and (meta-)xylene at 10 ppb.[133] In the case of the latter sensor, cross-selectivity to other VOCs including ethanol, formaldehyde and methane was low, although there was minimal cross- selectivity between TEX compounds. More recently, the doping of WO_3 nanofibres with Pd-ZnO nanocubes enabled the detection of 100 ppb of toluene with a response time of 20 seconds.[130] Cross-selectivity to non-aromatics such as acetone and ethanol was high, although cross-selectivity to aromatic compounds was not reported. Formaldehyde has been detected down to double[134] and single[135,136] figure ppb range. Although many resistive sensors are based on metal oxide materials, others have also been reported. It has been shown that graphene can be used as a sensing material to measure a wide range of VOCs, including BTEX and solvents such as tetrahydrofuran, chloroform and hexane.[137]

Optical Sensors

It is possible to measure VOCs via a range of optical methods, such as UV-vis spectroscopy. As with MOX VOC sensors, few optical VOC sensors have been reported with a ppb-range sensitivity.[138–141] For example, a compact portable UV spectroscopy-based BTX sensor capable of measuring in the single figure ppb range after sampling vapours into a silica-packed concentration cell.[138,139] Despite this sensitivity, the sensor has a 30 minute response time, limiting the usefulness of such sensors for practical real-time VOC measurement applications. In recent years, light emitting diodes (LEDs) for the deep UV-range have become available, with emission bandwidths suitable for measuring VOCs. In 2016, a BTEX sensor based on vapour absorbance in a 40 cm length measurement cell illuminated with light from a UV-LED in a recorded a LoD of 1 ppm.[142]

1.3.4 Improving Sensor Selectivity

In the above section, many VOC sensing methods have problems with cross-sensitivity. Different approaches have been developed in order to introduce additional selectivity. Two such approaches are the development of molecular receptors for target analytes, or the use of multiple sensors as part of sensor arrays.

Molecular Receptor Sensors

Molecular receptors are materials that have a cavity or binding region for analytes of interest. They are analogous to many specific binding interactions in nature, such as enzymes and substrates, or antigens and antibodies. Consequently, molecular receptors have potential to address issues regarding VOC sensor selectivity.[143] Inspired by biological systems, chemists have sought to synthesise molecular receptors that recreate the specificity and selectivity of biological receptors, by bringing concepts around shape recognition and binding site complementary to gas phase receptors.[144] Most of this work has focussed on developing gas sensors based on organic molecules that contain enforced cavities with molecular dimensions that function as molecular recognition sites for target analytes.[143] Molecules that have been used to selectively detect VOCs include cyclodextrins for benzene (23 ppm LoD),[145] calixarenes[146] and cavitands (Figure 1.10).[147–149]

It is possible to modify molecular receptors during synthesis, which can further increase selective performance.[143] For example, the use of a cavitand (EtQxBox) as a preconcentrator adsorbent has been shown to have a sub-ppt detection limit for BTEX compounds.[150] Despite the choice and availability of synthesised molecular receptors, they are yet to make a significant impact on sensors used for practical applications. This is due to complex syntheses of receptors, long gas sampling times (typically over 15 minutes) and limited control of molecular recognition at the adsorbent interfaces.[143,145,150]

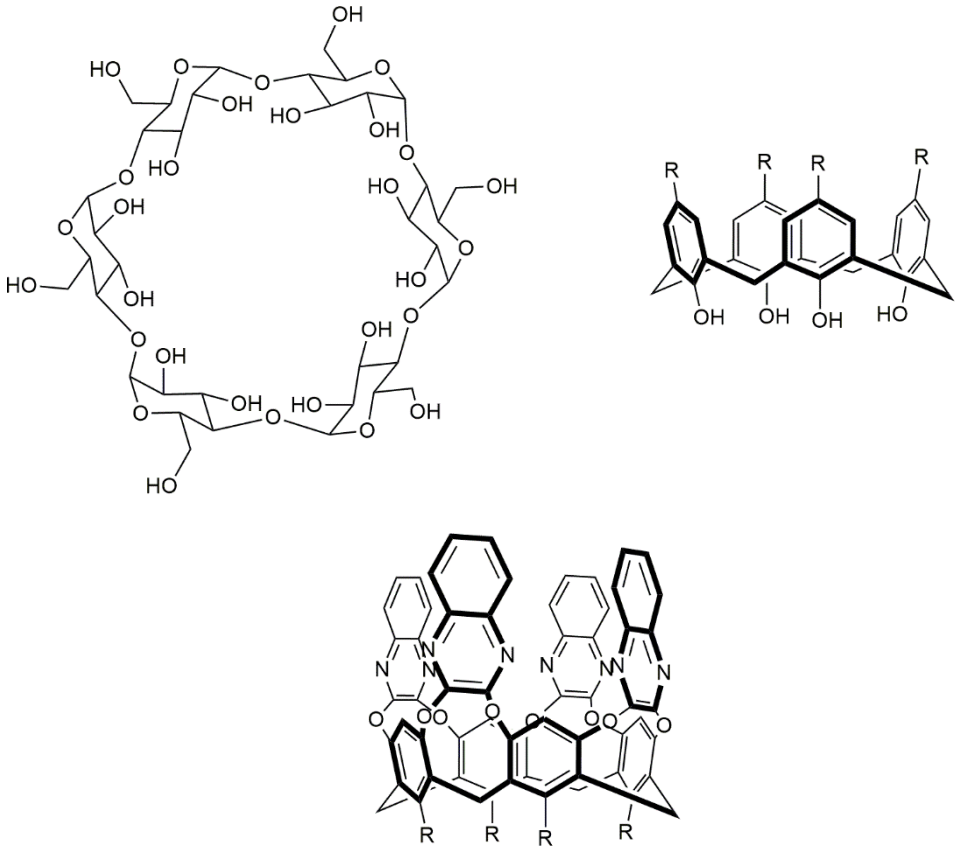

Figure 1.10. Structures of common molecular receptors. Clockwise from top left: cyclodextrin, calixarene (cone calix[4]arene) and cavitand (QXCav).

Sensor Arrays

Devices that contain multiple sensors of different type or configuration are commonly known as sensor arrays or electronic noses (e-noses).[105] Each sensor within the array has a different response to a given compound or class of compounds. Therefore, individual selectivity of each sensor is not required as the range of responses from all the sensors in the array can provide collective selectivity. This multivariate response from an array of sensors with a variety of selectivities can therefore produce "electronic fingerprints" that can be used to detect VOCs via pattern recognition.[151]

The response of a sensor tends to change in response to the concentration of target vapour, such as the total concentration of VOCs in a gas sample corresponding to the resistance of a MOX sensor. These are examples of data *features*: patterns that are typically, either individually or in combination with others, indicative of a target vapour.[151] Initially, the most common practice for gas detection was to use the steady state responses of the sensors as the feature,[152] but it is possible to extract these and a variety of other features from sensor output data. In order to process the features produced from sensors, it is

necessary to introduce elements of intelligence, such as statistical analysis techniques. In general, the stages involved in data analysis are:[151]

1. **Signal Pre-processing** – extraction of the feature vector (which contains information describing an object's important characteristics, i.e. individual features).
2. **Dimensionality Reduction** – projection of the feature vector onto a lower dimensional space and avoid problems associated with large and sparse datasets.
3. **Problem Prediction** – use of the low-dimensional feature vector to solve a given prediction problem, typically classification, regression, or clustering.
4. **Validation** – estimation of analysis error rates.

Examples for VOC sensing include temporal parameters from the response curves, such as the integral of the sensor response curve,[153] or the maximum change in resistance.[137] In these examples, different vapours produce different response profiles, such that features extracted from the responses can be used to select between analytes. This type of selectivity can address issues with sensors that aim to achieve selectivity with an on-sensor material, which tend to have significant cross-sensitivity problems.[153] Numerous types of sensor have been used in arrays for VOC detection, including MOX,[90,137,153] acoustic wave resonators,[154] paper-based colorimetrics,[155] optoelectronics[155,156] and fabric sensors.[157] It is also possible to create a virtual array, by applying signal processing analysis techniques to a single sensor operated with different settings. For example, varying the temperature of a sensor means a different signal can be taken for each temperature. It has been shown that using a temperature gradient for a tin oxide nanowire allows 5 different signals to be extracted from a single sensor, achieving a toluene detection limit of 300 ppb.[158]

1.4 Gas Adsorption and Desorption

VOC can be separated through adsorption and desorption of vapours to and from adsorbents. Adsorption is the adhesion of atoms, ions or molecules from a gas to a surface, leading to the formation of an adsorbate film on the surface of an adsorbent. It occurs as a result of the surface energy of atoms at the surface of the adsorbent. In the bulk of the absorbent, atoms are completely bound by other atoms in all directions, whereas atoms at the surface of the adsorbent are incompletely bound. This means they are able to form adsorptive bonds with atoms, ions or molecules (the adsorptives) in the gas phase above the surface (Figure 1.11).

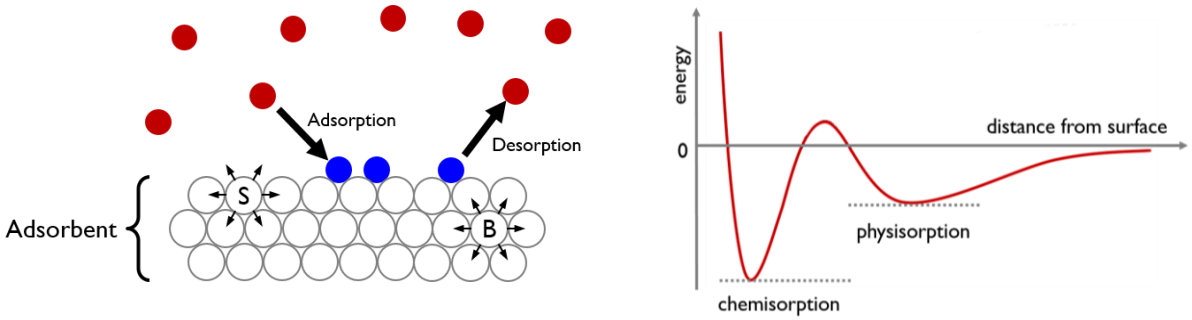

Figure 1.11. Gas Adsorption Process and Energy Profile. *Left:* Adsorption at the surface of an adsorbent. Atoms in the bulk (atom B) are *completely* bound to other atoms in the adsorbent, whereas atoms at the surface (atom S) are *incompletely* bound and free to interact with adsorptives (red circles) in the gas phase. When adsorption occurs, adsorptives become adsorbates (blue circles) on the surface. Conversely, desorption occurs when adsorbates are released. *Right:* Potential energy of a gas phase adsorptive versus distance from the surface.

The strength of the interaction between the adsorbent and the adsorptive depends on whether adsorption is physical (physisorption) or chemical (chemisorption). Physisorption is a weaker type of adsorption and is caused by van-der-Waals (dispersive) interactions. The enthalpy of adsorption for these interactions is typically less than 50 kJ/mole. As a general phenomenon, physisorption occurs whenever an adsorbable gas is brought into contact with a solid surface.[159] Chemisorption leads to the formation of chemical bonds: interactions that are covalent, metallic (both typically > 50 kJ/mole) or ionic (> 100 kJ/mole). Desorption is the opposite of adsorption, i.e. the process by which atoms, ions or molecules are released from a surface, and can be attained through swings in temperature and pressure. When adsorbed molecules are heated, they gain sufficient kinetic energy to 'escape' the energetic well

(Figure 1.11). Lowering gas pressure increases the likelihood of adsorbate escape as there are fewer molecular impacts to rebound adsorbed molecules back to the surface.

1.4.1 Adsorbents

Porosity

Porous adsorbents have internal and external surfaces. The external surface is defined as the surface outside the pores and the internal surface is then the surface of all pore walls.[159] Pores can be classified according to their size:[160]

- **Macropores** are pores with widths greater than 50 nm (nanometres).
- **Mesopores** are pores with widths between 2nm and 50 nm.
- **Micropores** are pores with widths less than 2 nm.

All of the accessible volume in micropores can be considered as adsorption space. When adsorption occurs here, the process is known as micropore filling, which is distinct from the surface coverage that takes place on the walls of macropores or mesopores.[159] Physisorption in mesopores starts with monolayer adsorption, where all adsorbate molecules are in contact with the adsorbent surface. For multilayer adsorption, there is more than one layer of adsorbate, but not all molecules are in contact with the surface. The final stage of adsorption is called *capillary condensation*. This occurs when a gas condenses within the pore at a pressure less than the saturation pressure of the bulk liquid. It is distinct from micropore filling, which does not involve a vapour-liquid phase transition.[161] The pore features of an adsorbent can be determined through interpretation of its adsorption isotherm.

VOC Adsorbents

Activated Carbon and Carbon Nanotubes

Activated carbon is produced from carbon-rich materials, such as coal and nutshells, by the processes of carbonization and activation. It is one of the most popular VOC adsorbents due to its stability, capacity and cost efficiency.[162] At 25 °C activated carbon has been shown to have a high capacity for BTX compounds: adsorption capacities of 27.5, 59.2 and 90.4 mg g^{-1} for benzene, toluene and *ortho*-xylene, respectively.[163] The drawbacks of activated carbon adsorbents include its nonpolar nature, limiting its ability to adsorb hydrophilic VOCs; its mostly microporous nature, limiting adsorption of larger molecular sizes; and difficulty in adsorbent regeneration (due to slow desorption rates and high

regeneration temperatures: typically over 300-350 °C).[162,164–166] Other disadvantages include posing fire risks, hygroscopicity[vi] and pore clogging (due to polymerization of VOCs, catalysed by surface ash).[167]

Carbon nanotubes (CNTs) are engineered carbon nanomaterials formed of cylindrical graphene sheets. They are usually produced by arc discharge, laser ablation, and chemical vapour deposition.[162] CNTs are promising adsorbents due to their large specific surface area, controlled cylindrical hollow structure, hydrophobic wall and easily modified surfaces.[162] The adsorption of many gases, including CO_2,[168] NOx,[169] H_2,[170] NH_3[171] and VOCs,[162] have been widely reported. The adsorption capacities of organic compounds onto CNTs are usually higher than that onto activated carbon and other carbon adsorbents.[162] The highly hydrophobic nature of CNTs enables strong adsorption of aromatic ring VOCs.[172] CNTs are limited by their tendency to aggregate, as well as their harmful and toxic effects on the human body.[173]

Metal Organic Frameworks

Metal organic frameworks (MOFs) are a class of hybrid porous solid consisting of ordered 3D frameworks of strong metal–ligand bonds between metal cations and organic linkers. They have been shown to have exceptionally large pore volumes and surface areas (typically in excess of 3000 m^2/g).[174] These properties have led to MOFs being used for gas storage, separation, heterogeneous catalysis and sensing.[175] A range of MOF materials, such as MIL-101, ZIF-8 and BUT-66, have been shown to have high capacities for BTEX compounds.[176,177] Despite this, the capacity and loading figures for many MOFs are measured at partial pressures far in excess of the partial pressures of trace level VOCs.[178] In addition, MOFs typically require high temperatures in order to regenerate the adsorbent, so that although they have considerable potential for VOC sequestration, their usefulness as a reversible VOC adsorber is still questionable.

Zeolites

Zeolites (aluminosilicate minerals) have found use as VOC adsorbents and catalysts due to their large surface areas, well-defined micropores, high adsorption capacity and high thermal stability.[179] Zeolites are able to accommodate different ions, atoms and molecules within their structures, which enables the development of advances materials that can offer selectivity for VOCs.[179] For example, zeolite microcantilevers have been shown to be able to detect ethanol in the ppm range.[180]

[vi] i.e. readily attracts water from its surroundings, typically through absorption or adsorption

Silica

Silica (silica dioxide) is a popular adsorbent for air dehumidification and pollutant removal.[181,182] These processes, when occurring simultaneously known as co-sorption, are energy efficient as it removes the need to cool air below its dew point temperature to remove water vapour.[182] Silicas have been shown to be effective at removing VOCs, including (toluene, formaldehyde, ethanol and 1,2-dichloroethane) from ambient air over a wide humidity range.[182] Mesoporous silica is a sub-type of silica characterised by structured mesopores, high surface area and high pore volume. Two of the most common mesoporous silicas, MCM-41 and SBA-15, have been used as adsorbents for VOCs, including benzene and toluene.[167,183] Although capable of adsorbing large volumes of VOCs, the synthesis of mesoporous silicas is involved and time consuming.[184] However, a significant advantage of silica materials is the relatively simple methods that can be used to modify the surface functionality and hydrophobicity (such as silanisation).[185] This renders them as a useful base material to investigate further in this thesis for separation of BTEX compounds as a function of their respective adsorption and desorption properties.

1.5 Aims and Objectives

1.5.1 Aims

This thesis considers the challenge of selective VOC sensing at concentration levels required in air quality monitoring applications. Gas sensors' size and cost make them suitable for use as part of dense sensor networks, but they currently lack selectivity for VOCs. A central hypothesis of this work is that mixtures of VOCs can be separated by their different physiochemical properties, such as boiling point, polarity and functionality. Consequently, the research seeks to establish the extent to which adsorption thermodynamics can be manipulated to achieve selective detection of gaseous volatile compounds. More specifically, the work explores how adsorbent chemistry, and different chemical functionality, can be used to influence the phase equilibrium between gaseous species and solid adsorbents.

1.5.2 Objectives

Silica was chosen as the base adsorbent material due to its low cost and potential for easy chemical modification, and a photoionisation detector (PID) was chosen as the detection component owing to its broadband response, ease of use and high sensitivity. Based on these selections, this thesis has the following primary objectives:

1. Design, build and optimise a VOC speciation platform, which is:
    - Able to achieve temperature controlled adsorption and desorption of VOCs in air.
    - Suitable for AQ monitoring applications: i.e. small, inexpensive and automated.
2. Synthesize and characterise a library of modified silica adsorbents, with a range of chemical functionalities.
    - Examine the kinetic and thermodynamic adsorption and desorption properties.
3. Develop adsorption/desorption control regimes to exploit kinetic and thermodynamic differences of different VOCs on absorbent library.
4. Use Principle Component Analysis (PCA) and other data separation analysis techniques to characterise the capability of the sensor device to discriminate VOC mixtures.

Chapter 2 Materials, Methods and Sensor Setup

2.1 Generating VOCs

2.1.1 Target Compounds

For this thesis, benzene, toluene, ethylbenzene and *para*-xylene (BTEX) were chosen as the primary target compounds due to their role as common pollutants with proven health impacts. The key properties of the BTEX compounds are shown in Table 2.1. Also included are: methyl ethyl ketone (MEK, also known as 2-butantone), a polar VOC with a similar boiling point to benzene, as well as being a compound of interest for breath analysis applications; acetone, another polar solvent and compound of interest for breath analysis; hexane, an apolar solvent.

Table 2.1. Key properties for volatile organic compounds (VOCs) used in this work.[186]

	Name	Molecular weight, g/mol	Boiling point, °C	Ionization potential, eV	Dipole moment, D
1	Benzene	78.1	80.1	9.24	0
2	Toluene	92.1	111.0	8.82	0.36
3	Ethylbenzene	106.2	136.0	10	0.58
4	*para*-Xylene	106.2	138.4	8.44	0
5	MEK*	72.11	79.6	9.54	2.76
6	Acetone	58.08	56.1	9.69	2.91
7	n-Hexane	86.18	68.7	10.18	0.08

* MEK: methyl ethyl ketone, also known as 2-butantone

2.1.2 Permeation Tubes

The preparation of standard gas mixtures can be broadly divided into static or dynamic methods.[187] Static methods are typically based on the dilution of a known amount of a target component by a diluting gas. Dynamic methods are based on the introduction of target components into a flow of a dilution gas. Permeation tubes are one of the most common dynamic techniques for the preparation VOC vapours.[188] They use a permeable membrane to distribute a small and consistent flow of VOCs into a diluting gas such as nitrogen or air. The analyte 'permeates' (diffuses) through the walls of the tube into the diluting stream. The vapours of all VOCs for this thesis were generated from calibrated permeation tubes. The tubes were made of PTFE (Teflon) and were sealed with PTFE caps and stainless steel crimps (Figure 2.1).

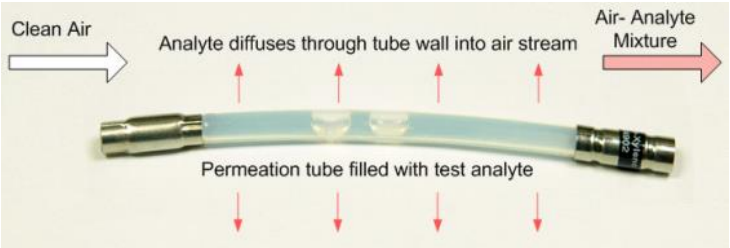

Figure 2.1. Permeation tube principle of operation (Credit: Owlstone Ltd)

Permeation is a temperature-sensitive process.[188] Therefore, to generate a consistent and reliable permeation rate, the tubes must be used with precise temperature control. For this work, permeation tubes were used with Owlstone V-OVG and OVG-4 Calibration Gas ovens.[189,190] Both V-OVG and OVG-4 ovens have temperature and flow rate control. The flow control systems comprise of a two vapour outlets (sample and exhaust flows). This split allows the control of sample concentration. For example, a high exhaust flow to sample flow ratio lowers the output concentration. Vapour permeation rates are constant at constant temperature, hence by maintaining the tubes at constant temperature and periodically weighing the tube over several days or weeks the permeation rates were calculated. Permeation rates are typically in the nanogram per minute range, and produce VOC vapours in the ppb and ppm (parts-per-million) concentration range at flow rates of 0-500 mL/min. Both the diluting gas and carrier gas were clean (i.e. no VOCs) compressed air. All permeation tubes used were calibrated gravimetrically at a given temperature until a stable permeation rate was achieved.

2.2 Adsorbent Library Preparation

2.2.1 Overview

A library of adsorbent materials were prepared for use in the Adsorption Device described below. In keeping with the design specifications of the device, the used adsorbents had to be:

- Large enough to ensure a relatively large volume could be sampled in a given analysis period.
- Modifiable through relatively simple chemistry.
- Stable enough to adsorb and desorb over a long time period.
- Regenerated at modest temperatures – up to approximately 120 °C.

These specifications led to the selection of silica as the base adsorbent material for this project. Silica is commercially available in a wide range of sizes, surface areas and prices. Consequently, it was possible to readily purchase a material that had a high surface area, low cost and dimensions large enough to ensure unrestricted vapour flow through the Adsorption Device. The preparation of complex adsorbents, such as cavitands,[143,150] were not considered as part of this work due to the intricate multi-step syntheses required.

2.2.2 Silanisation

One of the most simple and effective methods of modifying the surface of silica is via silanisation. This consists of reactions that cover a surface in a network of disiloxane (Si-O-Si) bonds. Organosilanes (Figure 2.2) contain at least one functional group, thus allowing a straightforward method of changing surface functionality, and in turn adsorption processes on them. The first step of silanisation is the hydrolysis of the alkoxysilane groups to form highly reactive silanol groups (Figure 2.3). When brought into contact with an activated surface, such as silica, silanol groups form hydrogen bonds with the surface, as well as other silanol groups to produce a network of associated organosilane derivatives. This is then followed by a condensation reaction to form a polymerized coating of the organosilanes covalently bonded to the substrate surface.

Materials

Materials sourced from Sigma Aldrich: silica (high-purity grade, pore size 60 Å, 35-60 mesh {250-500 μm} particle size), (3-Aminopropyl)triethoxysilane (APTES), 3-Chloropropyl)triethoxysilane (CLTES), triethoxyphenylsilane (PhTES), 1-chloro-4-triethoxysilylbenzene (PCTES), 1H,1H,2H,2H-Perfluorooctyltriethoxysilane (POTES), n-Octyltriethoxysilane (C8TES), toluene (high performance liquid chromatography grade), molecular sieves (3 Å, 4-8 mesh), acetic acid.

Silanisation Reaction Protocols

There are four standard silanisation reaction methods.[191] Reactions can be carried out in aqueous solution, solely organic solvent, in organic solution with a small proportion of water, or in the vapour phase.[191] Only the first three of these methods were considered for this work, as vapour phase disposition was deemed incompatible with small and unbound silica particles.

Organic Solvent Silanisation

Silica particles were activated by stirring in piranha solution[i] for 15 minutes, then oven dried. The organosilane was dissolved in in dry toluene to produce a 5% (v/v) silane solution. Dry silica was then added to the silane solution with mixing. Reactants were heated to reflux and left to react with gentle stirring overnight (~12–16 hours). The reaction was cooled to room temperature, then the silica particles

[i] a mixture of sulfuric acid (H_2SO_4) and hydrogen peroxide (H_2O_2)

were washed three times with dry toluene to remove excess silane reagent and reaction by-products. The modified silica particles were then cured by incubation at 110 °C overnight.

Aqueous-Organic Solvent Silanisation

Silica particles were activated by stirring in piranha solution for 15 minutes, then oven dried. A solution of 5 % water in ethanol (v/v) was prepared and the pH adjusted to 4.5–5.5 with acetic acid. The silane coupling agent was dissolved in the acidic water/ethanol solution with stirring to a final concentration of 5% (v/v). The reaction was left for 5 minutes at room temperature to allow hydrolysis to occur to form reactive silanols groups. Dry silica was added to the silane solution with mixing and the reactants were left to react with gentle stirring overnight (~12–16 hours). Silica particles washed three times with ethanol to remove excess silane reagent and reaction by-products. The modified silica particles were then cured by incubation at 110 °C overnight.

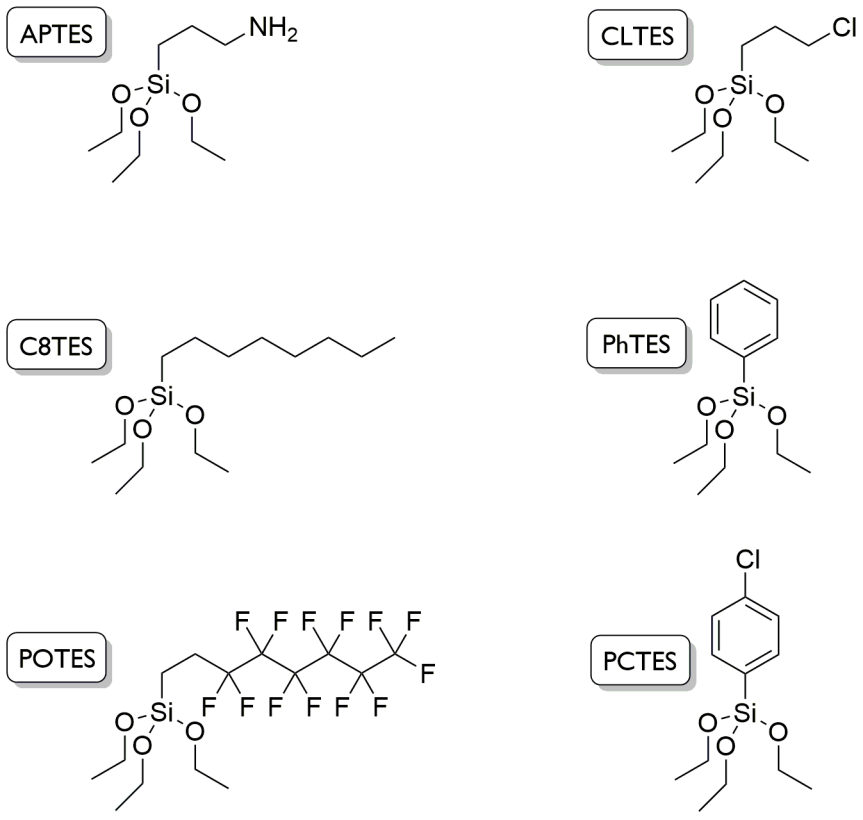

Figure 2.2. Organosilane Structures. 3-Aminopropyl)triethoxysilane (APTES), (3-Chloropropyl)triethoxysilane (CLTES), triethoxyphenylsilane (PhTES), 1-chloro-4-triethoxysilylbenzene (PCTES), 1H,1H,2H,2H-Perfluorooctyltriethoxysilane (POTES), n-Octyltriethoxysilane (C8TES).

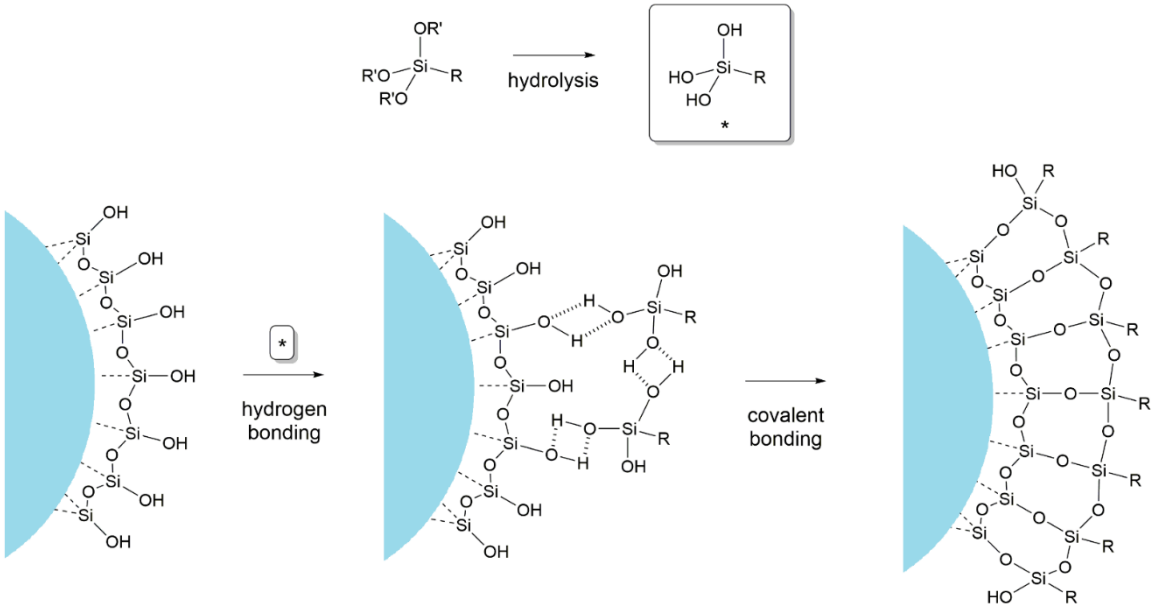

Figure 2.3. General Silanisation Scheme. Organosilanes are first hydrolysed to form reactive silanol groups (*). Silanol groups from the organosilane derivative and the silica surface form a hydrogen bonded network, before condensation reactions lead to a covalently bonded polymerized coating.

Aqueous Silanisation

Silica particles were activated by stirring in piranha solution for 15 minutes, then oven dried. An aqueous silane solution was prepared by dissolving the silane in water at a concentration of 2 % (v/v). If the silane was poorly soluble in water, Triton X-100 (a non-ionic detergent) was added at 0.1% (v/v) to promote solubility. The pH was adjusted to 5.5 with acetic acid. Dry silica was added to the silane solution with mixing and the reactants were left to react with gentle stirring overnight (~ 12–16 hours). Dried and activated silica were added to the silane solution, and stirred for up to 16 hours. Silica particles washed (three times) with water to remove excess silane reagent and reaction by-products. The modified silica particles were then cured by incubation at 110°C overnight.

List of Adsorbents

In total, six modified adsorbents were synthesised. In this thesis, the names given to these adsorbents are shown in Table 2.2 below.

Table 2.2. Names assigned to silica adsorbents

Name	Silane Modification
Unmodified	None
Amino	APTES
Chloro	CLTES
Alkyl	C8TES
Fluoroalkyl	POTES
Phenyl	PhTES
Chlorophenyl	CBTES

2.2.3 Characterisation

Modified adsorbents were characterised visually using optical microscopy; by surface chemistry using contact angle measurements and infrared (IR) spectroscopy; by porosity using nitrogen gas isotherms; and by heat stability using thermal gravimetric analysis (TGA).

Optical Microscopy

Bright field optical microscope images were taken with a Nikon Optiphot-2 microscope. Silica particles were spread on glass microscope slides to form a disperse layer. The microscope slides were supplied by VWR.

Contact Angle

A packed bed of particles was created using a small square (approximately 6 mm x 6 mm) of double-sided tape on a glass microscope slide. The taped area was then completely covered in a monolayer of particles. Contact angles were measured using a Dataphysics Contact Angle System OCA. 5 µl of distilled water was dropped vertically from a pipette on to the particle bed and the instantaneous contact angle was measured.

Infrared Spectra

Fourier-transform infrared (FTIR) spectra were recorded with a Perkin Elmer Spectrum One IR spectrometer. Silica particles were manually crushed with a spatula to form a powder before recording the spectra.

Thermogravimetric Analysis

Thermogravimetric analysis results were obtained with a Perkin Elmer Pyris 1 Thermogravimetric Analyzer. Samples were heated from 30 °C to 800 °C in nitrogen. The heating rate, unless otherwise stated, was 30 °C/min.

Nitrogen Isotherms

N_2 gas adsorption/desorption studies were carried out using a Micromeritics 3Flex Surface Characterisation Analyzer at 77 K. Samples were degassed overnight before the collection of isotherm data. Surface area was calculated by the BET method based on the linear part of BET plot (P/P_0 = 0.06–0.21). In addition, adsorption data were fitted to the Freundlich and Langmuir adsorption isotherm models. Pore volume and pore size was estimated using the Barrett, Joyner and Halenda (BJH) model.[192]

2.3 Adsorption Device

2.3.1 Overview

The principle function of the Adsorption Device was to separate multi-component VOC mixtures via temperature-controlled desorption from silica based adsorbents. The device consisted of three key components: a separation 'chip', which acted as closed adsorbent flow chamber; a peltier based temperature control unit, and a downstream photoionisation detector (PID), from which adsorption or desorption in the separation chip was inferred (Figure 2.4). The device was designed such that there was a continual, and constant flow rate of air at the detector. All components were connected using PTFE tubing (outer diameter 3.2 mm, internal diameter 1.5 mm). During the design of the device, the research aim of creating a small and inexpensive device directed the choice of materials and dimensions. Aluminium was chosen as chip metal as it would allow fast heat transfer from the peltier module. Similarly, the size of the chip was chosen to match the size of the most commonly available peltier modules (20 mm x 20 mm). The tubing material was PTFE to minimise adsorption along the flow path.

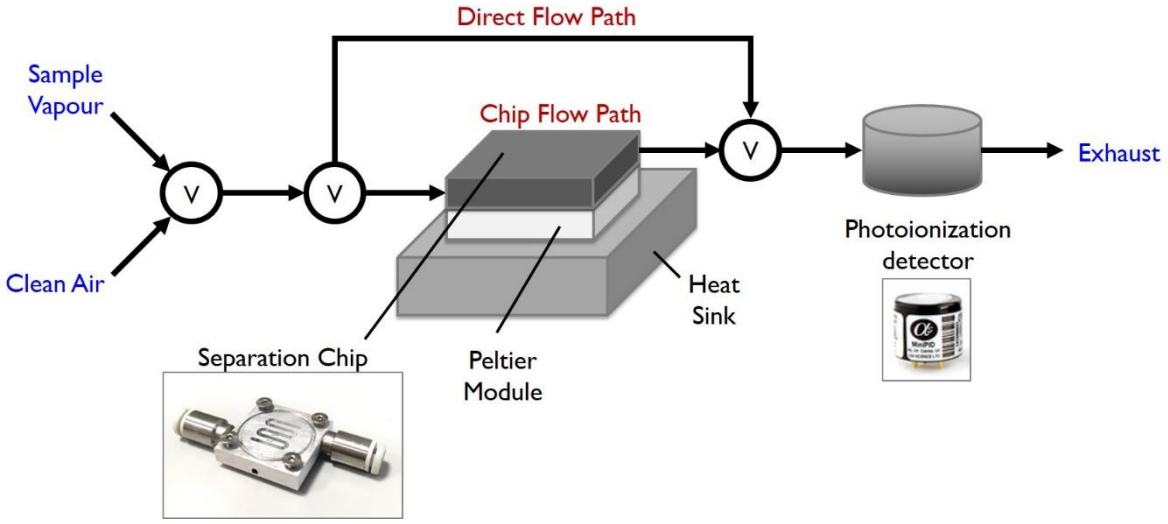

Figure 2.4. Diagram of experimental set up. The circles labelled 'V' represent 3-way solenoid valves (SMC VDW250-6G-1-M5, RS Components), controlled via a pre-programmed Arduino Uno microcontroller. Both the 'Clean Air' and 'Sample Vapour' streams come from an Owlstone calibration gas oven. *Inset left* – adsorbent chip, shown without enclosing cap. *Inset right*– Alphasense PID-AH photoionisation detector.

2.3.2 Chip

The adsorbent chip was made from a machined aluminium plate (20 mm x 20 mm, height 4 mm) with a serpentine channel produced with a CNC (computer numerical control) mill (Figure 2.5). The channel dimensions were 30 mm (length) x 1 mm (width) x 2 mm (height). The chip was connected to the other device components via 1/8″ inch M3 push-fit connectors (KQ2S23-M3G, SMC Pneumatics). A closed channel was created by placing another piece of 20 mm x 20 mm (height 1.5 mm) aluminium on top of the base plate, secured via 4 M3 screws. To ensure a gas-tight seal, a <1 mm circular groove was milled into the base plate, where a nitrile O-ring (Nitrile 70 ShA, Polymax) was placed prior to fixing the lid.

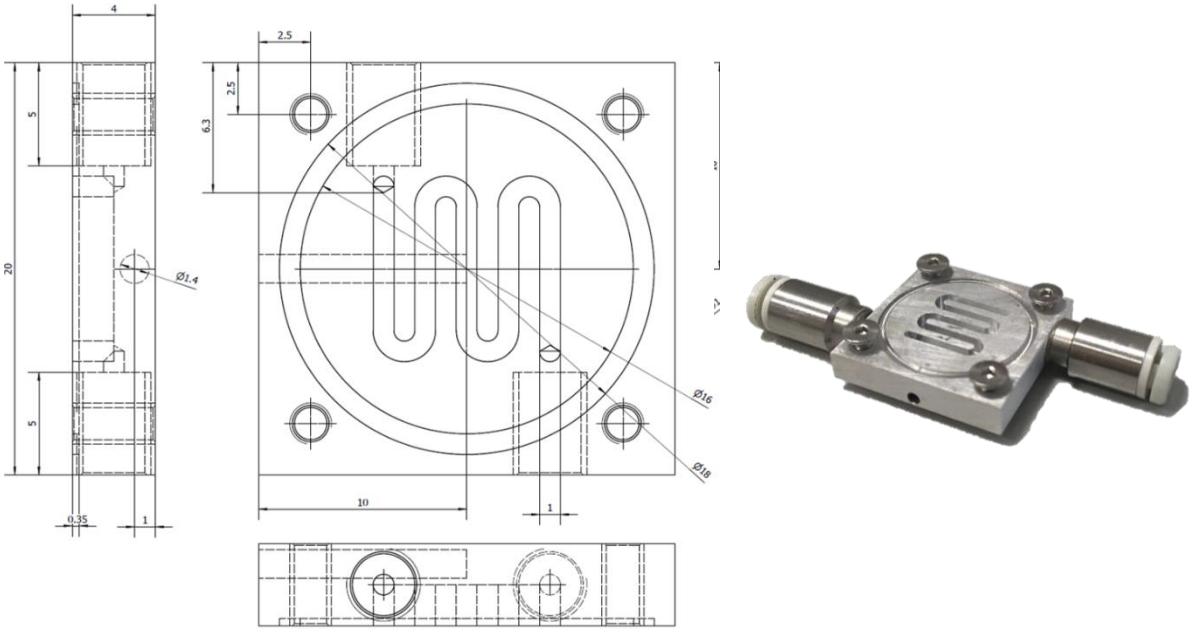

Figure 2.5. Adsorbent Chip. *Left*: Design and size specifications of the chip base plate. *Right*: the milled base plate, shown with push-fit connectors, and without cap.

2.3.3 Detector

A photoionisation detector (PID) was chosen for the detection component owing to its superior limit of detection (LoD) over other VOC gas sensors. The Alphasense PID-AH model PID has a quoted LoD for benzene of >500 ppb, and 1 ppb for isobutylene.[105,193] The sensor was mounted on an Alphasense test board (ISB Iss 2), and connected to the other parts of the device – the separation chip upstream and exhaust downstream – via a machined PTFE hood (Figure 2.6). To ensure a close seal, the hood and PID control board were secured with a clamp.

Figure 2.6. Detection Component. Different angles of the PTFE housing built for the PID (photoionisation detector, bottom right). The housing consisted of an input and output flow paths. The PID was mounted on a control board, which was then held in place with a clamp.

The PID detection limits benzene, toluene, ethyl benzene and para-xylene were calculated by varying the concentration of vapour from the permeation oven and recording the (stable) PID response. The data points were collected non-progressively, i.e. not by simply increasing the concentration, and with exposure to zero air between concentration changes (Figure 2.7). The limits of detection (LoD) and quantification (LoQ), which were calculated from Eqn. 2.1 and Eqn. 2.2, are shown in Table 2.3.

$$LoD = \frac{3.3\sigma_r}{S_l} \qquad \text{Eqn. 2.1}$$

$$LoQ = \frac{10\sigma}{S_l} \qquad \text{Eqn. 2.2}$$

Where σ_r is the deviation of the blank (i.e. 0 ppb) response and S_l is the slope of the linear region of the calibration curve (shown by the straight line).[194]

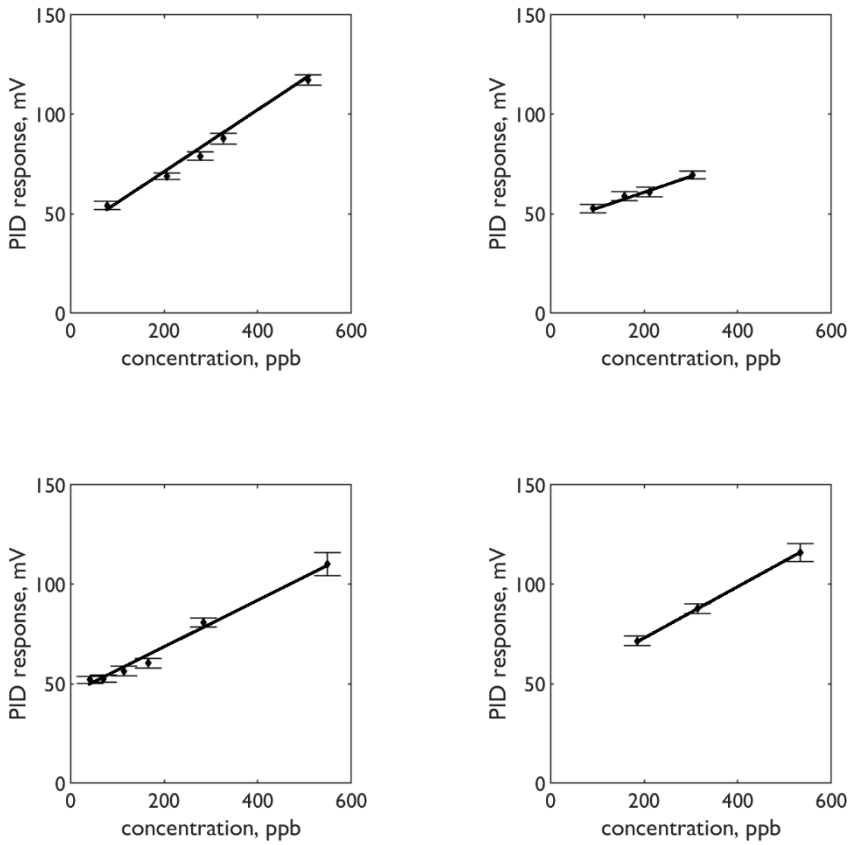

Figure 2.7. Calibration plots of benzene (top left), toluene (top right), ethyl benzene (bottom left) and *para*-xylene (bottom right). Average PID response (diamonds) was taken as mean over 3 minute period. Error bars represent standard deviation (over the 3 minute period). Note: maximum concentration generated from ethyl benzene was ~1050 ppb.

Table 2.3. Limits of detection (LoD) and quantification (LoQ)

VOC	LoD, ppb	LoQ, ppb
Benzene	47	141
Toluene	118	358
Ethyl Benzene	106	321
para-Xylene	118	357

2.3.4 Heating Unit

Peltier modules are a type of heat pump that transfers heat from one side to the other in the presence of an applied voltage. The direction of heat transfer is dependent on the direction of electrical current, thus allowing peltier modules to operate as heaters and coolers. Similarly, the magnitude of heat directly related to the magnitude of the current. The fan-assisted heat sink (5V, RS Components) provided additional cooling capability, permitting faster cooling as heat is removed from the adsorbent chip. The chip was mounted firstly on a peltier module (8.8 V, 6 A, 20 mm width, 20 mm length, RS components) and secondly on a fan-assisted aluminium heat sink (5 V, RS Components), as shown in Figure 2.8. A thin coating of thermal paste (metal oxide, RS components) was placed on either side of the peltier module. Thermal adhesive tape or a metal clamp was used ensure a good contact between the chip, peltier and heat sink. Power was provided via a variable direct current (DC) power supply.

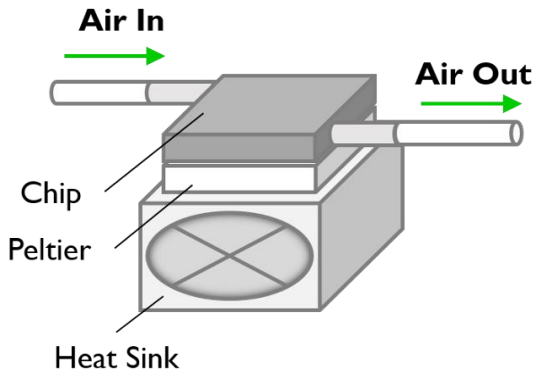

Figure 2.8. Diagram of Adsorption Device Heating Module.

2.3.5 System Control

The temperature of the chip was measured via a thermistor (10 kohm NTC, Farnell) placed in hole drilled into the side of the chip. This thermistor formed the input of an Arduino Uno based proportional–integral–derivative (p-i-d) controller. The controller continually measured the temperature (the process variable) and calculated the difference to a pre-programmed set point. Depending on the magnitude of the temperature difference, the controller would then apply an electrical current 'correction' to the peltier module. This allowed accurate control of chip temperature with minimal delay and under-/over-shoot. The Arduino was also used as a controller for the 3-way solenoid valves (SMC VDW250-6G-1-M5, RS Components) that directed vapour and zero air through the device (Figure 2.9).

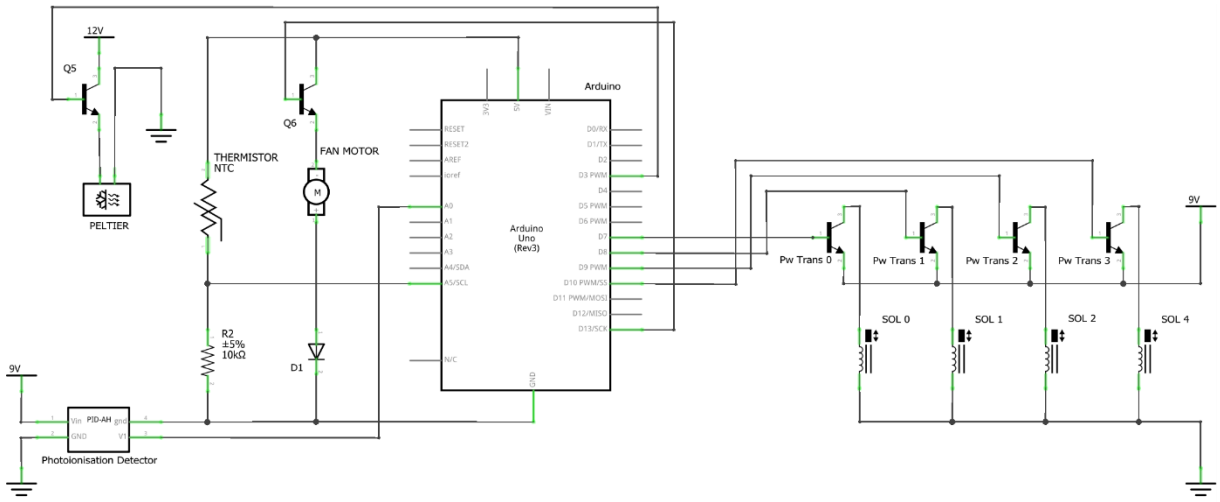

Figure 2.9. Circuit Diagram of the Electrical Components of the Adsorption Device. Peltier: 8.8 V, 6 A module (RS components); Photoionisation Detector: PID-AH (Alphasense UK); Thermistor: 10 kohm NTC (Farnell); Q2: BC547B NPN Transistor (RS Components); Fan Motor: 5V aluminium (RS Components); D1: 1N4001 Diode; Pw Trans 0-3: IRL520NPBF N-Channel MOSFET (RS Components); SOL 0-3: SMC VDW250-6G-1-M5, (RS Components). Not shown is the USB connection between the Arduino Uno and computer used for data logging.

All control scripts were written in C++ and uploaded to the Arduino from a PC via USB (Universal Serial Bus) prior to device operation. All scripts were written by the author and examples are shown in Appendix 1.

2.3.6 Data Recording and Logging

The voltage output of the PID was measured via the Arduino Uno, and data transmitted to a PC (personal computer) via a USB serial connection and stored as a .txt file using CoolTerm, a serial port terminal programme. The final data was then cleaned and stored as an .xlsx file before further data analysis.

Comparison of Arduino and PicoScope

To ensure that the ADC (analog-to-digital converter) reading was sensitive enough to measure the target VOCs in the ppb range, a linear run calibration using the Arduino and a PicoScope PC Oscilloscope (model 4224) was performed (Figure 2.10).

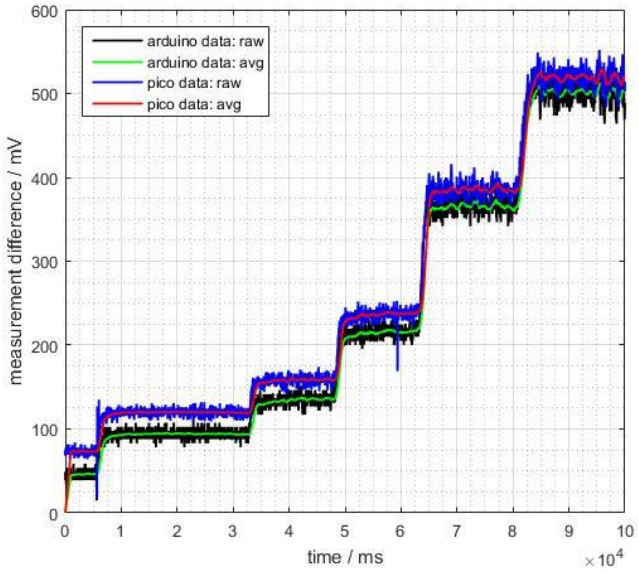

Figure 2.10. Comparison of Arduino Uno and PicoScope 4224 Oscilloscope measurements of an Alphasense PID-AH detector. The concentration of benzene was increased from 0 to ~3 ppm.

Despite the higher resolution offered by the PicoScope (12-bit, 4096 vertical levels) over the Arduino (8-bit, 256 vertical levels), the additional detail was not sufficient enough to justify using a separate oscilloscope. As shown in Figure 2.10, there was a small difference in measured voltage between the Arduino and the PicoScope, but this difference is consistent over a wide range of vapour concentrations. The noise level is also consistent for both measurements methods. Given the size, cost and convenience benefits, the Arduino was selected as the measurement component for the development of the lab-based Adsorption Device.

2.4 Device Operation

2.4.1 Principle of Operation

The standard test cycle consisted of five phases (Table 2.4). Each phase has different combinations of vapour input (sample or clean air) and flow path (direct sensor or via separation chip), as shown in Figure 2.11.

Table 2.4. Description of test cycle phases

#	Phase	Vapour source	Flow path
1	Conditioning	Clean air	Chip
2	Sample Reference	Sample	Direct
3	Baseline Reference	Clean air	Direct
4	Sampling	Sample	Chip
5	Analysis	Clean air	Chip

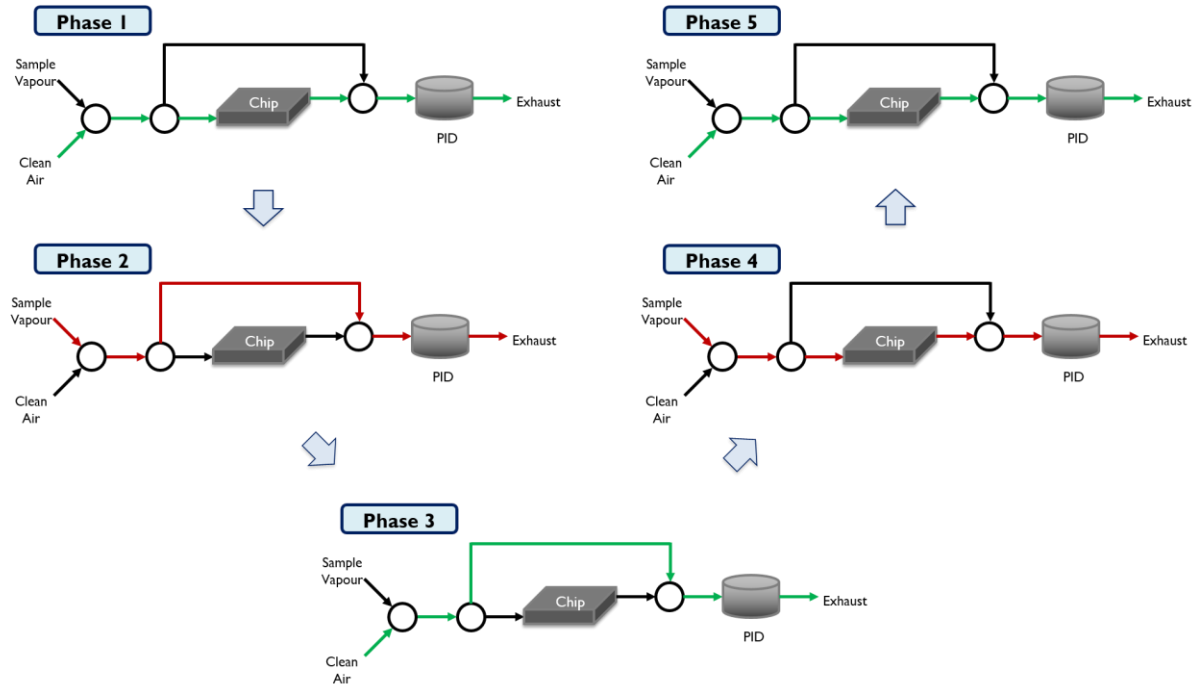

Figure 2.11. Flow Path Directions for Each Test Cycle Phase. The flow path is highlighted in green for phases with clean air input and red for phases with sample vapour (i.e. VOC) input.

Photoionisation detector (PID) response was continuously measured throughout the entire test cycle. During the conditioning phase, the chip was heated to > 80 °C under the flow of clean air in order to remove any pre-adsorbed species. The sample reference and baseline reference phases allow the respective expected PID responses for given input concentrations and background. The sampling phase exposes the adsorbent chip to the sample vapour for a given time. The analysis phase typically involved a both non-thermal and thermal desorption of adsorbates. Three heating profiles were used for thermal desorption: binary (single step); stepwise (multiple step); exponential increase; and pulsed (on-off). The phase durations, temperature set points and heating profile are specified in the relevant sections below. Note that before the use of new material, the adsorbent chip was treated to a long condition, where the chip was heated to 105 °C for at least 15 minutes under high flow.

Data Cleaning and Analysis

The PID voltage and chip temperature data measured by the Arduino Uno was transmitted to a PC via Serial (USB), and stored as a .txt file. The voltage data was then converted from ADC counts to millivolts (mV) and cleaned with a moving average filter (window size 10) and saved as an .xls file containing only temperature and voltage data. Data for each experiment were then compiled into the same .xls file. Interpretation and statistical analyses were conducted using the Statistical and Machine Learning Toolbox for MATLAB (R2018b; MathWorks, Natwick, MA). Data files were loaded into the programme, and then visualised and analysed with custom scripts. Depending on the specific information required, the specific data analyses varied between experiments and relevant details are highlighted where appropriate.

2.4.2 VOC Isotherms

Data Collection

The test cycle used to collect VOC isotherm data is shown in Table 2.5.

Table 2.5. Test cycle conditions for VOC isotherm analysis

Phase	Duration, mins	Chip temperature set point (°C)
Conditioning	5	80
Sample Reference	5	25*
Baseline Reference	5	25*
Sampling	15	25
Desorption	8	80

* chip cooling during this phase

PID data was collected for benzene, toluene, ethylbenzene and xylene on all adsorbents (Table 2.2). The generated concentration range of the vapours was dependent on the permeation rate of the permeation tubes for each VOC, but concentrations were in the range of 0 – 3,000 ppb and are specified in the results. Sufficient data points were collected to establish the adsorption behaviour of each adsorbent-vapour combination. The input concentration was changed non-sequentially between each test cycle.

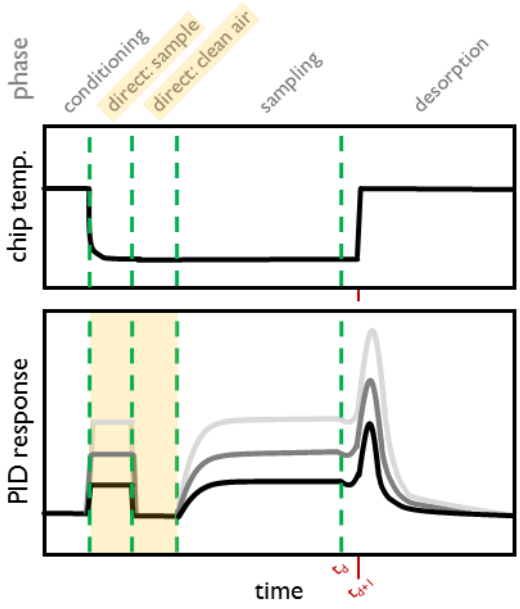

Figure 2.12. VOC Isotherm Test Cycle. The response of the photoionisation detector (PID) was recorded as VOC sampling concentrations was varied. The response to direct flow, highlighted in yellow, involved measuring the PID response to the sample air (with VOCs) and clean air (no VOCs). The 'direct' phases was the only period that vapour was not directed from the adsorbent chip.

Data Interpretation

A basic adsorption process can be represented as:

$$G + S \rightleftharpoons GS \qquad \text{Eqn. 2.3}$$

Where G is the gas-phase species, S is the adsorption sites on the solid adsorbent surface, and GS is surface adsorbed species, or adsorbate. The concentration of adsorbate, $[GS]$, can be estimated through analysis of the concentration detected by the PID location downstream of the adsorbent chip (Figure 2.4). As the system is closed, it was assumed that any VOCs not detected by the PID were adsorbed by the adsorbent material. With prior knowledge of the expected signal of the PID, obtained during the Sample Reference phase (Table 2.5), the mass of VOC adsorbed at a particular time can be calculated. For example, if the PID signal is 25% of the Sample Reference reading (correcting for background, calculated during the Baseline Reference phase), then it can be assumed that 75% of the input sample vapour has been adsorbed. Combining knowledge of the vapour input concentration, sampling time and the fraction of adsorption during the sampling phase, the total adsorbate concentration was calculated (see below). Using this method, adsorbate data were fitted to linear equations of the Freundlich and Langmuir adsorption models.

2.4.3 Adsorption Thermodynamics

Data Collection

The test cycle used to collect VOC isotherm data is shown in Table 2.6.

Table 2.6. Test cycle conditions for thermodynamic analysis

Phase	Duration, mins	Chip temperature set point (°C)
Conditioning	5	80
Sample Reference	5	25*
Baseline Reference	5	25*
Sampling	45	25-52
Desorption: Spontaneous	15	25-52
Desorption: Thermal	5	80

* chip cooling during this phase

PID data was collected for benzene, toluene, ethylbenzene and xylene on all adsorbents (Table 2.2), at sampling temperatures between 25 °C to 55 °C.

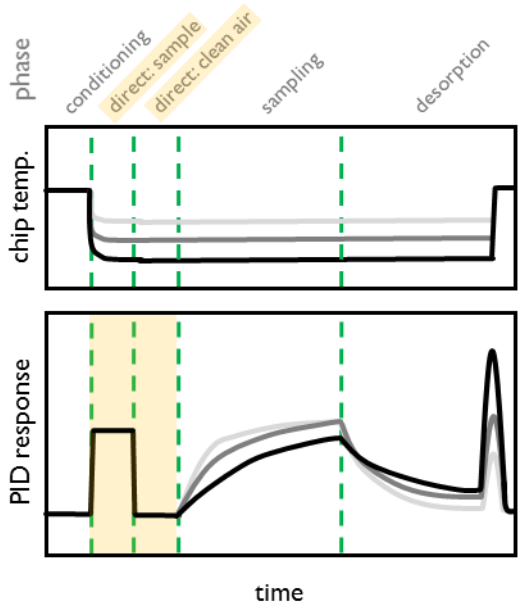

Figure 2.13. VOC Thermodynamic Analysis Test Cycle. Photoionisation detector (PID) response was recorded for the constant sampling concentration, as chip sampling temperature was varied. PID response to direct flow is highlighted in yellow.

Data Interpretation

Adsorbate Estimation

The mass adsorbed, m_{ad} (i.e. the adsorbate), during the sampling phases of device operation was estimated by multiplying the mass 'injected' during sampling, m_{inj}, by the proportion of VOC adsorbed, p_{ad}:

$$m_{ad} = m_{inj}.p_{ad} \quad \text{Eqn. 2.4}$$

The proportion of VOC adsorbed was calculated through interpretation of PID output during sampling:

$$p_{ad} = \frac{A_0 - A_{obs}}{A_0} \quad \text{Eqn. 2.5}$$

Where A_0 is the theoretical area under the PID output for a process with no adsorption, and A_{obs} is actual area observed:

$$A_0 = t_{sam}.r_{eq} \quad \text{Eqn. 2.6}$$

$$A_{obs} = \int_{t_1}^{t_2} r \quad \text{Eqn. 2.7}$$

Where t_{sam} is the sampling time, r is the baseline adjusted sensor response, r_{eq} is the sensor response at equilibrium, t_1 and t_2 are the start and end time of the sampling region (such that: $t_{sam} = t_2 - t_1$). In this work, the numerical integration of Eqn. 2.7 was calculated using the trapezoidal method.[ii] Finally, the mass sampled, or 'injected', into the device was calculated using:

$$m_{inj} = t_{sam}.R_f.c_{VOC} \quad \text{Eqn. 2.8}$$

Where R_f is the flow rate of sample stream and c_{VOC} is the VOC concentration.

Mass Desorbed Estimation

The desorption phase was divided between distinct thermal desorption and non-thermal desorption phases. The latter, labelled here as the *spontaneous desorption* phase, involved maintaining the chip temperature from the sampling temperature. The thermal desorption phase involved a binary step

[ii] approximates the integration over an interval by breaking the area down into trapezoids with more easily computable areas

increase in chip temperature from the sampling temperature to 80 °C. The mass desorbed during each desorption sub-phase was calculated via:

$$m_{SD} = m_{ad}\frac{A_{SD}}{A_{SD} + A_{TD}} \quad \text{Eqn. 2.9}$$

$$m_{TD} = m_{ad}\frac{A_{TD}}{A_{SD} + A_{TD}} \quad \text{Eqn. 2.10}$$

Where m_{SD} is the mass spontaneously desorbed, m_{TD} is the mass thermally desorbed, A_{SD} is the baseline adjusted area of the sensor response during spontaneous desorption and A_{TD} is the baseline adjusted area of the sensor response during thermal desorption.

Equilibrium Constant

Following from Eqn. 2.3, the rates of the forward reaction (adsorption) and the backward reaction (desorption) can be described as:

$$k_a[G][S] \quad \text{Eqn. 2.11}$$

$$k_d[GS] \quad \text{Eqn. 2.12}$$

Where the square brackets represent the concentration of each component. Given the difficulty in describing the concentration of adsorption sites, $[S]$, Eqn. 2.11 can be rewritten as:

$$k_a[A](1 - \theta_m) \quad \text{Eqn. 2.13}$$

Where θ_m represents the fraction of filled *monolayer* adsorption sites. Therefore, the equilibrium constant, K_{eq}, can be expressed as:

$$K_{eq} = \frac{k_a}{k_d} = \frac{[GS]}{[G](1 - \theta_m)} \quad \text{Eqn. 2.14}$$

The fraction of filled monolayer adsorption sites can be estimated with prior knowledge of the adsorbent surface area (such as the BET surface area obtained via N_2 isotherm analysis) and the molecular cross sectional area, σ, of the sample VOC vapour. The molecular cross sectional areas and dimensions of the BTEX compounds are shown in Table 2.7.

Table 2.7. Molecular dimension of N_2 and BTEX gases

Gas	σ,[195] nm^2	width,[196] nm	thickness,[196] nm	length,[196] nm
N_2	0.162	-	-	-
Benzene	0.305	6.628	3.277	7.337
Toluene	0.344	6.625	4.012	8.252
Ethylbenzene	0.368	6.625	5.285	9.361
para-Xylene	0.380	6.618	3.810	9.146

σ = molecular cross sectional area

Van't Hoff Equation

The van't Hoff equation relates the change in the equilibrium constant, K_{eq}, of a chemical reaction to the change in temperature given the standard enthalpy change, $\Delta H^{\emptyset}$, for that reaction.[197] Under standard conditions, the equation is:

$$\frac{d}{dT} ln(K_{eq}) = \frac{\Delta H^{\emptyset}}{RT^2} \quad \text{Eqn. 2.15}$$

Where ln is the natural logarithm and R is the ideal gas constant. The Gibbs free energy is defined as:

$$\Delta G^{\emptyset} = \Delta H^{\emptyset} - T\Delta S^{\emptyset} \quad \text{Eqn. 2.16}$$

Where $\Delta S^{\emptyset}$ is the standard entropy of the system. The Gibbs free energy isotherm equation is:

$$\Delta G^{\emptyset} = -RTln(K_{eq}) \quad \text{Eqn. 2.17}$$

Combining Eqn. 2.16 with Eqn. 2.17 produces the following linear form of the van't Hoff equation:

$$ln(K_{eq}) = \frac{\Delta S^{\emptyset}}{R} - \frac{\Delta H^{\emptyset}}{RT} \quad \text{Eqn. 2.18}$$

Therefore, a plot of $ln(K_{eq})$ versus $1/T$ can provide a means of estimating enthalpy and entropy change of a reaction or process, i.e. adsorption. The slope of the plot gives $-\Delta H/R$ and the y-axis intercept gives $\Delta S/T$.

2.4.4 Thermal Desorption Profiles

As mentioned above, a range of heating profiles were used to initiate the thermal desorption of adsorbed VOCs. Three heating profiles were developed:

1. **Pulsed** – an on/off profile, where heat was applied in 1 minutes 'pulses'
2. **Gradual** – set point exponentially increased from sampling temperature
3. **Stepwise** – the set point increased in gradual steps

Each profile was applied during the thermal desorption phase of an otherwise identical test cycle, as shown in Table 2.8.

Table 2.8. Test cycle conditions for controlled desorption experiments

Phase	Duration, mins	Chip temperature set point (°C)
Conditioning	5	80
Sample Reference	5	25*
Baseline Reference	5	25*
Sampling	15	25
Desorption: Spontaneous	1	25
Desorption: Thermal	5	25-105

* chip cooling during this phase

Data Collection

PID data was collected for benzene, toluene, ethylbenzene and xylene on all adsorbents (Table 2.2), for the gradual, pulsed and stepwise heating profiles. Examples of the temperature and PID response for each cycle are shown in Figure 2.14.

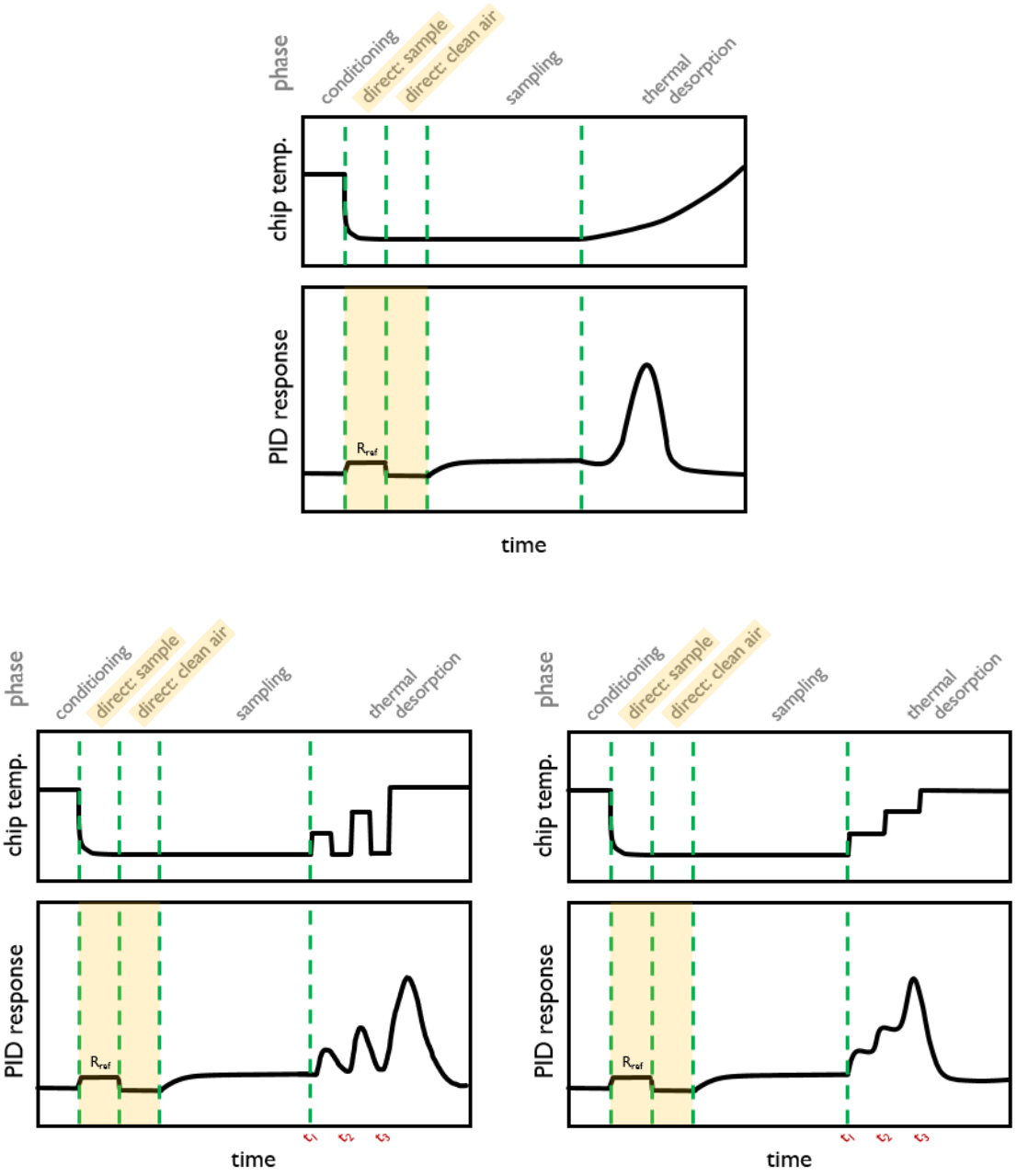

Figure 2.14. Typical Test Cycles for the Gradual (top), Pulsed (bottom left) and Stepwise (bottom right) and Heating Profiles. The response of the photoionisation detector (PID) was recorded in relation to chip temperature and vapour flow path. The response to direct flow, highlighted in yellow, involved measuring the PID response to the sample air (with VOCs) and clean air (no VOCs). The 'direct' phases was the only period that vapour was not directed from the adsorbent chip.

2.5 Data Processing

Analysis of sensor data involved some or all of the following stages, as visualised in Figure 2.15:

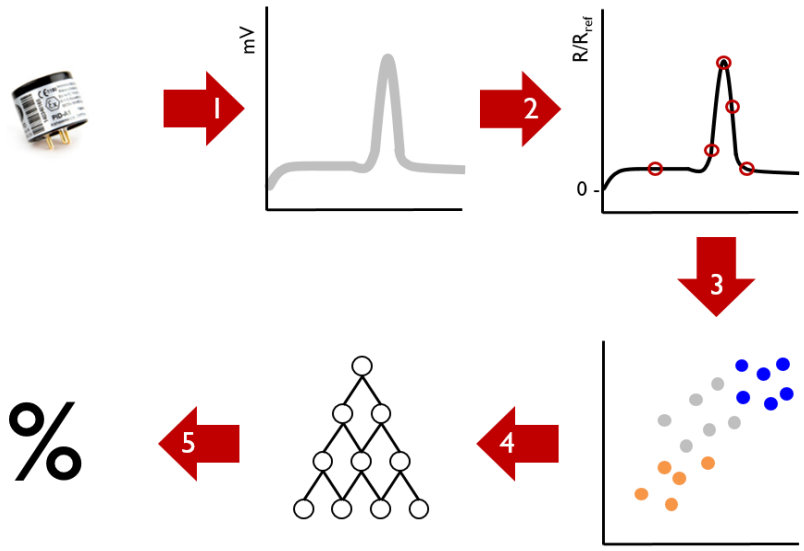

Figure 2.15. Data Processing Block Diagram. 1) data collection, 2) data normalisation, 3) feature extraction, 4) analysis and prediction, 5) classification accuracy.

2.5.1 Data Pre-Processing

Step 1 represents the collection of PID data from the Adsorption Device. The pre-processing step (2) includes:

- **Cleaning** of detector response using a moving average filter (window size = 10),
- **Normalisation** of the average signal of the plateau region of the sample reference phase (R_{ref}).
- **Feature extraction** of important characteristics.

The range of possible features for the gradual, pulsed and stepwise heating profiles are specified in the relevant results chapters.

2.5.2 Principle Component Analysis

Data features were extracted for all vapours and mixtures and evaluated with Principle Component Analysis (PCA). This method was chosen as it allows data with many variables (in this case data features) to be visualised. Data sets with many variables often have groups of variables that change simultaneously. This can be due to there may be more than one variable measuring the same underlying principle in the behaviour of a system. PCA is a quantitative method that can take advantage of the redundancy of information.[198] Groups of variables can be replaced with a single new variable, called a principle component, which are linear combinations of the original variables. All of the principle components are orthogonal to each other, meaning there is no redundant information. Each principle component is a single axis in space. Each observation is projected on a given axis, and the values form a new variable with maximum variance among all possible choices for that axis. There are as many principle components as there are original variables (or in the case of this thesis, features), but it is standard practice to include enough components that account for > 80% of the total variance of the original data.

In this work, principle components were calculated using the Matlab Statistics and Machine Learning Toolbox. Principal component coefficients, scores and variances of the components were calculated for the feature data. Feature data was standardised (mean = 0, variance = 1), and then reduced to either two dimensions (2D) or three dimensions (3D). The explained variance of each principle component was also calculated and are presented with the corresponding principle components.

2.5.3 Problem Prediction and Validation

Problem prediction can be undertaken with regression techniques to quantify concentrations, classification techniques to discriminate between different groups, or clustering techniques to group similar responses.[199] Algorithms can be supervised or unsupervised. Supervised algorithms take a known set of input data and the known responses to the data (the training set), and then trains a model to make predictions based on the responses of new data (the testing set). Unsupervised algorithms are generally used to explore data with unknown contents, or as a dimension reduction method.

In this thesis, supervised algorithms were chosen as data was available for a specific output, i.e. VOC selectivity. There are a range of models that can be used in a given scenario, and selecting the 'right' algorithm is often a process of trial and error. In this thesis, the following classification tasks were applied and later assessed for accuracy.

k-Nearest Neighbour (kNN)

k-Nearest Neighbour (kNN) categorizes objects based on the classes of their (k) nearest neighbours in the dataset. Predictions assume that neighbours, i.e. objects in close proximity, are similar. It is a simple algorithm that is effective when memory usage and prediction speed are lesser concerns, as is the case during the development of the sensor device.

Support Vector Machine (SVM)

Support Vector Machine (SVM) classifies data by finding the linear decision boundary (hyperplane) that separates all data points of one class from those of the other class. The best hyperplane for an SVM is the one with the largest margin between the two classes, when the data is linearly separable. If the data is not linearly separable, a loss function is used to penalize points on the wrong side of the hyperplane. Like kNN, it is a simple classifier, but it tends to favour data with fewer classes.

Random Forest (RF)

A random forest (RF), or decision tree, predicts response to data by following decisions from the beginning to an end node. The decision path consists of branching conditions where the values of a predictor is compared to a trained weight. The number of branches and weightings are determined in the training process. It is a fast and easily interpretable model, but can have poor accuracy.

Linear Discriminant Analysis (LDA)

Linear Discriminant Analysis (LDA) classifies data by finding linear combinations of features. It assumes that different classes generate data based on Gaussian distributions. Training the model involves finding the parameters for a Gaussian distribution for each class. The distribution parameters are used to calculate boundaries, which then determine the class of test data.

Chapter 3 Adsorbent Library

3.1 Introduction

The first step in answering the main research question of this thesis – *to what extent can temperature controlled adsorption and desorption be used to achieve selective detection of mixtures of volatile organic compounds (VOCs) in the parts-per-billion range?* – was to develop a library of adsorbents that could exploit the different physiochemical properties of the target VOC analytes. The previous chapter presented the design and setup of the VOC Adsorption Device, which consisted of an adsorbent chamber where the adsorption and desorption of VOCs could be achieved with the modulation of temperature.

In this chapter, a library of silica based adsorbents is presented, along with data on their hydrophilicity, functionality and thermal stability. Different surface functionalities should have different interactions with different VOCs, hence providing a basis for diagnostic or selective sensing. Adsorbent characterisation was achieved through water droplet contact angle measurement, thermogravimetric analysis (TGA) and infrared (IR) spectroscopy. In addition, the adsorbent surface was characterised via analysis of the adsorption and desorption of nitrogen gas (N_2) at 77 K. Langmuir, Freundlich and BET (Brunauer, Emmett and Teller) isotherm models were then applied to the adsorption data and corresponding adsorption parameters were calculated.

3.2 Isotherm Models

3.2.1 Adsorption Isotherms

Many adsorption capacities are reported at relatively high VOC partial pressures. For example, the benzene sorption capacity of NENU-513, a MOF material, was reported as 1,687 mg/g, This capacity was obtained at a benzene partial pressure of 12,700 Pa (i.e. approximately 13% benzene in air).[178,200] It is important to know the adsorbent capacity at partial pressures that are typical for air quality monitoring. Adsorption isotherms show how much gas an adsorbent will adsorb for a given range of pressures at a constant temperature. They indicate the capacity of the adsorbent over a range of partial pressures, as well as providing information regarding surface area and porosity. According to the International Union of Pure and Applied Chemistry (IUAPC), isotherms, specifically physisorption isotherms, can be grouped into six different types, as shown in Figure 3.1.[159,160]

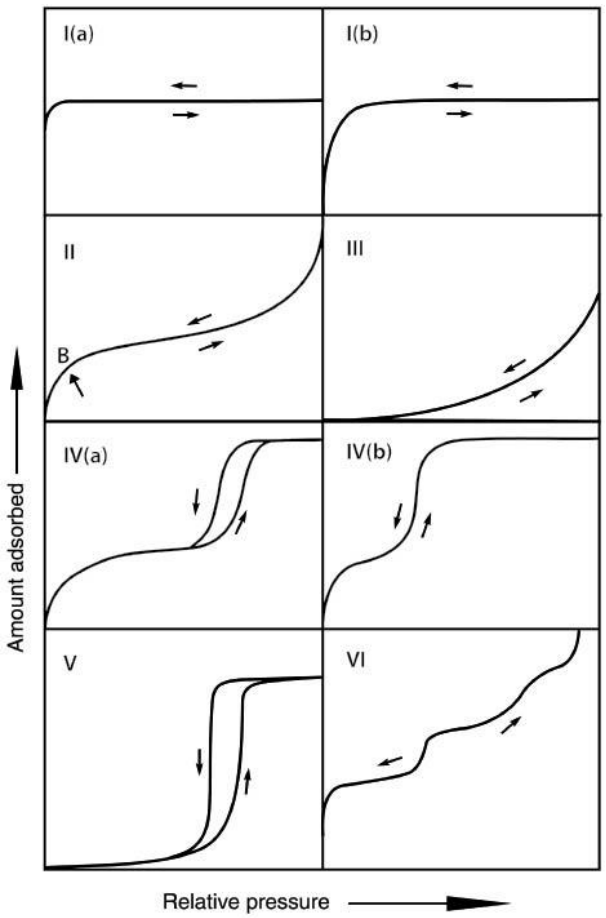

Figure 3.1. Physisorption Isotherms Classifications. B indicates the stage at which monolayer formation is complete and the onset of multilayer formation. Image from reference.[159]

Type I isotherms, also known as pseudo-Langmuir isotherms, are given by microporous materials. They are concave to the relative pressure (p/p_0) axis and depict the formation of a monolayer. Reversible Type II isotherms are obtained with a non-porous or macroporous adsorbent, and typically represent the formation of an initial monolayer then unrestricted multilayers. Reversible Type III isotherms indicate the immediate formation of unrestricted multilayers. Type IV and V isotherms are the result of multilayer adsorption and capillary condensation on mesoporous solids. The distinction between Type IV and V isotherms is analogous to the difference between Type II and III isotherms: Types II and IV reflect monolayer-multilayer adsorption whereas Types III and V reflect multilayer adsorption. Type IVa (and Type V) isotherms show hysteresis, which is when the adsorption and desorption processes do not coincide. This occurs when pore width exceeds a certain critical width, which is dependent on the adsorption system and temperature (e.g. for nitrogen adsorption in cylindrical pores at 77 K hysteresis starts to occur for pores wider than ~ 4 nm).[159] When adsorbents have mesopores with smaller widths, it is possible to get completely reversible (Type IVb) isotherms.[201] Finally, Type VI isotherms are caused by layer-by-layer adsorption on uniform nonporous surfaces, with the step-height indicative of each adsorbed layer.

3.2.2 Langmuir Model

A basic adsorption equilibrium can be represented as:

$$G + S \rightleftharpoons GS \quad \text{Eqn. 3.1}$$

Where G is the gas-phase species, S is the adsorption sites on the solid adsorbent surface, and GS is surface adsorbed species. The rates of adsorption and desorption can be described as:

$$k_a[G][S] \quad \text{Eqn. 3.2}$$

$$k_d[GS] \quad \text{Eqn. 3.3}$$

Where the square brackets represent the concentration of each component. As described in the previous chapter, $[S]$ can be represented as $(\theta - 1)$, and $[GS]$ as θ, such that:

$$k_a[G](1 - \theta) \quad \text{Eqn. 3.4}$$

$$k_d(\theta) \quad \text{Eqn. 3.5}$$

At equilibrium, the rate of adsorption and desorption will be equal, such that:

$$k_a[G]_{eq}(1 - \theta) = k_d(\theta) \quad \text{Eqn. 3.6}$$

$$\frac{k_a}{k_d} = \frac{\theta}{[G]_{eq}(1 - \theta)} \quad \text{Eqn. 3.7}$$

$$K_L = \frac{\theta}{[G]_{eq}(1 - \theta)} \quad \text{Eqn. 3.8}$$

Where K_L is the Langmuir adsorption equilibrium constant. Rearranging gives the Langmuir isotherm:

$$\theta = \frac{K_L[G]_{eq}}{1 + K_L[G]_{eq}} \quad \text{Eqn. 3.9}$$

Taking θ as q_e/q_m, where q_e is the equilibrium quantity adsorbed and $q_m$is the monolayer quantity adsorbed, and rewriting $[G]_{eq}$ as C_e, the Langmuir isotherm becomes:

$$q_e = \frac{q_m K_L C_e}{1 + K_L C_e} \quad \text{Eqn. 3.10}$$

Which can be represented in linear form is:

$$\frac{C_e}{q_e} = \frac{1}{q_m} C_e + \frac{1}{q_m K_L} \qquad \text{Eqn. 3.11}$$

Therefore via a plot of C_e/q_e versus C_e, q_m and K_L can be calculated.

3.2.3 Freundlich Model

The Freundlich isotherm is an empirical isotherm. It assumes that non-ideal adsorption occurs on heterogeneous surfaces.[202] The isotherm expresses surface heterogeneity and the exponential distribution of active sites and their energies. The Freundlich equation can be written as:

$$q_e = K_F C_e^{1/n} \qquad \text{Eqn. 3.12}$$

Where K_F is the Freundlich constant ($mg^{1-(1/n)} L^{1/n} g^{-1}$) indicative of the relative adsorption capacity of the adsorbent, and n is a constant that indicates the relative distribution of the energy and the heterogeneity of the adsorbate sites. The linear form of the Freundlich equation is:

$$\ln(q_e) = \ln(K_F) + \frac{1}{n}\ln(C_e) \qquad \text{Eqn. 3.13}$$

3.2.4 BET Model

Below the critical temperature of a gas, Type II isotherms dominate over Type I, which indicates that multilayer build up occurs before the formation of a complete monolayer.[203] To account for this, Brunauer, Emmett and Teller extended the Langmuir isotherm model to create the BET model.[204] In this model, each site can accommodate 0 to i adsorbate molecules, which are not mobile on the surface. For the first layer, the rate of condensation on unoccupied sites is equal to the rate of evaporation from the sites that are covered by only one adsorbate molecule. Similarly, equilibrium is established for all layers with i number of equations. Key assumptions are: firstly, the heat of adsorption beyond the first layer is constant and is equal the heat of liquefaction; secondly, the ratio of adsorption and desorption rate constants (α/β) is constant for layers beyond the first. Summing over all layers then yields the BET equation:[203]

$$\frac{p}{v(p_0 - p)} = \frac{1}{v_m c} + \frac{c-1}{v_m c}\left(\frac{p}{p_0}\right) \qquad \text{Eqn. 3.14}$$

Where p is total pressure, p_0 is saturation vapour pressure, v is amount adsorbed in volume (STP)/g, v_m is monolayer amount adsorbed and c, the BET constant, is given by:

$$c = \frac{\alpha_1 \beta_2}{\alpha_2 \beta_1} e^{\left(\frac{Q_1 - Q_L}{RT}\right)} \approx e^{\left(\frac{Q_1 - Q_L}{RT}\right)} \qquad \text{Eqn. 3.15}$$

Where α is the adsorption rate constant, β the desorption rate constant, Q_1 the heat of adsorption (first layer), Q_L the heat of adsorption (liquefaction), R the gas constant and T is temperature. Plotting the left side of the BET equation against relative pressure using experimental data in range of p/p_0 = 0.05 to ~0.25 produces BET plots with a slope corresponding to v_m and intercept c.[203] Prior knowledge of the adsorbate molecular area, such as 0.162 nm^2 for nitrogen at 77 K, allows the BET surface area of the adsorbent surface area to be directly calculated from v_m.[203]

3.3 Silanisation Protocol

While the main purpose of silanisation was to modify the silica surface, maintenance of the particle size was required. Fine powders compact in the channel – restricting air flow, preventing efficient air-adsorbent interaction and in turn leading to poor adsorption. In this work, all three liquid phase techniques (described in Chapter 2) were attempted. Modification with the aqueous and aqueous/organic methods led to breakup of the silica particles into a powder, as shown in Figure 3.2. The organic solvent silanisation technique avoided particle breakup (Figure 3.3), meaning the particles could act as adsorbents with the Adsorption Device.

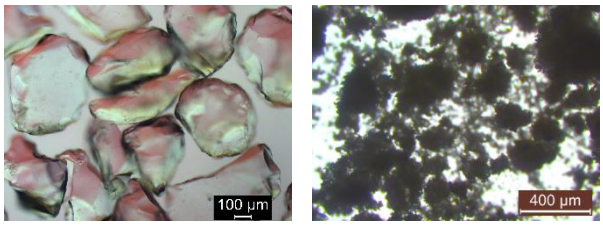

Figure 3.2. Optical microscope images of silica particles before and after aqueous-organic silanisation. *Left* – unmodified silica particles before any silane deposition. *Right* – silica particles following aqueous-organic deposition protocol. The aqueous only protocol had the same effect as the aqueous-organic protocol.

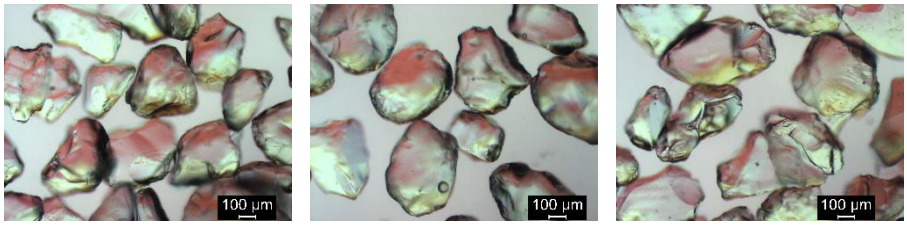

Amino Silica | n8 Alkyl Silica | Phenyl Silica

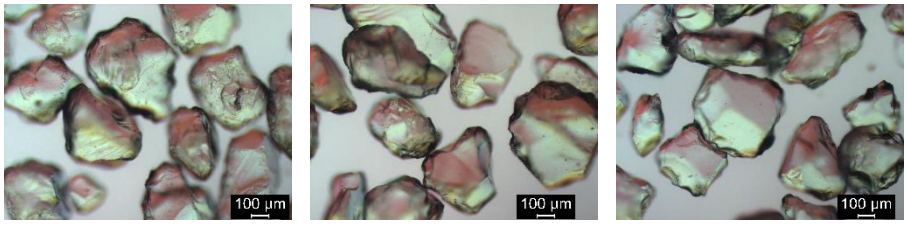

Chloro Silica | Alkylfluoro Silica | Chlorophenyl Silica

Figure 3.3. Optical microscope images of silica particles after organic solvent silanisation.

3.4 Adsorbent Characterisation

3.4.1 Contact Angle

Contact angle measurements quantify the wettability of a surface, and indicate the hydrophobicity of a given material. Small contact angles (< 90°) correspond to high wettability and large contact angles (> 90°) correspond to low wettability.[205] Consequently, small contact angles correspond to high *hydrophilicity* and large contact angles to high *hydrophobicity*. Instantaneous contact angles for the silica library are shown in Figure 3.4.

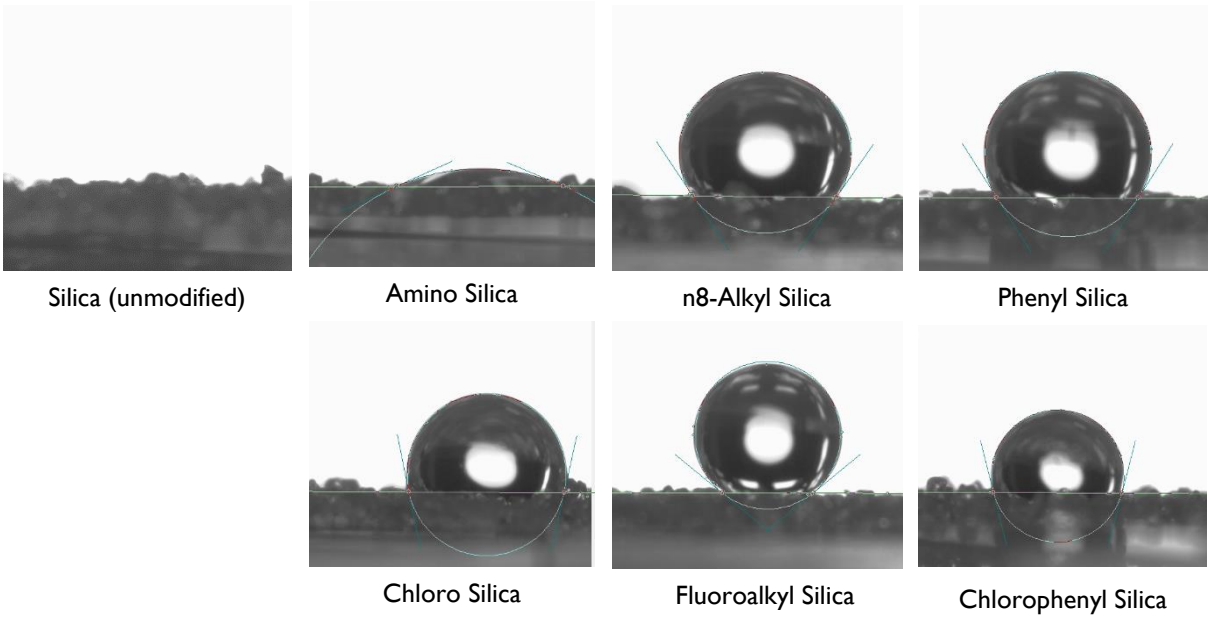

Silica	Contact Angle
Unmodified	n/a
Amino	24°
Chloro	102°
n8-Alkyl	123°
Fluoroalkyl	141°
Phenyl	122°
Chlorophenyl	119°

Figure 3.4. Contact angle measurement of silica particles. No contact angle was measured for the unmodified silica as the water droplet immediately spread across the surface.

It was impossible to measure a contact angle for unmodified silica as the water droplet was immediately adsorbed and spread across the surface. This is due to the presence of surface silanol (hydroxyl) groups that can form strong (hydrogen) bonds make the surface highly hydrophilic, such that any contact with water led to immediate surface wetting and coating. Of the remaining silicas, only aminosilica was found to be hydrophilic. A contact angle of 24° indicates that the adsorbent is less hydrophilic that unmodified silica. Although the terminal amino group (-NH_2) is also able to form hydrogen bonds with water, the coating of surface silanols and the presence of a propyl chain before the amino group has likely caused a reduction in surface hydrophilicity (in comparison to unmodified silica).[206]

All other silicas were hydrophobic, in the order fluoroalkyl > n8-alkyl ≈ phenyl ≈ chlorophenyl > chloro. None of these compounds are able to form hydrogen bonds, therefore any interactions with water are inherently weak, such that the droplet doesn't wet the surface and retains a spherical shape. This is due to the *hydrophobic effect*, when it is energetically and entropically favourable for water molecules to bond to each other rather than the surface.[207,208] Consequently, if water cannot form strong interactions with an adsorbent surface, an interface is formed.[209] Hydrophobicity is a desired feature of VOC adsorbents, as it enables the adsorbents to be used in humid environments.[185] In the case of ambient air quality measurement, it is a significant challenge to control fluctuating humidity levels, hence it is favourable to have a sensor system that can operate across a wide humidity range.

3.4.2 Thermal Gravimetric Analysis (TGA)

The strong temperature stability of the modified materials was confirmed via thermogravimetric analysis (TGA), heating from 25 to 800 °C (Figure 3.5). These data reveal two features that are consistent with all silicas analysed. Firstly, there is a small mass change up to 100 °C, which is caused by the evaporation of surface water. Secondly, between 100 and approximately 250 °C, the masses of the particles remain constant, indicating that all silicas are thermostable to this upper value. Above 250 °C, amino, chloro and alkyl silica particles begin to break down (at rates in the order of amino > alkyl > chloro), as the silica side groups break off. Around 550 °C, the phenyl-functionalised silicas break down. The similar shape of the mass changes for phenyl and chlorophenyl silicas indicates that the side groups cleave at the Si-Ph bond initially, rather than Ph-Cl for chlorophenyl silica.

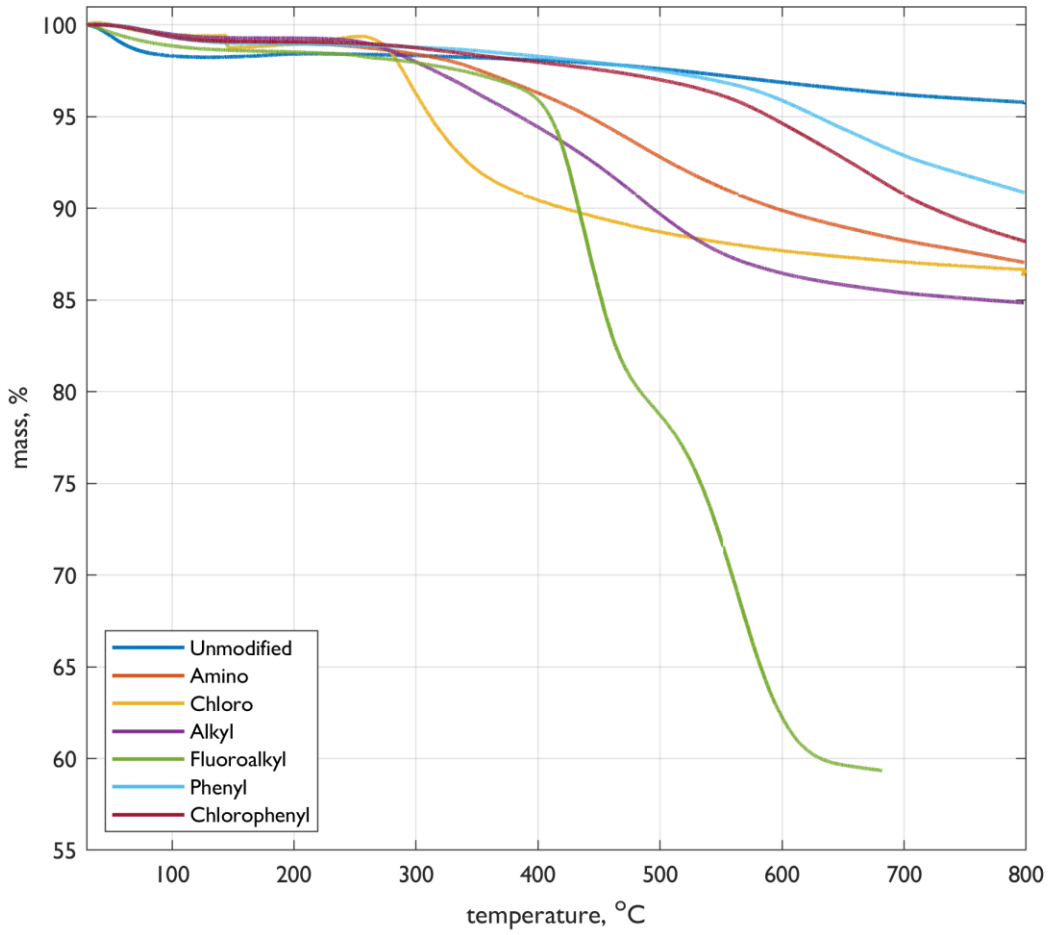

Figure 3.5. Thermal gravimetric analyses (TGA) of silica particles after silanisation (except unmodified silica). Note: the recording for fluoroalkyl silica stopped at 680 °C due to equipment error.

Table 3.1. Comparison of Silanisation Masses with TGA

Silica	Mass Change Increase after Silanisation, %	TGA Change*, %
Amino	4	9
Chloro	3	7
n8 Alkyl	9	11
Fluoroalkyl	38	37 **
Phenyl	5	5
Chlorophenyl	5	7

* Relative to the mass loss of unmodified silica at 800 °C (i.e. 96%).
** Taken at 680 °C (Figure 3.5).

Fluoroalkyl silica loses a small proportion of mass up to approximately 400 °C, followed by a large decrease in mass, which is likely caused by the removal of the dense fluoroalkyl moiety. The obvious difference in magnitude of mass loss for the fluoroalkyl silica versus other silica functionalities is due to the significant mass added with silanisation. This mass change during TGA is consistent with the mass deposited during silanisation, as shown in Table 3.1. As shown in Figure 3.4, the fluoroalkyl silane is the most hydrophobic material used. TGA indicates that during silanisation, the POTES silane could be polymerising away from the surface and then attaching to the surface of the silica, rather than the surface tethered mechanism shown in Figure 2.3. Alternatively, and perhaps more likely, silanisation of POTES could have occurred within silica pores, as indicated by the relatively low pore volume post-silanisation (see Table 3.4 below).

3.4.3 Infrared Spectra

The IR spectra for all silicas were recorded and are shown in Figure 3.6. The most obvious and consistent feature of the spectra is the large broad peak at ~1,090 cm^{-1}, which is the vibrational frequency of the disiloxane bond (Si-O-Si). Given the low mass of each silane relative to the mass of the silica particles (typically 10% or lower, Table 3.1), the disiloxane bond is the dominant feature of all spectra. Despite this, there are characteristic frequencies in the spectra of the functionalised silicas, the assignments of which are shown in Table 3.2. The data are, in their own right, insufficient to confidently characterise the adsorbents. Despite this, in combination with other characterisation data they indicate functional group difference between the materials and indicate that modification has occurred.

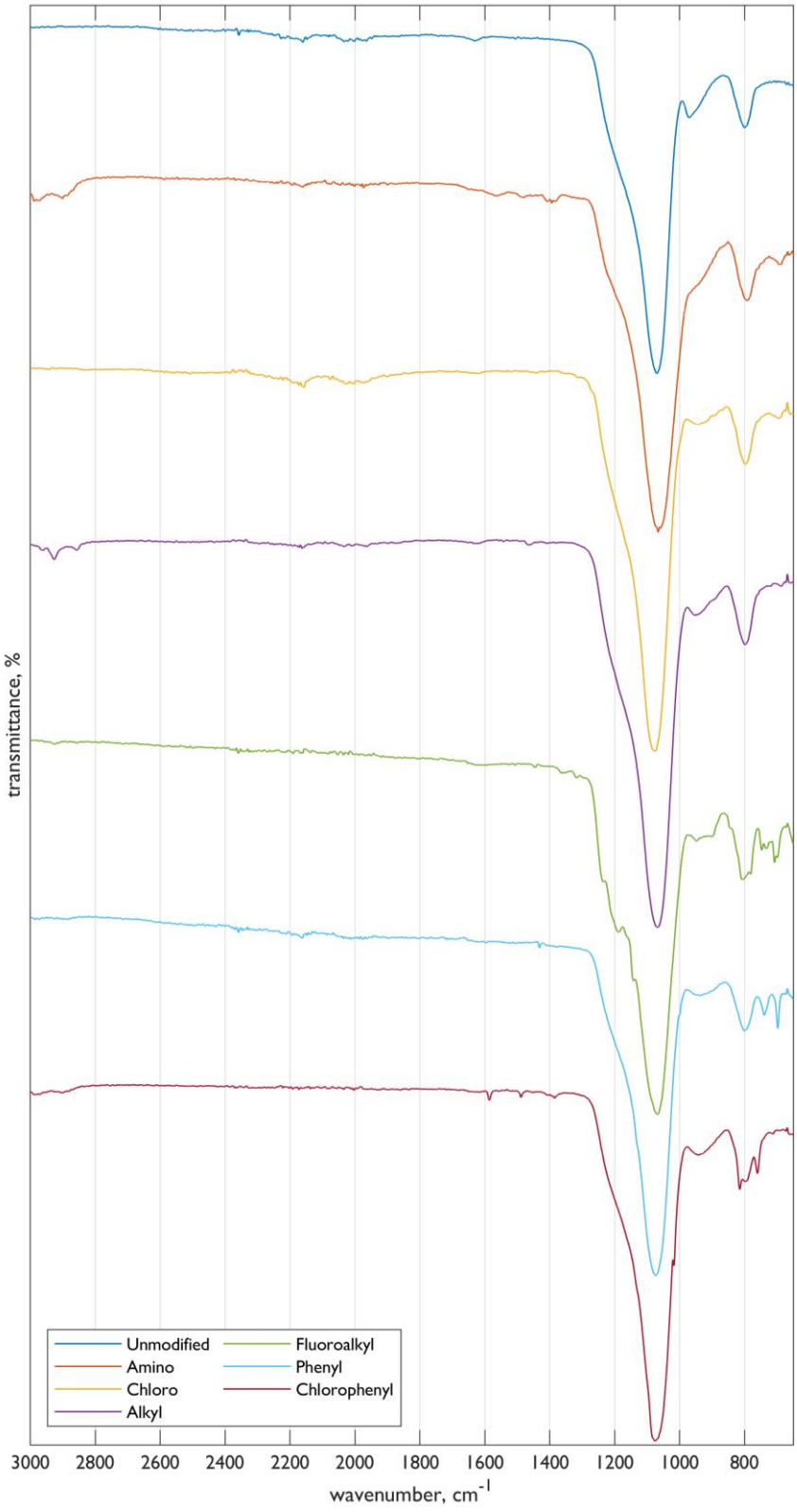

Figure 3.6. Infrared spectra of unmodified and silanised silicas. Note the apparent peak at approximately 2100 cm^{-1} is due to a verified artefact of the spectrometer.

Table 3.2. Assignment of IR bands of spectra shown in Figure 3.6

Silica	Wavenumber (cm^{-1})	Intensity	Vibrational Modes	Ref
ALL	1090	strong, br	Si-O-Si	210
Amino	1394	weak	C-N (str)	211
	2897	weak	C-H (str), sp3	211
	2976	weak	C-H (str), sp3	211
Chloro	696	weak	C-Cl (str)	211
(n8) Alkyl	1460	vw	C-H (str), sp3 (Me)	211
	2897	weak	C-H (str), sp3	211
	2927	weak	C-H (str), sp3	211
Fluoroalkyl	805	medium	C-F (str), CF_3	212,213
	899	weak	C-F (str), CF_3	212,213
	1144	medium	C-F (str)	212,213
	1190	medium	C-F (str)	212,213
	1238	medium	C-F (str)	212,213
	1320	vw	C-F (str), CF_3	212,213
Phenyl	697	medium	O-Si-Ph	210
	739	medium	C-H (b), sp2	211
	1432	vw	Si-Ph (narrow)	210
	2992	vw	C-H (str), sp2	211
Chlorophenyl	760	medium	C-H (b), sp2 (monosub)	211
	815	medium	C-H (b)	214
	1017	medium	C-H (b)	214
	1386	weak	Si-Ph	210
	1489	vw	Si-Ph	210
	1586	vw	C-C (str)	214
	2901	weak	C-H (str), sp2	211
	2990	weak	C-H (str), sp2	211

b = bend, br = broad, monosub = monosubstituted, str = stretch, vw = very weak

3.5 Nitrogen Isotherms

Isotherms for the adsorption and desorption nitrogen gas (N_2) to and from silica adsorbents at 77 K are presented in Figure 3.7. The isotherms for all adsorbents are classified as Type IV, according to the IUPAC definitons.[159] This indicates the formation of an initial monolayer at lower pressures (0 to ~0.4 p/p_0), then multilayer adsorption at higher pressures, followed by capillary condensation. In addition, all isotherms show hysteresis between adsorption and desorption processes, which indicates the presence of mesopores of widths higher than 4 nm.[159] N_2 adsorption for most adsorbents from 0 to 0.4 p/p_0 are similar, indicating comparable N_2 capacity in the low-to-middle relative pressure range. Relative to the other adsorbents, amino and fluoroalkyl silicas adsorb less N_2, from 0 to 0.4 p/p_0. These adsorption capabilities become more distinct at higher pressures, i.e. above 0.4 p/p_0, with chloro, alkyl, phenyl and chlorophenyl derivatives all adsorbing similar amounts, and more that the amount adsorbed by the amino silica and the fluoroalkyl derivatised silica. In all cases the modified silicas appear to adsorb less than unmodified silica.

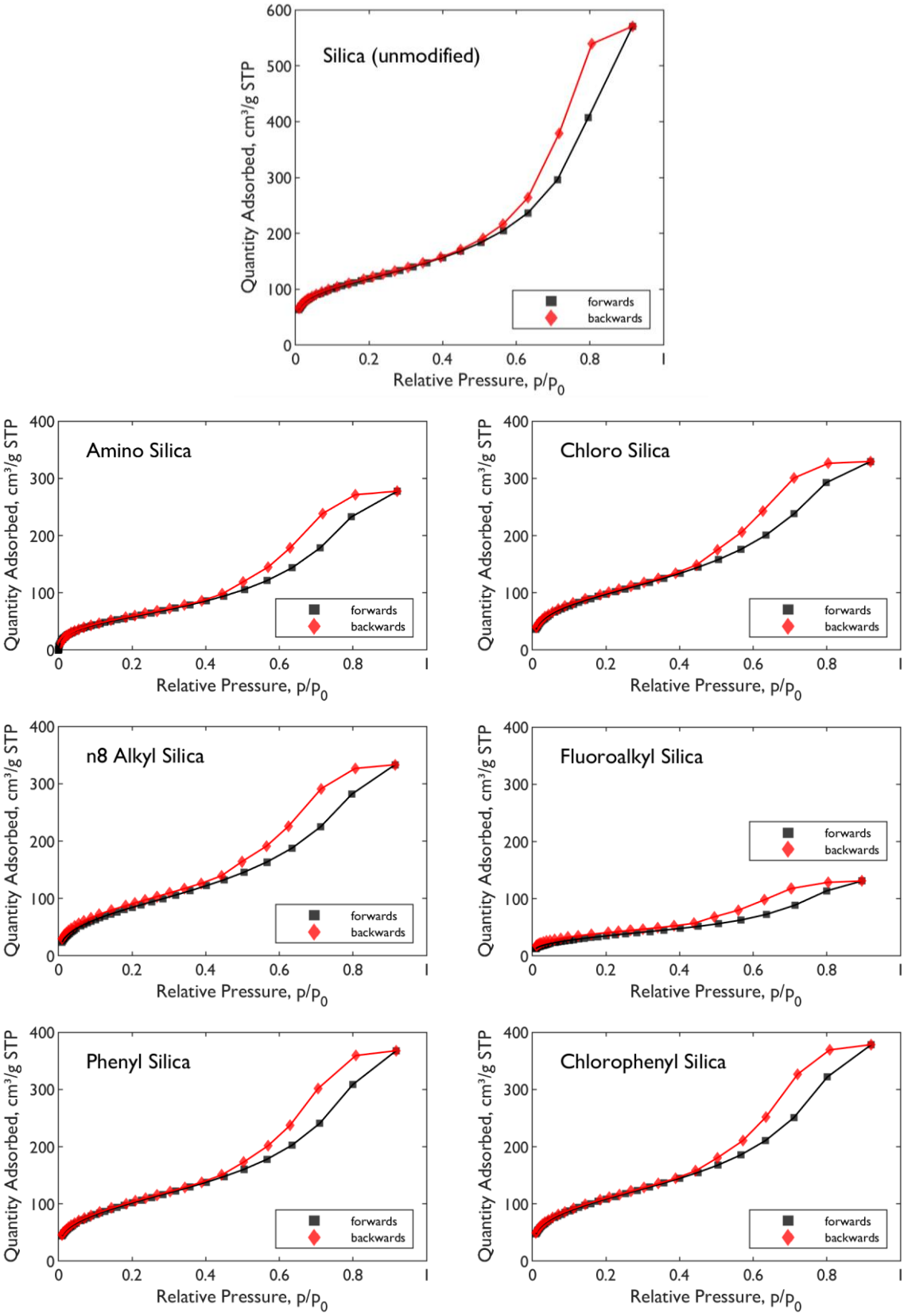

Figure 3.7. Nitrogen Adsorption and Desorption Isotherms for silica adsorbents. N2 gas adsorption/desorption studies were carried out using a Micromeritics 3Flex Surface Characterisation Analyzer at 77 K. Samples were degassed overnight before the collection.

Surface areas were calculated by the BET method based on the linear part of BET plot in the relative pressure range of 0.06 to 0.21 (Figure 3.8). These data revel that the surface areas of chloro, alkyl, phenyl and chlorophenyl silicas were of similar magnitude (540 ± 40 m^2/g), but there was a significant reduction for amino and fluoroalkyl silicas. For the former material, it could be that the organic solvent used for silanisation (toluene) causes amino silane (APTES) to silanise in the pore of the silica. Pore volume data, estimated using the Barrett, Joyner and Halenda (BJH) model (Table 3.4), indicate that this could be the case, although the volume of amino silica is not significantly lower than other modified silicas, excluding fluoroalkyl silica. The BET constant, *c*, is a dimensionless measurement that relates to the enthalpy of adsorption of the adsorbate gas, with lower values indicating stronger interactions. The BET constants of modified silica adsorbents are not significantly different from each other, although they are all lower than unmodified silica, indicating stronger adsorption for functionalised materials.

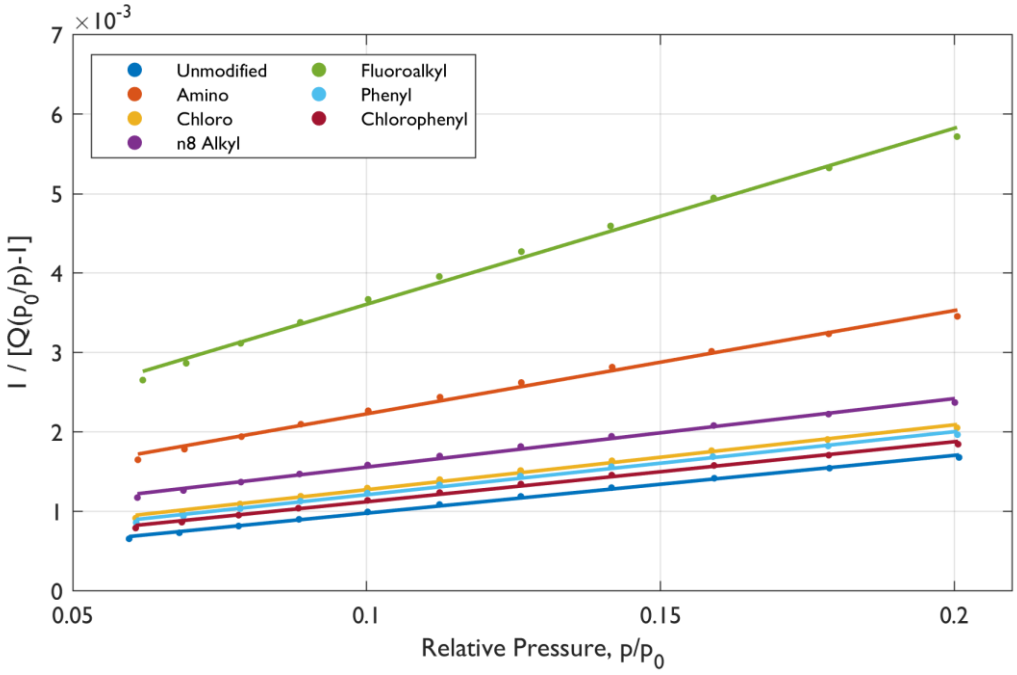

Figure 3.8. BET Plots for silica adsorbents.

Table 3.3. Isotherm parameters of nitrogen (N_2) adsorption on silica adsorbents

Isotherm Model	Isotherm Constants	Silica						
		Unmod-ified	Amino	Chloro	n8 Alkyl	Fluoro alkyl	Phenyl	Chloro-phenyl
BET	SA (m^2/g)	578	312	505	467	185	521	549
	BET constant, c	29.7	15.0	18.8	13.3	16.9	19.9	21.6
	R^2	0.99	0.99	0.99	0.99	0.99	0.99	0.99
Freundlich	n	0.28	0.59	0.38	0.53	0.63	0.34	0.33
	K_F ($mg^{1-(1/n)}$ $L^{1/n}$ g^{-1})	1.22	1.46	1.38	1.50	1.38	1.31	1.31
	R^2	0.99	0.99	0.99	0.99	0.99	0.99	0.99
Langmuir	q_m (mg/g)	119.4	55.1	93.9	78.3	32.4	94.7	103.5
	K_L (L/mg)	0.041	0.014	0.019	0.013	0.021	0.028	0.027
	R^2	0.99	0.99	0.99	0.99	0.99	0.99	0.99

SA = surface area

Table 3.4. Pore volume and pore size estimates, as estimated using the BJH method

	Silica						
	Unmodified	Amino	Chloro	n8 Alkyl	Fluoroalkyl	Phenyl	Chlorophenyl
Pore volume (cm^3/g)	0.91	0.45	0.51	0.52	0.24	0.61	0.59
Pore diameter (Å)	75	60	55	55	55	55	53

3.5.1 Adsorption Isotherm Models

Two different models – Langmuir and Freundlich – were applied to fit the adsorption isotherms. The linear forms of the models (Eqn. 3.11 and Eqn. 3.13 for Langmuir and Freundlich models, respectively) were used calculate the adsorption parameters. These, together with values of R^2 are summarised in Table 3.3.

Freundlich Model

For the Freundlich model, the $1/n$ term can be between 0 and 1, hence the model equation (Eqn. 3.12) only applies over a limited pressure range. When $1/n = 0$, q_e is constant and adsorption is independent of gas pressure. When $1/n = 1$, $q_e = K_f C_e$, meaning adsorption is directly proportional to gas pressure. The model is only applicable for physisorption, so does not account for the multilayer adsorption that occurs at higher pressures (beyond the range of interest to low concentration VOCs). Consequently, it tends to fail at higher pressures as secondary and higher layers are formed. This can be seen clearly in the linear fits of the Freundlich model to N_2 adsorption data (Figure 3.9), where at higher pressures (represented by hollow circles) the data become non-linear. Due to this observation, the Freundlich model was only fitted in the linear region (represented by filled circles). The coefficients of correlation values, shown in Table 3.3, are very high (0.99) showing excellent linearity. The magnitude of the exponent n indicates the favourability of adsorption. Values of n in the range 2-10 represent good, 1-2 moderate and < 1 represent poor adsorption characteristics.[215] According to these classifications, all silica adsorbents exhibit poor characteristics for N_2 adsorption. It is important to note that the meaning of 'good' adsorption characteristics in this sense reflect a capability to trap a large quantity of a target gas, as is the gas with air purification applications.[162,177,203,216] Given that the aim of this project is to detect vapours, capability to adsorb is required to the extent that sensitive and selective detection is possible. Consequently these adsorbents may be adequate for this application despite their low n values.

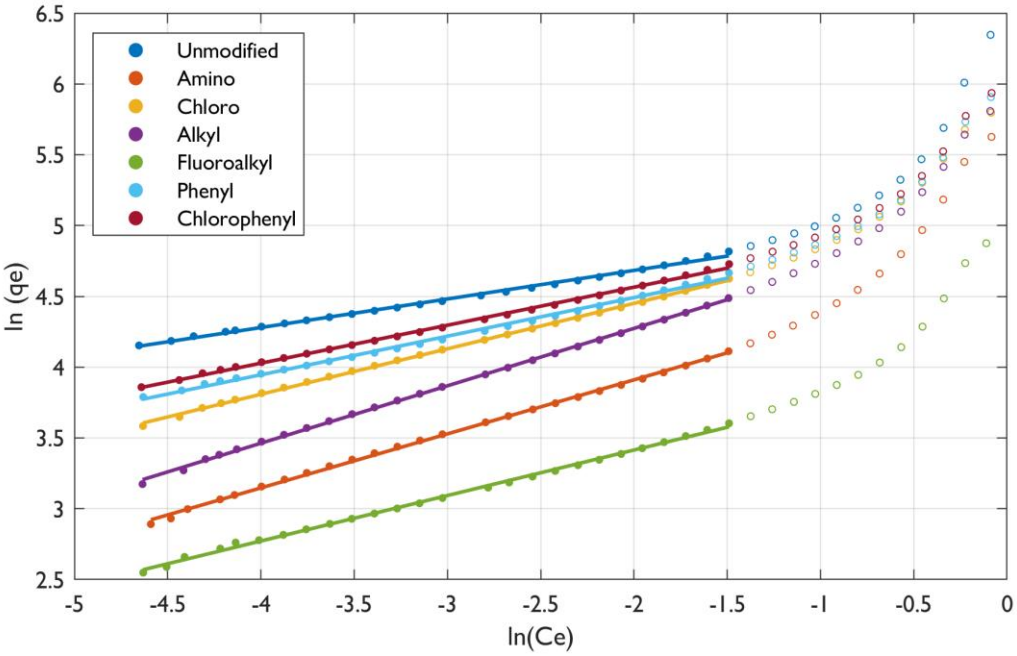

Figure 3.9. Linear Fit of the Freundlich Adsorption Isotherm. The data points not included in the fit are shown as hollow circles.

Langmuir Model

As with the Freundlich model, adsorption data for N_2 onto the silica adsorbents were analysed by a regression analysis to fit to the linearized equation (Eqn. 3.11) of the Langmuir model (Figure 3.10). Given the central assumption of the Langmuir model of a monolayer formation, the equation was fitted to the data points corresponding to monolayer formation. The Langmuir adsorption parameters calculated from these fits, K_L and q_m, are shown in Table 3.3. As would be expected, the quantities required to form a monolayer (q_m) correspond to the calculated BET surface areas. The Langmuir constant (K_L) indicates the extent of interaction between adsorbate and adsorbent. In general, this reflects the order of surface area, for example the largest K_L value is for unmodified silica, which also has the largest BET surface area. A notable exception is the alkyl functionalised silica, which has the lowest the K_L despite having a surface area 2.5 times larger than the fluoroalkyl silica. This indicates that there could be stronger interactions between N_2 and the surface when the surface is fluorinated.

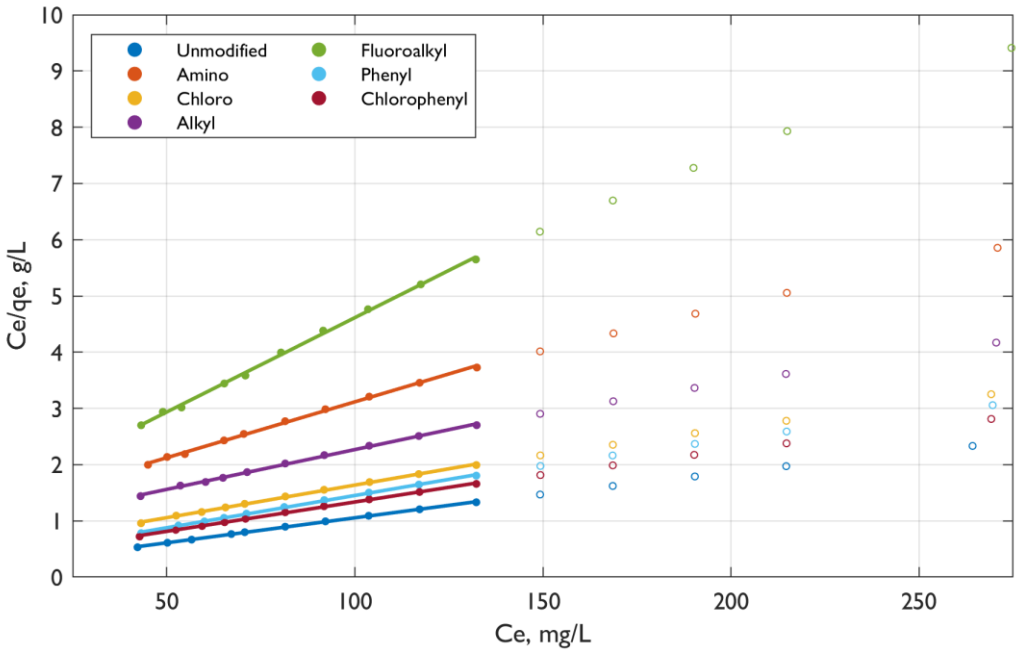

Figure 3.10. Linear Fit of the Langmuir Adsorption Isotherm. The data points not included in the fit are shown as hollow circles.

3.6 Discussion

This primary motive of this chapter was to synthesize and characterise a library of modified silica adsorbents with a range of chemical functionalities, suitable for use in the Adsorption Device. Six modified silica adsorbents were prepared, which were modified through organic solvent silanisation and introduced amino, chloro, alkyl, fluoroalkyl, phenyl and chlorophenyl functionalities to the adsorbent surface. Contact angle measurements revealed that unmodified and amino silica were hydrophophilic and all others were hydrophobic.[i] Thermogravimetric analysis indicated that all adsorbents are thermostable in the proposed operational temperature range of the Adsorption Device (20-105 °C). With the exception of fluoroalkyl silica, silanisation added between 5-11% of functionalised silanes to silica. IR spectra of the adsorbents, although not conclusive, was able to suggest that different chemical functionalities had been incorporated, although the low silane mass relative to the silica particles meant that the characteristic bands were weak.

Nitrogen isotherms for all adsorbents were Type IV, indicating that nitrogen adsorption proceeds from monolayer formation to multilayer and then capillary condensation at high pressures. This finding agrees with previously reported isotherms for unmodified, phenyl-grafted and amino-grafted silica.[185,217] Subsequent BET and BJH analyses of adsorption data indicated a range of surface areas and pore sizes, respectively. The relatively low surface area (185 m^2/g) and pore volume (0.24 cm^3/g) for fluoroalkyl silica (together with TGA data) suggests that the silane may have polymerised in the pores of the silica, reducing its adsorption capacity. Unmodified, alkyl, phenyl and chlorophenyl silicas were estimated to have surface areas of approximately 520 ± 55 m^2/g, and amino silica approximately 312 m^2/g. Pore volume sizes corresponded with surface area calculations (i.e. high for unmodified silica and low for fluoroalkyl).

Analysis of adsorption using the Freundlich model revealed that, at least when compared to 'traditional' adsorbents like activated carbon, the silica materials would be categorised as 'poor' adsorbents.[215] Given that good adsorption characteristics signify a capability to trap a large quantity of a target gas, a poor adsorbent could still have utility and effectiveness as a sensing material. For sensing materials - rather than extraction materials – the ability to trap a high concentrations is not necessary, provided that a difference in adsorption can be observed. The Langmuir adsorption model indicated that the monolayer quantity reflected the same trend found for surface area and pore volume calculated from the BET model. However, the Langmuir constants, which indicates the extent of interaction between the gas and

[i] Given that contact angles were measured from a bed of particles rather than a uniform flat surface, these values are more relative than absolute, but still provide a good indication of hydrophobicity.

adsorbent, indicated that fluoroalkyl silica adsorbed a comparable volume of nitrogen gas per unit as amino, chloro, phenyl and chlorophenyl silicas. Despite this, the capacity of the adsorbents is still a key factor in gas sensing. This chapter has shown that, through silanisation, a range of functionalised silicas can be produced. Based on the nitrogen isotherms, the adsorbents show some promise for gas adsorption for sensing applications, although their capacity is unlikely to be high enough for pollutant removal.

Chapter 4 VOC Adsorption

4.1 Introduction

Adsorption and desorption studies with nitrogen gas (N_2) shown in the previous chapter indicated that the silica adsorbents facilitate the adsorption of the gas at different rates and at different capacities, based on their functionalities, surface area and pore volume. This chapter presents the examination of the adsorption of four VOCs: benzene, toluene, ethylbenzene and *para*-xylene (collectively termed BTEX) on each material in the adsorbent library. Unlike the N_2 adsorption analysis, BTEX studies were undertaken at ambient temperature (273 K) and at partial pressures that are typically observed in the atmosphere and indoor environments, i.e. in the low parts-per-millions range (0 – 3 ppm).

The chapter begins by estimating the BTEX adsorption capacity for the silica adsorbents, based on isotherms collected at standard temperature and pressure. The isotherms were then modelled using Langmuir and Freundlich adsorption models, and the estimation of enthalpy of adsorption ($\Delta H^{\emptyset}$), entropy of adsorption ($\Delta S^{\emptyset}$) and change in Gibbs free energy ($\Delta G^{\emptyset}$). Finally, the adsorption 'patterns' of the different BTEX-adsorbent combinations are analysed, and input vapour selectivity considered *during* vapour adsorption – i.e. the sampling phase.

4.2 VOC Isotherms

The adsorbed quantities of benzene, toluene, ethylbenzene and *para*-xylene (BTEX) on unmodified silica and the six modified silica adsorbents were estimated with the method described in Chapter 2. Different concentrations of BTEX, in the range of 0 to 2,000 parts-per-billion (ppb) were generated from pre-calibrated permeation tubes and sampled with the Adsorption Device for 15 minutes. This was possible due to the downstream measurement of VOCs by the photoionisation detector (PID), which was located at the exhaust end of the Adsorption Device (as shown in Figure 2.12). As the device is a closed system, the concentration measured at the PID corresponds to the concentration that has been adsorbed in the adsorbent chamber of the device (Figure 4.1). Unlike the nitrogen isotherms shown in the previous chapter, which were collected at the condensation temperature of N_2 (77 K) and varying N_2 pressures, BTEX isotherms were collected at standard temperature and pressure: 273 K and atmospheric pressure. The quantities of vapour adsorbed (q_{15}) for each BTEX-adsorbent combination are shown in Figure 4.2 (per BTEX) and Figure 4.3 (per adsorbent).[i]

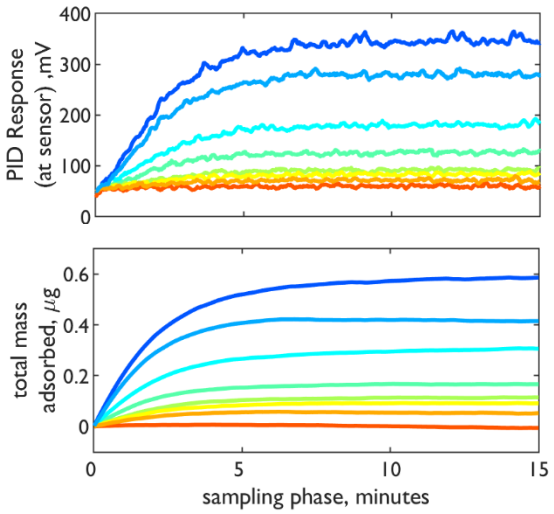

Figure 4.1. Benzene Adsorption on unmodified silica, ranging from 200 ppb (red) to 1,900 ppb (blue). *Top* – PID response during the sampling phase. *Bottom* - the inferred adsorbent concentration during the sampling phase. Values of q_{15}, used in VOC isotherms, were calculated from the masses at 15 minutes.

[i] Note: the quantity adsorbed values for the VOC isotherms are q_{15} (quantity adsorbed after 15 minutes of sampling) rather than q_e (quantity adsorbed at equilibrium). Although in some cases adsorption-desorption equilibrium had been established, this was not the case for all adsorbents, most notably phenyl and chlorophenyl silicas, which both had additional capacity for adsorption beyond the 15 minute sampling time. Given the design parameters of the sensor device (i.e. short sampling time) it was decided that going significantly beyond 15 minutes sampling time to establish q_e values was not necessary and sufficient information regarding the relative capacities of the adsorbents was obtained for understanding the varying adsorption capacities.

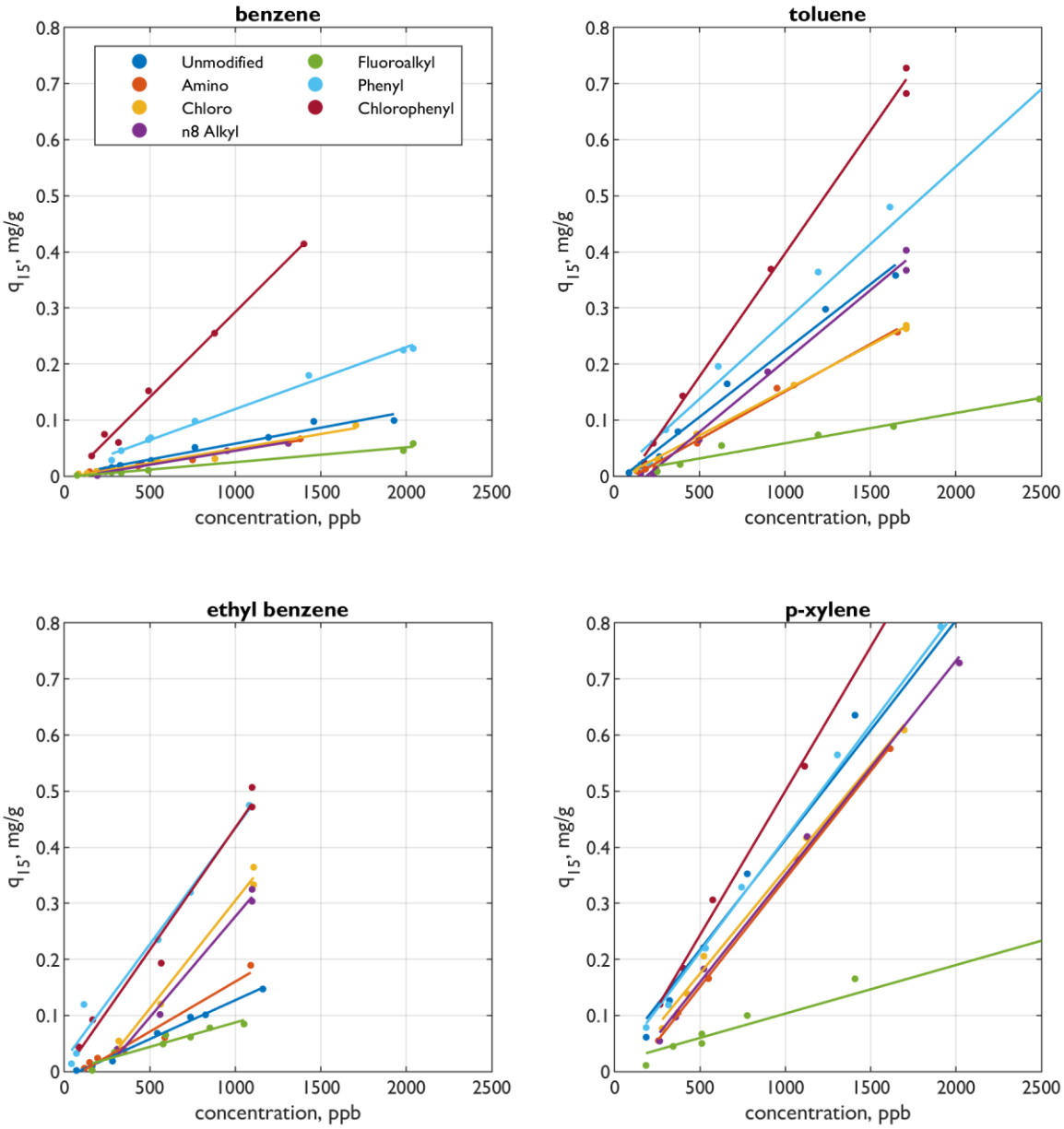

Figure 4.2. VOC Isotherms. Benzene (top left), toluene (top right), ethylbenzene and (bottom left) and *para*-xylene (bottom right). Note: for ethylbenzene, the concentration values are lower due to the concentration limit of the permeation tube used.

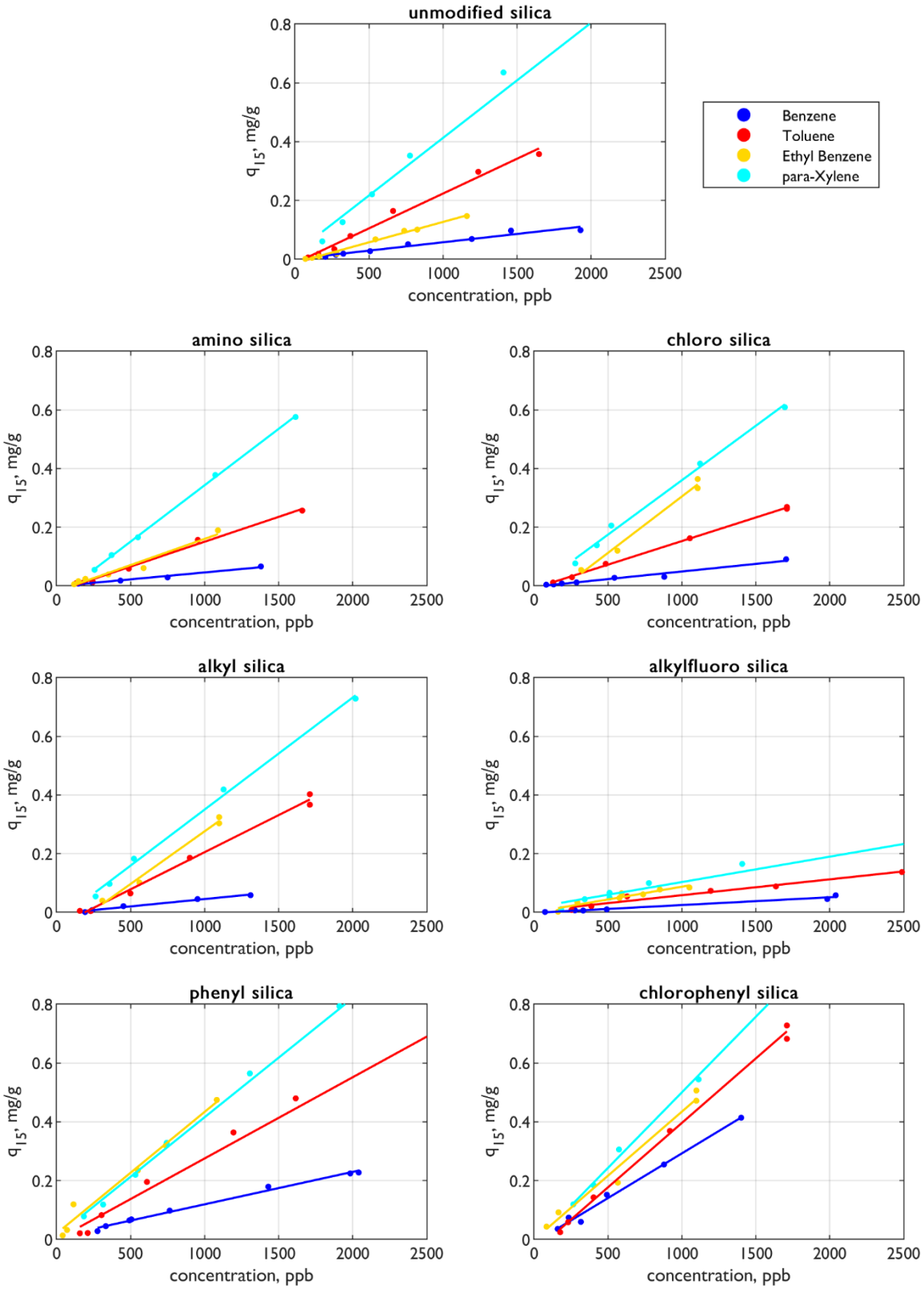

Figure 4.3. BTEX Isotherms. Note: data is the same as in Figure 4.2, but presented per silica adsorbent (rather than per BTEX).

Chlorophenyl and phenyl silicas were the adsorbents with the highest capacities for all four BTEX vapours. This a significant difference to nitrogen gas adsorption, which had capacities that generally corresponded to the BET surface areas of each adsorbent, with unmodified silica having the highest capacity (Figure 3.7 and Table 3.3). The increase in capacity for chlorophenyl and phenyl silicas is likely due to the energetically favourable interactions between the aromatic pi-systems of both the vapours and adsorbent surface. Pi stacking, or pi-pi interactions, are attractive non-covalent interactions between aromatic rings. Although benzene lacks a dipole moment, it has a strong quadrupole moment. The local C-H dipole results in a positive charge on the ring atoms and a negative charge on the electron density above and below the ring (Figure 4.4). These charges allow interactions between aromatic compounds where δ+ and δ– forces are favourably aligned.

Figure 4.4. *Left* – p-orbitals within benzene. *Right* – quadrupole moments of benzene.

Although the capacity of chlorophenyl silica is consistent across all vapours, the adsorbate concentration for phenyl silica is more varied, with a lower capacity for benzene compared to TEX. Substitution of the aromatic ring with a chlorine atom clearly affects adsorption behaviour. As an electronegative element, chlorine is a withdrawing group, removing electron density from the aromatic ring by induction. It is proposed here that this has the effect of reducing electron density in the aromatic ring, reducing repulsion (or increasing attraction) between electron density in the aromatic quadrupole. Although little empirical evidence exists regarding substituent effects of pi-pi interactions, reported theoretical calculations support the theory proposed here.[218,219] In general, adsorbate capacity for alkyl, amino, chloro and unmodified silicas are similar for each vapour. All four adsorbents have a lower capacity than phenyl and chlorophenyl silicas. Due to the lack of delocalised electrons in these adsorbents, pi-stacking cannot occur with the adsorbent, meaning energy stabilisation can only occur via van der Waals (dispersion) interactions. These interactions are lower energy than pi-stacking, so lead to less adsorption. Fluoroalkyl silica had the lowest capacity for all vapours. Unlike the phenyl and chlorophenyl silicas, this is consistent with the BET surface area and BJH pore volume, for which fluoroalkyl silica had the lowest surface area of all the adsorbents (Table 3.3). These observations indicate that the interactions between fluoroalkyl silica and BTEX compounds are not sufficiently favourable to make up for a relatively lower surface area.

4.2.1 Isotherm Models

BTEX isotherm data was analysed using Freundlich and Langmuir adsorption isotherm models. Experimental data was plotted using the linearized forms of the equations, Eqn. 3.12 and Eqn. 3.10 for Freundlich and Langmuir respectively. The data are well fitted to the Freundlich equation (Figure 4.5), with only one vapour (benzene on silica) having an R^2 value of less than 0.95 (0.91). Adsorption parameters for these models are shown in Table 4.1. Given the empirical nature of the model, and the very low concentration (i.e. partial pressure) of vapours, it was expected that the model fits well in this range. As mentioned in section 3.5, the values of n may correspond to adsorption characteristics of the adsorbents.[215] As was the case with nitrogen gas, adsorption of BTEX compounds all returned n values less than 1, signifying 'poor' adsorption characteristics. Statistical analysis of Freundlich n and K_f values (Table 4.2) reveals that only benzene adsorption is statistically different to other vapours (t-test values for n, comparing each vapour with other vapours, e.g. B against TEX, T against BEX etc). The Freundlich constant, K_f, may indicate relative adsorbent capacity. Calculated K_f values (Table 4.1) are of a similar magnitude, and reveal little relative adsorbent capacity, especially as the units of K_f ($mg^{1-(1/n)}\ L^{1/n}\ g^{-1}$) are dependent on n. As a result of this, the largest values of K_f, such as 7.47 for toluene on alkyl silica, correspond to lower values of n (0.11).

Direct comparison of n values between N_2 and BTEX adsorption is not expected. Firstly, there was a significant temperature difference: 77 K for N_2 and 273 K for BTEX. Given the temperature dependence of the Freundlich model (i.e. the values are valid for the temperature at which they were collected), it was expected that the model parameters would change significantly across this temperature range. In addition, the adsorbate quantity for BTEX was q_{15} rather than q_e, so the equilibrium concentration was not necessarily established for all vapour-adsorbent combinations. Despite this, the isotherms allow the estimation of adsorption behaviour for BTEX vapours, and a comparison to be made of the different materials. These data show that, in terms of a fit to the Freundlich model, adsorption kinetics are not expected to yield a high retention of the BTEX VOCs. In general terms this is favourable for the design of a *reversible* affinity column that can be configured for real time measurement to distinguish between the BTEX VOCs (as targeted in this thesis) but would not be the desired characteristics of a sorption tube model, which would require remote sample acquisition and later laboratory measurement.

The fit of the data to the Langmuir model equation used in the previous chapter is poor (Figure 8.1, Appendix 2). As shown by the R^2 values for the absorbent-vapour combinations (Table 4.1), the correlation of data with the model is very poor, indicating that this form of the model doesn't apply in this low concentration (and partial pressure) of BTEX compounds. A significant contributing factor is

the q_{15} value not representing an equilibrium quantity, a key assumption of the model. Due to the poor fit, Langmuir adsorption parameters were not calculated.

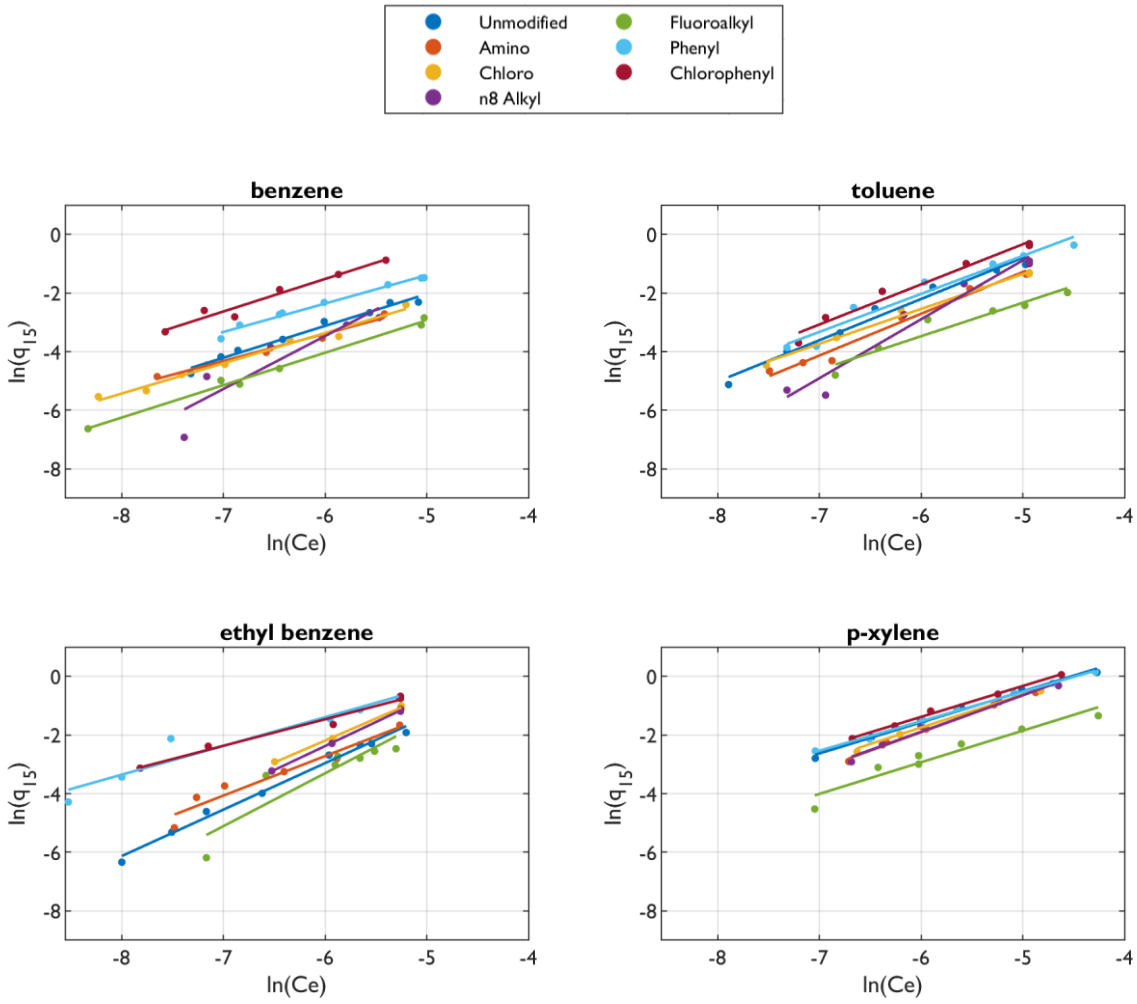

Figure 4.5. Freundlich model fitting to VOC Isotherms.

Table 4.1. Isotherm parameters of VOC adsorption on silica adsorbents

Isotherm Model	VOC	Isotherm Constants	Silica						
			Unmodified	Amino	Chloro	n8 Alkyl	Fluoroalkyl	Phenyl	Chlorophenyl
Freundlich	Benzene	n	0.16	0.46	0.35	0.14	0.38	0.29	0.19
		K_F *	5.30	2.54	2.81	6.09	3.02	2.64	3.04
		R^2	0.91	0.98	0.98	0.83	0.99	0.98	0.96
	Toluene	n	0.16	0.17	0.22	0.11	0.30	0.17	0.15
		K_F *	4.09	4.15	3.29	7.47	3.14	3.66	3.93
		R^2	0.98	0.98	0.99	0.95	0.92	0.95	0.97
	Ethylbenzene	n	0.33	0.19	0.15	0.13	0.13	0.22	0.25
		K_F *	2.95	3.85	4.50	5.15	6.08	2.67	2.47
		R^2	0.95	0.94	0.99	0.99	0.82	0.92	0.98
	p-Xylene	n	0.21	0.18	0.20	0.18	0.28	0.22	0.20
		K_F *	2.89	3.52	3.08	3.48	2.94	2.74	2.87
		R^2	0.99	0.99	0.98	0.98	0.92	0.99	0.99
Langmuir	Benzene	R^2	0.32	0.03	0.09	0.28	0.48	0.12	0.17
	Toluene	R^2	0.41	0.55	0.55	0.51	0.09	0.27	0.43
	Ethylbenzene	R^2	0.21	0.98	0.98	0.95	0.37	0.01	0.14
	p-Xylene	R^2	0.03	0.63	0.26	0.42	0.00	0.00	0.27

SA = surface area, * units: $mg^{1-(1/n)}\ L^{1/n}\ g^{-1}$)

Table 4.2. Statistical analysis of Freundlich *n* and K_f values

Value		B	T	E	X
n	Mean	0.281	0.183	0.200	0.210
	SD	0.122	0.061	0.073	0.034
	Variance	0.015	0.004	0.005	0.001
	t-test	0.019	0.200	0.510	0.762
K_F	Mean	3.634	4.247	3.953	3.074
	SD	1.438	1.472	1.361	0.308
	Variance	2.067	2.168	1.853	0.095
	t-test	0.826	0.211	0.592	0.113

4.3 Adsorption Thermodynamics

In order to further examine the adsorption mechanisms between vapour and adsorbent, the sampling temperature of the chip was varied between 25 °C and 55 °C, while sample concentration was kept constant. The temperature of the chip was preprogramed in C++ and uploaded to the Arduino Uno microcontroller. The test cycle conditions are shown in Table 2.6. By calculating adsorbate concentration at a range of temperatures at constant concentration, it was possible to use the van't Hoff equation (Eqn. 2.18) to estimate the enthalpy and entropy of adsorption for different adsorbent-VOC combinations. Examples of data used to calculate these parameters is shown in Figure 4.6. The data are taken from the sampling phase of the test cycle (i.e. during adsorption).

As sampling temperature is increased from 25 °C to 55 °C the PID responses tend to become higher, as less vapour is adsorbed and therefore reaches the detector. At higher temperatures and longer sampling times, the signal saturates, which indicates that the rates of adsorption have reached an equilibrium and the concentration of adsorbate has plateaued. This is most obvious for sampling recorded at the highest temperature (red lines), where equilibrium is reached more quickly into the sampling period. At lower temperatures, such as 25 °C (navy blue line), the PID response rises more slowly, indicating slower vapour adsorption. Data from the sampling temperatures that reached equilibrium were used to calculate the equilibrium rate constant, K_{eq} (Eqn. 2.14). By plotting K_{eq} against $1/T$ (Figure 4.6, right), the enthalpy ($\Delta H^{\emptyset}$) and entropy ($\Delta S^{\emptyset}$) of adsorption can be calculated from the slope and intercept, respectively (Figure 4.6, right). This analysis was repeated for all BTEX-adsorbent combinations. Estimated enthalpies and entropies of adsorption for all adsorbent-BTEX combinations, together with the Gibbs energy of adsorption at 25 °C to 55 °C, are shown in Table 4.3.

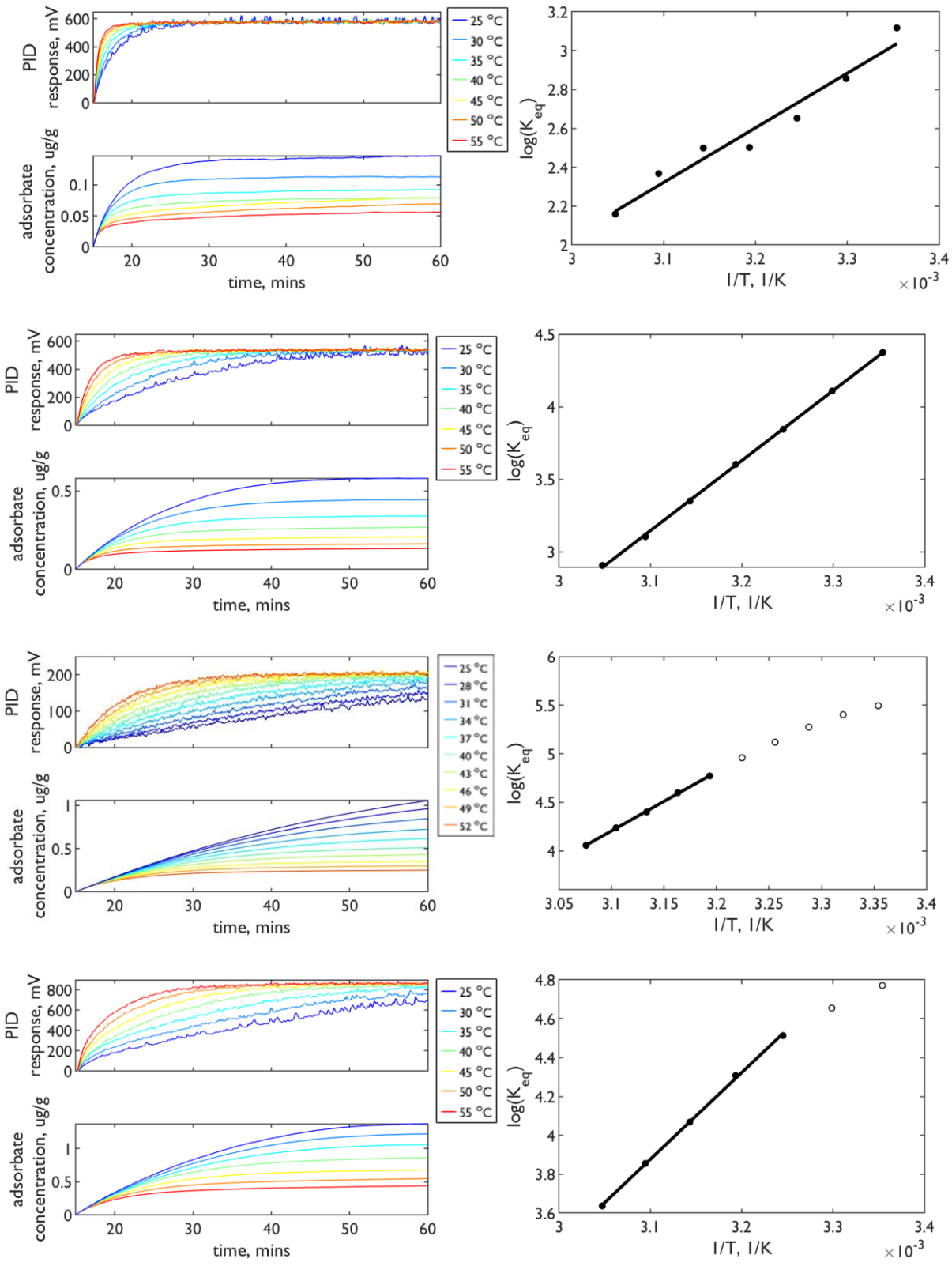

Figure 4.6. *Left* – PID (photoionisation detector) responses on phenyl silica during sampling phase (15 to 60 minutes) of a test cycle at temperatures from 25 °C to 55 °C at constant concentration (1 ppm), and corresponding adsorbate concentration during the sampling phase (*top-bottom*: benzene, toluene, ethyl benzene, *para*-xylene). *Right* – van't Hoff plot. The data points that are

not included in the fit (temperatures at which equilibrium had not been reached) are shown as hollow circles.

Table 4.3. Enthalpy and entropy estimates for adsorbent-BTEX combinations, calculated from corresponding van't Hoff equation analysis.

VOC	Parameter	Silica							units
		Unmodified	Amino	Chloro	n8 Alkyl	Fluoroalkyl	Phenyl	Chlorophenyl	
Benzene	ΔH°	-17.9	-28.2	-25.0	-26.5	-28.6	-20.5	-55.9	kJ mol^{-1}
	ΔS°	-39.0	-68.7	-63.0	-55.8	-70.9	-44.3	-142.0	J K^{-1} mol^{-1}
	R^2	0.97	0.90	0.65	0.91	0.92	0.95	0.97	
	ΔG° (T = 25 °C)	-6.3	-7.7	-6.2	-9.8	-7.5	-7.3	-13.5	kJ mol^{-1}
	ΔG° (T = 55 °C)	-5.1	-5.7	-4.3	-8.2	-5.4	-6.0	-9.3	"
Toluene	ΔH°	-33.4	-43.8	-30.7	-51.9	-31.4	-40.2	-57.1	kJ mol-1
	ΔS°	-79.8	-111.6	-72.9	-141.3	-76.0	-98.4	-141.7	J K^{-1} mol^{-1}
	R^2	0.99	0.94	0.88	0.98	0.89	0.99	0.99	
	ΔG° (T = 25 °C)	-9.6	-10.5	-8.9	-9.7	-8.7	-10.8	-14.8	kJ mol^{-1}
	ΔG° (T = 55 °C)	-7.2	-7.1	-6.7	-5.5	-6.4	-7.9	-10.5	"
Ethyl Benzene	ΔH°	-30.0	-33.0	-42.3	-50.6	-36.8	-50.5	-56.3	kJ mol^{-1}
	ΔS°	-64.5	-69.7	-103.6	-129.9	-90.8	-121.6	-134.4	J K^{-1} mol^{-1}
	R^2	0.97	0.96	0.97	0.92	0.99	0.99	0.97	
	ΔG° (T = 25 °C)	-10.8	-12.2	-11.4	-11.9	-9.8	-14.3	-16.2	kJ mol^{-1}
	ΔG° (T = 55 °C)	-8.9	-10.1	-8.3	-8.0	-7.0	-10.6	-12.2	"
p-Xylene	ΔH°	-35.5	-31.3	-35.4	-42.3	-32.9	-37.1	-52.2	kJ mol^{-1}
	ΔS°	-79.7	-62.1	-82.1	-102.5	-79.2	-82.7	-124.6	J K^{-1} mol^{-1}
	R^2	0.99	0.96	0.98	0.99	0.99	0.99	0.99	
	ΔG° (T = 25 °C)	-11.7	-12.8	-10.9	-11.8	-9.3	-12.4	-15.1	kJ mol^{-1}
	ΔG° (T = 55 °C)	-9.3	-10.9	-8.4	-8.7	-6.9	-9.9	-11.3	"

Negative adsorption enthalpy (i.e. $\Delta H^{\emptyset} < 0$), indicates an exothermic process. Adsorption leads to a decrease in the surface energy of the adsorbent, as incompletely bound surface atoms interact with gas molecules (Figure 1.11). The magnitude of the adsorption enthalpy indicates the type of interactions and in all cases the adsorption is consistent with physical (physisorption) and not chemical bond-forming (chemisorption). In the case of strong interactions between the adsorbent surface and gas molecules, a higher enthalpy of adsorption would be expected, and in turn a higher concentration of adsorbate on the surface. The strongest interactions for all adsorbents was found chlorophenyl silica, which achieved the largest adsorption enthalpy for all four vapours. Of the individual BTEX compounds, benzene had the smallest adsorption enthalpies. TEX vapours all had higher enthalpies, but had variability between different adsorbents. For example, enthalpies for chlorophenyl silica are consistently larger for chlorophenyl silica over amino silica. These variances for each BTEX vapour could be exploited for an adsorption based selective gas sensor, as different behaviour provides points of difference that can be interpreted through analysis of PID response. This is discussed in detail in the following chapters.

Entropy was also negative in all cases. When gas molecules are adsorbed and bind to the surface of an adsorbent, the free movement of the molecules is restricted and entropy is decreased. At higher temperatures, molecule are less likely to bind because the gain in entropy outweighs the enthalpy gained from adsorption. This can be clearly seen through comparison of the Gibbs free energy of adsorption at 25 °C and 55 °C. The Gibbs energy ($\Delta G^{\emptyset}$) is more negative at 25 °C than at 55 °C, meaning that spontaneous adsorption is more likely. This is expected and these data indicate that a lower sampling temperature is beneficial for achieving more BTEX adsorption. Significantly, more adsorption means a higher adsorbate concentration and, so long as the adsorption remains reversible, an increased potential for sensitivity improvements.

4.4 Adsorption Patterns Based on PID Response

Due to the design of the Adsorption Device, adsorption can be monitored in real time. Any input vapours that aren't adsorbed are eluted from the sensor via the detection component, where their concentration can be calculated. The adsorption of each BTEX vapour on the seven silica adsorbents was studied. The normalised PID responses during a sampling phase of 15 minutes are shown in Figure 4.7. These responses show the extent and speed of adsorption in the upstream affinity chamber. In most cases, the response plateaus at 1 – the point at which the concentration eluted from the adsorbent chip is the same as the concentration measured during the sample reference phase – which represents the point at which an adsorption equilibrium has been reached. The speed that equilibrium is established correlates to the speed of adsorption. For example, benzene on unmodified, amino and chloro silica reaches equilibrium ($R/R_{ref} = 1$) at ~6 minutes into the sampling phase. At equilibrium no more net adsorption occurs. Conversely, response curves for BTEX vapours on chlorophenyl indicate that adsorption equilibrium is not reached during the 15 minute sampling period, and more adsorbate would likely have adsorbed if the sampling period were continued.

It is important to note that there isn't necessarily a 'good' or 'bad' level of adsorption with regards to the sensing application proposed in this work – so as long as adsorption/desorption can be reversible, multiple sampling cycles can be performed over extended time periods. The key factors are that adsorption is occurring to an extent that it is detectable by the PID, and that the adsorption behaviour for each vapour and adsorbent is *different*. Consequently, there is potential for adsorbents that don't adsorb as much material as other adsorbents to have utility as a sensing material. For example, these data indicate that fluoroalkyl silica adsorbs the least of the BTEX vapours, but the pattern that is produced through that adsorption could provide means for selectivity.

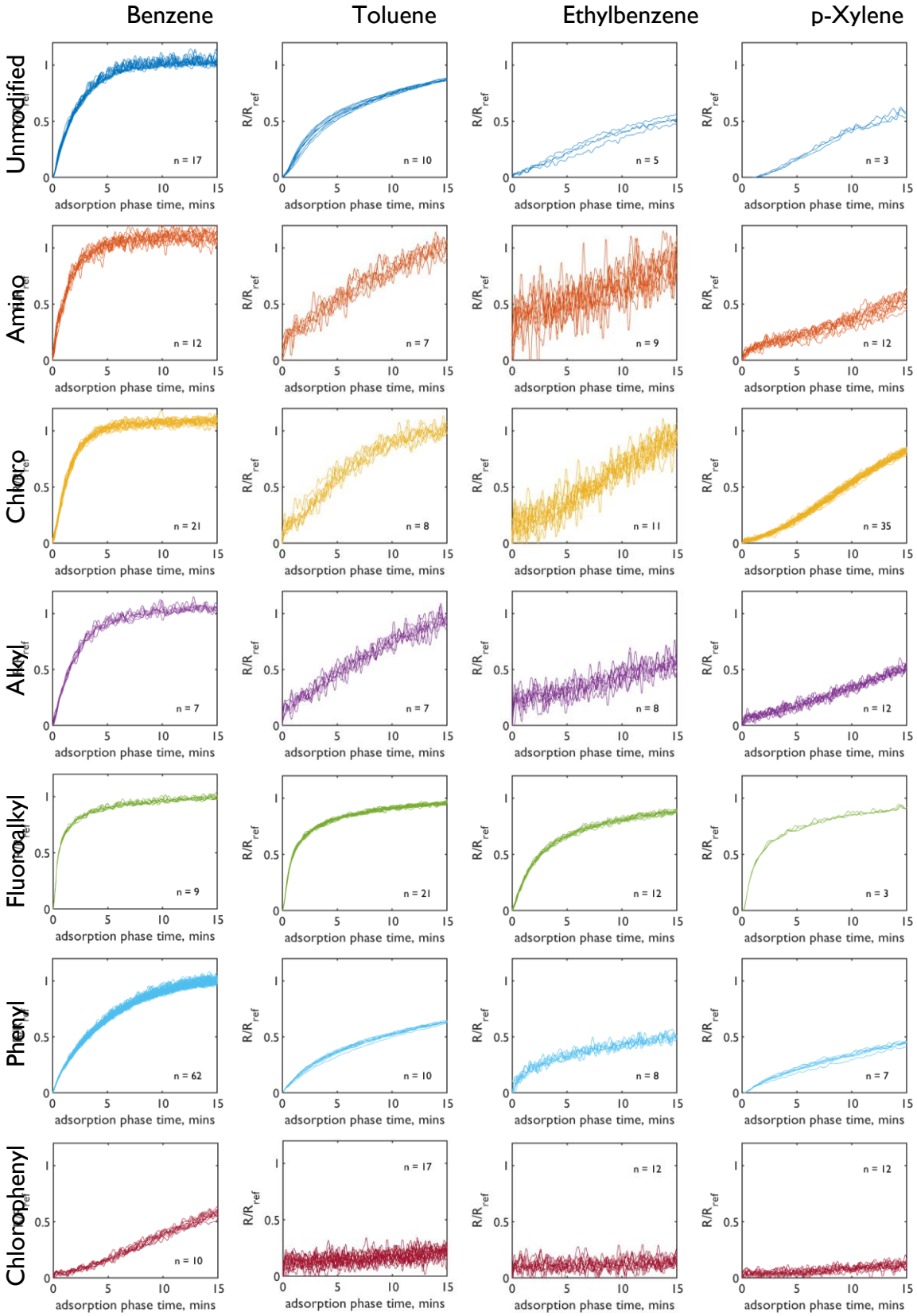

Figure 4.7. Normalised detector responses (R/R_{ref}) during the adsorption (sampling) phase. The adsorbents (t-b): unmodified (blue), amino (orange), chloro (yellow), alkyl (purple), fluoroalkyl (green), phenyl (sky blue) and chlorophenyl (red) silica.

The difference in responses for vapours on each adsorbent can be visualised with Principal Component Analysis (PCA). PCA is a statistical data reduction technique that transforms a set of original variables into a set of weighted linear combinations of the original variables that account for the majority of the variance of the original dataset. The resulting analysis produces a set of principal components, with each component giving a weighting to each of the original variables. These variable weightings can then be interpreted for their inter-relationships by examining the magnitude of the weighting and the sign of the weighting. The input variable for these analyses were R/R_{ref} values taken at 30 second intervals during the sampling phase (Figure 4.8). Corresponding PCA plots are shown per BTEX compound (Figure 4.9) and per silica adsorbent (Figure 4.10).

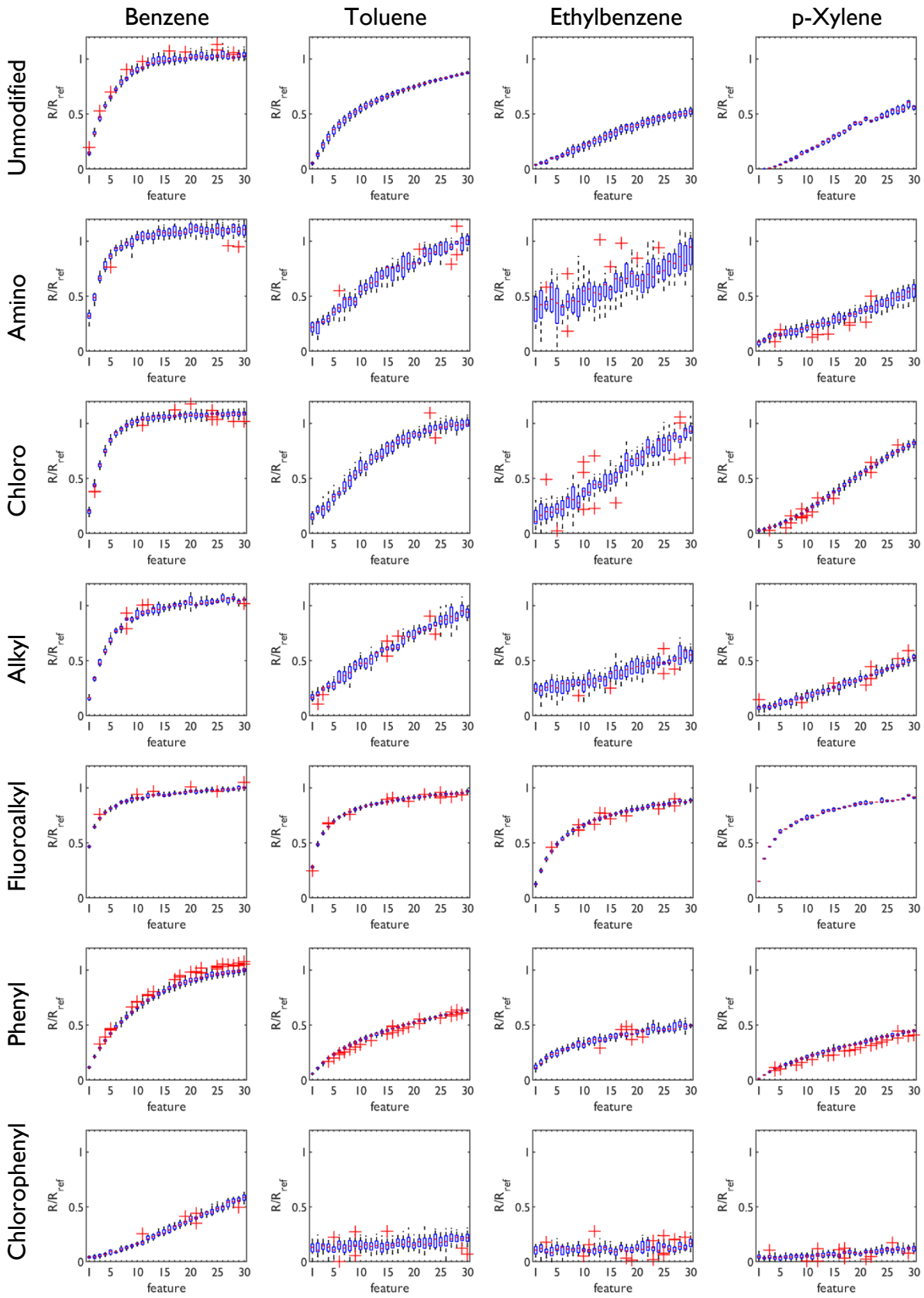

Figure 4.8. Box plots of input variable used for Principle Component Analyses (PCA). Variables were taken as R/R_{ref} values were taken at 30 second intervals during the sampling phase.

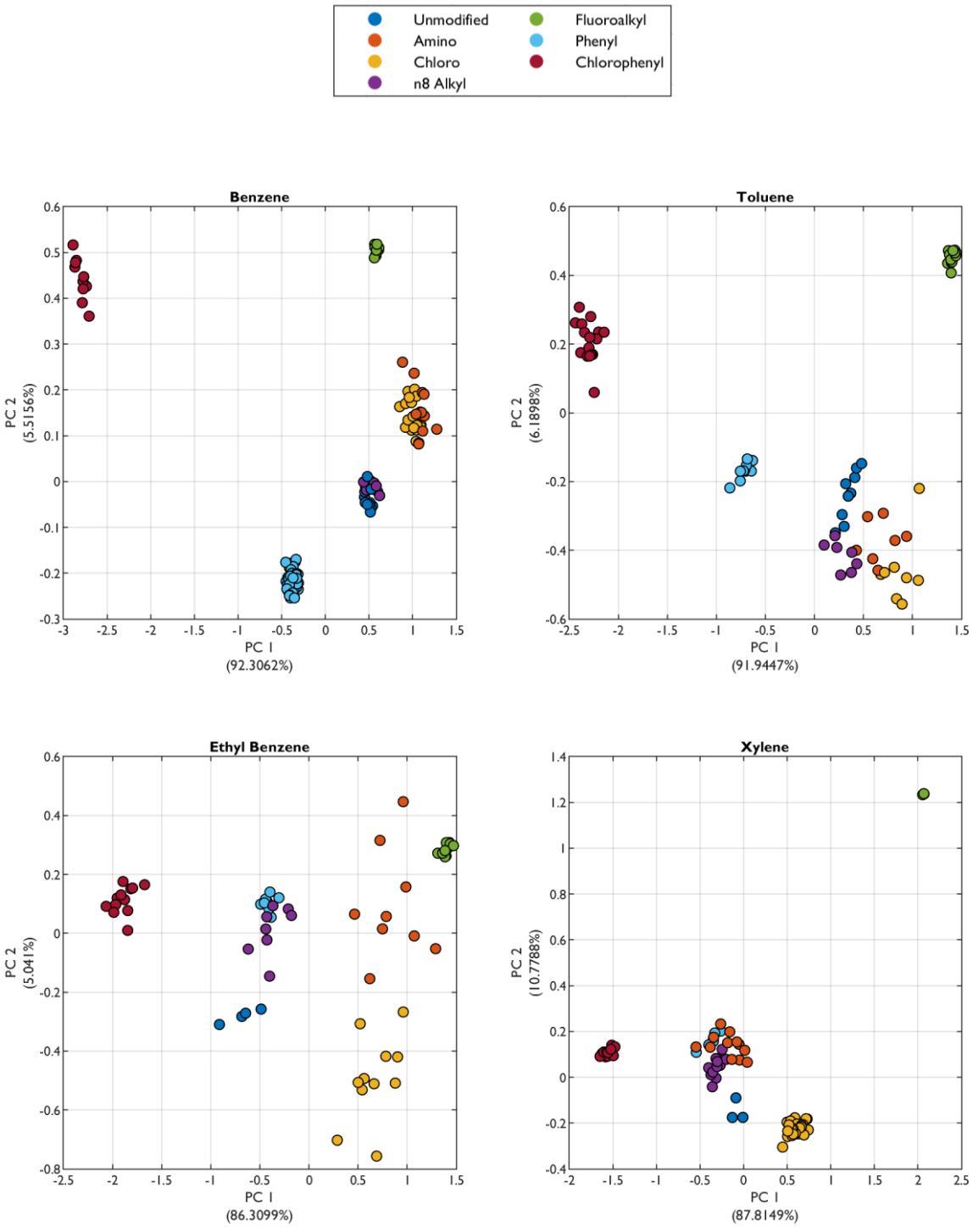

Figure 4.9. Principle Component Analyses (PCA) of the adsorption of benzene, toluene, ethylbenzene and para-xylene on seven silica adsorbents. The normalised response at 30 second intervals of the sampling phase for each adsorbent-vapour combination were used as input values. The explained variance of each principal component is shown in parentheses.

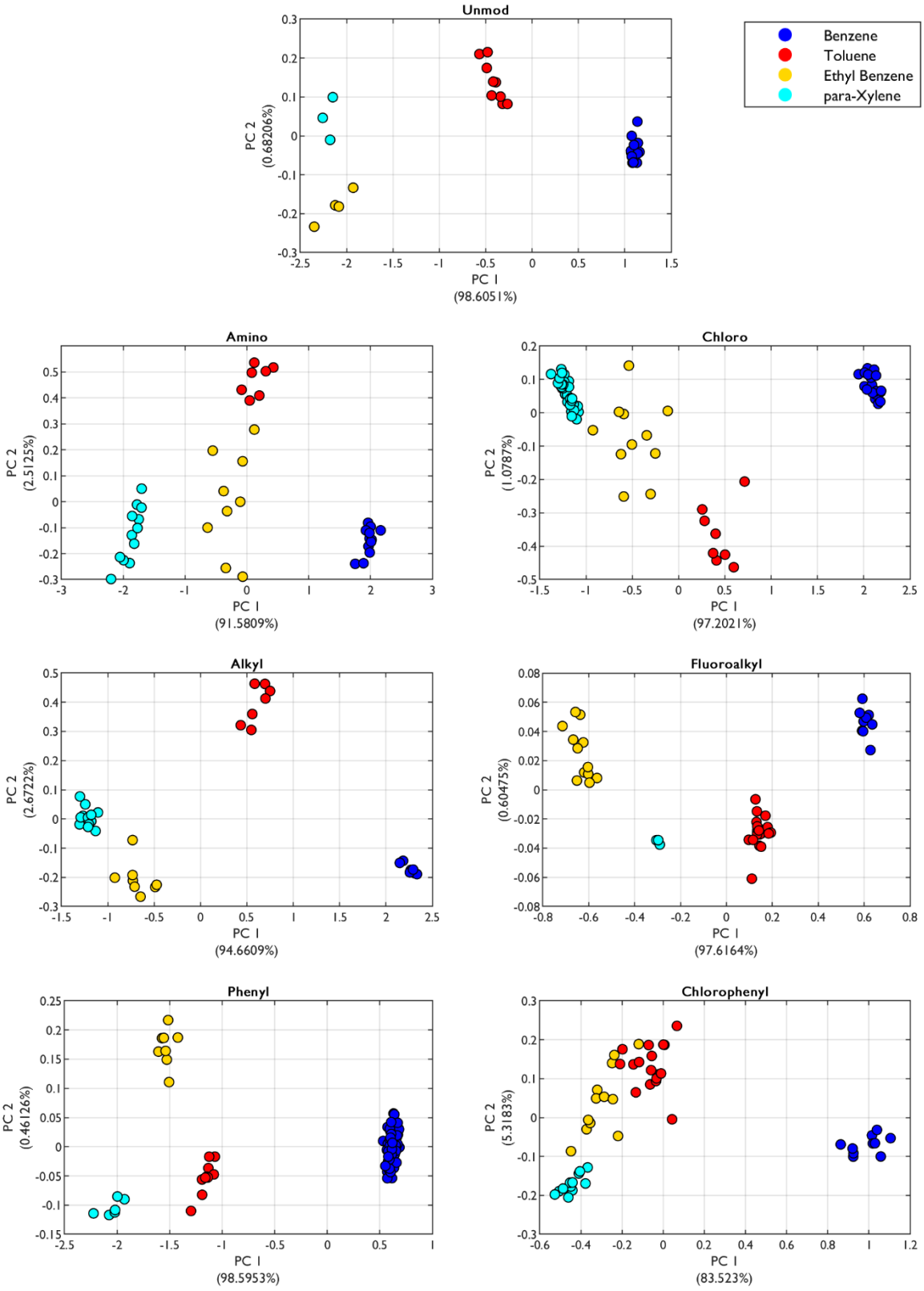

Figure 4.10. Principle Component Analyses (PCA) of the adsorption of benzene, toluene, ethylbenzene and para-xylene on seven silica adsorbents, using the same input variables as Figure 4.9. The explained variance of each principal component is shown in parentheses.

In general, the PCA data points for each adsorbent are well grouped for all vapours, showing that the adsorbent patterns are consistent between test runs. One exception to this is for ethylbenzene, which has more dispersed data for silicas with polar functional groups – amino and chloro silica – which is most likely due to the higher level of noise for these adsorbents. The extent to which the responses from different adsorbents are distinguishable from each other varies across vapours. Chlorophenyl, phenyl and fluoroalkyl adsorbent data are well separated for all adsorbents, with the only exception being the overlap of phenyl and amino silica data for xylene. The reason that these adsorbents produce well separated data in PCA is because they represent the extremes of BTEX adsorption capacity: chlorophenyl adsorbs the most and fluoroalkyl the least. Adsorption behaviour on phenyl silica follows a similar, but less intense, trend to chlorophenyl, hence the PCA data is generally distinct from the other adsorbents. In the case of xylene and amino/phenyl silica, the similar appearance appears to be coincidental. Of the polar functional adsorbents (unmodified, chloro and amino silicas), chloro silica produces the most unique data, especially for xylene vapour. It does, however, overlap with amino silica for benzene and (slightly) for toluene.

In general, there are particular combinations of adsorbents that could provide selectivity for given BTEX vapours. For example, aromatic functionalised silicas (phenyl or chlorophenyl) with polar functionalised silicas (such as unmodified, chloro or amino). This concept is explored in more detail in Chapter 6. The potential for speciation *during* sampling with this technique is limited by the limit of detection of the detector. Normalisation is a key step in the analysis, so when the sample being measured is below the limit of detection of the detector the normalisation is redundant and provides little additional information. An exception could be an indication of noise, which itself could be a diagnostic feature in data analysis. Even if adsorption isn't detected by the PID, it would likely still occur, and will lead to some degree of vapour (pre-)concentration on the adsorbent. Consequently, desorption of adsorbate can still provide information on the sample, which is the focus of the following chapter.

4.5 Discussion

The main focus of this chapter was to investigate the adsorption behaviour of BTEX vapours on the silica adsorbents characterised in the previous chapter. This began with the collection of BTEX isotherms and estimation of quantities adsorbed. In general, the quantities adsorbed correspond to the boiling point of the vapours – xylene (138 °C), ethyl benzene (136 °C), toluene (111 °C) and benzene (80 °C). The quantity of benzene adsorbed was the lowest for all adsorbents, but the amount varied significantly between each adsorbent. Phenyl and chlorophenyl silica appeared to show significant adsorption, likely due to the extra energy stabilisation offered from pi-pi interactions. This analysis agreed with the findings of Liu et al, who found that the quantity of adsorbed toluene vapour on mesoporous silica increased as phenyl group functionality was added, in the pressure range of 0 to 100 Pa.[220] The results of this chapter also agree with previous research by Ncube et al, who, as one part of their study, investigated benzene, toluene and meta-xylene adsorption on mesoporous silica (KIT-6) and APTES-modified KIT-6 at pressures between 400 and 8,000 Pa.[206] They reported the capability for BTEX compounds to have affinity with hydrophilic surfaces, and found that the adsorbed quantity corresponded to the boiling point of the vapours (i.e. xylene > toluene > benzene), as was the case with this work.

In general, most published work on BTEX and VOC adsorption focusses on removing pollutants at high concentrations and pressures. For example, Hong et al have reported the removal of toluene and ortho-xylene using silica gel.[221,222] Although found to be efficient, the concentrations were 12,000 ppm and 4,000 ppm, respectively. As this corresponds to vapour concentrations of 0.4-1.2 %, comparison to the results of this work are difficult. In addition, the availability of VOC adsorption data on modified silica adsorbents is sparse. The results of this chapter build upon previously published data for aromatic- and amino- functionalised silica by examining low concentration adsorption on a range of functional groups. Perhaps the most significant case is the study of a substituted aromatic functional group – chlorophenyl silica – which was found to adsorb relatively large quantities of BTEX. It is proposed here that chloro substitution of the aromatic ring in chlorophenyl silica causes more adsorption through electron withdrawing effects that reduce electron density in the aromatic ring, leading to reduced repulsion between adsorbent and vapour. Although the generalisability of this specific result is limited by having looked at a single substituted aromatic, it suggests that further investigation of different ring substituents may be worthwhile and could potentially offer a route towards effective silica based VOC adsorbents.

A computational study by Coasne et al found that surface chemistry is a key parameter in benzene molecule orientation during adsorption on silica surfaces.[223] It was beyond the scope of this study to investigate how the conformation of vapours influenced adsorption, but it is assumed that ring

substituents would have an impact on adsorptive conformations, and therefore adsorption quantity. BTEX adsorption on fluoroalkyl silica highlighted the need to maintain a high surface area and pore volume with modification. Despite having potentially useful apolar functionality, the low surface area and pore volume led to the adsorbent adsorbing the least of all four BTEX vapours. The previous work of Liu et al suggested that surface area and pore volume effects dominated over vapour-functional group interactions in the pressure range of 100-1,500 Pa.[220] The results of this chapter indicate that the balance of physical features and functionality are important at a much lower pressure range.

Thermodynamic analyses of adsorption at sampling temperatures between 25 °C and 55 °C enabled the estimation of the enthalpies and entropies of adsorption for all BTEX-adsorbent combinations. The study indicated that adsorption in all cases was physisorption, although the magnitude of adsorption enthalpy varied. The values estimated are consistent with those previously reported (i.e. physisorption, approximately 20-60 kJ mol^{-1}), and allowing for small variations caused by differences in pore size and functionality.[220,224] In general, enthalpy was found to correlate to the adsorption capacity observed in the isotherms. For example, chlorophenyl had the largest adsorption enthalpy. Perhaps surprisingly, and despite having the significantly lowest capacity, fluoroalkyl silica was found to have enthalpies and entropies of adsorption of a similar value to other adsorbents. Consequently, this indicates that fluoroalkyl silica may be a useful adsorption materials for sensing applications, provided significant surface area and pore volume can be maintained with modification. Adsorption entropy in all cases was negative, as was the Gibbs energy between 25 °C and 55 °C – signifying that adsorption would occur spontaneously in this range. As expected, Gibbs energy was more negative, indicating more adsorption would occur, at lower temperatures. Although not explored in this work, lowering the sampling temperature of the adsorption channel would be possible with the peltier device. Although this could lead to increased adsorption, it could also lead to increased condensation (of VOCs and water), would therefore likely change the adsorption model.

This chapter also examined the capability of the Adsorption Device to discriminate signals during the sampling phase. Adsorption signals corresponded to the estimated capacities and adsorption enthalpies. For example, adsorption response for fluoroalkyl silica indicated little adsorption whereas chlorophenyl silica indicated the most adsorption. Readings of the normalised photoionisation detector (PID) response for each BTEX-adsorbent combination were examined with Principle Component Analysis (PCA), which indicated that the signals for each combination were discriminable. Owing to the different adsorption behaviour, real-time observation may itself provide a means of selective sensing. Although restricted by the detector limit of detection (during adsorption), additional information provided by desorption analysis could provide a simple and inexpensive means of significantly enhancing sensor selectivity.

Chapter 5 VOC Desorption

5.1 Introduction

This chapter focusses on desorption of BTEX from the library of the seven silica adsorbents. The principle control method for desorption was through the accurate and specific control of the temperature of the adsorbent chip, which was controlled through a programmed peltier module. The chapter begins by exploring the difference between desorption that occurs *spontaneously* from the adsorbents, and desorption that occurs in the response to *thermal* modulations of the adsorbent chip. This leads to the development and application of three different heating profiles – pulsed (on/off heating phases), gradual (exponential increase in chip temperature) and stepwise (gradual three step increase). These profiles are then applied to each of the BTEX-adsorbent combinations. The resulting range of desorption patterns are shown to contain unique properties, which offer a route towards selective detection of BTEX vapours with the Adsorption Device.

5.2 Spontaneous and Thermal Desorption

Desorption of BTEX vapours from each adsorbent was investigated by first sampling each vapour for 45 minutes, followed by a 20 minute period where but the input vapour was switched from the VOC stream to clean air (i.e. 0 ppb VOCs). After this 20 minute desorption phase, the chip was heated (in a single step) to 80 °C in order to trigger thermal desorption of any remaining adsorbate molecules. The response of the photoionisation detector (PID) was monitored throughout all phases of the test cycle. The response during the 20 minute phase immediately following the adsorption sampling phase was named *spontaneous desorption*, and the succeeding 5 minute phase which heated the chip to 80 °C, was named *thermal desorption*.

As discussed in the previous chapters, gas adsorption can be described as an equilibrium between gas molecules (G), adsorption sites (S) and adsorbate (GS), as shown in Eqn. 3.1:

$$G + S \rightleftharpoons GS \qquad \text{Eqn. 3.1}$$

Where the rates of reaction for adsorption and desorption can be represented by Eqn. 3.2 and Eqn. 3.3, respectively:

$$k_a[G][S] \qquad \text{Eqn. 3.2}$$

$$k_d[GS] \qquad \text{Eqn. 3.3}$$

When the input vapour is switched from VOC stream to clean air (i.e. $G = 0$), Eqn. 3.1 shifts to the left such that adsorbate (GS) desorbs to correct the equilibrium. Under spontaneous desorption conditions, the rate of desorption (Eqn. 3.3) is the same as it was during sampling, but for thermal desorption conditions the rate of desorption changes. Examples of the total desorption phase (i.e. spontaneous and thermal) for ethylbenzene from unmodified and phenyl silica is shown in Figure 5.1, together with calculations of the proportion of the adsorbate that is desorbed during the spontaneous and thermal desorption phases.

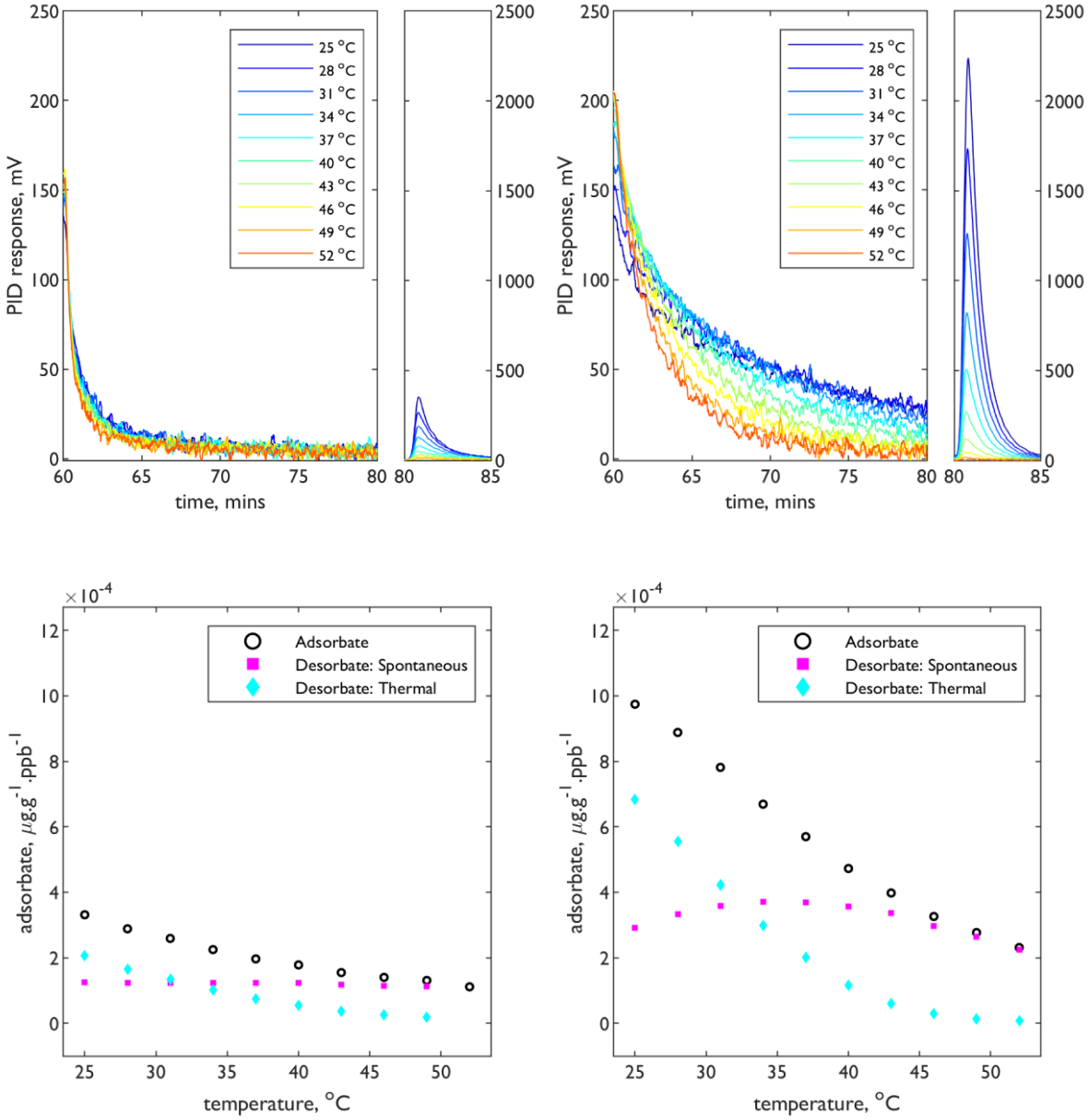

Figure 5.1. *Top* – Photoionisation detector (PID) response during the spontaneous and thermal desorption regions for ethylbenzene from unmodified (left) and phenyl (right) silicas. *Bottom* – Proportion of desorbate measured during each phase for ethylbenzene from unmodified (left) and phenyl (right) silicas. Note the units: mass of *adsorbate* per gram of *adsorbent* per concentration of vapour.

As shown in the previous chapter, more adsorption occurs on phenyl than unmodified silica. The masses adsorbed (i.e. the adsorbate) during the sampling phases for each test run are indicated by the black circles of the lower plots. For unmodified silica at higher temperature test cycles the PID response drops off quickly before reaching a plateau (around 0 mV), indicating ethylbenzene is predominately detected early in the spontaneous desorption phase. This is followed by the lack of a signal in the thermal desorption phase, indicating that all adsorbate has already desorbed. For phenyl silica, there is a similar trend at higher temperatures – a levelling out during spontaneous desorption followed by little to no peak during thermal desorption. Both observations together indicate that at 52 °C the adsorbate molecules are quickly and completely desorbing from the adsorbent to the gas phase without additional heat. At lower temperatures the fall in PID response during spontaneous desorption is flatter, and a clear peak is observed during thermal desorption. This is more pronounced for phenyl silica, which at low temperatures (e.g. 25 °C) retains significant adsorbate even after 20 minutes (of the spontaneous desorption phase).

This analysis was repeated for all BTEX-adsorbent combinations (Figure 5.2). For benzene and toluene, only the aromatic functionalised adsorbents (chlorophenyl and phenyl, for toluene) are able to trap adsorbate beyond the 20 minute spontaneous desorption period. For benzene this appears to be due to the very low quantities of adsorbate retained in the sampling period (shown by the black circles). There is more toluene adsorbate, although, with the exception of amino silica, this all desorbs spontaneously (pink squares) within 20 minutes. Conversely, ethylbenzene and xylene adsorbed on all adsorbents, and, at lower temperatures, thermal desorbate was observed for all adsorbents. Like with benzene and toluene, the aromatic adsorbents adsorbed more vapour and trapped more throughout the spontaneous phase. In general, these results indicate that by controlling the temperature and the *time* of thermal desorption, the rate of desorption from adsorbents can be influenced. In turn this would provide a potential means by which desorption patterns could be used as a means of selective detection. This concept is built upon in the following section, where desorption patterns for different temperature profiles are characterised.

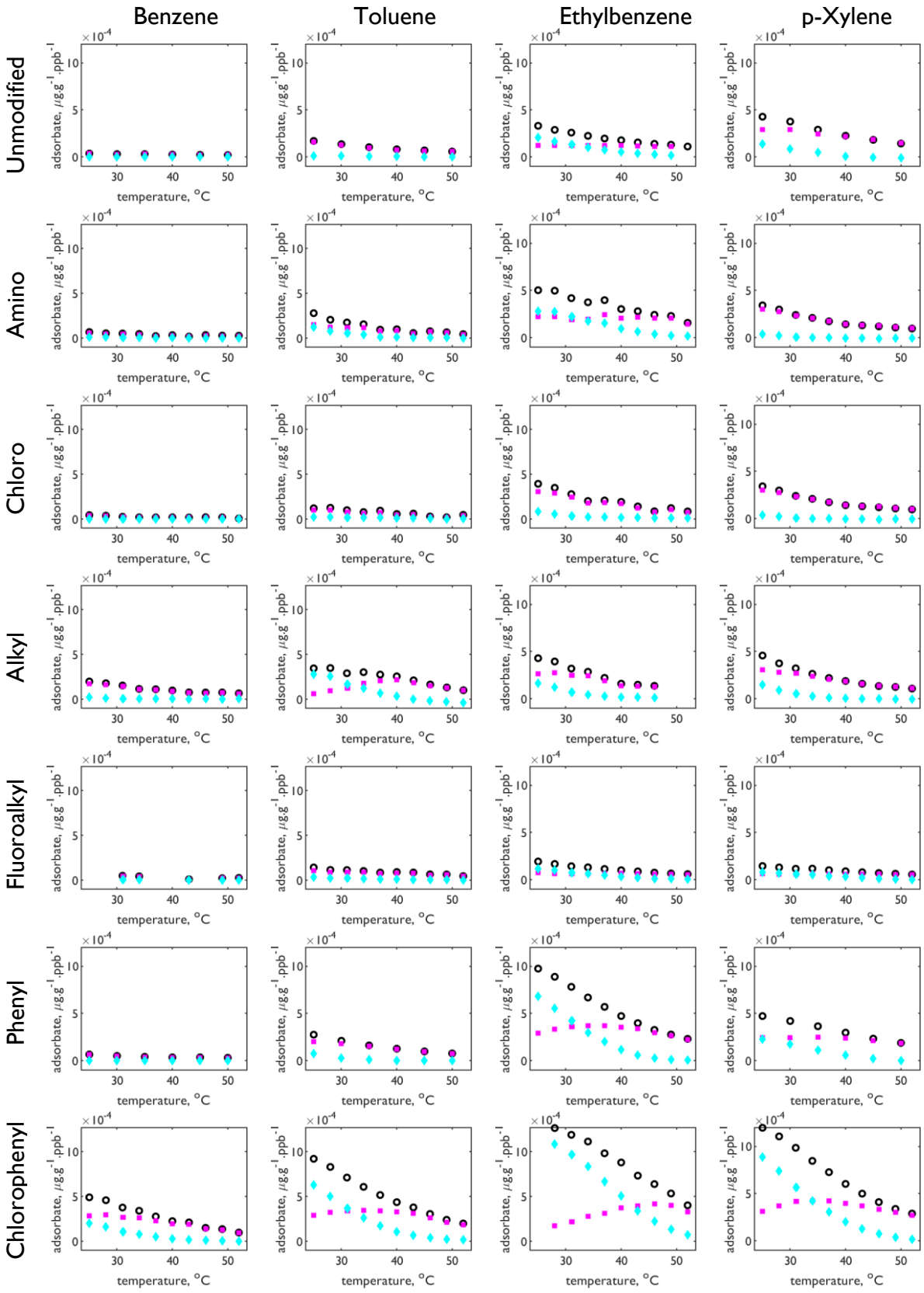

Figure 5.2. Proportion of desorbate measured during the spontaneous and thermal desorption phases for all BTEX-adsorbent combinations. Note the units: mass of adsorbate per gram of adsorbent per concentration of vapour. Note: same legend from Figure 5.1 (lower) applies here.

5.3 Vapour Differentiation

Following from the spontaneous and thermal desorption experiment above, desorption patterns of each BTEX vapour from the seven silica adsorbents were investigated. Spontaneous desorption was not used as specific analysis phase, although a 1 minute delay between the end of the sampling phase and the initiation of heating profile was used. The primary motivation for this delay was to provide time for headspace vapour to pass through the channel. Three heating profiles were developed and used to test the vapour-adsorbent combinations: pulsed (on-off heating steps of increasing temperature), gradual (exponential increase in chip temperature) and stepwise (gradual three step increase), as shown in Figure 5.3. The profiles were applied to all of the BTEX-adsorbent combinations and the corresponding desorption patterns were measured with the photoionisation detector (PID) of the Adsorption Device. With the exception of the thermal desorption phase, the test cycles were identical for each vapour-adsorbent combination. The phase durations and temperatures used are shown in Table 5.1.

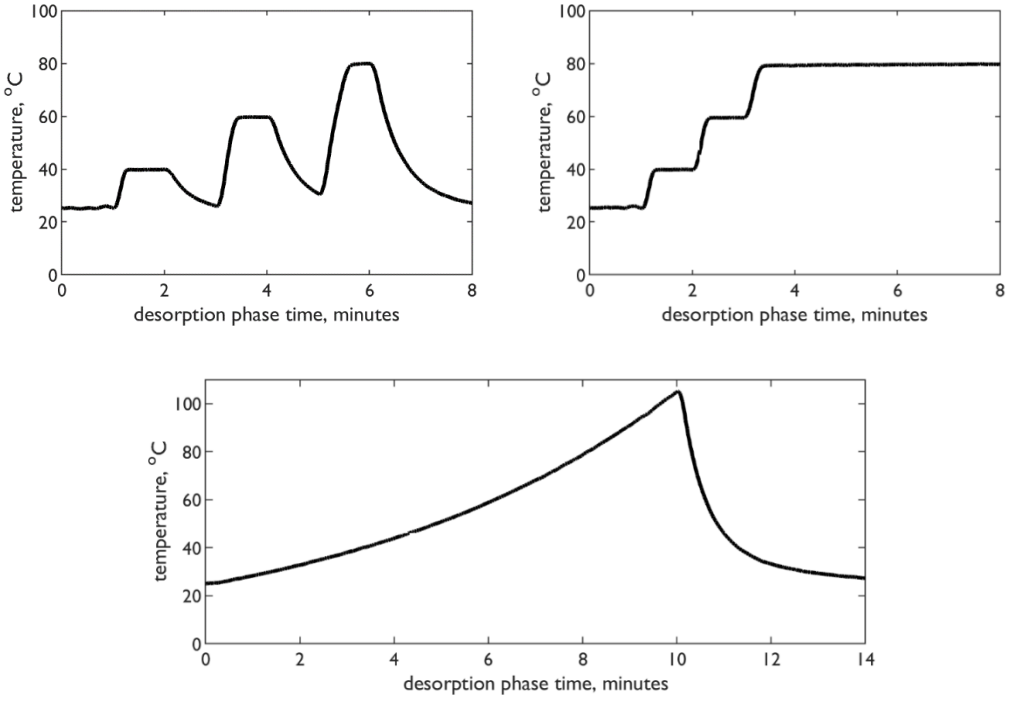

Figure 5.3. Heating Profiles: pulsed (*top left*), step-wise (*top right*) and gradual (*bottom*). The pulsed profile involves three separate heating steps, the first from the sampling temperature (25 °C) to 40 °C, 60 °C and finally 80 °C. The steps were initiated after 1, 3, and 5 minutes of the desorption phase, and the duration of each heating pulse was 1 minute. The stepwise profile involves three consecutive heating steps, from the sampling temperature to 40 °C, 60 °C and 80 °C. The steps were initiated after 1, 2 and 3 minutes of the desorption phase, and the duration of each heating step was 1 minute. The gradual profile involved heating exponentially from the sampling temperature to 105°C over a 10 minute period.

Table 5.1. Test cycle conditions for desorption study

Phase	Duration, mins	Chip temperature set point (°C)
Conditioning	5	80
Sample Reference	5	25*
Baseline Reference	5	25*
Sampling	15	25
Desorption	varied	varied

* chip cooling during this phase

5.3.1 Pulsed Profile

The normalised responses (R/R_{ref}) during the desorption phase for each BTEX vapour on the seven silica adsorbents, when heated with the pulsed heating profile, are shown in Figure 5.4. There is a clear difference between the vapours (comparing vertically) and between the different adsorbents (comparing horizontally). In general, the magnitude of desorption peaks increase in the order benzene < toluene < ethylbenzene ≈ xylene. This indicates greater adsorbate concentration as substitution of the benzene ring increases, and is consistent with the trends of enthalpy of adsorption values calculated in the previous chapter (Table 4.3), i.e. higher enthalpy of adsorption values correlate to more adsorbate, and in turn larger desorption peaks.

These data suggest that, of the four VOCs tested, benzene adsorbs the least. Adsorption is strongest for the chlorophenyl silica, which has clear desorption peaks for all three temperature pulses for all four vapours. Phenyl silica also has significant, but smaller, peaks for all four vapours. Other adsorbents have poor responses for benzene (with a small peak for the 40 °C pulse), but then little to no peak for the subsequent heat pulses. This indicates that a relatively low quantity of benzene is adsorbed during the sampling phase, (and is consistent with the previous section) and any adsorbed species rapidly desorb ≥ 40 °C. The common factor among these other adsorbents is a lack of pi-electron functionality. As discussed in the previous chapter, phenyl and chlorophenyl silicas are able to form pi-stacking interactions with the BTEX molecules (Figure 4.4), and the presence of the chlorine atom in chlorophenyl silica may have an inductive electron withdrawing effect on the aromatic ring that stabilises adsorption.

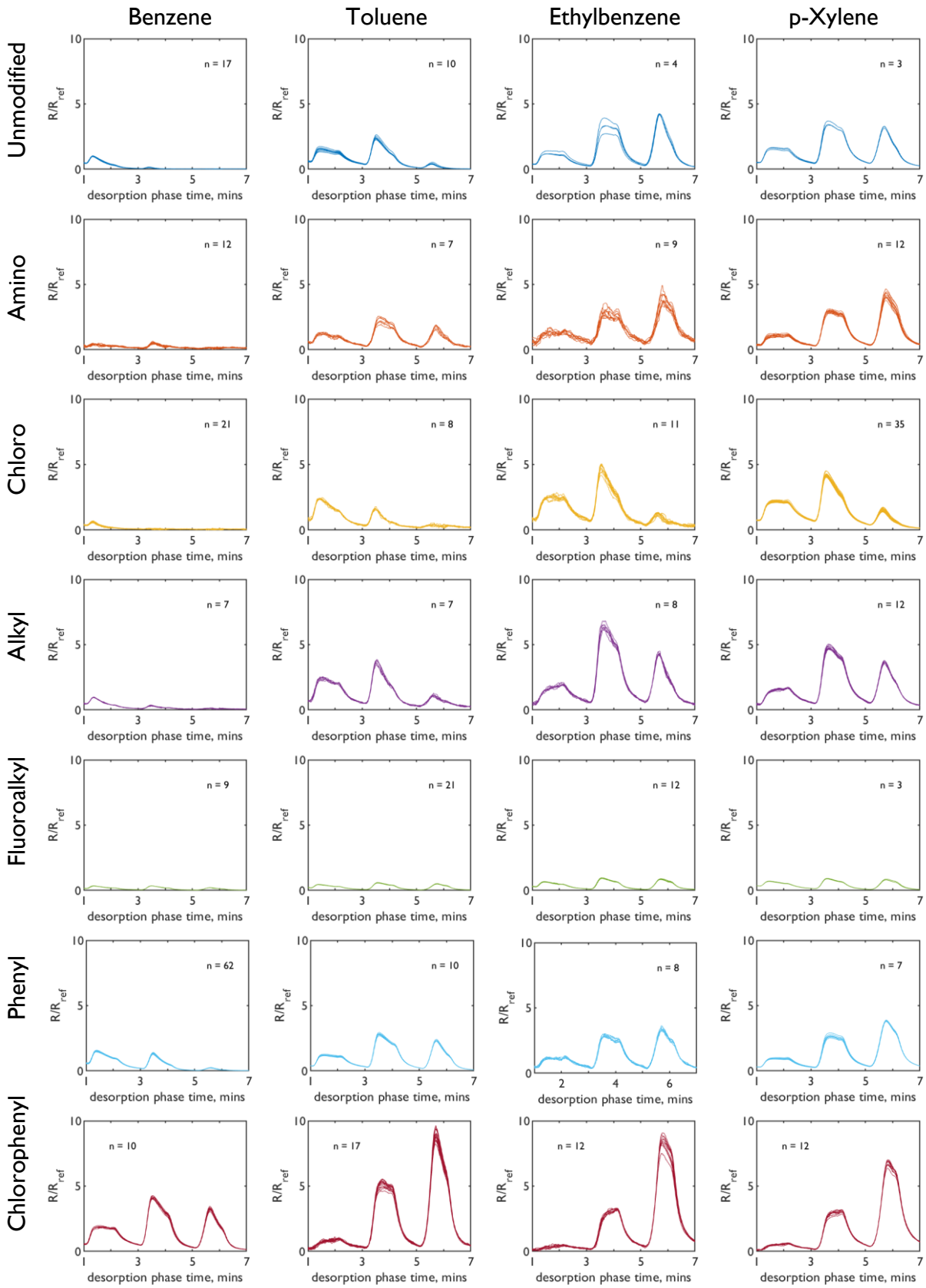

Figure 5.4. Desorption Patterns for all BTEX-adsorbent combinations in response to a pulsed heating profile during the desorption phase. The pulses were 40, 60 and 80 °C, and lasted for 1 minute. The number of repeats (n) is indicated in each plot. R_{ref} was taken as the average signal of the plateau region of the sample reference phase.

Of the adsorbents without functional groups containing delocalised electrons, alkyl silica had the largest desorption peaks, especially for the 60 °C and 80 °C temperature pulses. As shown by water contact angle measurements in Chapter 3 (Figure 3.4), alkyl silica has a highly hydrophobic surface, approximately equal to both phenyl and chlorophenyl silicas (all 121° ± 2°). Due to its apolar surface, alkyl silica is a good adsorbent for apolar and highly non-polar molecules, such as BTEX.[56] In addition, the n8 alkyl chain can freely rotate to form van der Vaals interactions. There is some increase in desorption signal from the polar functional adsorbents (unmodified, amino and chloro silicas) for toluene to ethylbenzene. As the most polar of the BTEX[i] compounds (Table 2.1), it is possible that this creates a slight electrostatic interaction that favours adsorption. Fluoroalkyl silica had consistently poor adsorption for all BTEX vapours. The cause of this is most likely due to the relatively low surface area of the adsorbent (185 m^2/g), limiting the mass of adsorbate trapped during sampling. Critically, the normalised response is approximately, or slightly lower than, 1, which means that vapour detection would be more difficult for this silica at low concentrations.

Feature Extraction and PCA

In order to better visualise the variance in these desorption data, 'features' were taken from the desorption patterns and used in a principle component analysis (PCA). The following features were chosen to form the original variable set of the desorption data above: the median peak heights of the three pulse steps (Figure 5.5); the skewness (a measure of symmetry) of each heating pulse signal (Figure 5.6) and the kurtosis (a measure of 'tailing', i.e. steepness) of each heating pulse signal (Figure 5.7). The latter two were chosen so as to attempt to capture information regarding the rate of desorption during each pulse. For example, a steeper drop-off (i.e. high kurtosis) could represent a faster desorption rate. Looking at the shape of the pattern could provide a simple means of inferring this information. All features were then used as variables for a PCA with each adsorbent (Figure 5.8).

[i] considering only para-xylene in this instance

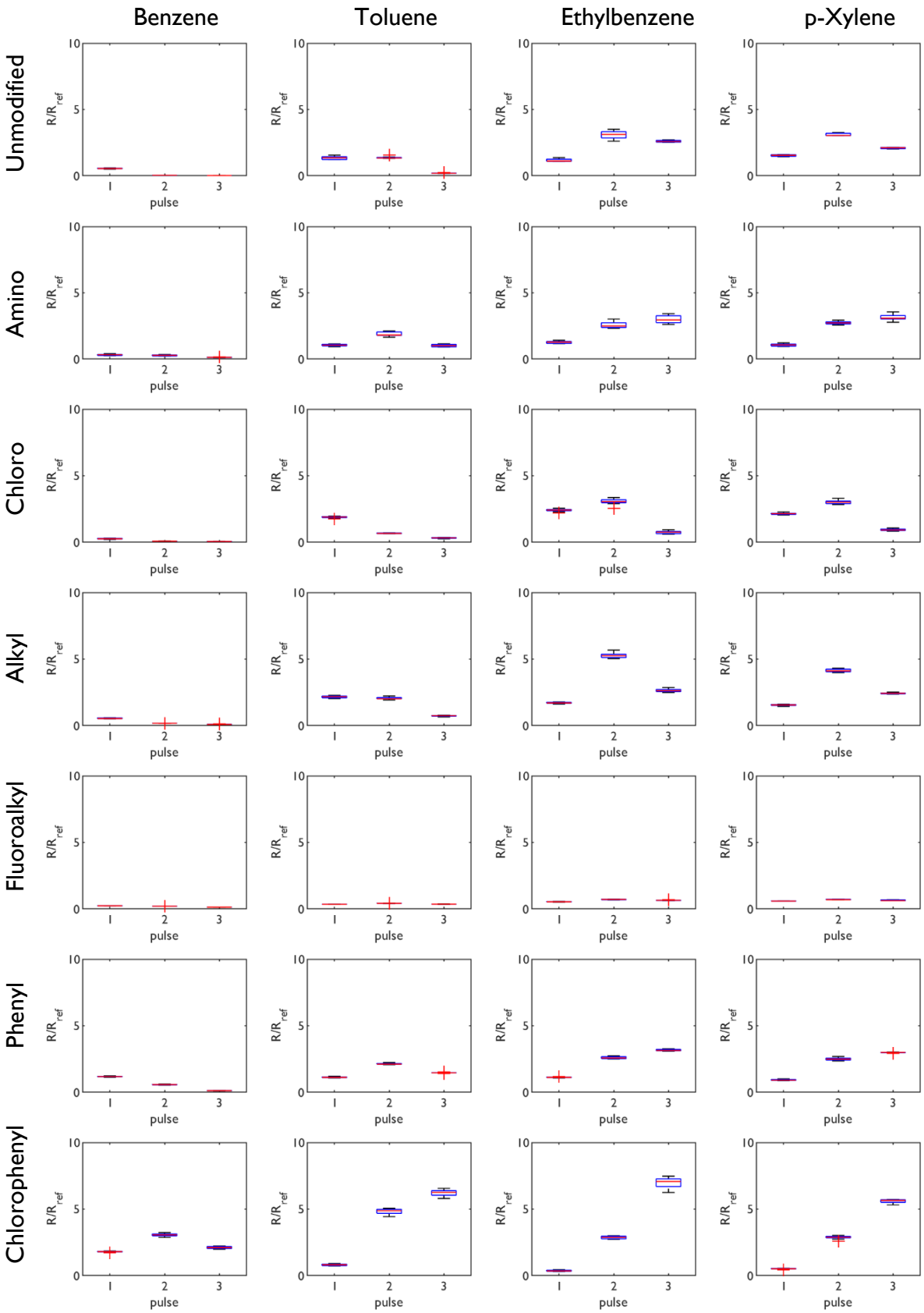

Figure 5.5. Box plots of peak heights, taken as a median of the R/R_{ref} value during each heating pulse. For each box, the central line indicates the median (of the medians, in this case), and the bottom and top edges of the box indicate the 25th and 75th percentiles, respectively. The whiskers extend to the most extreme data points not considered outliers, and the outliers are plotted individually using the '+' symbol.

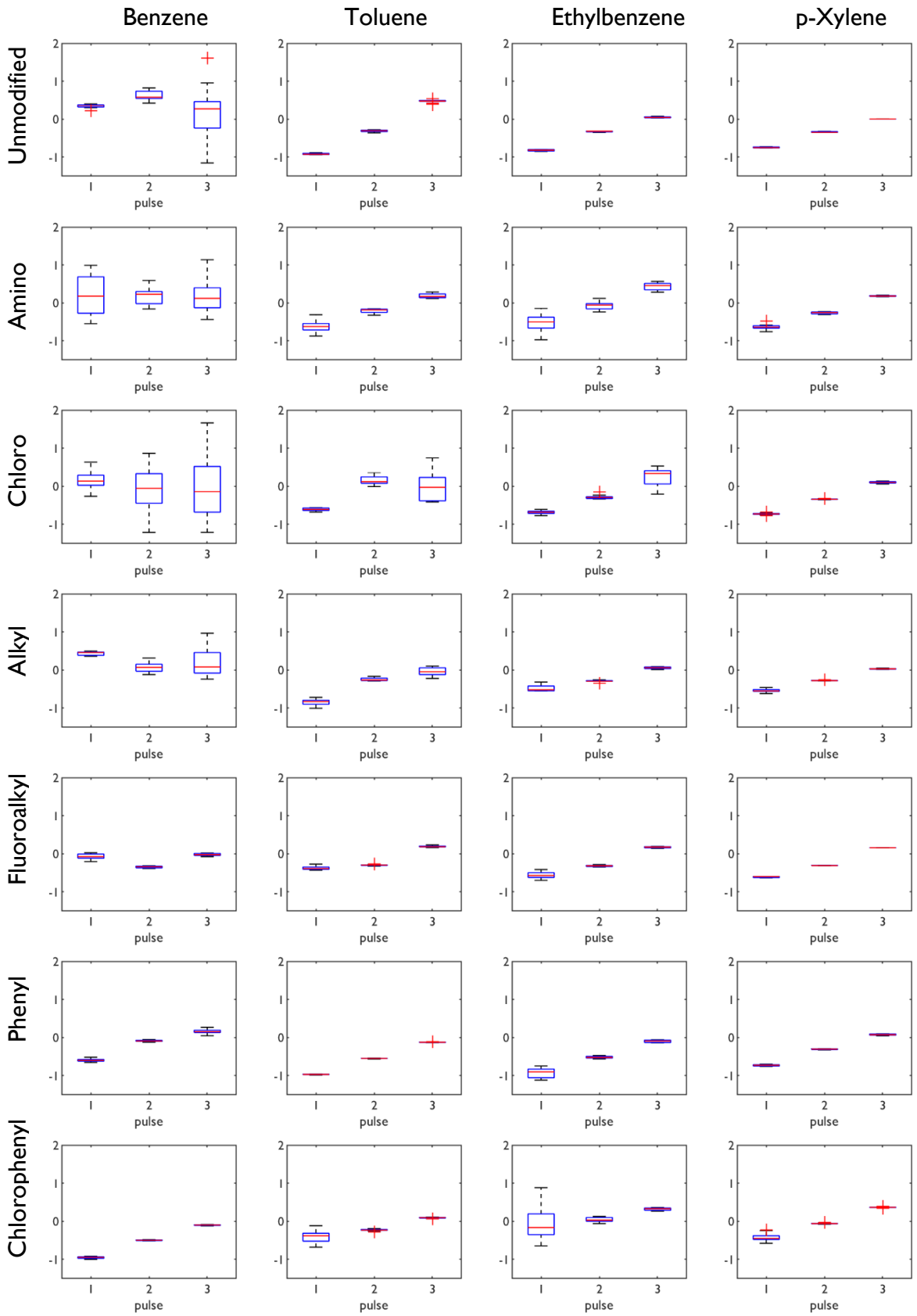

Figure 5.6. Peak skewness, measured during each heating pulse. For each box, the central line indicates the median, and the bottom and top edges of the box indicate the 25th and 75th percentiles, respectively. The whiskers extend to the most extreme data points not considered outliers, and the outliers are plotted individually using the '+' symbol.

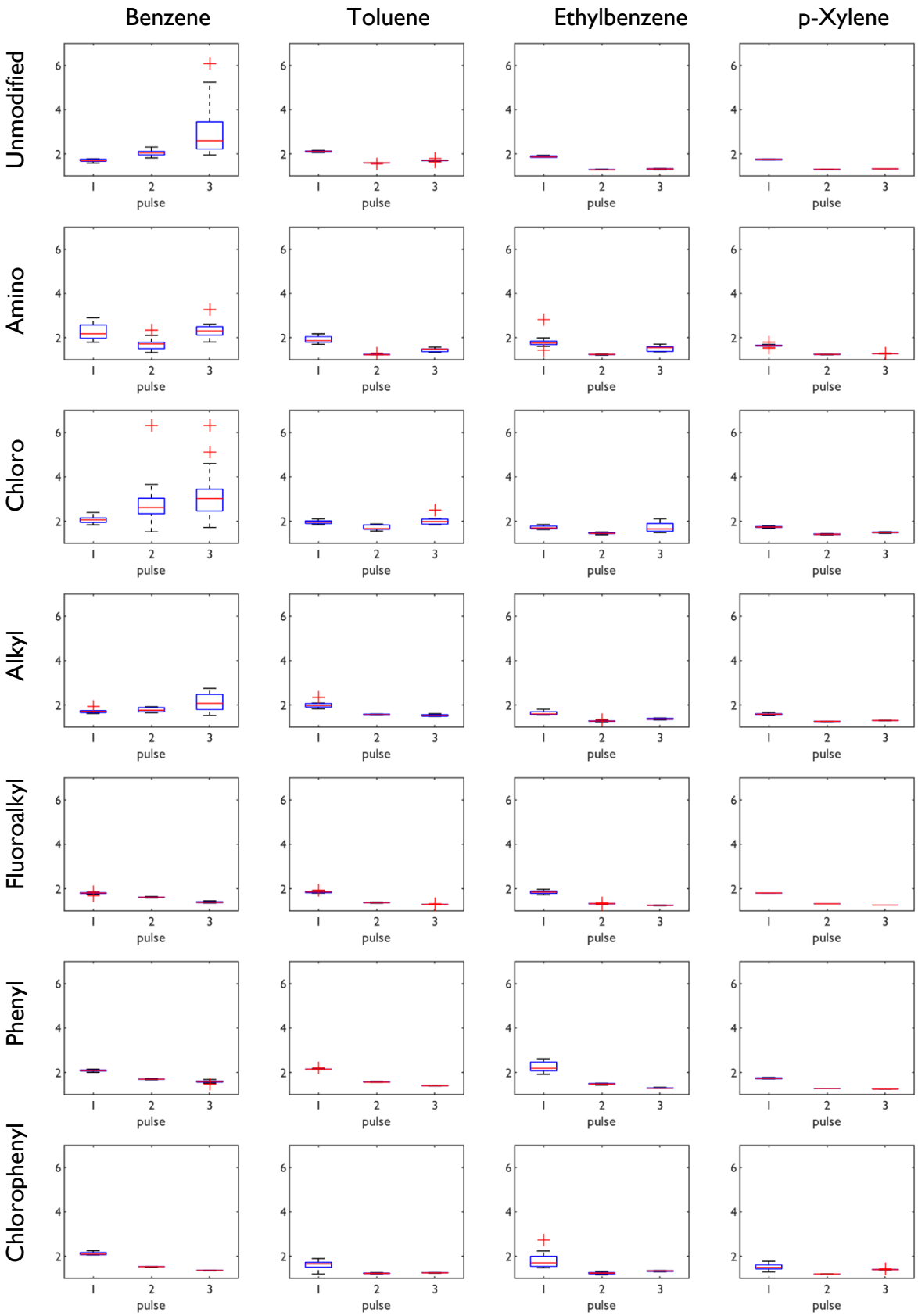

Figure 5.7. Peak kurtosis, measured during each heating pulse. For each box, the central line indicates the median, and the bottom and top edges of the box indicate the 25th and 75th percentiles, respectively. The whiskers extend to the most extreme data points not considered outliers, and the outliers are plotted individually using the '+' symbol.

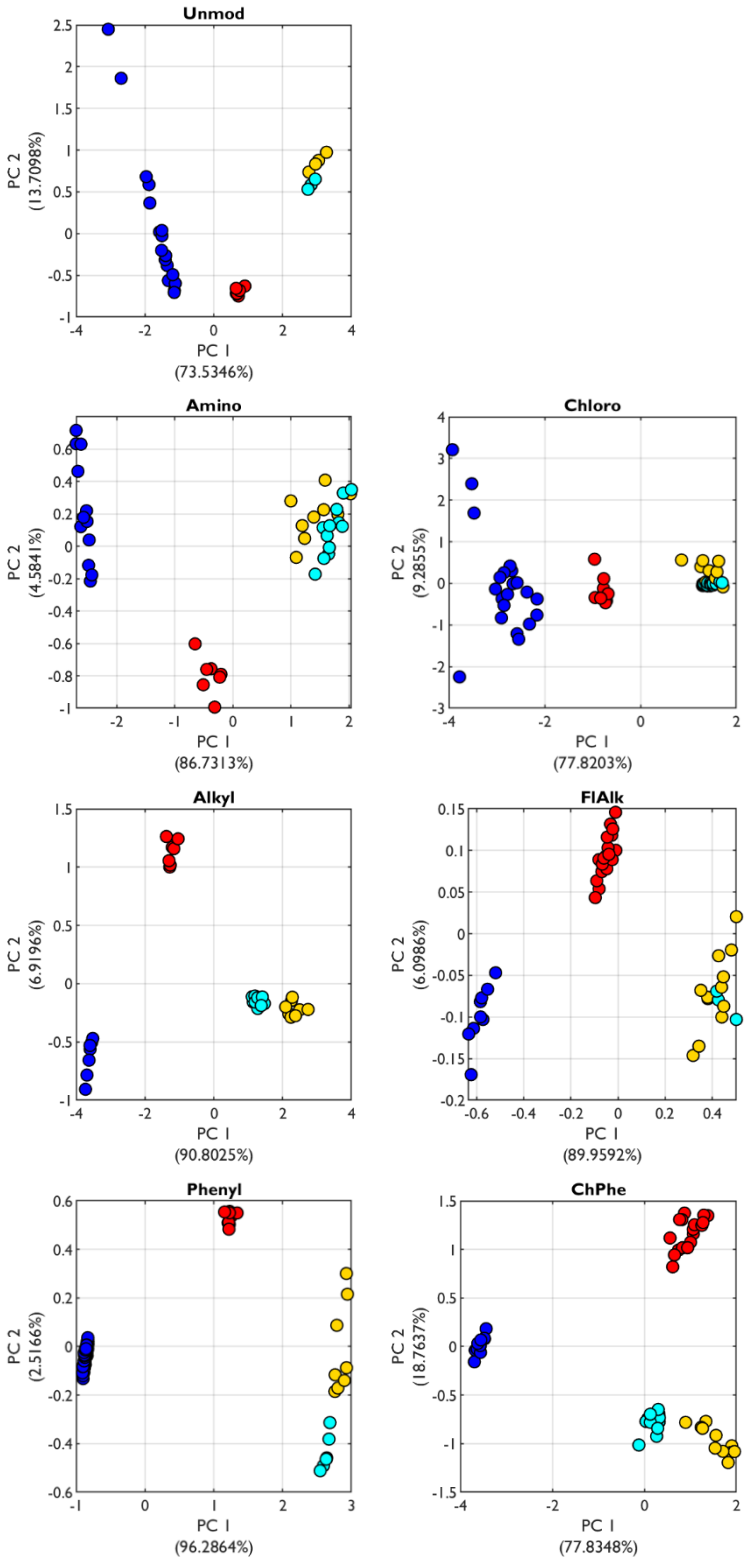

Figure 5.8. Principle Component Analyses (PCA) of the benzene, toluene, ethylbenzene and *para*-xylene desorption phase feature vectors for each adsorbent, in response to the pulsed heating profile. The explained variance of each principal component is shown in parentheses.

These principle component analyses reveal that, in general, the features described above are sufficient to distinguish between BTEX vapours with the pulsed heating profile. For two adsorbents – chloro and fluoroalkyl silica – there is overlap between the feature vectors[ii] of ethylbenzene and xylene vapours. For two other adsorbents – unmodified and amino silica – the feature vector of ethylbenzene and xylene are not quite overlapping, but are very close, so achieving selective detection with these adsorbents may be less effective.

The data points of some vapours form a streaked line along the second principle component (PC2). For example, benzene desorbate from unmodified, amino and fluoroalkyl silica. The common factor among these combinations is that skewness (Figure 5.6) and kurtosis (Figure 5.7) were measured in situations where there was no peak (i.e. no desorbate), for example, the third heating pulse of benzene from unmodified silica. This has the effect of producing a 'random' feature value that, in turn, leads to artefacts in the variance highlighted by PCA.

[ii] Defined as vectors that contain information describing an object's important characteristics, i.e. individual features

5.3.2 Gradual Profile

The gradual heating profile involved the exponential increase in chip temperature, from the sampling temperature (25 °C) up to 105 °C over a desorption phase over 10 minutes. This represents a heating profile more akin to those in conventional GC ovens. The normalised responses (R/R_{ref}) during the desorption phase for each BTEX vapour on the seven silica adsorbents are shown in Figure 5.9. As with the pulsed profile, there is a clear difference between the vapours (comparing vertically) and between the different adsorbents (comparing horizontally). In general, the magnitude of the desorption peaks increase in the order benzene < toluene < xylene ⩽ ethylbenzene. Unsurprisingly, this is a similar trend to the pulsed profile desorption patterns, and is again consistent with the trends of enthalpy of adsorption values calculated in the previous chapter (Table 4.3). This profile provides a more pronounced difference in desorption from phenyl and chlorophenyl silicas. In general, there is a higher response at lower desorption temperatures and the maximum value is lower than for the pulsed profile. For example, the normalised PID response for toluene between 0 and 4 minutes is higher for phenyl silica, but the peak maximum is higher for chlorophenyl silica from 4 minutes onward. This suggests that the adsorbate desorbs more readily from phenyl silica at lower temperatures. With the exception of fluoroalkyl silica, all adsorbents provide a clear desorption curve. Compared to the pulsed heating profile, there is a more distinct difference in appearance for the non-conjugated adsorbents. For example, the time where the peak of the desorption curve occurs follows the order of: chloro > alkyl > unmodified > amino.

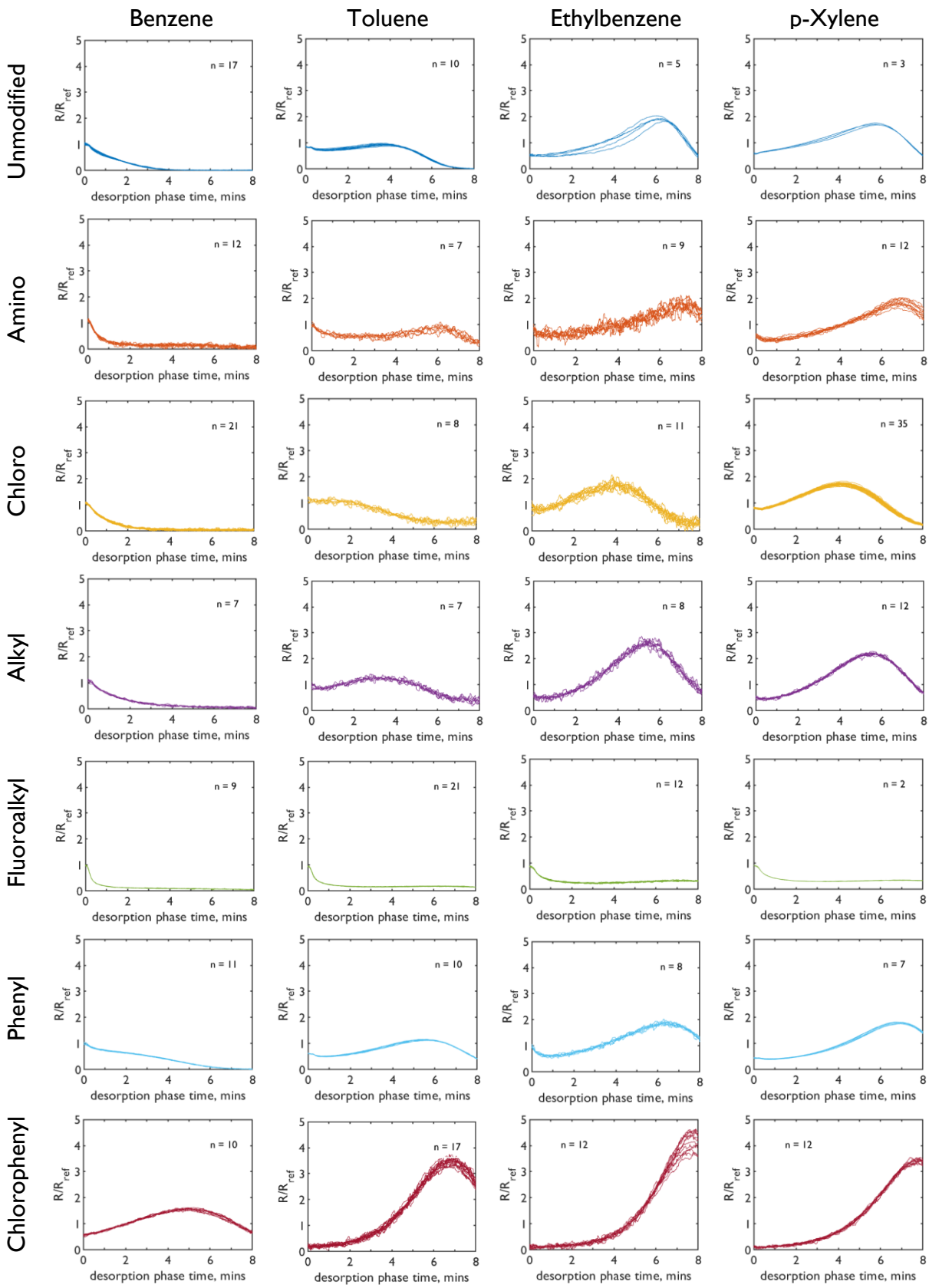

Figure 5.9. Desorption Patterns for all BTEX-adsorbent combinations in response to a gradual heating profile during the desorption phase. The chip set point was increased exponentially from the set point (25 °C) to 105 °C over 10 minutes. R_{ref} was taken as the average signal of the plateau region of the sample reference phase.

Feature Extraction and PCA

Unlike the Pulsed heating profile, the features selected from the gradual profile were based only on time points throughout the desorption phase. For this profile, the normalised sensor responses at 0.5, 1, 1.5, 2, 3, 4, 5, 6, 7 and 8 minutes were selected as features (Figure 5.10). The variance in the desorption profile was again examined with PCA (Figure 5.11). These analyses reveal that the selected features are sufficient to distinguish between BTEX vapours. The separation of the data points for each vapour is more distinct than for the pulsed heating profile. Only amino and chlorophenyl silicas produce some overlap, which is very slight. Unlike the PCA for the pulsed heating profile, there is little to no smearing of data points along either principal component, indicating that the selected features have fewer false features than those selected for the pulsed heating profile. Despite this, the gradual profile is limited by the relatively long time for the desorption phase. Although the 10 minutes could be shortened, which would be necessary for a deployed sensor, this would likely involve significant loss of feature detail.

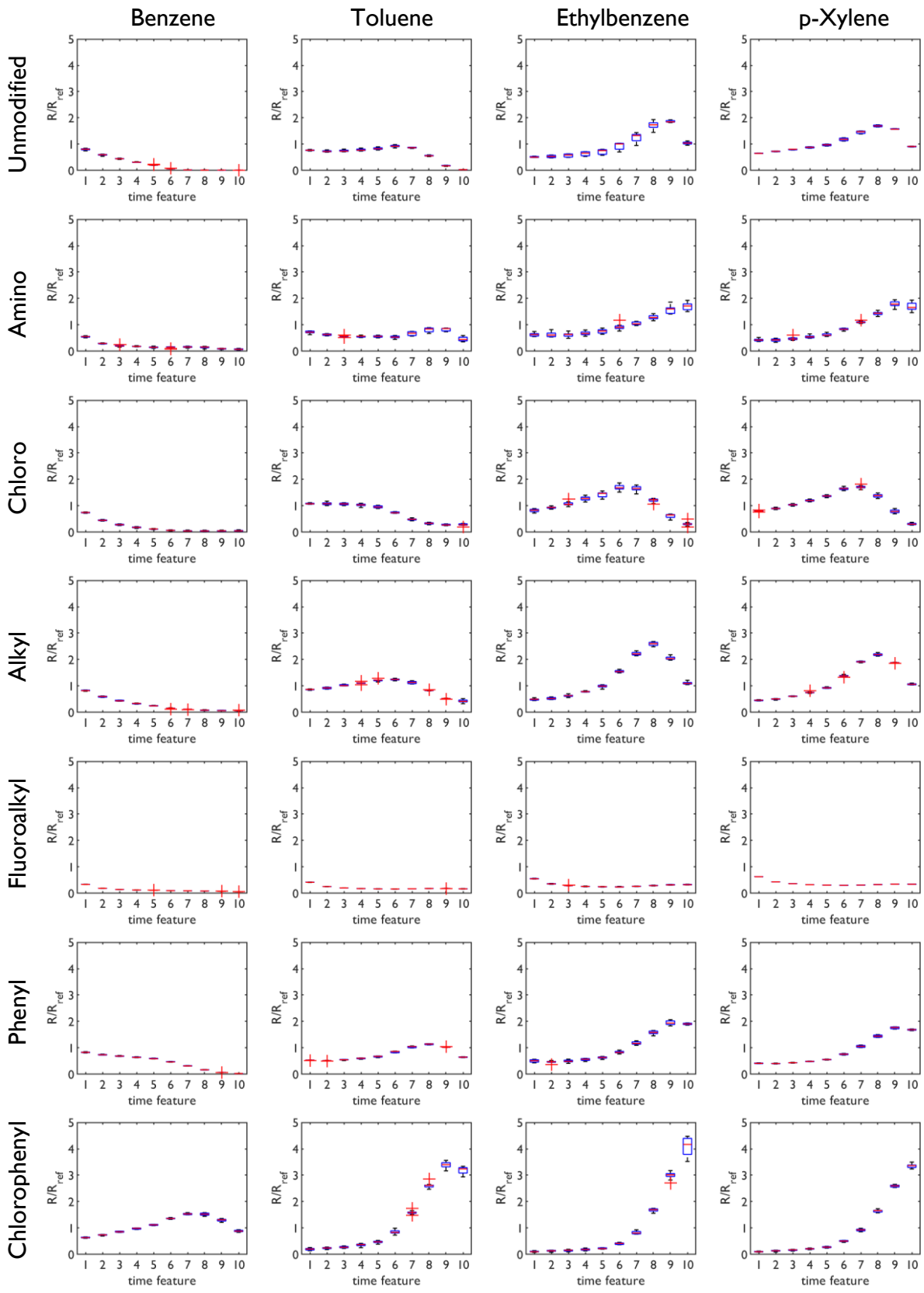

Figure 5.10. Box plots of time features, taken as a median of the R/R_{ref} value at 0.5, 1, 1.5, 2, 3, 4, 5, 6, 7 and 8 minutes. For each box, the central line indicates the median (of the medians, in this case), and the bottom and top edges of the box indicate the 25th and 75th percentiles, respectively. The whiskers extend to the most extreme data points not considered outliers, and the outliers are plotted individually using the '+' symbol.

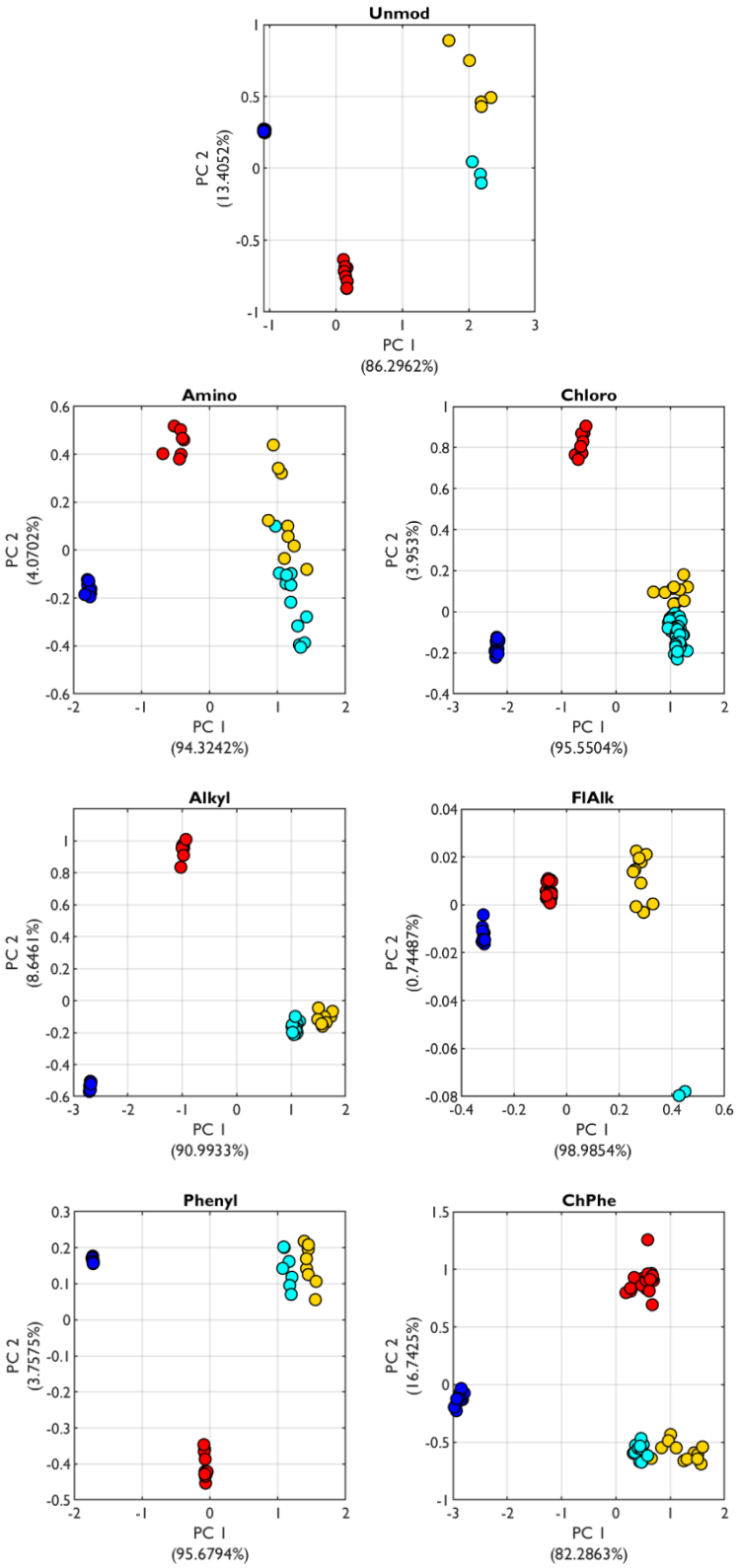

Figure 5.11. Principle Component Analyses (PCA) of the benzene, toluene, ethylbenzene and para-xylene desorption phase feature vectors for each adsorbent, in response to the pulsed heating profile. The explained variance of each principal component is shown in parentheses.

5.3.3 Stepwise Profile

The third and final heating profile developed was the continuous version of the pulsed profile, named 'stepwise'. The same chip temperatures were chosen – 40, 60 and 80 °C – but unlike the pulsed profile the temperature was immediately increased after the preceding step. Once the temperature was increased to 80 °C, it was maintained for 5 minutes, and continued directly into the conditioning phase of the next cycle. The normalised responses (R/R_{ref}) during the desorption phase for each BTEX vapour on the seven silica adsorbents are shown in Figure 5.12. As with the previous two profiles, there is a clear difference between the vapours (comparing vertically) and between the different adsorbents (comparing horizontally). In general, the majority of the trends discussed for the previous profiles apply to the stepwise profile. For instance, benzene again shows the lowest amount of adsorbate, fluoroalkyl silica has the lowest response and chloro silica has the highest. Despite this, there are some subtle differences in desorption patterns. The *magnitudes* of response for toluene, ethylbenzene and xylene are consistent (whereas previously they have shown more variation) and there is a more pronounced difference in the peaks for ethylbenzene and xylene.

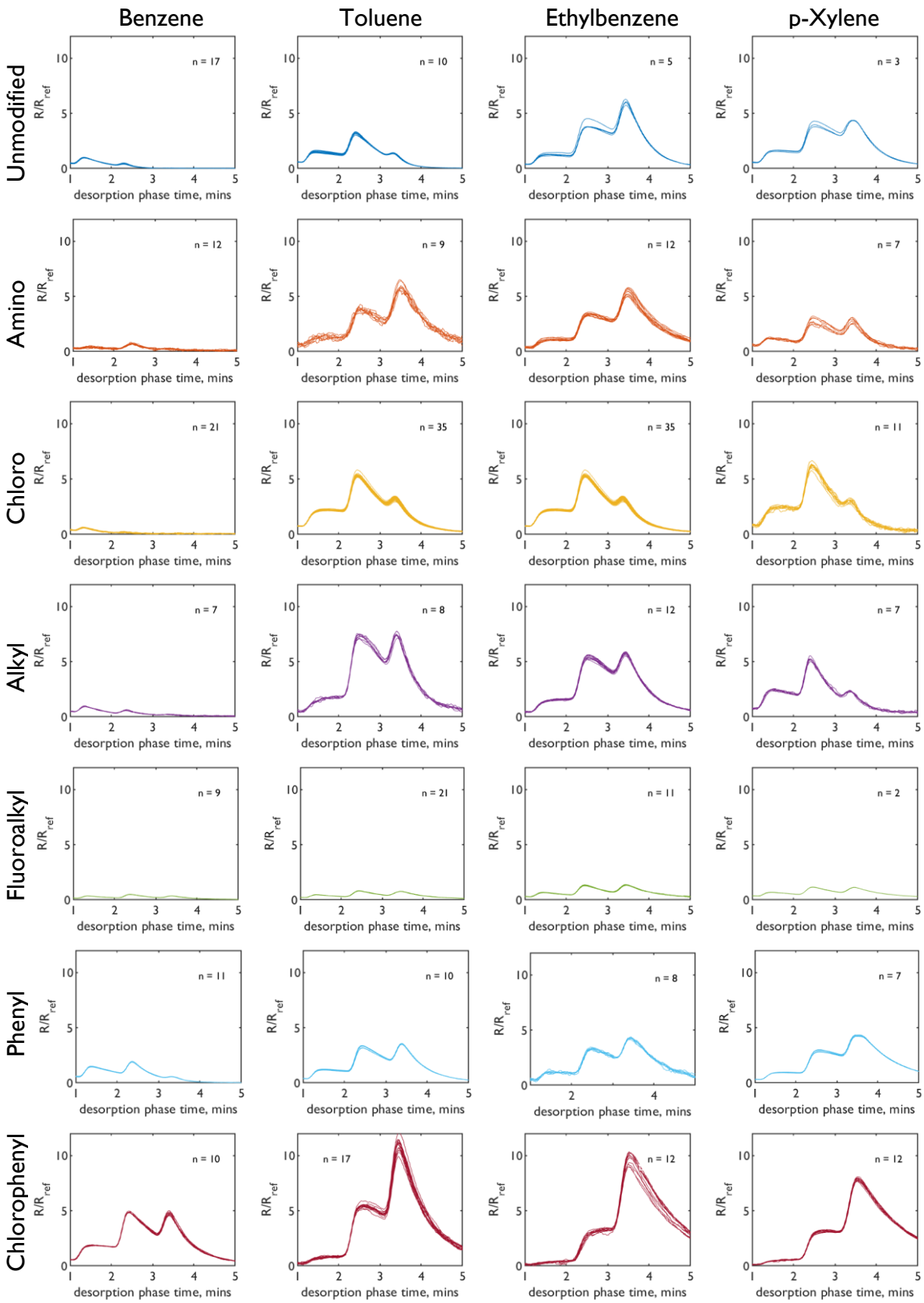

Figure 5.12. Desorption Patterns for all BTEX-adsorbent combinations in response to the stepwise heating profile, during the desorption phase. The pulses were 40, 60 and 80 °C, and lasted for 1 minute. R_{ref} was taken as the average signal of the plateau region of the sample reference phase.

Feature Extraction and PCA

The following features were chosen to form the original variable set of the desorption data above: the median peak heights of the three heating steps (Figure 5.13), and the skewness (Figure 5.14) and kurtosis (Figure 5.15) of each heating pulse signal. The variance in the desorption profile was again examined with PCA (Figure 5.16). These analyses reveal that the selected features are sufficient to distinguish between BTEX vapours. In general, the data points for each vapour are well separated, where only amino silica produces some overlap between ethylbenzene and xylene. As was observed with the pulsed heating profiles, there is some smearing of data points along the second principle component (PC2), indicating that the selected features are capturing artificial variances in the desorption profiles. Following from this repeated observation (having also occurred for the pulsed profile), the selection of more appropriate features, specific to more practical sensor use cases, are discussed in more detail later in the following sections. The stepwise profile is the fasted of the profiles tested, and also ends at a temperature that can be used to ensure the adsorbent is conditioned ahead of the next test cycle, lending itself well to fast continuous monitoring.

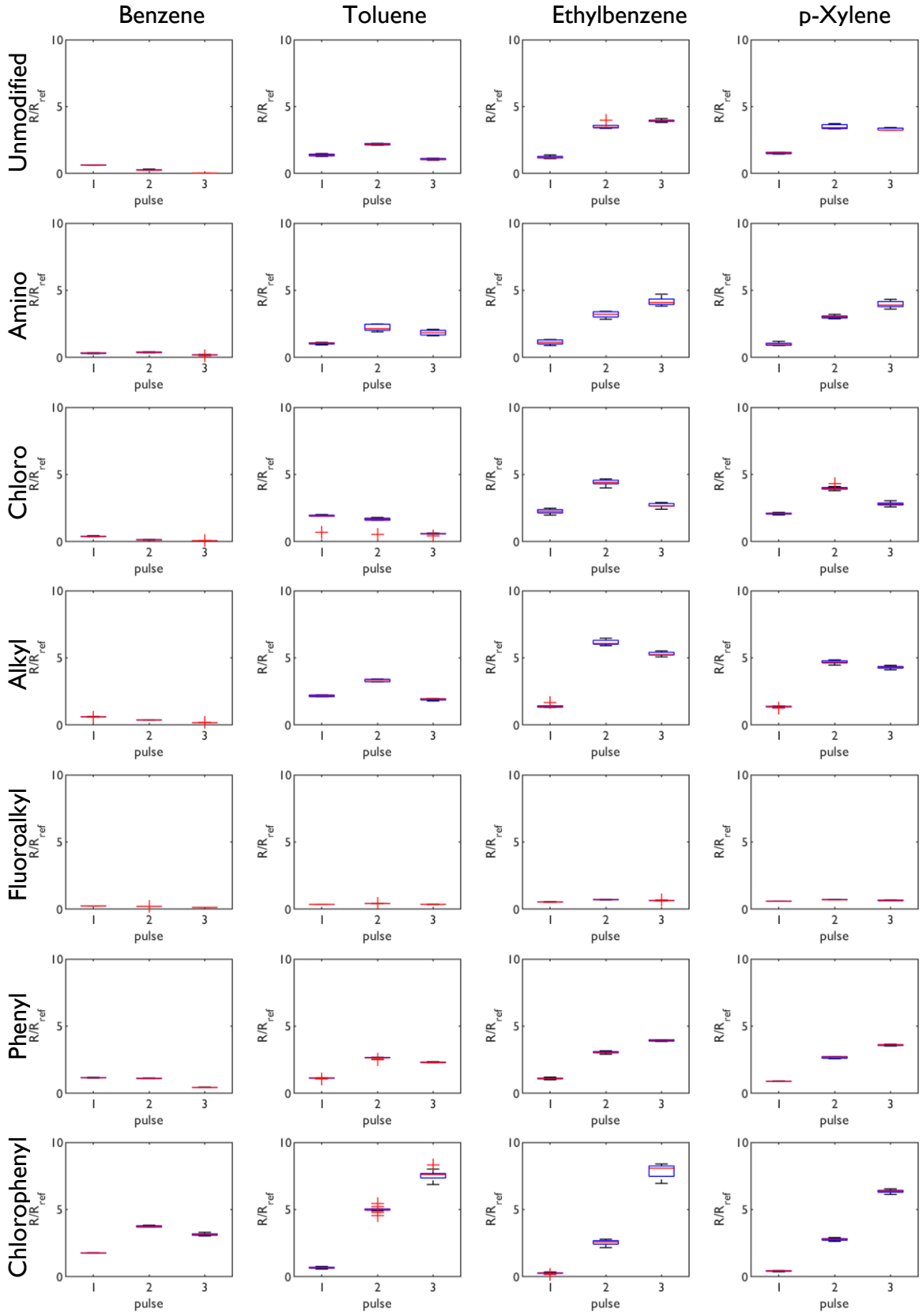

Figure 5.13. Box plots of peak heights, taken as a median of the R/R_{ref} value during each heating step. For each box, the central line indicates the median (of the medians, in this case), and the bottom and top edges of the box indicate the 25th and 75th percentiles, respectively. The whiskers extend to the most extreme data points not considered outliers, and the outliers are plotted individually using the '+' symbol.

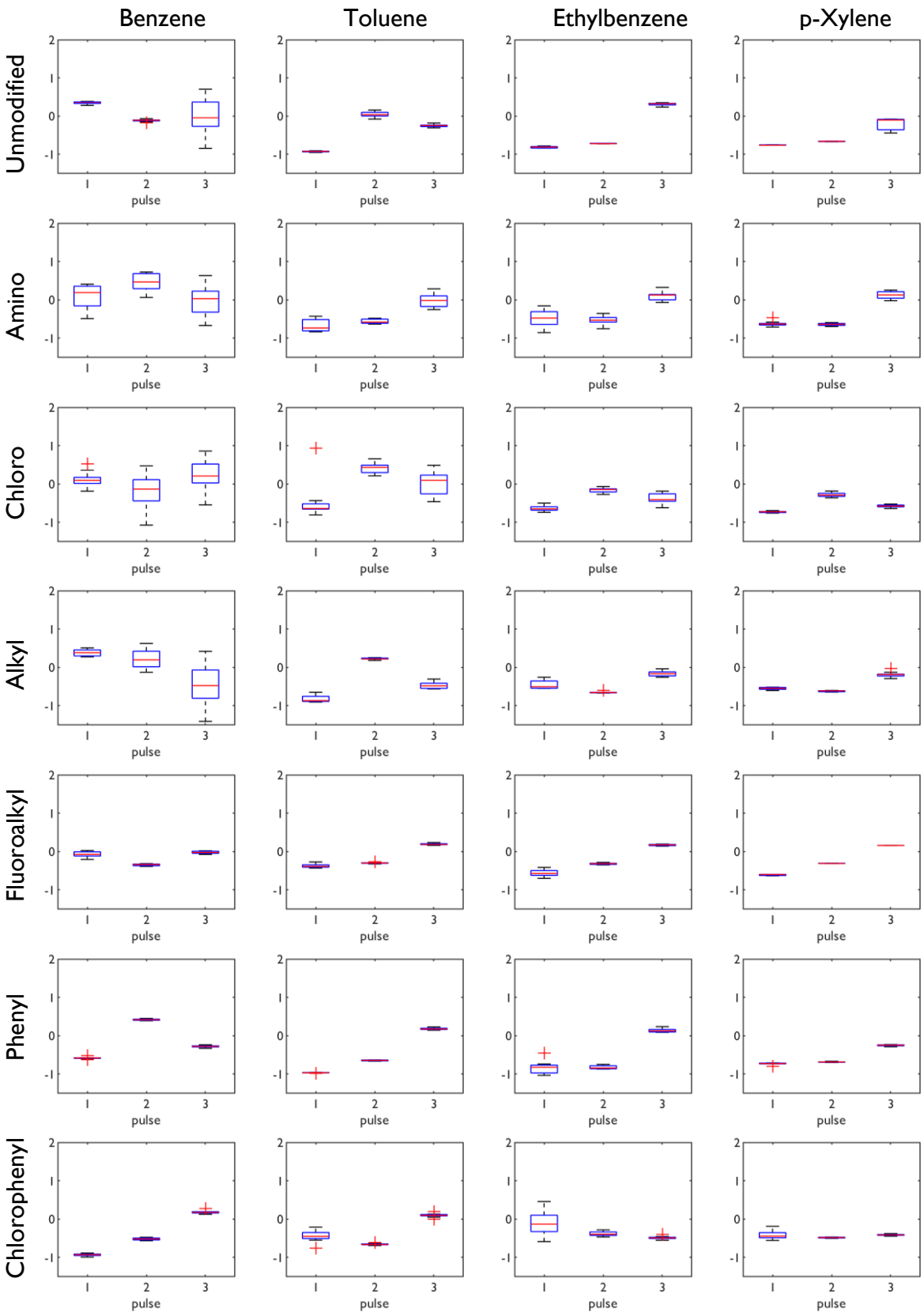

Figure 5.14. Peak skewness, measured during each heating step. For each box, the central line indicates the median, and the bottom and top edges of the box indicate the 25th and 75th percentiles, respectively. The whiskers extend to the most extreme data points not considered outliers, and the outliers are plotted individually using the '+' symbol.

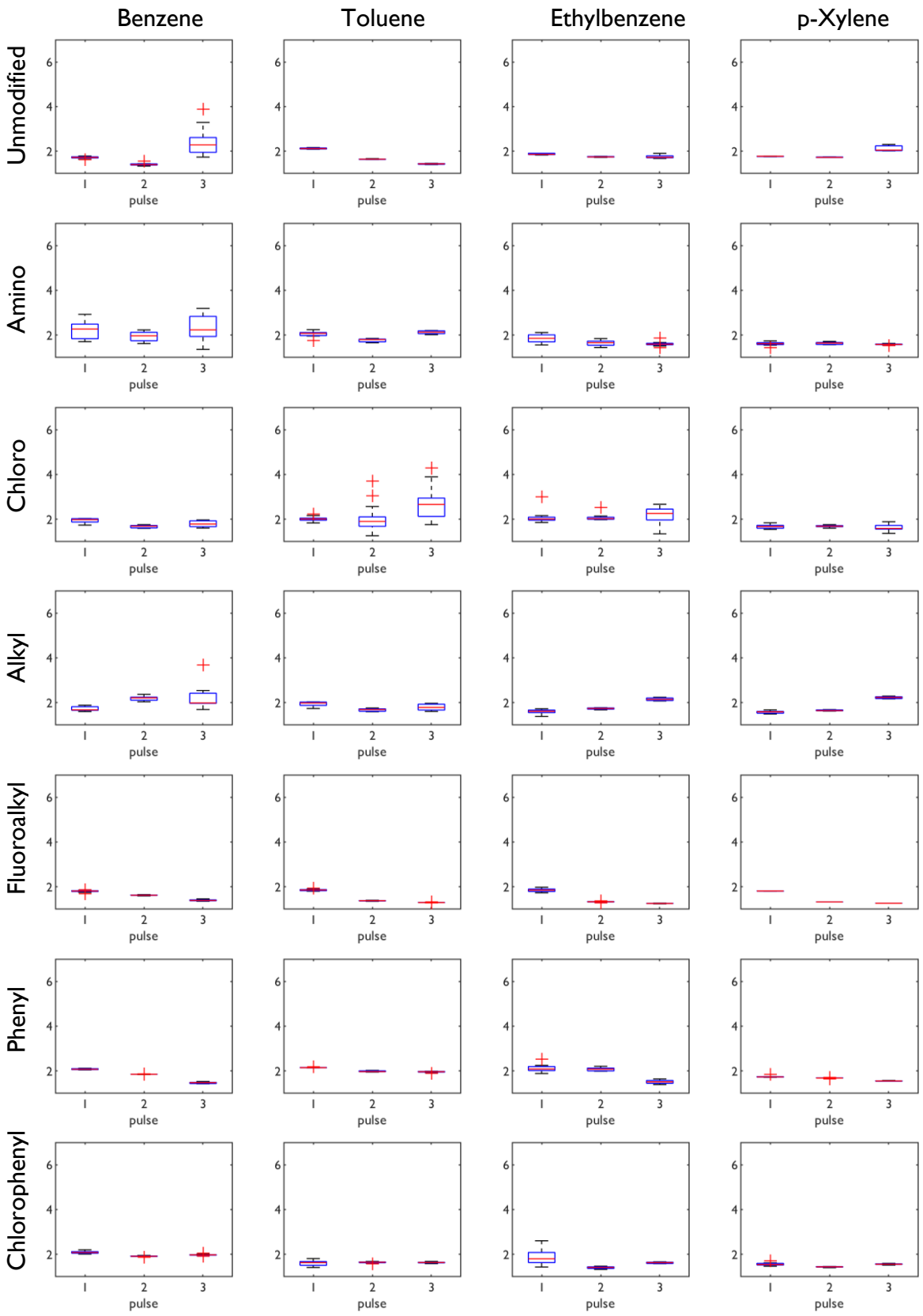

Figure 5.15. Peak kurtosis, measured during each heating pulse. For each box, the central line indicates the median, and the bottom and top edges of the box indicate the 25th and 75th percentiles, respectively. The whiskers extend to the most extreme data points not considered outliers, and the outliers are plotted individually using the '+' symbol.

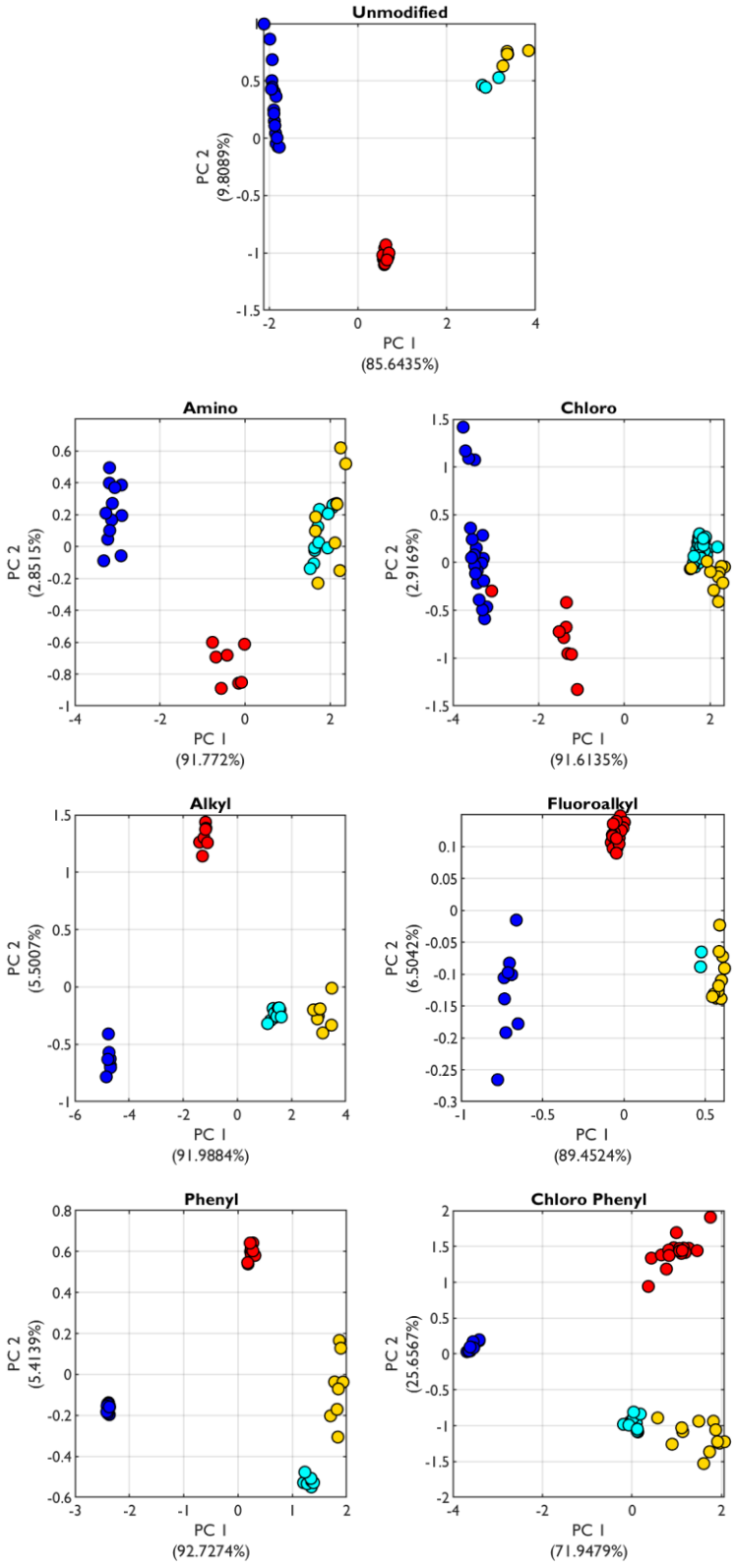

Figure 5.16. Principle Component Analyses (PCA) of the benzene, toluene, ethylbenzene and para-xylene desorption phase feature vectors for each adsorbent, in response to the stepwise heating profile. The explained variance of each principal component is shown in parentheses.

5.4 Concentration Dependence

The primary goal of the introducing desorption profiles was to aid vapour selectivity, rather than concentration estimation, which can be calculated from the (calibrated) PID response (*R*). One of the main motivations for normalising the response to R/R_{ref} was to compensate for differences in concentration of the analyte, therefore allowing for desorption patterns to be used to try and elucidate vapour selectivity, i.e. which vapour, or vapours, are present in the sample? For PIDs, drift manifests as a reduction of signal as the sensor ages and the UV lamp become dirty due to exposure to contaminants in the vapour sample.[225,226] As this approach effectively calibrates the desorption units in each cycle, issues regarding PID response drift over time can also be reduced. A drawback of this approach is that it assumes that the concentration of the sample is maintained throughout the test cycle. To investigate the concentration dependence of the three desorption profiles, each one was tested with benzene at concentrations between 10 and 100 ppb (Figure 5.17).

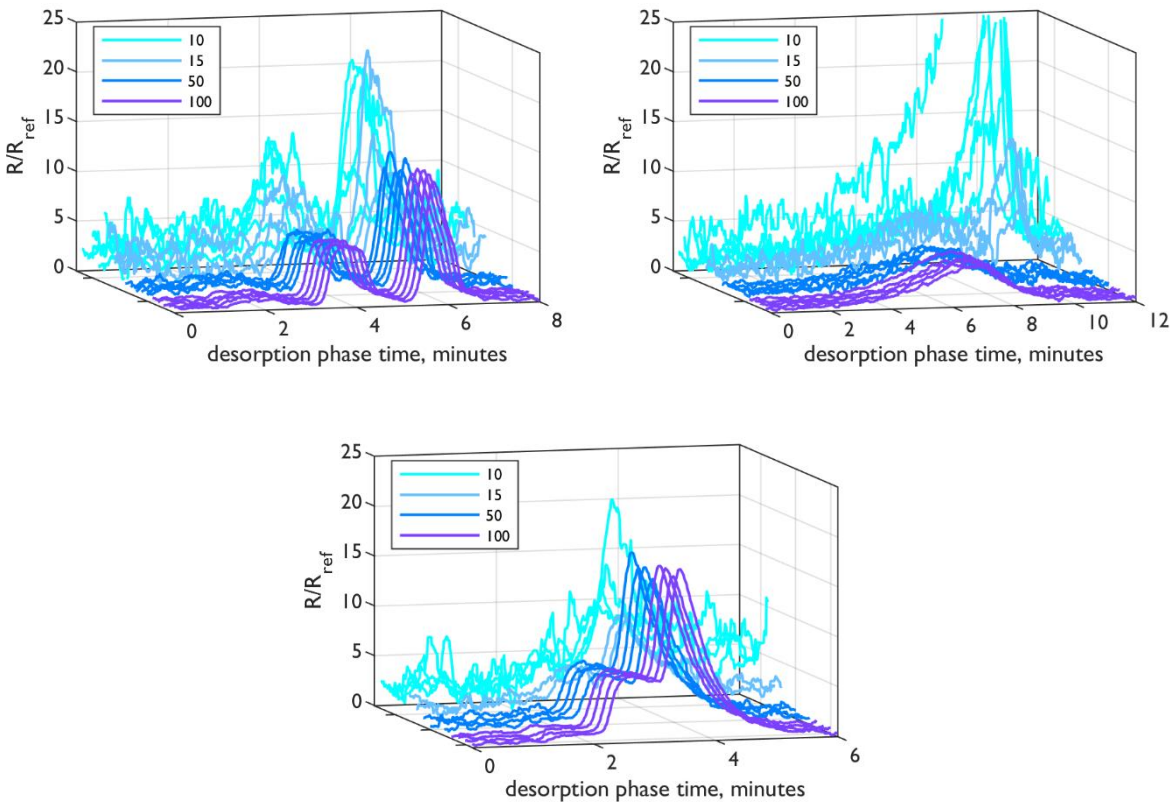

Figure 5.17. Concentration Dependence of benzene for three desorption profiles: pulsed (*top left*), gradual (*top right*) and stepwise (*bottom*). The concentrations of benzene used are shown in the legend of each plot.

For all three profiles, the desorption patterns are consistent for 50 and 100 ppb. However, below 50 ppb, the profiles become significantly noisier. This is likely due to the noise that is captured during the normalisation process. At concentrations below the limit of detection (to standard, i.e. non-concentrated) samples, the reference period and R_{ref} has a high noise-to-signal ratio. Both 10 ppb and 15 ppb samples are below the limits of detection recorded for this sensor (as shown in Figure 2.7), so the level of noise observed is expected. Despite this, there are details within the desorption profile that are consistent with higher concentration samples. For instance, the heating pulses and steps of the respective pulsed and stepwise profiles for low concentration samples are generally matched to the higher concentration samples, indicating that enough vapour is desorbed during these periods to temporarily exceed the LoD of the PID. While still noisy, there are features of the data that could be applied to selective sensing, even at low concentration. This is explored in more detail in the following chapter.

5.5 Discussion

The purpose of this chapter was to explore the extent to which desorption of BTEX compounds could be used to achieve selective detection. The concepts of spontaneous and thermal desorption were introduced, and data shows that some adsorbents (e.g. phenyl and chlorophenyl silica) are able to trap adsorbate for over 20 minutes, whereas for some other adsorbents, vapours desorb quickly and completely. Following from this, three heating profiles – pulsed, gradual and stepwise – were used to thermally initiate desorption. Desorption phase PID data were normalised to the sample reference reading (R_{ref}) and selected features for each profile were analysed with principle component analysis (PCA). These results indicate that desorption control regimes produce different desorption patterns for different vapour-adsorbent combinations. The analysis shows that skewness and kurtosis measures are only of practical use when there is a consistent peak in the desorption pattern. Further data suggests that speciation information is unlikely to be concentration dependent above the direct[iii] limit of detection of the sensor to respective vapours, at least in the concentration range tested.

The results indicate that adsorption is readily reversible under the conditions tested. Adsorbents with efficient regeneration capability would be necessary for an automated sensor that performs multiple test runs sequentially. Even for adsorbents with large and relatively stable adsorption capacities, the adsorbent was successfully regenerated between each run and produced consistent desorption patterns. There has been little previous research on VOC desorption from silica for sensing applications, with a tendency for desorption studies to focus on regeneration of VOC removal devices (e.g. desiccants) and preconcentraters for chromatography. For the former, silica gel has been shown to remove toluene from air at 609 ppm.[166] The study demonstrated that the silica gel desiccant could be regenerated to 80% of the original capacity in approximately 90 minutes by heating to 60 °C. Despite operating at concentrations multiple orders of magnitude lower, the results of this chapter add to such reports by showing that complete regeneration is possible in 10 minutes or fewer by heating up to 105 °C (in the case of the gradual profile). For thermal desorption from preconcentraters, fast desorption (for efficient sample injection into chromatographs) is desired. Therefore, heating is typically both fast and high temperature. For example, in a portable GC, the preconcentrater was heated to 200 °C in 8 seconds, and then the desorbate was injected with the application of 0.07 mL of carrier gas.[45]

In line with the assumption that favourable intermolecular forces would increase the amount of adsorption and slow the spontaneous rate of desorption, the adsorbents with aromatic functionality – phenyl and chlorophenyl silica – demonstrated strong desorption signals for each BTEX vapour,

[iii] i.e. not having been preconcentrated

although signals for benzene were weaker compared to TEX. Although this was largely due to the lower quantities of benzene adsorbed, a strong desorption signal would be important for selective benzene detection, given the low exposure limits, including 17 μg/m^3 (5.2 ppb) recommended by WHO.[35] This also highlights the need, in a sensor using this approach, for relatively high and stable adsorption capacity (while still retaining the capability for facile reversibility of adsorption). While the non-aromatic adsorbents, excluding fluoroalkyl silica, have weak signals for benzene, they have strong signals for TEX compounds. This could allow for efficient detection of those compounds, but a sensor that could employ two or more adsorbents with different signal intensities, such as an aromatic *and* a non-aromatic adsorbent, could have potential as a selective low concentration benzene sensor.

PCA plots for the three heating profiles indicate a similar degree of variance in the feature variables extracted from raw data. However, the profiles vary in the length of desorption period: from 6 minutes for stepwise up to 10 minutes for gradual. This should be taken into account when considering the preference for short sampling times, hence the stepwise profile provides an advantage in this regard. Although the gradual profile did not exhibit the streaking seen in PCA of stepwise and pulsed profiles, these artefacts could be significantly reduced through more appropriate application of the measures such as skewness and kurtosis – i.e. only when there is a peak in the desorption profile. Alternatively, they could be replaces with additional time-based variables that capture the same variability in the data set.

A limitation of this chapter is the varying quantities of adsorbate present on the adsorbents before the start of the desorption phase. Therefore, direct comparisons between different adsorbents, specifically with regards to desorption, should only be viewed in this context, i.e. that valuable desorption information is dependent on an adequate adsorbate to begin with. In addition, the methodological choices were constrained by the temperature range of the peltier module (i.e. approximately 105°C). In the scope of developing a practical BTEX sensor, these results are limited by the relatively long test cycle times – typically longer than 35 minutes – as well as a relatively high concentration of sample – above 500 ppb. While these methodological choices were necessary for this stage of investigation, a gas sensor in the field would likely need to be able to produce results in under 15 minutes and at concentrations in the single to double digit ppb range. Notwithstanding, this chapter has demonstrated that selective desorption offers a promising means of vapour differentiation, and the methods applied are built upon in the following chapter, where selectivity at lower concentrations and faster cycle times is examined.

Chapter 6 VOC Discrimination

6.1 Introduction

The previous two chapters explored the adsorption and desorption of benzene, toluene, ethylbenzene and para-xylene (BTEX) vapours on and from seven silica based adsorbents. Behaviour for adsorption and desorption were found to offer a possible route towards selective detection. This chapter demonstrates how the combination of adsorption and desorption control can be used produce a range of responses from the Adsorption Device. It focusses on testing mixtures of VOCs, and benzene and toluene in particular, beginning with a proof-of-concept of the Adsorption Device, showing how mixtures are able to produce different signals. This is built upon throughout the chapter, testing the three desorption profiles described previously, and moves to testing at low concentrations (i.e. low ppb range) and at test cycle times of 10 and 5 minutes. Emphasis is given to taking feature variable data and using classification algorithms to predict the vapour or vapours that are being sampled.

6.2 Proof of Concept

An initial hypothesis of this thesis was that the adsorption and desorption behaviour of VOCs will vary between different adsorbents. For instance, it was assumed that a polar VOC would have stronger interactions with a polar, rather than apolar, adsorbent. If heat were applied to an adsorbent after sampling with VOCs, the rate of desorption would vary depending on the strength of the interactions between the VOC and adsorbent. In order to further test this assumption with the Adsorption Device, vapours of benzene, toluene, ethylbenzene and methyl ethyl ketone (MEK) were sampled at the concentrations of which are shown in Table 6.1. MEK was chosen due to having a similar boiling (79.6 °C) to benzene (80.1 °C), but opposing polarity. The total sampling time was 30 minutes, and thermal desorption was performed using a pulsed heating profile.

Table 6.1. Concentrations of benzene, toluene, ethylbenzene and methyl ethyl ketone (MEK)

Vapours	**Vapour concentration, ppb**
Benzene	350
Toluene	350
Ethylbenzene	350
MEK	350
Benzene; Toluene	500; 500
Benzene; MEK	500; 500
Benzene; Toluene; Ethylbenzene	1,000; 500; 1,000

Given the boiling points and the polarity of these compounds (Table 2.1), it was assumed that the rate of desorption would follow the order of benzene > toluene > ethylbenzene > MEK, due to the increasing polarity of the VOCs, which would favour strong polar-polar electrostatic interactions between the vapour and the silica adsorbent surface. The complete test cycle for each sample is shown in Figure 6.1, along with the normalised response during the desorption phase. As was observed in the results of Chapter 3, more desorbate is observed when the temperature pulses correspond to the boiling point of the vapour, and the functionality of the adsorbent 'matches' the VOC. For example, in the mono-component benzene sample, the vapour desorbs at 40 °C, but toluene mostly desorbs at 60 °C or higher.

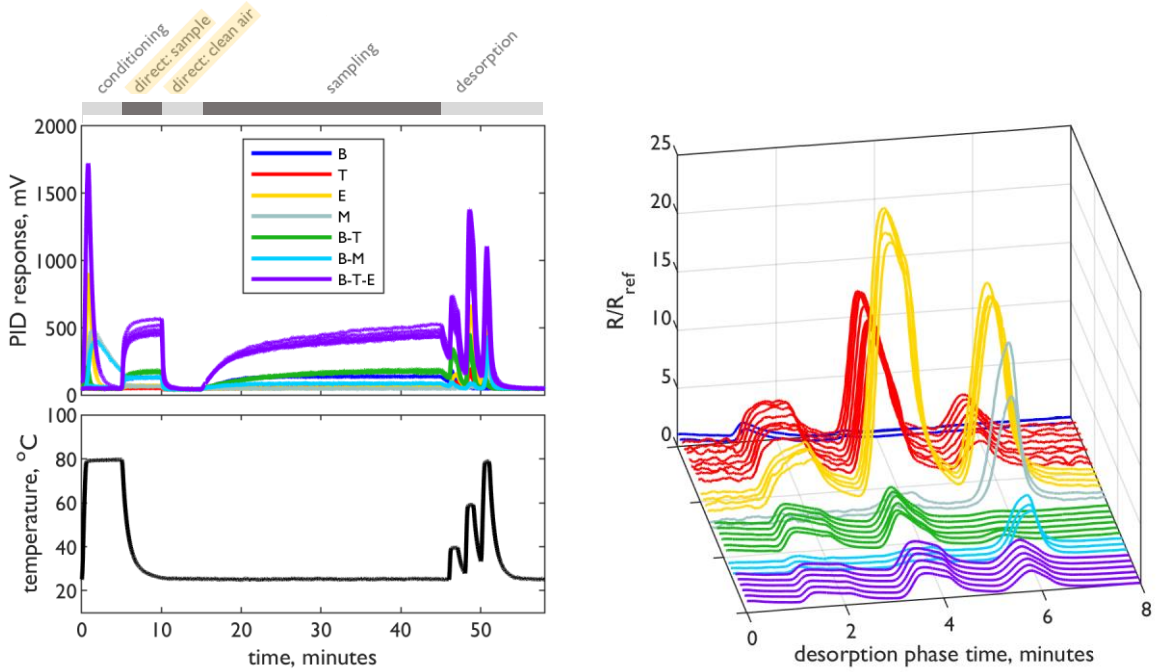

Figure 6.1. *Left* – photoionisation detector (PID) response for the benzene (B), toluene (T), ethylbenzene (E), methyl ethyl ketone (M) and three mixtures: benzene and toluene (B-T); benzene and methyl ethyl ketone (B-M); benzene, toluene and ethylbenzene (B-T-E), to and from unmodified silica with a pulsed heating profile, *Right* – normalised sensor response (R/R_{ref}), where R is PID response and R_{ref} is the PID response during the sample reference region (5-10 minutes of test cycle). Note: the desorption phase is 45-53 minutes of test cycle.

In order to make a direct comparison between samples the detector response was normalized to the sample reference response, R_{ref} (Figure 6.1, right). The responses of the aromatic compounds are markedly different, both in terms of magnitude and proportionality between the three heating zones (at 1-2, 3-4 and 5-6 mins). This analysis further validates the earlier finding that benzene has poor affinity for silica, as any adsorbed species are quickly desorbed at 40 °C. Both toluene and ethylbenzene are significantly more stable on silica, and require higher and sustained temperatures to complete vapour desorption. The relative sizes of the peaks for ethylbenzene are significantly larger than any other vapour sample tested, with the 60 °C peak reaching ~ 24 R/R_{ref}. In the case of the aromatic mixtures (BT and BTE), the reduction in the relative sizes of the peaks is likely due to the presence of benzene in the sample, which has an inherently large PID response but adsorbs poorly on silica.

MEK remains adsorbed for the first two heating steps, almost entirely desorbing at 80 °C (its boiling point). Benzene has almost exactly the same boiling point but no desorption was observed at 80 °C, indicating that the polarity of the compounds plays a significant role in adsorbate stability on silica.

Owing to the normalisation method, the size of the peaks for mixtures are skewed by vapours, like benzene, that have a large PID signal but poor affinity for silica. For example, the benzene-MEK mixture has an 80 °C peak that is approximately half the size of the single vapour MEK sample. This effect can also be seen when comparing the benzene-toluene-ethylbenzene mixture with the single vapour ethylbenzene samples.

Feature Selection and Principle Component Analysis (PCA)

For this proof of concept experiment, only the height of the normalised response during each heating zone was selected as features. In order to make this consistent between vapours and runs, the peak height was taken from the median smoothed normalised response (Figure 6.2, bottom left). These features were then used as inputs for principle component analysis (Figure 6.2, right). The first principle component (PC1) accounted for the most of the data variance (>91%). With the exception of MEK (for which there are only two data points), all of the data points for each VOC sample are well grouped and distinct from each other. The single vapour samples are well separated and the mixture data points are positioned between the corresponding single vapour data points. These proof of concept data indicate that the Adsorption Device in combination with triple step analysis, data feature extraction and PCA, offer a means of differentiating signals produced by mixtures of vapours. Despite this, the variance in the feature vectors may be increased by using additional data features (i.e. more than the three used here), which is incorporated in analyses presented in the following sections.

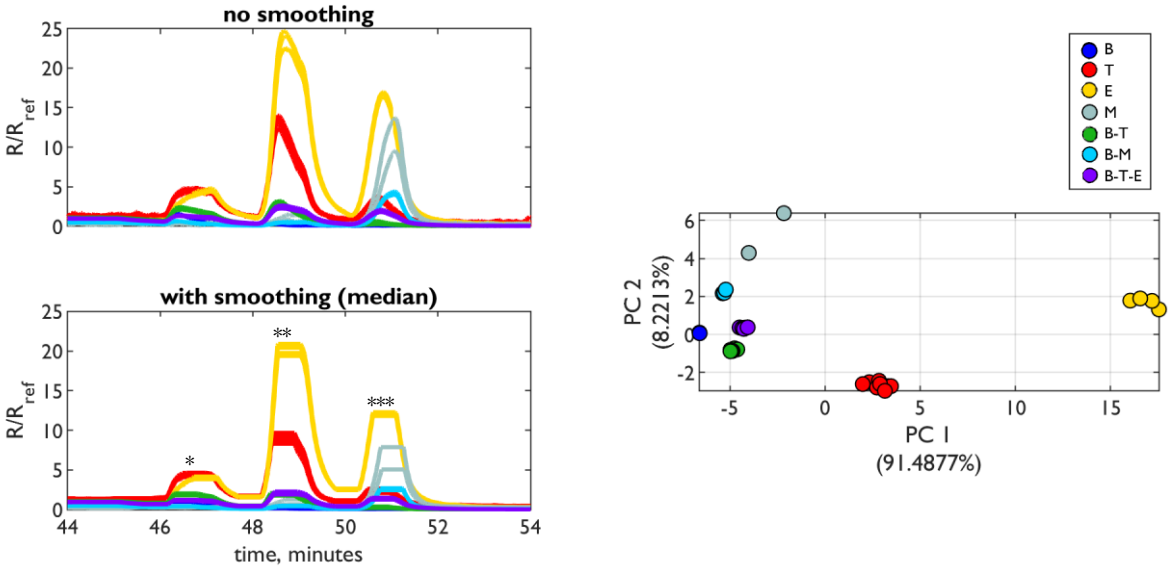

Figure 6.2. *Left* – normalised sensor response (R/R_{ref}) before and after median smoothing (window taken as 30 seconds). Data features were taken as the median at 46.5 (*), 48.5 (**) and 51 (***) minutes. *Right* – Principle Component Analyses (PCA) of the feature data extracted from the normalised sensor response (R/R_{ref}) for the desorption of the following vapours: benzene (B), toluene (T), ethylbenzene (E), methyl ethyl ketone (M) and three mixtures: benzene and toluene (B-T); benzene and methyl ethyl ketone (B-M); benzene, toluene and ethylbenzene (B-T-E). The explained variance of each principal component is shown in parentheses.

6.3 Speciation at Low Concentrations

6.3.1 Benzene and Toluene Mixtures

The previous section shows how a pulsed heating profile can used to elicit a different desorption patterns in mixtures of BTEX vapours. In this section, all three heating profiles are used to examine the capability of the Adsorption Device for discriminating benzene vapour mixtures down to 5 ppb. This value was targeted because it is the concentration at which the World Health Organisation (WHO) Air Quality Guidelines for Europe state are associated with an elevated excess lifetime risk (1/10,000).[35] Concentrations of benzene in the range of 5 to 100 ppb were mixed with 220 ppb of toluene and sampled onto phenyl silica. This adsorbent was chosen due to the capacity for, and difference in signal between, benzene and toluene (as shown in Chapter 5). Given the strong adsorption observed for 30 minute sampling (in the previous section), 15 minutes was deemed sufficient to adsorb enough vapour during the sampling phase, even at significantly lower concentrations.

Pulsed Heating

The pulsed heating profile was applied to the benzene, toluene and mixed vapours, as shown in Figure 6.3 (left). The magnitude of the PID response increases as the benzene concentration is increased, both as a mono-component and in the toluene mixtures. The height of each desorption peak (relative to the others) corresponds with the boiling point of the vapour. For example, the third (80 °C) desorption peak for toluene is approximately 5 times the magnitude of the second (60 °C) peak, whereas for the 100/220 ppb benzene-toluene the third desorption peak is approximately 1.2 the size of the second. The PID response data was normalised to the plateau region of the sample reference region (R/R_{ref}, Figure 6.3, right). For the benzene-toluene mix data (green), it can be seen that the ratio of the second and, in particular, third peaks change in height as the vapour fraction changes. It was expected that the ratios for the mono-component benzene peaks would be the same, irrespective of concentration, owing to the normalisation to the sample reference. Despite this, at 10 and 15 ppb the peaks are slightly larger than at 50 and 100 ppb. The most likely cause of this observation is the high noise for the PID response of these cycles, which is magnified in the normalisation process. However, it is possible that adsorption at low concentrations may occur via a different mechanism to higher concentrations, and subsequently interfere with desorption.

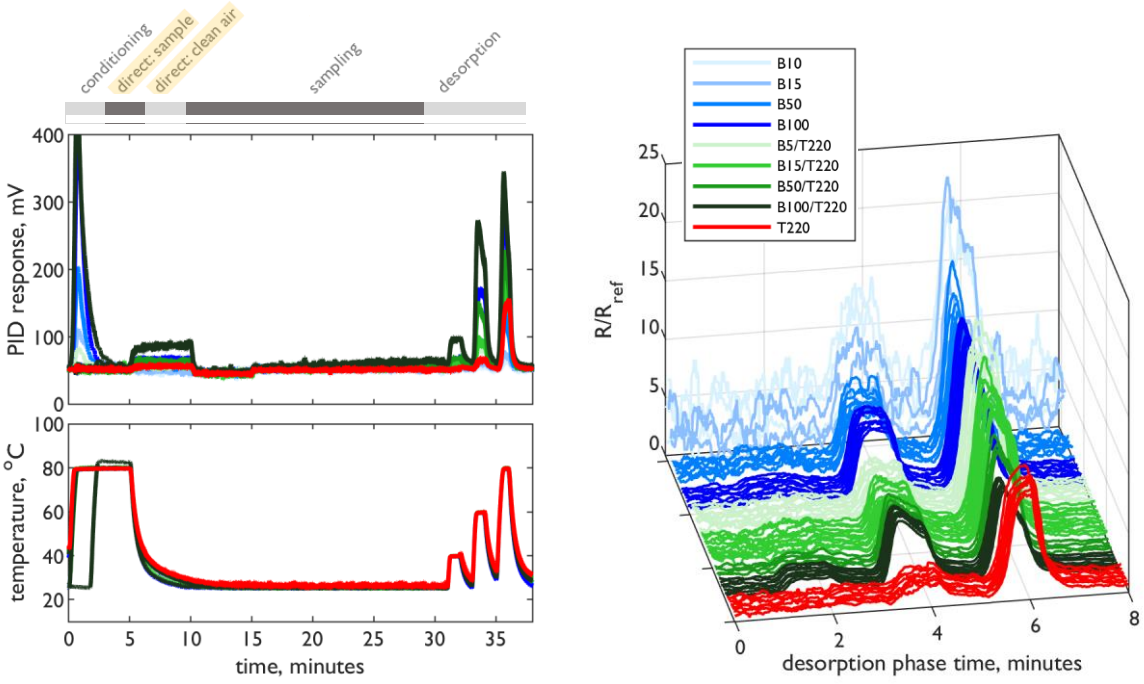

Figure 6.3. *Top* – Photoionisation detector (PID) response to the pulsed heating desorption profile (with 40, 60 and 80 °C degree heating pulses). *Bottom left* – normalised sensor response (R/R_{ref}), where R is PID response and R_{ref} is the PID response during the sample reference region (5-10 minutes of test cycle). The desorption phase is 30-42 minutes of test cycle. *Right* – normalised sensor response with smoothing (taking the median over a 60 element, 1 per second, window),

From these data, smoothed[i] R/R_{ref} values at 0.5, 1, 2, 4, 6, 9 and 12 minutes of the sampling phase, and at 1, 2, 3, 4, 5, 6, 7, 8, 9, 10 minutes of the desorption phase were selected as feature variables (Figure 6.4). With the exception of the 10 and 15 ppb benzene samples, all plots show that the selected features are consistent across sampling runs. These two samples have significant noise, as a result of measuring below the PID limit of detection, especially during the sampling phase. Despite this, the features at 4 and 6 minutes of the desorption phase correspond to the heating pulses. The adsorption region variables show minimal variation between the sample, with the exception again of the 10 and 15 ppb benzene samples. Given the low concentration of the samples in this case, observing a signal during this period would be unlikely, especially with adsorption occurring before the PID. From these variables it appears that benzene desorbs more during the first (40 °C) heating pulse than toluene, which is consistent with the boiling points and vapour pressures of the compounds. In general, the repeatability between sample runs is good, and the variances subtle, so PCA was used for visualisation.

[i] With Savitzky-Golay filter

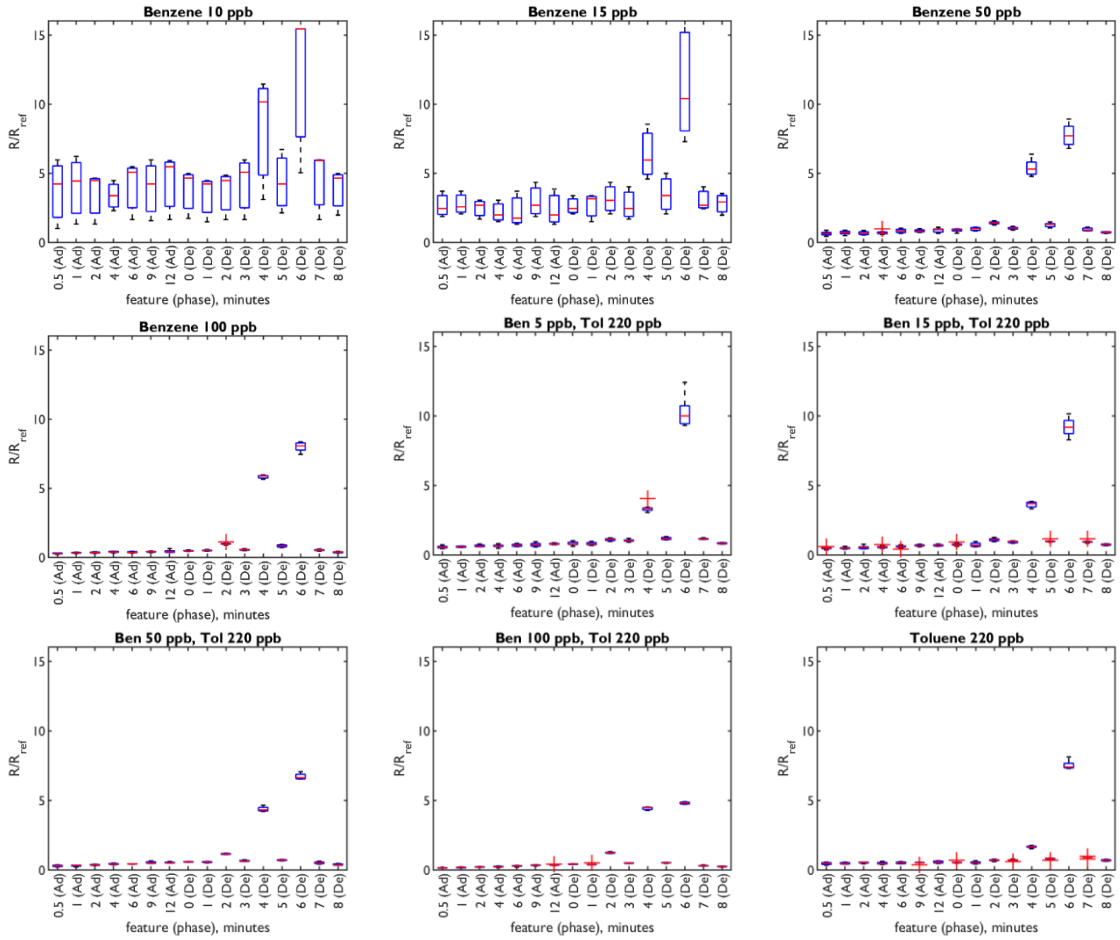

Figure 6.4. Boxplots of feature variables, where on each box the central mark indicates the median, and the bottom and top edges of the box indicate the 25th and 75th percentiles, respectively. The 'whiskers' extend to the most extreme data points not considered outliers, and the outliers are plotted using the '+' symbol. Abbreviations: Ad: adsorption (sampling phase), De: desorption (desorption phase).

As was the case with the gradual heating data, two PCA plots were generated in order to examine the variance with and without the noisy low mono-component (10 ppb and 15 ppb) benzene vapour data. In the first PCA plot (Figure 6.5, left), each vapour is well grouped, with the exception of the low concentration benzene vapour responses, as was the case with the all-data PCA from the gradual profile. In the second plot (Figure 6.5, right), the three different vapour components – toluene (red) , benzene (blue) and benzene-toluene mix (green) – are all well separated, and the variation vapour fractions of the mixed vapour are well separated. These plots indicate that, for the pulsed heating profile, there is more variance than the gradual profile. As a consequence, pulsed heating could provide more potential for vapour speciation. In addition, the desorption phase is much shorter – 8 minutes rather than 12– and

the maximum temperature much lower (80 °C rather than 105 °C) meaning this profile could be both quicker and more energy efficient.

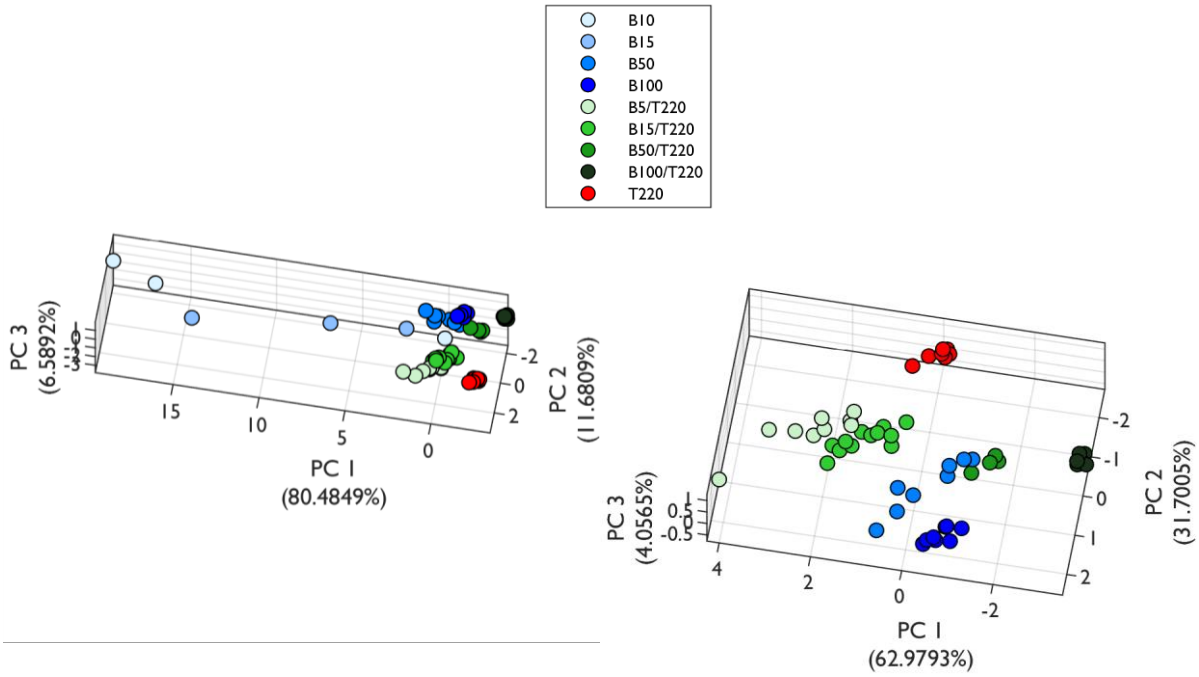

Figure 6.5. Principle Component Analyses (PCA) of the feature data extracted from the normalised sensor response (R/R_{ref}) for the benzene-toluene vapour desorption in combination with the pulsed heating desorption profile (see Figure 6.3). The left PCA includes all concentrations, whereas the right PCA omits the 10 ppb and 15 ppb benzene mono-component vapour data.

Gradual Heating

The PID response to the range of benzene-toluene vapours for the gradual heating profile is shown in Figure 6.6. Darker shades of blue and green represent increasing concentrations of benzene as a mono-component and dual-component vapour (benzene/toluene), respectively. In both cases, the magnitude of the PID response increases as the benzene concentration is increased, which is clearly observable in the desorption phase (30 minutes onwards). The peak of the desorption response indicates that toluene desorbed at a higher temperature than both benzene and benzene-toluene adsorbates, which is consistent with its higher boiling point (111 °C versus 80 °C). The benzene-toluene mixture PID patterns have peaks in between the peaks of the toluene and mono-component benzene peaks, in terms of both peak height and time within the phase. As can be seen in during the conditioning phase (0-5 minutes), not all of the adsorbate is removed during the desorption phase. It is possible that towards the end of the cycle, approaching 100 °C, small amounts of water are released and produce a PID signal. The 10 ppb sample could then be amplified, relative to 15 ppb sample, due to the normalisation process.

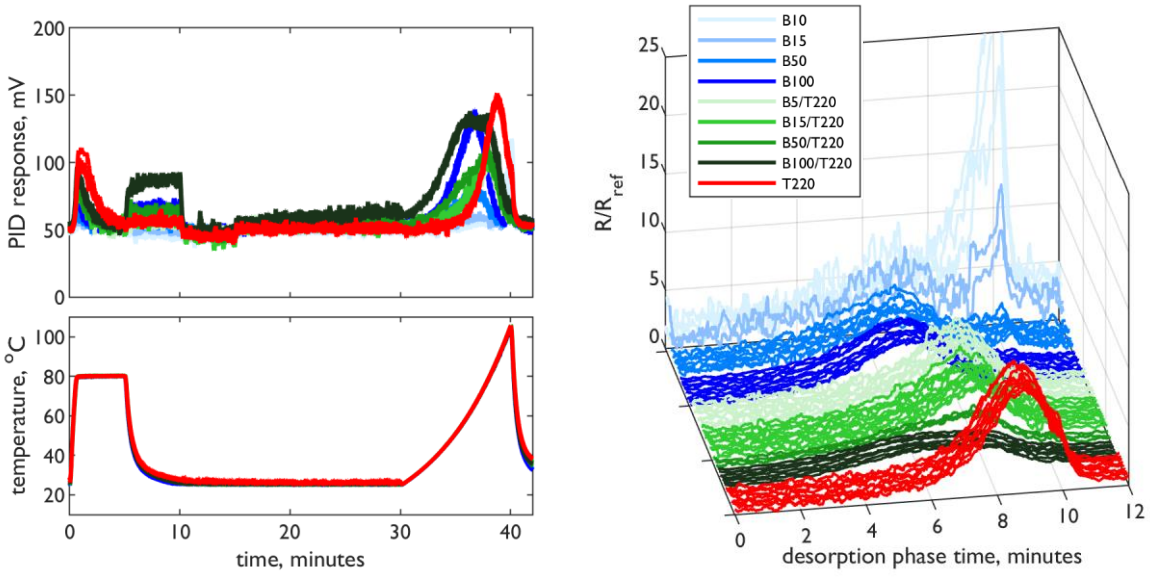

Figure 6.6. *Left* – Photoionisation detector (PID) response to the gradual heating desorption profile. *Right* – normalised sensor response (R/R_{ref}), where R is PID response and R_{ref} is the PID response during the sample reference region (5-10 minutes of test cycle). The desorption phase is 30-42 minutes of test cycle.

PID response data were then normalised to the plateau region of the sample reference region (R/R_{ref}, Figure 6.6 right). From these data, smoothed[ii] R/R_{ref} values at 0.5, 1, 2, 4, 6, 9 and 12 minutes of the sampling phase, and at 1, 2, 3, 4, 5, 6, 7, 8, 9, 10 minutes of the desorption phase were selected as feature variables (Figure 6.7). In general, all plots show that the selected features are consistent across sampling runs, with the exception of the 10 and 15 ppb benzene samples. These two samples have significant noise, as a result of measuring below the PID limit of detection, especially during the sampling phase. In addition, the desorption phase features of the 10 and 15 ppb samples further highlight the unexpected finding of peaks at ~10 minutes of the desorption phase, which are absent from all other samples. Again, benzene desorbs earlier in the desorption cycle than toluene. Other differences between samples are more subtle, and PCA was used to visualise the variance between them (Figure 6.8)

[ii] With Savitzky-Golay filter

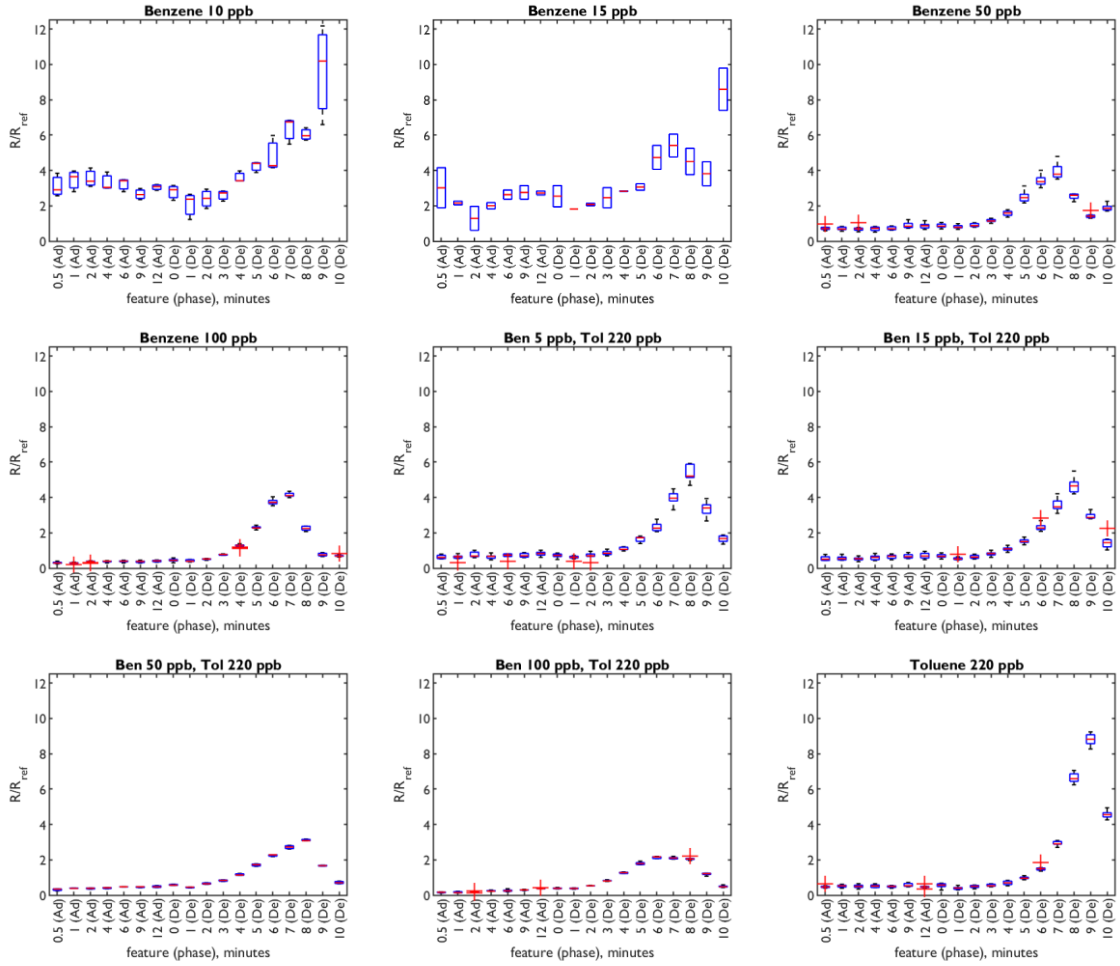

Figure 6.7. Boxplots of feature variables, where on each box the central mark indicates the median, and the bottom and top edges of the box indicate the 25th and 75th percentiles, respectively. The 'whiskers' extend to the most extreme data points not considered outliers, and the outliers are plotted using the '+' symbol. Abbreviations: Ad: adsorption (sampling phase), De: desorption (desorption phase).

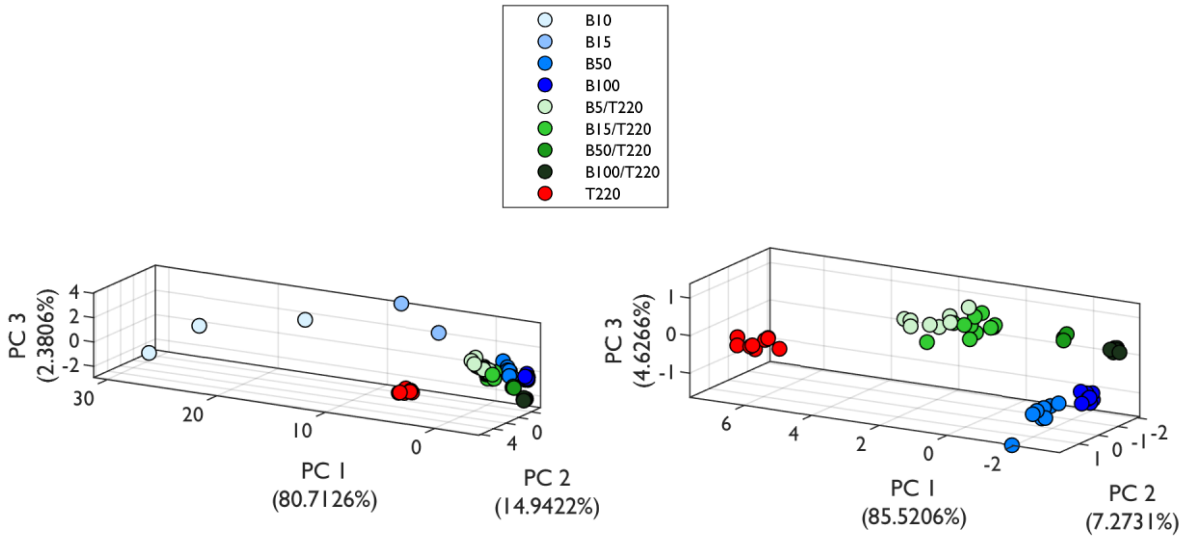

Figure 6.8. Principle Component Analyses (PCA) of the feature data extracted from the normalised sensor response (R/R_{ref}) for the benzene-toluene vapour desorption in combination with the gradual heating desorption profile (see Figure 6.6). The left plot includes all concentrations, whereas the right plot omits the 10 ppb and 15 ppb benzene mono-component vapour data. The explained variance of each principal component is shown in parentheses.

Two principle component analyses are presented in Figure 6.8, one including all mono-component and dual-component vapours (left) and the other (right) omitting the 10 ppb and 15 ppb concentration benzene mono-component vapour data (to better visualise the variance between these samples). PCA reduces the dimensionality of a dataset and aids the visualisation of multidimensional data. In the first PCA (Figure 6.8, left), each vapour is well grouped, with the exception of the low concentration benzene vapour responses. The wide spread of 10 and 15 ppb benzene vapour represents the largest variance along the primary principle component (PC1), which has an explained variance of 82%. For this reason, the 10 and 15 ppb benzene vapour data was omitted from the second analysis (Figure 6.8, right), to examine the variance in the other vapour data features. The three different vapour components – toluene (red), benzene (blue) and benzene-toluene mix (green) – are all well separated, and the variation vapour fractions of the mixed vapour are well separated. These analyses suggest that there is sufficient information in these features to differentiate between benzene and toluene, and vapour fractions, but signal variability in low benzene concentration mixtures (i.e. 10 and 15 ppb benzene) reduces accuracy.

Stepwise Heating

The stepwise profile is same as the pulsed profile, but with no breaks between the steps to 40, 60 and 80 °C (Figure 6.9, top). As with the two previous profiles, the magnitude of the PID response increases as the benzene concentration is increased, both as a mono-component and in the toluene mixtures. Overall, the appearance of this desorption pattern is a contracted version of the pattern from the pulsed heating profile, and the observation that the height of the height of each peak (relative to the others) corresponds to boiling point of the vapour carries over to this profile. The PID response data was normalised to the plateau region of the sample reference region (R/R_{ref}, Figure 6.9, bottom left). Unlike the previous two heating profiles, the low concentration mono-component benzene data show partial consistency with higher concentration runs. The peak corresponding to the third temperature step (60 to 80 °C) at 3 minutes desorption phase is mostly the same for all benzene concentrations. The appearance of the normalised responses for the toluene (red) and mixed (green) runs have consistent features as the pulsed heating profiles. Interestingly, the tail of toluene takes longer to plateau than the other samples. This is consistent with its lower vapour pressure, so is more likely to desorb at higher temperatures.

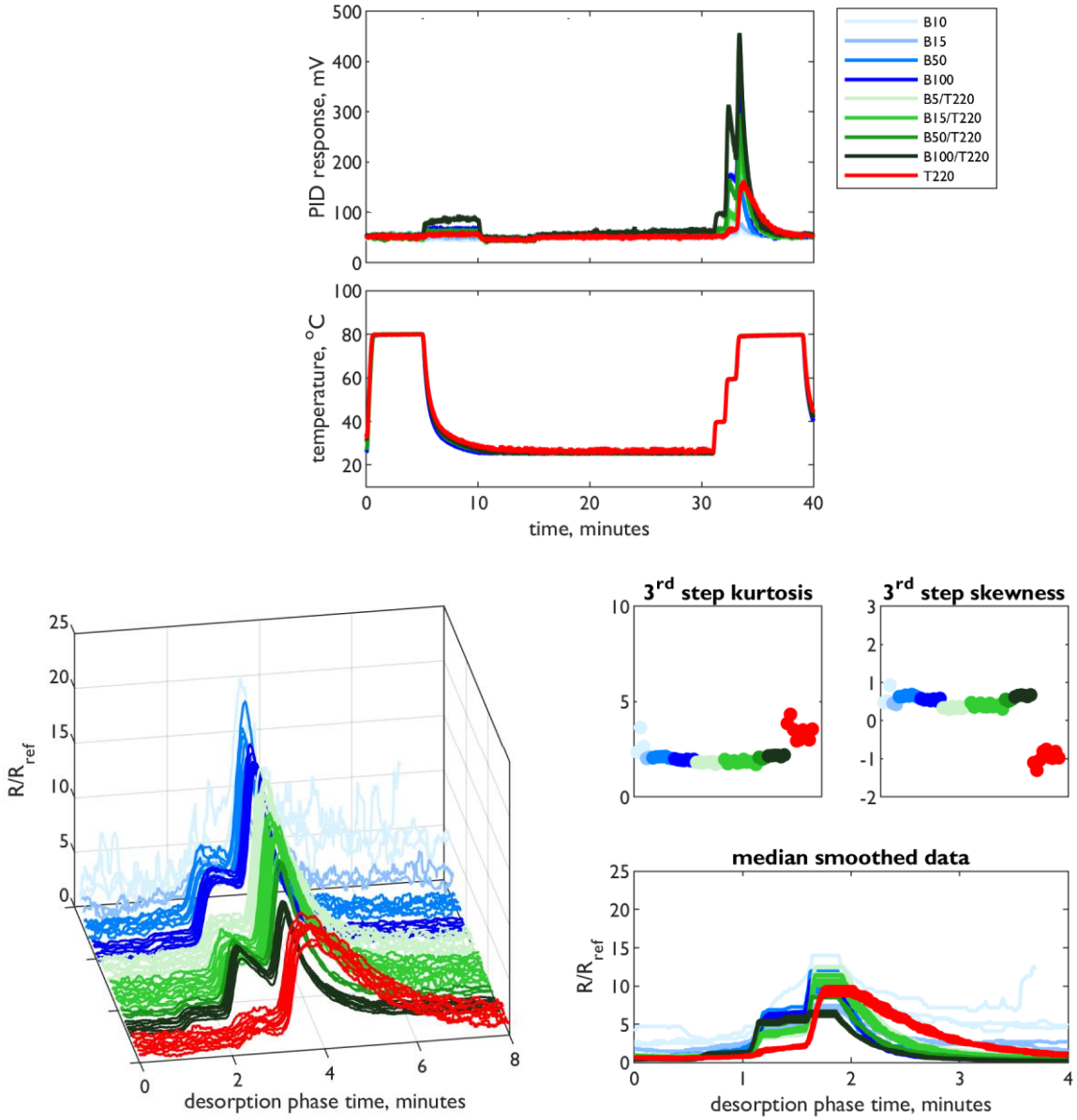

Figure 6.9. *Top* – Photoionisation detector (PID) response to the pulsed heating desorption profile (with 40, 60 and 80 °C degree heating pulses). *Bottom left* – normalised sensor response (R/R_{ref}), where R is PID response and R_{ref} is the PID response during the sample reference region (5-10 minutes of test cycle). The desorption phase is 30-42 minutes of test cycle. *Bottom right* – normalised sensor response with smoothing (taking median over a 60 element, 1 per second, window), as well as kurtosis and skewness measurements of the 3rd step desorption peak.

From the normalised responses, the following features were taken: the median smoothed values (Figure 6.9, bottom right) during the sampling region at 0.5, 1, 2, 4, 6,and 12 minutes, and during the desorption region at 0, 0.5, 1.5, 2, 2.5, 3, 3.5, 4 and 5 minutes (Figure 6.10). In addition, the kurtosis (a measure of heavy or light tails) and skewness (a measure of symmetry) of only the third peak (taken between 3.2 and 5 minutes of the desorption phases were also used as features. As was the case for the previous two profiles, the lower concentration mono-component benzene vapours are noisy, although the 15 ppb samples are considerably more consistent between runs.

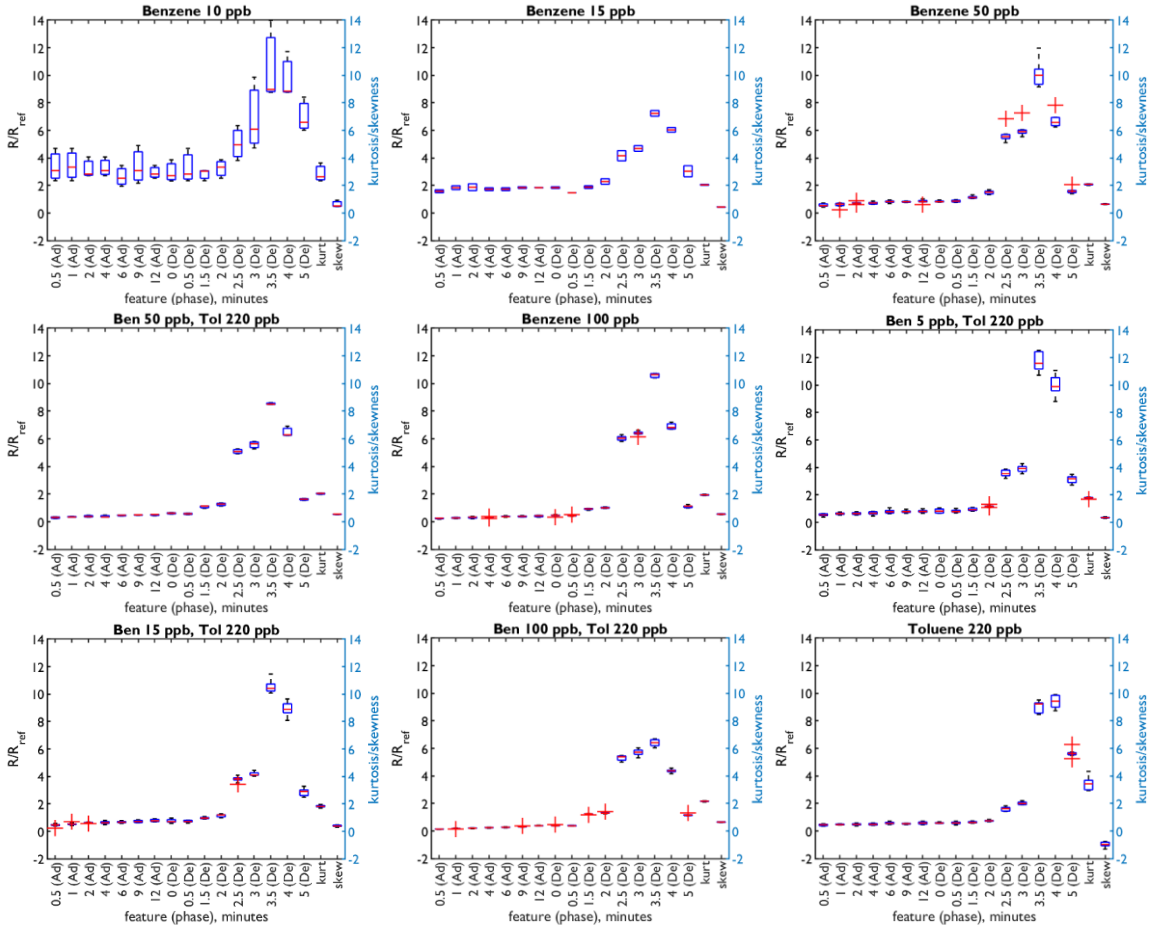

Figure 6.10. Boxplots of feature variables, where on each box the central mark indicates the median, and the bottom and top edges of the box indicate the 25th and 75th percentiles, respectively. The 'whiskers' extend to the most extreme data points not considered outliers, and the outliers are plotted using the '+' symbol. Abbreviations: Ad: adsorption (sampling phase), De: desorption (desorption phase).

The single PCA plot generated from this is shown in Figure 6.11. This is the first PCA plot where all vapours are well grouped, with the exception of a single point for 10 ppb mono-component benzene (light blue). Of the three heating profiles, stepwise is the only one with to have significant variance on three, rather than two, principle components. This is likely due to the increased number of features used for the analysis, as well as the difference in their nature. For example, kurtosis and skewness measurements capture may add detail to magnitude values at certain time points during desorption. In essence, it takes advantage of the redundancy of PCA as an analysis method. In effect, many practical features should be used as the technique will group together features that provide the same information.

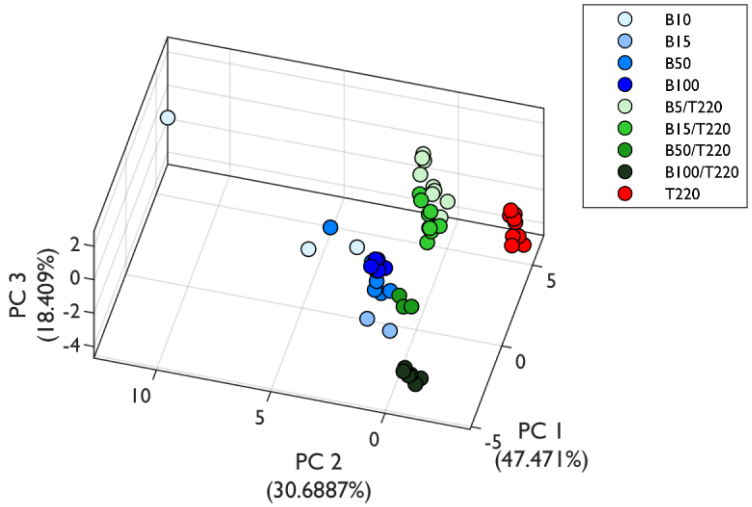

Figure 6.11. Principle Component Analyses (PCA) of the feature data extracted from the normalised sensor response (R/R_{ref}) for the benzene-toluene vapour desorption in combination with the stepwise heating desorption profile (see Figure 6.9).

6.4 Practical Cycle Times

Previous results have shown that it is possible to differentiate between the signals of individual vapours and different vapour fractions of multicomponent mixtures. Given that one of the key objectives of this work was to develop a device suitable for air quality monitoring applications, it was necessary to try and reduce the total cycle time. A benchmark of 10 minutes per cycle was established as industrially acceptable, as this would provide 6 readings per hour. In order to achieve this, the previously developed test scripts were modified to reduce the time of each test phase, as shown in Table 6.2.

Table 6.2. Conditions for 10 minute cycle time

Phase	Duration, mins	Chip temperature set point (°C)
Conditioning	1	80
Sample Reference	1	25*
Baseline Reference	1	25*
Sampling	5	25
Desorption (thermal)	2	40, 60, 80

* chip cooling during this phase

Stepwise heating was selected as the heating profile for these practical cycle times, as it was the best profile in the previous section, and the final step and hold of the desorption phase could be effectively carried over as the conditioning phase of the following test cycle, as shown in Figure 6.12. Previously presented data have shown sensor data for one adsorbent (either unmodified silica or phenyl silica). In this section, data are presented for both adsorbents, so as to demonstrate the difference in adsorption and desorption that is achieved when using materials with different functionalities and hydrophobicities.

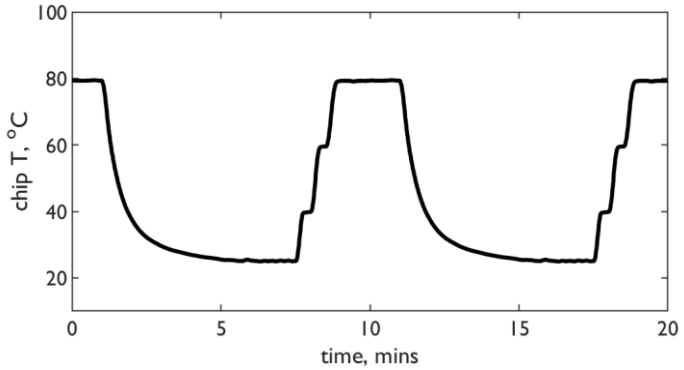

Figure 6.12. Continuous thermal desorption and conditioning phases.

6.4.1 Single Component Vapours

The first investigation undertaken with the above test conditions involved testing BTEX and MEK on unmodified and phenyl silica. As shown previously (Figure 3.4), unmodified silica is a hydrophilic adsorbent and phenyl silica is a hydrophobic. The normalised PID responses (R/R_{ref}) during the desorption phase (7-10 minutes of the test cycle) are shown in Figure 6.13. For both adsorbents, benzene is the only volatile that appears to completely desorb during the desorption phase – as shown by the reduction of the detector response towards baseline levels approaching 10 minutes. In the case of unmodified silica, the benzene response increases slightly at ~10 minutes. Given that benzene is the only volatile in the vapour stream, and that this increase is only seen for unmodified silica, it is possible that this increase is a result of water vapour, which may have adsorbed to the hydrophilic surface, and is desorbed when the chip is maintained at higher temperature.

Toluene, ethylbenzene and xylene have similar desorption profiles with both adsorbents, and none appear to be fully desorbed on either adsorbent during the desorption phase. This leads to an accumulation of adsorbate between runs, and the vertical spreading of lines during the third heating step (8.5-10 minutes). Higher temperatures, or longer conditioning times, may be required to fully regenerate the adsorbent for non-benzene VOCs. The fifth VOC tested, MEK, has significantly different behaviour between adsorbents. For unmodified silica, there is minimal desorption at any temperature, indicating that adsorbate is bound on the surface of the silica. There is significant desorption from phenyl silica – following the third temperature step to 80 °C at 8.5 minutes. MEK, a polar compound, is able to form hydrogen bonds with hydroxyl groups on unmodified silica. It is likely that higher temperatures, as suggested for TEX vapours above, would remove the adsorbates in this case.

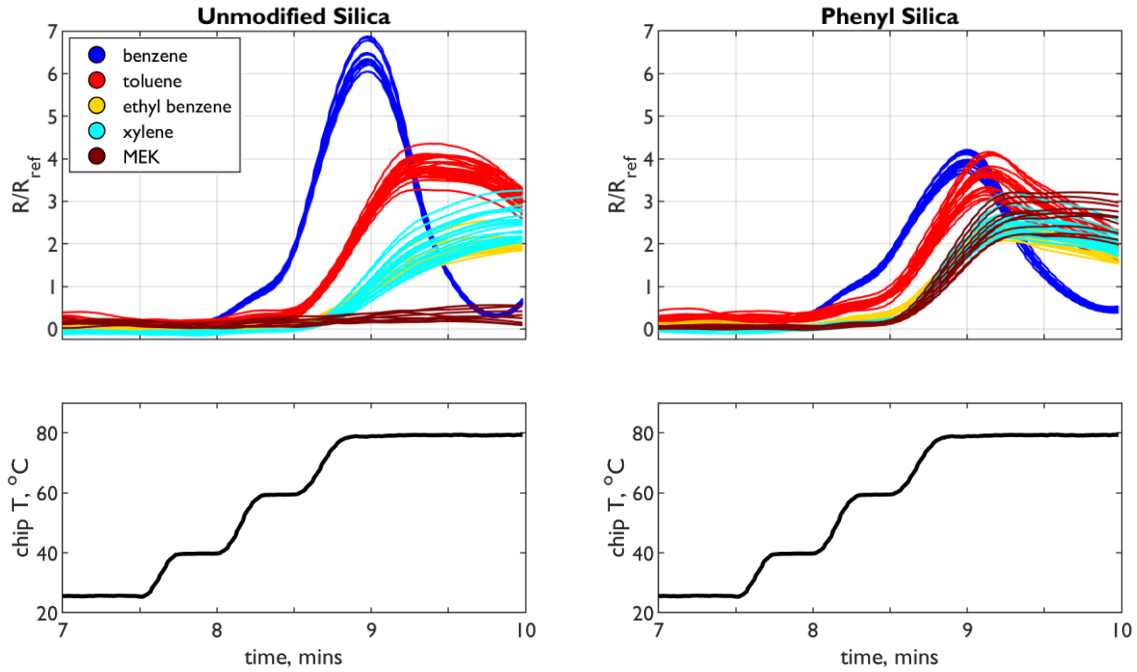

Figure 6.13. Normalised sensor response (R/R_{ref}) for unmodified (*left*) and phenyl (*right*) silica adsorbents with benzene, toluene, (para) xylene and methyl ethyl ketone (MEK). R is PID response and R_{ref} is the PID response during the sample reference region (1-2 minutes of test cycle). Only the desorption phases are shown.

Feature Selection and PCA

The normalised response at 3 points during the sampling phase (1.5, 3 and 4.5 minutes) and 9 points during the desorption phases (every 15 seconds from 0 to 3 minutes) were selected as data features and are shown in Figure 6.14.

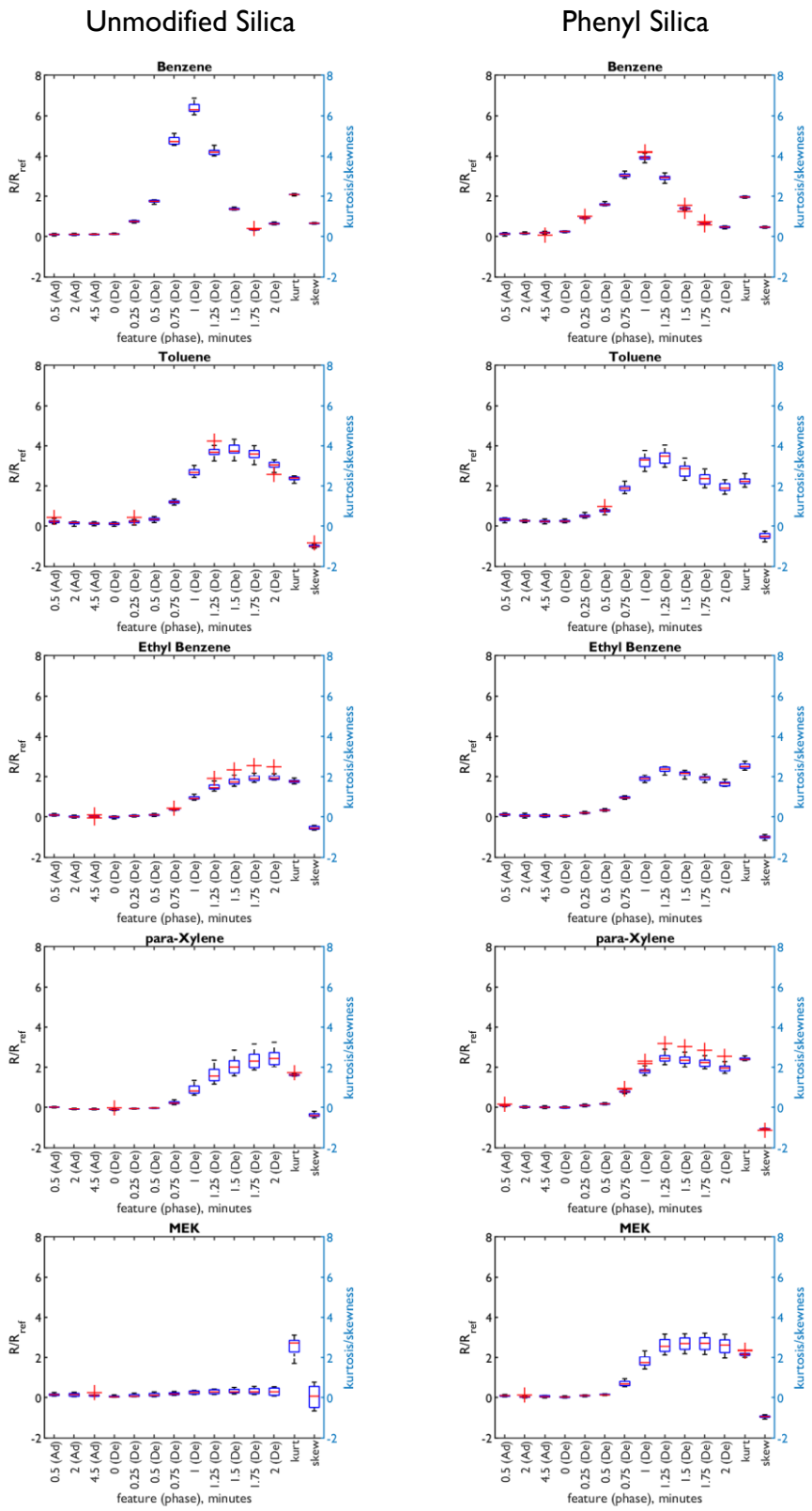

Figure 6.14. Boxplots of feature variables, where on each box the central mark indicates the median, and the bottom and top edges of the box indicate the 25th and 75th percentiles, respectively. The 'whiskers' extend to the most extreme data points not considered outliers, and the outliers are plotted using the '+' symbol. Abbreviations: Ad: adsorption (sampling phase), De: desorption (desorption phase), kurt: kurtosis, skew: skewness.

These feature variables were then used for PCA (Figure 6.15). The plots consist of two principle components, where in both cases these components account for >98% of variance. These analyses further validate the conclusions drawn from the normalized response curves. The Adsorption Device used with either adsorbent produces unique and well separated signals for benzene vapour and toluene. Although the other vapours are closer together, they are still distinct from each other with minimal overlaps. Incomplete desorption appears to correspond to spreading of data points along PC2. For example, benzene data points (for both adsorbents) have relatively little vertical spreading, but toluene, ethylbenzene and xylene are dispersed more.

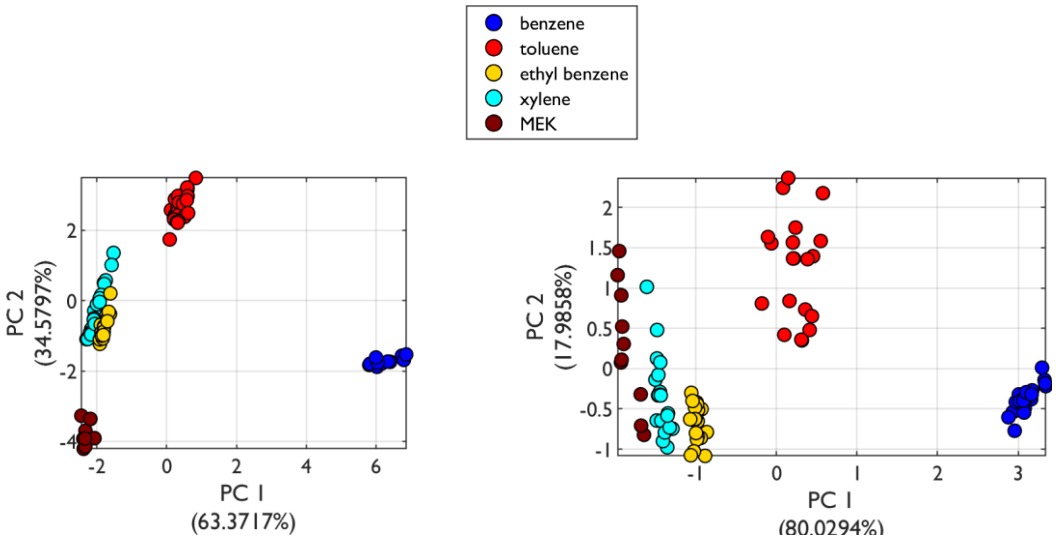

Figure 6.15. Principle Component Analyses (PCA) of the feature data for unmodified (*left*) and phenyl (*right*) silica adsorbents, using features selected from normalised sensor responses.

Classification Algorithms

PCA is a useful technique to visualise selected data features, and helps to describe the behaviour of data. Classification algorithms are functions that assess inputs – features, in this case – such that the output separates classes from each other. Classifier training generates functions that provide the most accurate separation of one or more classes of data. When applied to gas sensing, the responses from each vapour are a distinct class, and a classification function acts as means of vapour selectivity. Four supervised classification algorithms were tested with the features described above: linear discriminant analysis (LDA), k-nearest neighbours (kNN), support vector machines (SVM) and random forests (RF). These particular algorithms were chosen due to their relatively simple application, and to allow comparison with published sensors that describe their accuracy with these algorithms.[137,158] LDA is a basic classifer that identifies the linear weighting of multifactorial data, as a means to maximize the distance between the means of the two classes. kNN is another simple classifier that searches for the closest match of the test data in the feature space. SVM and RF are more computational processes that can create more complex divisions between classes. SVM separates classes in a training set with a straight line, or hyperplane, with the largest minimum distance (between the classes), while RF builds a decision tree (a series of binary questions) for a specific classification problem. The feature data were randomly split into training and test data, in ratios shown in Table 6.3. Training data were used to train the classification algorithms, and the accuracy assesed with test data. Confusion (error) matrices for these assessments are shown in Figure 6.16.

Table 6.3. Split of feature data (training/test)

VOC	Unmodified	Phenyl
Benzene	10/3	15/5
Toluene	20/6	16/4
Ethylbenzene	13/7	15/5
p-Xylene	13/6	15/5
MEK	4/4	7/3

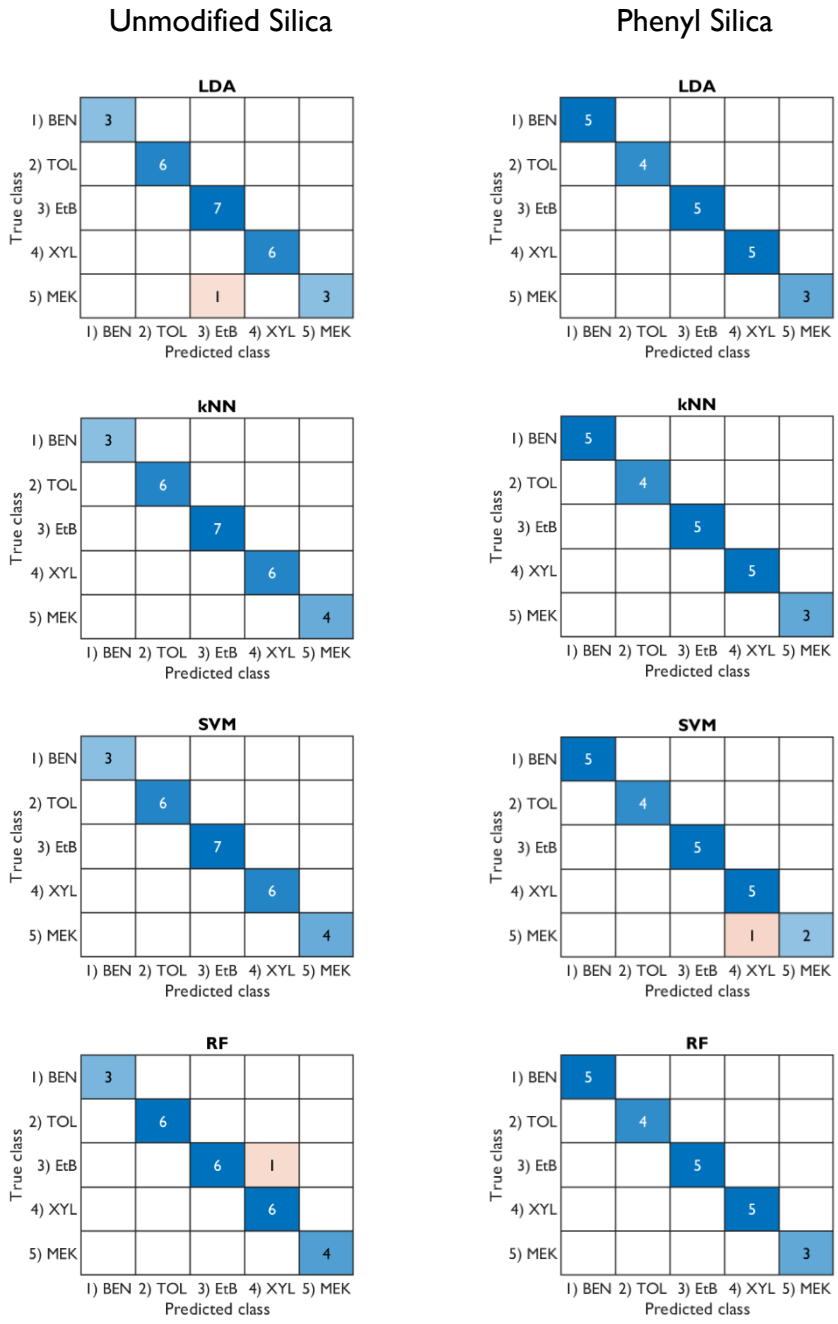

Figure 6.16. Confusion matrices for the application of the classification algorithms applied to feature data from the normalised sensor response (R/R_{ref}) for unmodified (left hand side) and phenyl (right hand side) silica adsorbents. LDA: linear discriminant analysis; SVM: support vector machine; kNN: k-nearest neighbours (k = 2 for both adsorbents); RF: random forest (number of trees: 24, unmodified; 12 phenyl). Abbreviations: BEN, benzene; TOL, toluene; EtB, ethylbenzene; XYL, para-xylene; MEK, methyl ethyl ketone.

In general, all four algorithms are accurate for both unmodifed and phenyl silicas. Benzene and toluene were correctly classfied 100% of the time, with both adsorbents. For unmodified silcia, RF incorrectly classfied ethylbenzene as xylene, and for phenyl silica, LDA and SVM incorrectly classified MEK as xylene. kNN correctly classifed 100% of the test VOCs on both adsorbents. These results indicate that such classification algorithms, in combination with the Adsorption Device, could provide a simple, fast and accurate means of achieving vapour selectivity. In particular, the accuracy of benzene selection is promising. The following section builds upon these results and examines the capability of the sensor and analysis algorithms with regards to achieving fast selectivity for low concentration benzene-toluene mixtures.

6.4.2 Benzene and Toluene Mixtures

As discussed in the introduction of this thesis, many reported VOC sensors that claim selectivity are only tested with mono-component vapours, and at relatively high concentrations (typically in the range of 1 ppm or higher). For this reason, the Adsorption Device proposed here was tested with low concentration mixtures of vapours. The two vapours chosen for this experiment were benzene and toluene, due to high level of interest in them as toxic pollutants. The Adsorption Device was tested with the following samples:

1. 200 ppb toluene
2. 100 ppb benzene
3. 100 ppb benzene in 200 ppb toluene
4. 50 ppb benzene in 200 ppb toluene
5. 10 ppb benzene in 200 ppb toluene
6. 5 ppb benzene in 200 ppb toluene

These tests sought to establish at what concentration benzene could be detected in the presence of another similar vapour that is likely to be present with. Initially, the vapours listed above were tested with unmodified and phenyl silica, the adsorbents used in the previous section. Normalised sensor responses (R/R_{ref}) for both adsorbents (for the test cycle described in Table 6.2) are shown in Figure 6.17. The responses for the benzene-toluene mixtures are only subtlety different. Despite this, there are a couple of key features that allow the inputs to be differentiated. Firstly, the first two temperature steps (to 40 and 60 °C) produce larger response from input samples that contain more benzene. In addition, the response peak associated with the third step (to 80 °C) occurs later for inputs with a higher toluene fraction.

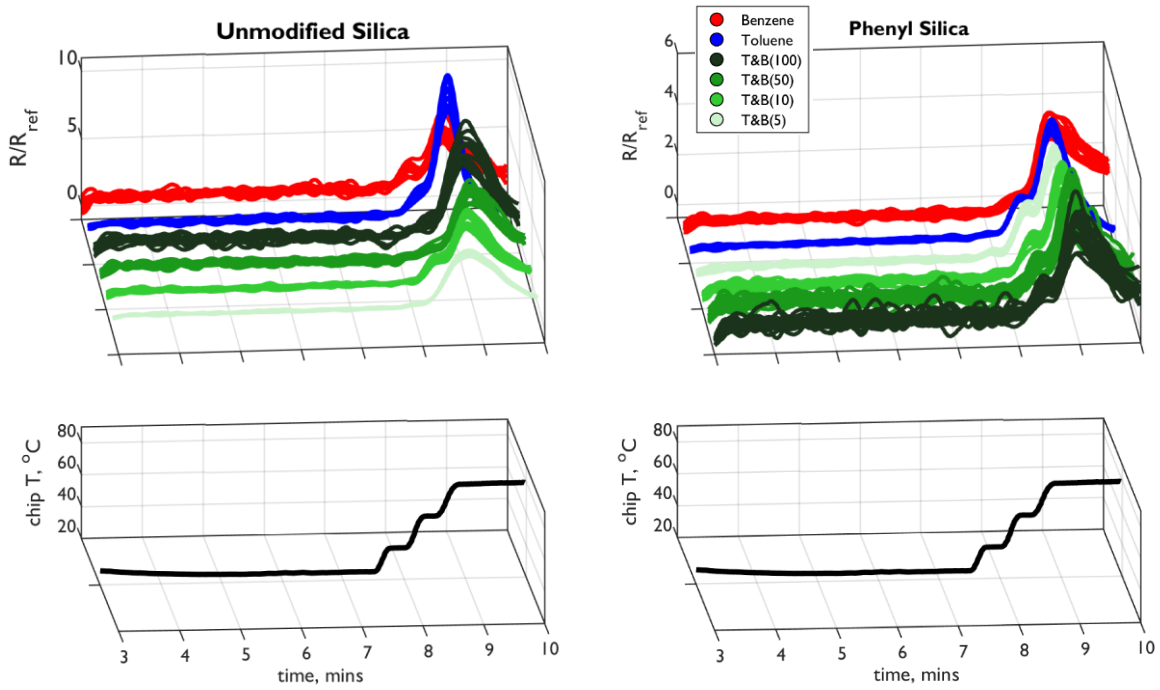

Figure 6.17. Normalised sensor response (R/R_{ref}) for unmodified (*left*) and phenyl (*right*) silica adsorbents with benzene (blue), toluene, (red) and a range of benzene concentrations in toluene (shades of green). R is PID response and R_{ref} is the PID response during the sample reference region (1-2 minutes of test cycle). Only sampling and desorption phases are shown.

The normalised response at 4 points during the sampling phase (3.5, 5, 6.5 and 8 minutes) and 8 points during the desorption phases (every 15 seconds from 8.25 to 10 minutes) were selected as features from the data presented in Figure 6.17. In general, the features are consistent between runs. As was also the case with the previous results of this chapter, the R/R_{ref} values during the sampling phase are low, and have minimal variation between the samples.

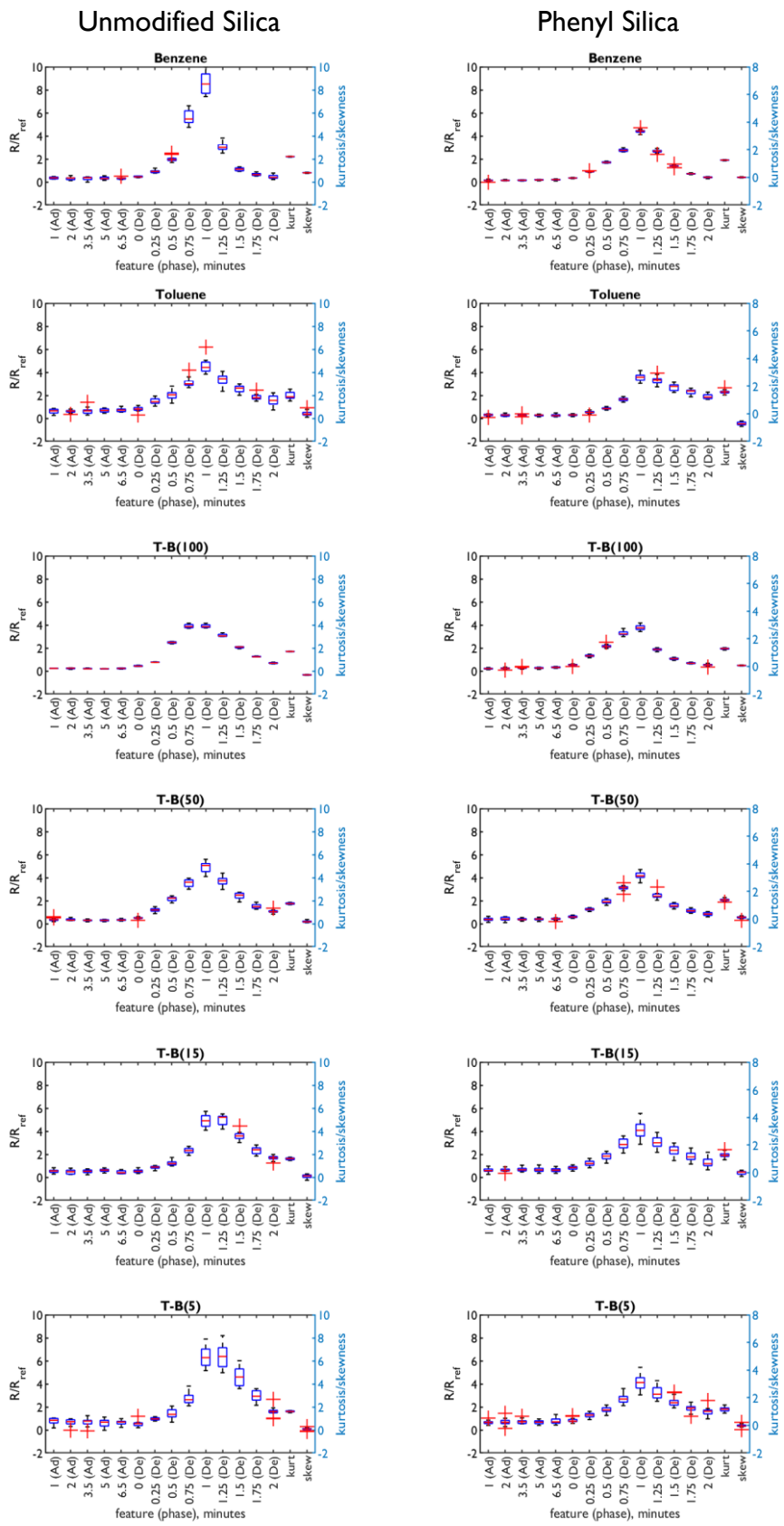

Figure 6.18. Boxplots of feature variables. The central mark indicates the median, and the bottom and top edges of the box indicate the 25th and 75th percentiles, respectively. The 'whiskers' extend to the most extreme data points not considered outliers, which are plotted using the '+' symbol. Abbreviations: Ad: adsorption (sampling phase), De: desorption (desorption phase), kurt: kurtosis, skew: skewness.

Features from both sets of adsorbent data were then used for principle component analyses (Figure 6.19). The PCA plots show that both unmodified and phenyl silica produce features that generally separate the input vapours. This is clearly the case for the mono-component benzene (blue) and toluene (red) data points, as well as the higher concentration (100 and 50 ppb benzene) mixtures. There is some overlap between the two lowest concentration (10 and 5 ppb benzene) mixtures, which means resolving these two samples is challenging.

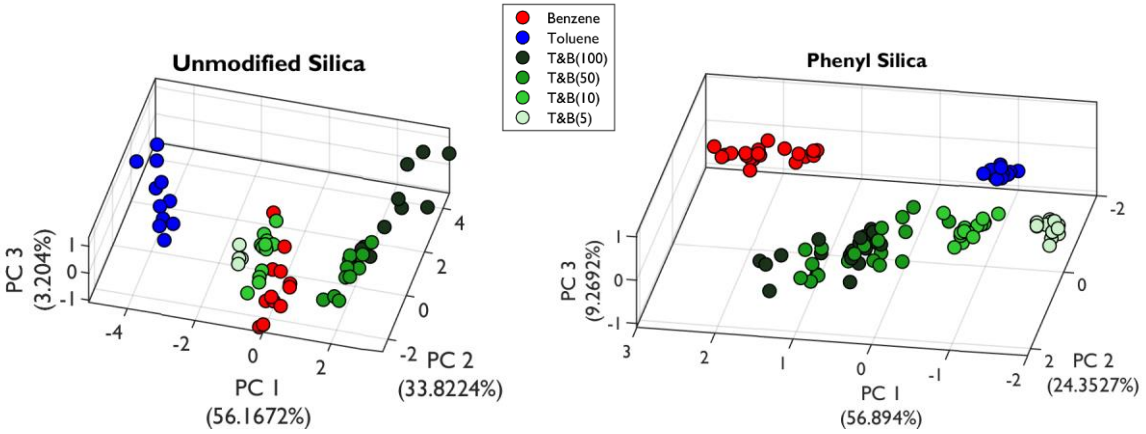

Figure 6.19. Principle Component Analyses (PCA) of the feature data for unmodified (*left*) and phenyl (*right*) silica adsorbents, using features selected from normalised sensor responses.

The same four supervised classification algorithms from the previous section - LDA, kNN, SVM and RF – were tested with the features described above. The feature data were randomly split into training and test data, as shown in Table 6.4. Training data were used to train the classification algorithms, and the accuracy assesed with test data. Confusion (error) matrices for these assessments are shown in Figure 6.20.

Table 6.4. Split of feature data (training/test)

VOC	Unmodified	Phenyl
Benzene	9/3	15/5
Toluene	8/4	16/4
B100-T	3/1	12/4
B50-T	8/4	12/4
B10-T	9/3	15/5
B5-T	8/4	14/6

The classification accuracies is again high for differentiating between mono-component vapours ('T only'and 'B only', as described in the matrices) with both adsorbents. The only exception to this is the incorrect prediction of toluene ('T only') for kNN with unmodified silica. This anomaly likely arose due to the relatively low number of data used, and the nature of the algorithm itself selecting the nearest data points (from this data set). In the PCA plot (Figure 6.19, left) there is an isloated red data point, which, if used as a training data point in kNN, would lead to an inaccurate classification. With more training data points, anomalous data points become less significant and the algorithm more robust. The only other inaccuracies are between the 10 and 5 ppb benzene input vapours. The accuracy at classifying between these two concentratins across all algorithms for both adsorbents is 69%.

Table 6.5. Classification Accuracy

	LDA	kNN	SVM	RF	Mean
Unmodified	95%	95%	90%	95%	94%
Phenyl	93%	82%	86%	82%	86%

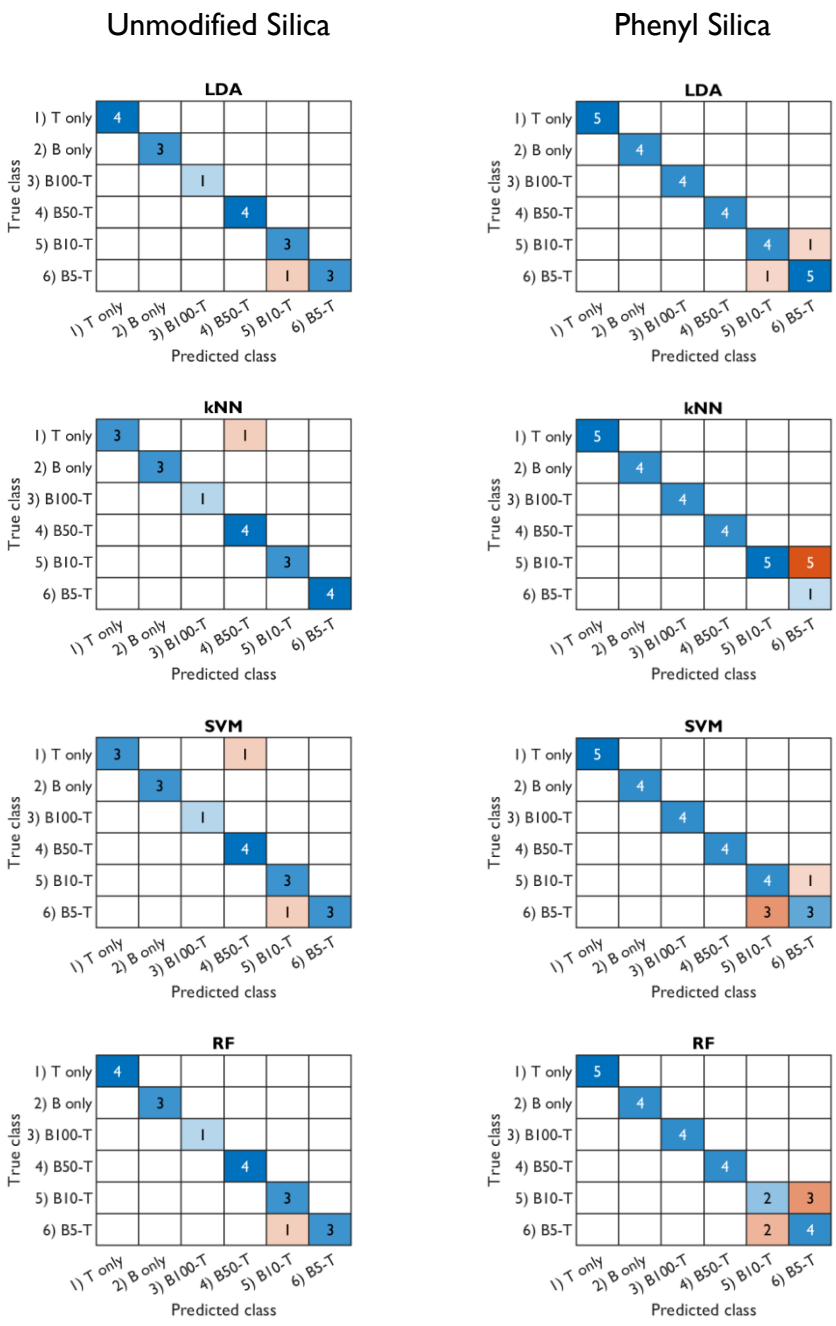

Figure 6.20. Confusion matrices for the application of the classification algorithms applied to feature data from the normalised sensor response (R/R_{ref}) for unmodified (left hand side) and phenyl (right hand side) silica adsorbents. LDA: linear discriminant analysis; SVM: support vector machine; kNN: k-nearest neighbours (k = 3 for unmodified and 6 phenyl); RF: random forest (number of trees: 25, unmodified; 12 phenyl). Abbreviations: B, benzene; T, toluene.

5 minute Cycle Time

Looking ahead to the practical application of the Adsorption Device, 10 minute cycle time could provide sufficient data points to reliably generate hourly readings. Despite this, as short as cycle time as possible is desirable. For this reason, the above experiments were repeated in half the time (total cycle time of 5 minutes). The phase conditions are shown in Table 6.6, and the normalised sensor responses (R/R_{ref}) for both adsorbents are shown in Figure 6.21. With the shorter cycle time, there is less time for the chip to cool and settle to the set point temperature following the conditioning and reference phases. Despite this, the sampling phase appears to be largely unaffected. The speed of the phases also affected the desorption phase, which rather than having distinct temperature steps, has more of a gradual increase.

Table 6.6. Conditions for 5 minute cycle time

Phase	Duration, mins	Chip temperature set point (°C)
Conditioning	0.5	80
Sample Reference	0.5	25*
Baseline Reference	0.5	25*
Sampling	2.5	25
Desorption (thermal)	1	40, 60, 80

* chip cooling during this phase

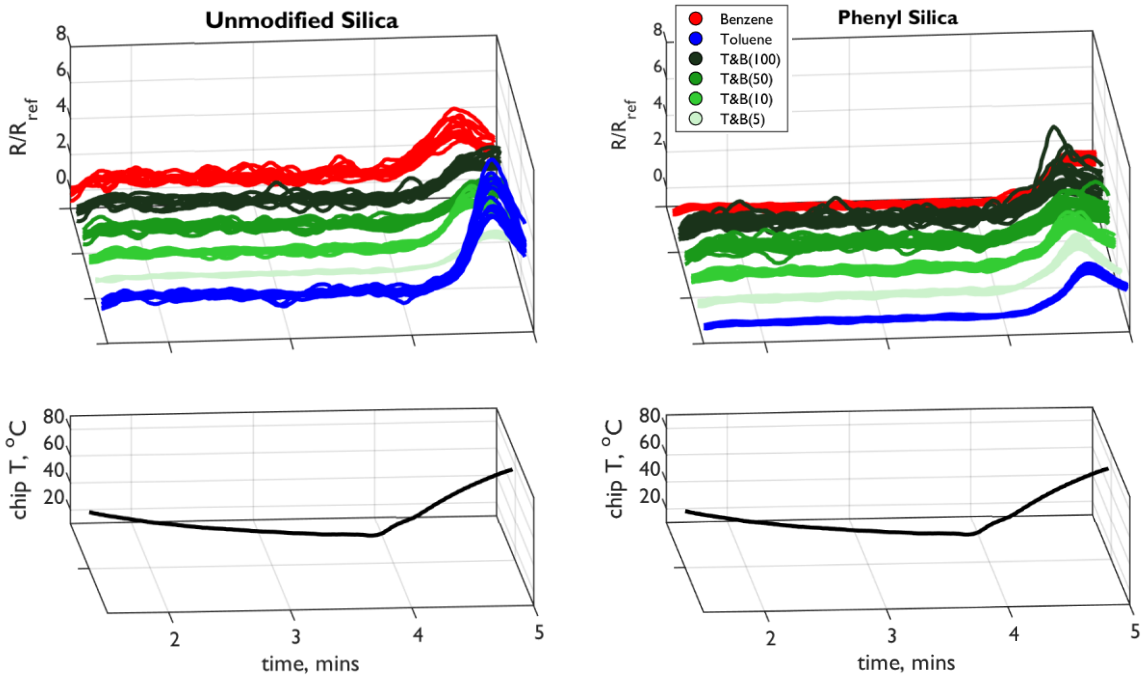

Figure 6.21. Normalised sensor response (R/R_{ref}) for unmodified (*left*) and phenyl (*right*) silica adsorbents with benzene (blue), toluene, (red) and a range of benzene concentrations in toluene (green). R is PID response and R_{ref} is the PID response during the sample reference region (0.5-1 minutes of test cycle). Only sampling and desorption phases are shown.

The normalised response at 5 points (0.25, 0.5, 0.75, 1 and 1.75 minutes) of the sampling phase and 9 points (approximately every 7 seconds from 0 to 1 minutes) of the desorption phases were selected as data features (Figure 6.22). These were then used for principle component analyses (Figure 6.23). The data points are generally well grouped, but are more overlapped than for the 10 minute cycle time data. A significant contributor to this is the increased susceptibility to noise that is an inherent effect of halving all cycle phases. As there is less time to generate a sample reference reading, the normalisation process effectively amplifies any noise captured during the reference phase. Despite this, the mono-component vapour data points are well separated, especially for the phenyl silica adsorbent.

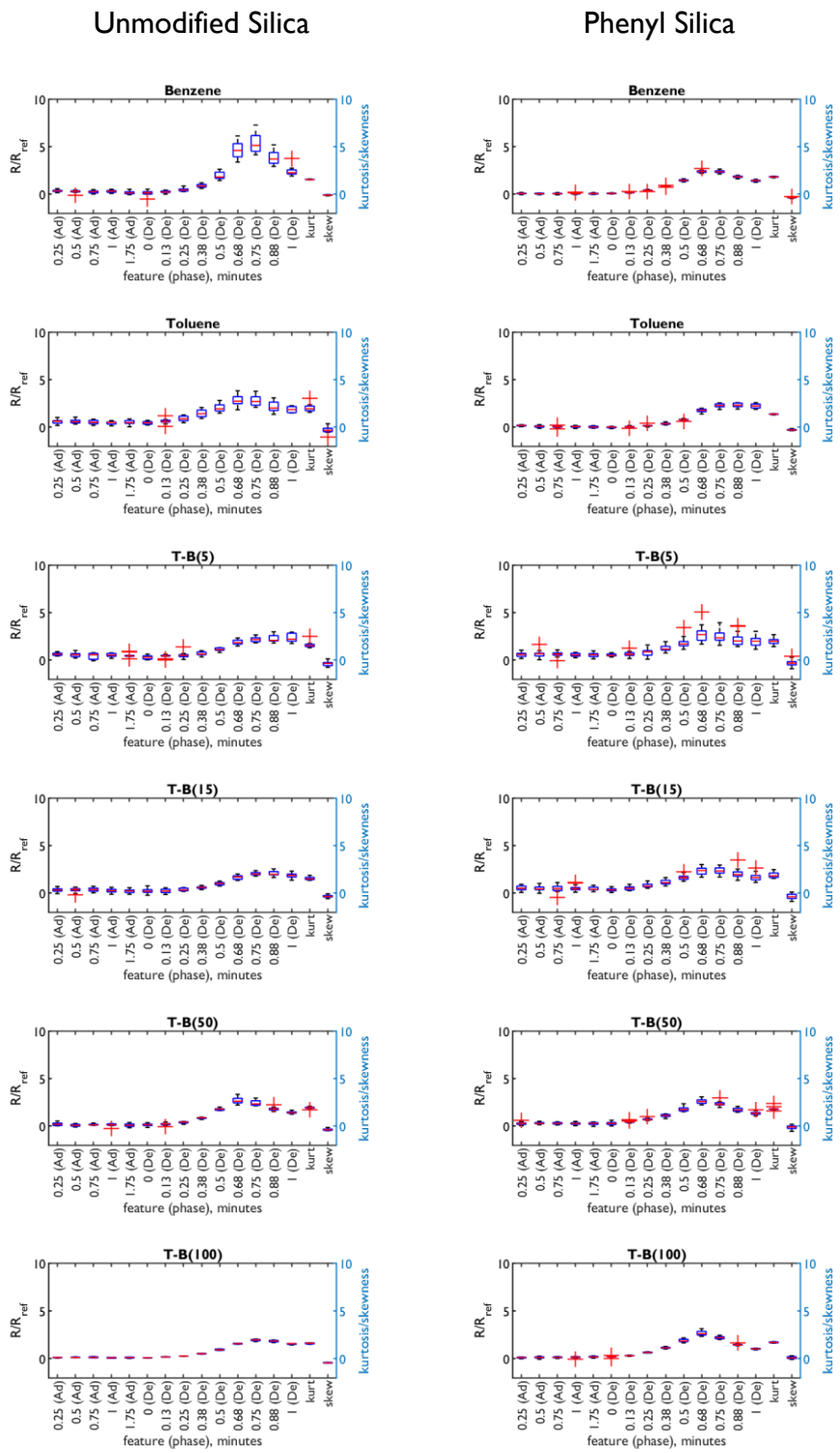

Figure 6.22. Boxplots of feature variables. The central mark indicates the median, and the bottom and top edges of the box indicate the 25th and 75th percentiles, respectively. The 'whiskers' extend to the most extreme data points not considered outliers, which are plotted using the '+' symbol. Abbreviations: Ad: adsorption (sampling phase), De: desorption (desorption phase), kurt: kurtosis, skew: skewness.

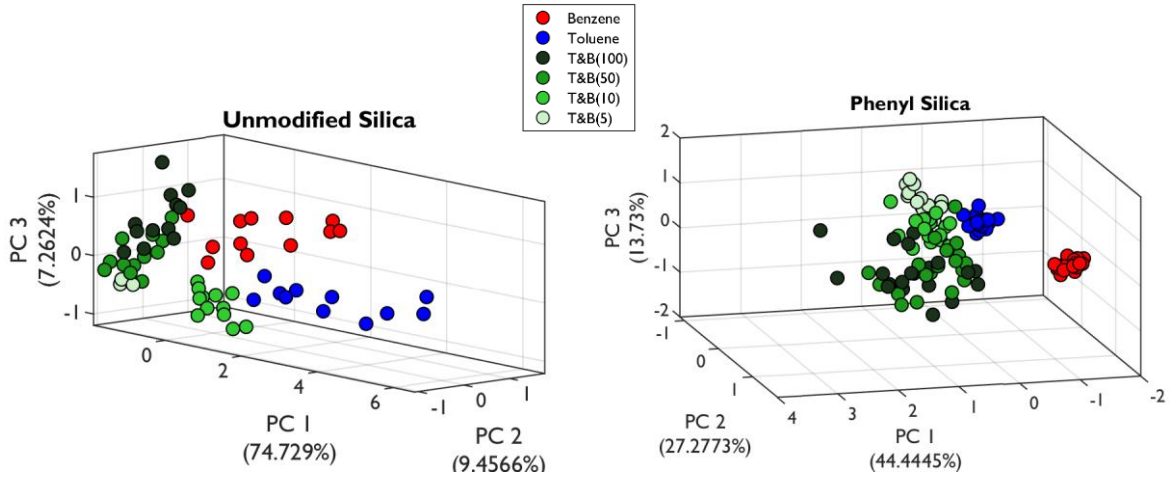

Figure 6.23. Principle Component Analyses (PCA) of the feature data for unmodified (*left*) and phenyl (*right*) silica adsorbents, using features selected from normalised sensor responses

As before, LDA, kNN, SVM and RF supervised classification algorithms were tested with the features described above. The feature data were randomly split into training and test data, as shown in Table 6.7. Training data were used to train the classification algorithms, and the accuracy assesed with test data. Confusion (error) matrices for these assessments are shown in Figure 6.24. The accuracy of the algorithms decreases for 5 minute cycle time, although a few notable cases have high accuracy. For example, LDA with unmodified silica, SVM with phenyl silica and RF with both adsorbents maintain high accruacy. The main conclusions to draw from the shorter, 5 minute, cycle time are that it is possible to shorten some aspects of the test cycle and maintain some selectivity. Most significantly, sampling time can be halfed and significant adsorption still occurs in order to be able to accurately classify many input vapours. Given the approach of data normalisation, the baseline reference phase benefits from more time, as this reduces 'trapped' noise maintained throughout the analysis.

Table 6.7. Split of feature data (training/test)

VOC	Unmodified	Phenyl
Benzene	9/3	15/5
Toluene	8/4	16/4
B100-T	3/1	12/4
B50-T	8/4	12/4
B10-T	9/3	15/5
B5-T	8/4	14/6

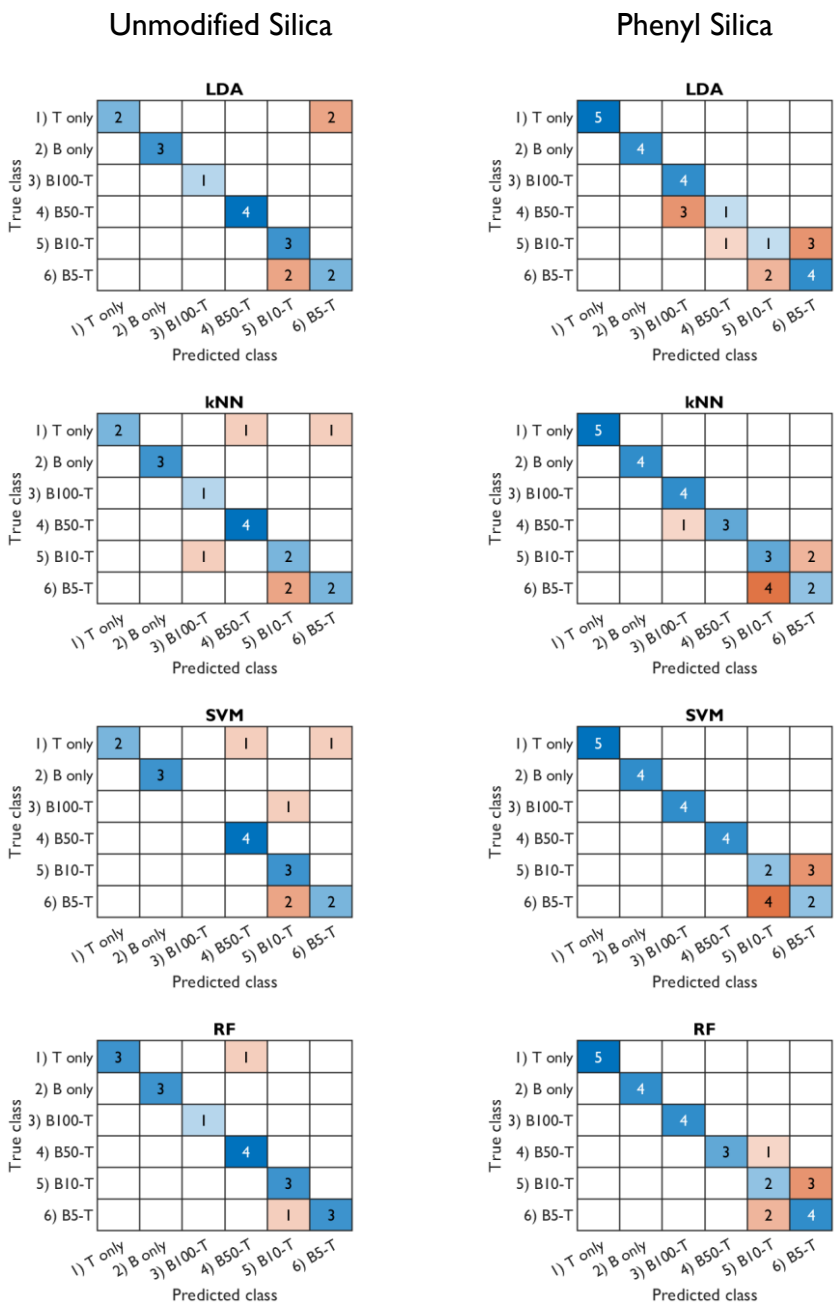

Figure 6.24. Confusion matrices for the application of the classification algorithms applied to feature data from the normalised sensor response (R/R_{ref}) for unmodified (left hand side) and phenyl (right hand side) silica adsorbents. LDA: linear discriminant analysis; SVM: support vector machine; kNN: k-nearest neighbours (k = 5 for unmodified. 3 for phenyl); RF: random forest (number of trees: 30, unmodified; 14 phenyl). Abbreviations: B, benzene; T, toluene

6.5 Vapour Fractions

This section examines the ability of the Adsorption Device to discriminate between different functional groups as mono-component samples, and then dual-component mixtures of benzene, toluene and ethyl benzene. The total cycle time was 10 minutes, but some slight alterations were made to the phases in the cycle (Table 6.8). A fourth temperature step (to 100 °C) was added to follow the 80 °C step, so as to fully desorb adsorbate and water (Figure 6.25). The 100 °C was carried over into the following conditioning phase. Owing to the higher conditioning temperature, the sampling temperature was raised slightly to 30 °C, so as to allow the channel to cool and stabilise prior to the start of sampling. The sampling phase was shortened to allow for more time to regenerate the adsorbent, which would now be maintained at 100 °C for two minutes. The concentrations and corresponding vapour fractions (expressed as percentages) are shown in Table 6.12.

Table 6.8. Updated conditions for 10 minute cycle time

Phase	Duration, mins	Chip temperature set point (°C)
Conditioning	1	100
Sample Reference	1	30*
Baseline Reference	1	30*
Sampling	3.5	30
Desorption (thermal)	3.5	40, 60, 80, 100

* chip cooling during this phase

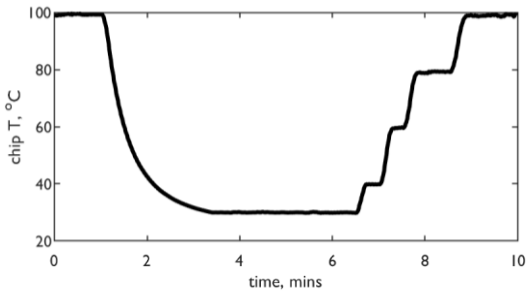

Figure 6.25. Temperature for updated test cycle (Table 6.8)

6.5.1 Single Component Discrimination

Chlorophenyl, chloro and alkyl silica were used as adsorbents for this section. Before examining their capability to discriminate mixtures, they were tested with single component samples (Table 6.9).

Table 6.9. VOCs and concentrations used in this section

VOC	Concentration, ppb
Benzene	250
Toluene	540
Ethyl Benzene	570
para-Xylene	950
MEK	910
Acetone	800
n-Hexane	980

Abbreviations: MEK, methyl ethyl ketone.

The normalised PID responses (R/R_{ref}) during the sampling and desorption phase (3-10 minutes of the test cycle) are shown in Figure 6.26. In general, across all three adsorbents, the similar desorption traces are observed as with the previous section. For example, quick desorption of benzene containing samples and late desorption of ethyl benzene containing samples. The desorption peaks are smaller, but this is to be expected given the shorter sampling time. Comparing between the adsorbents, there are a few key observations to note. Firstly, desorption peaks for benzene are strongest on chlorophenyl silica and weakest on chloro silica, which corresponds to the observations made in Chapter 5. The 100 °C step appears to have successfully desorbed ethyl benzene for all three adsorbents, and xylene for chloro and alkyl silicas. Peaks for ethyl benzene and xylene are shifted to the right, corresponding to their higher boiling points. MEK and acetone both have lower boiling points, but appear to mainly desorb for later, higher temperature steps. In general, the patterns for these two ketones are similar, as is expected given their chemical similarity. In addition, vapour breakthrough is more apparent for chloro silica, especially for benzene. This is also the case for hexane, which appears to only adsorb on chlorophenyl silica. The normalised response at four points during the sampling phase (0.5, 1, 1.5 and 2 minutes) and nine points during the desorption phase (0, 0.5, 0.75, 1, 1.25, 1.5, 1.75, 2, 2.25, 2.5 and 3 minutes) were selected as data features (Figure 6.27). Kurtosis and skewness were not measured.

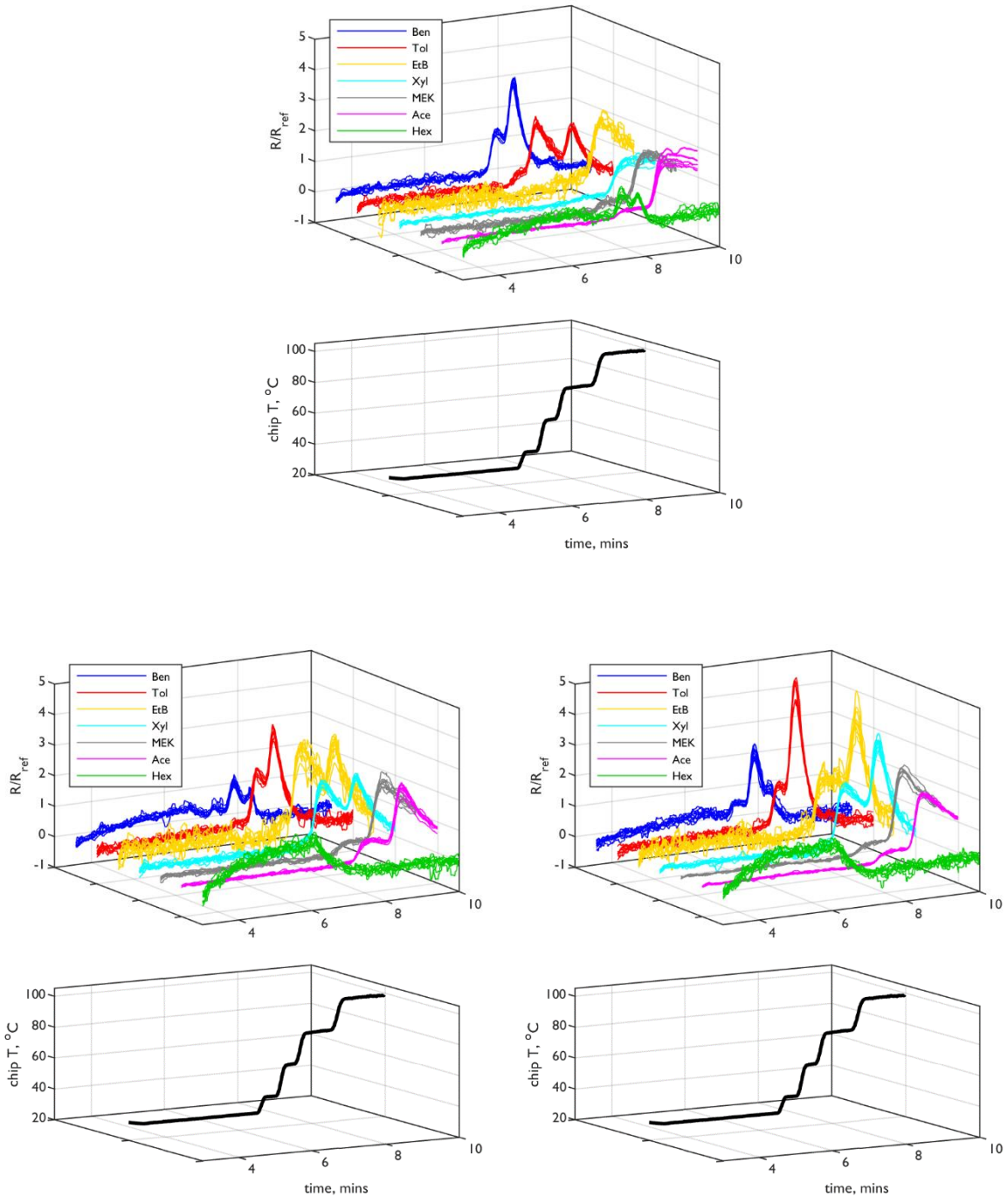

Figure 6.26. Normalised sensor response (R/R_{ref}) for chlorophenyl (*top*), chloro (*bottom left*) and alkyl (*bottom right*) silica adsorbents, for benzene, toluene, ethyl benzene, *para*-xylene, methyl ethyl ketone (MEK), acetone and n-hexane. R is PID response and R_{ref} is the PID response during the sample reference region (1-2 minutes of test cycle). Only sampling and desorption phases are shown. Abbreviations: Ben, benzene; Tol, toluene; EtB, ethyl benzene; Xyl, *para*-xylene; Ace, acetone; Hex, n-hexane.

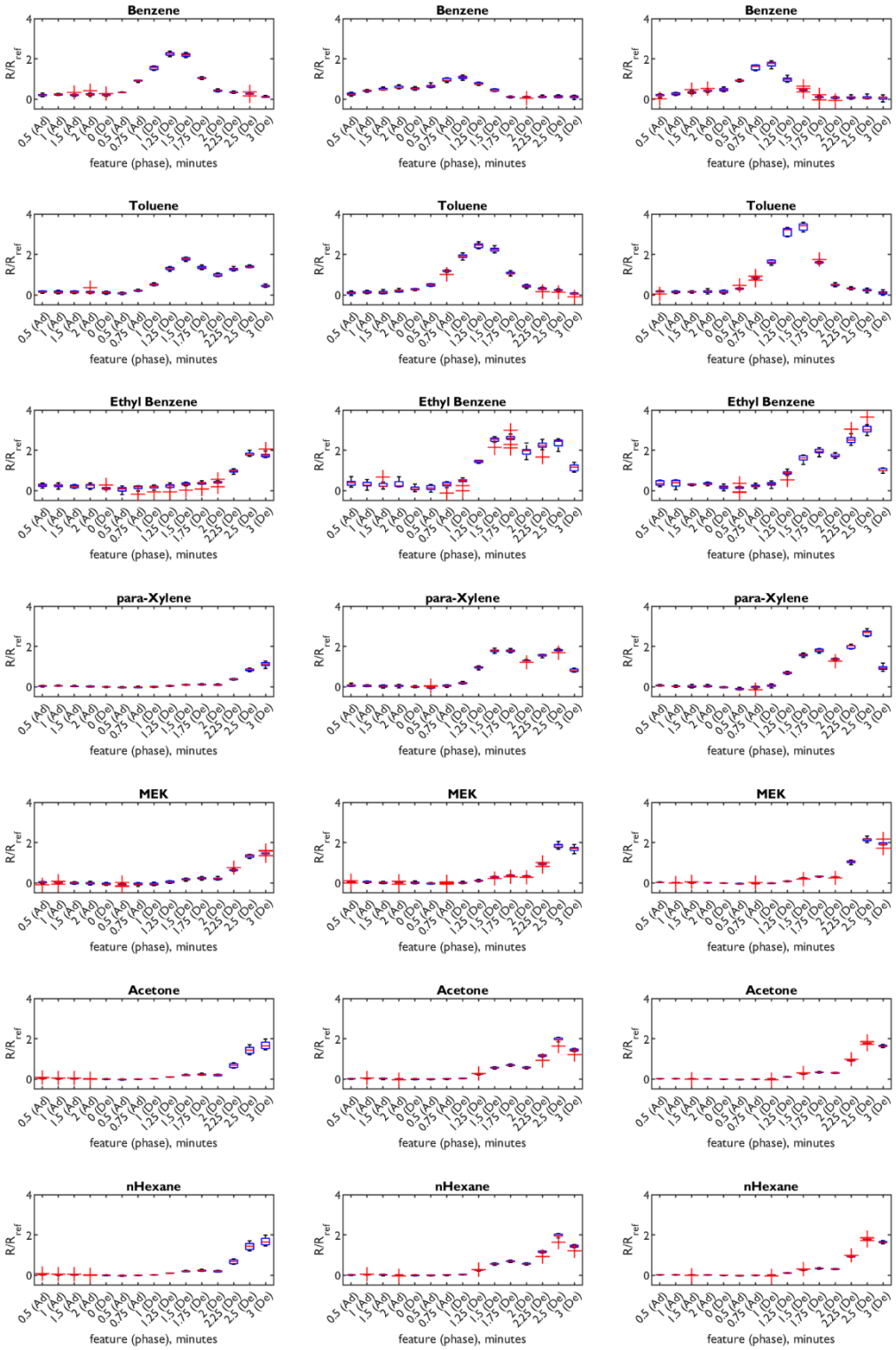

Figure 6.27. Boxplots of feature variables for chlorophenyl silica. The central mark indicates the median, and the bottom and top edges of the box indicate the 25th and 75th percentiles, respectively. The 'whiskers' extend to the most extreme data points not considered outliers, which are plotted using the '+' symbol. Abbreviations: Ad: adsorption (sampling phase), De: desorption (desorption phase).

These features were then used for principle component analysis (Figure 6.28). In general, these analyses suggest that the samples are well grouped and mostly distinct from each other, especially for chloro silica. There is some correlation, most significantly for acetone and MEK with chlorophenyl and alkyl silica, although the samples are clearly discriminable with chloro silica. Perhaps the most interesting observation is the extent to which benzene and toluene are discriminable for all adsorbents. These data indicate that building a selective sensor for these compounds would be possible.

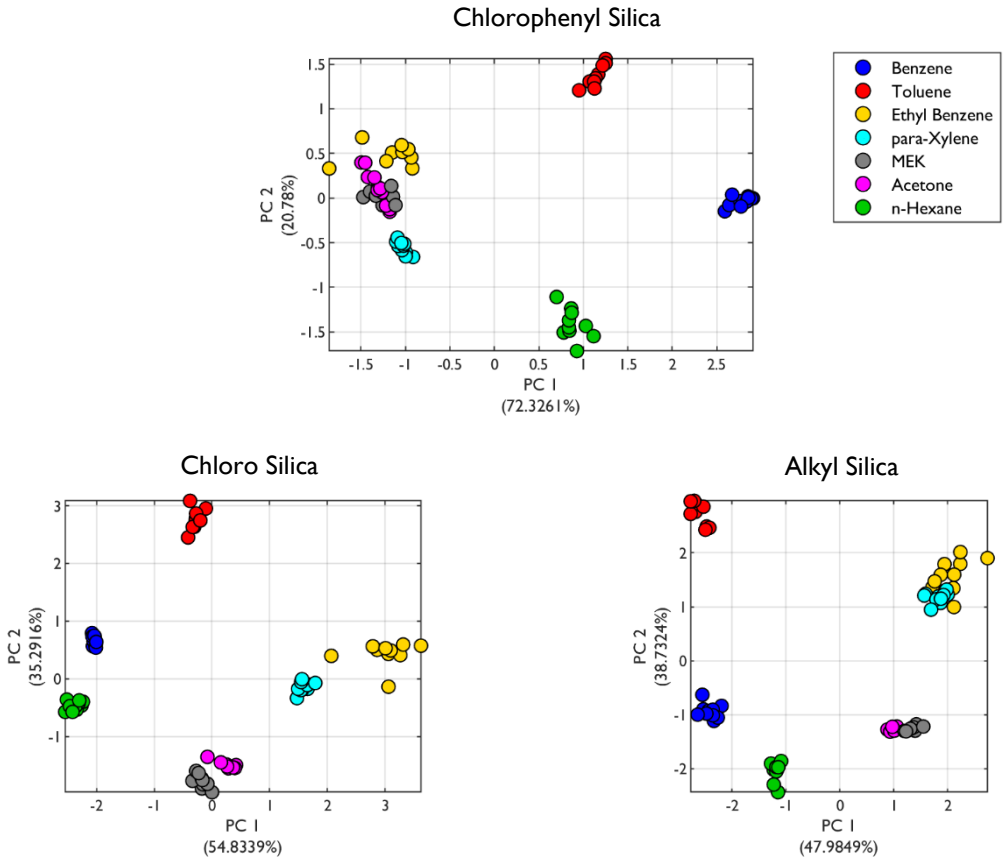

Figure 6.28. Principle Component Analyses (PCA) of the feature data for chlorophenyl (*top*), chloro (*bottom left*) and alkyl (*bottom right*) silica adsorbents, using features selected from normalised sensor responses. Abbreviations: MEK, methyl ethyl ketone.

As before, LDA, kNN, SVM and RF supervised classification algorithms were tested with these features. Feature data were randomly split into training and test data, as shown in Table 6.10. Training data were used to train the classification algorithms, and the accuracy assesed with test data. Confusion (error) matrices for these assessments are shown in Figure 6.29. The classfication accuracy for the algorithms is shown in Table 6.11.

Table 6.10. Split of feature data (training/test)

VOC	chlorophenyl	chloro	alkyl
Benzene	7/3	7/3	7/3
Toluene	7/3	7/3	7/3
Ethyl Benzene	7/3	7/3	7/3
para-Xylene	7/3	7/3	7/3
MEK	7/3	7/3	7/3
Acetone	7/3	7/3	7/3
n-Hexane	7/3	7/3	7/3

Abbreviations: MEK, methyl ethyl ketone

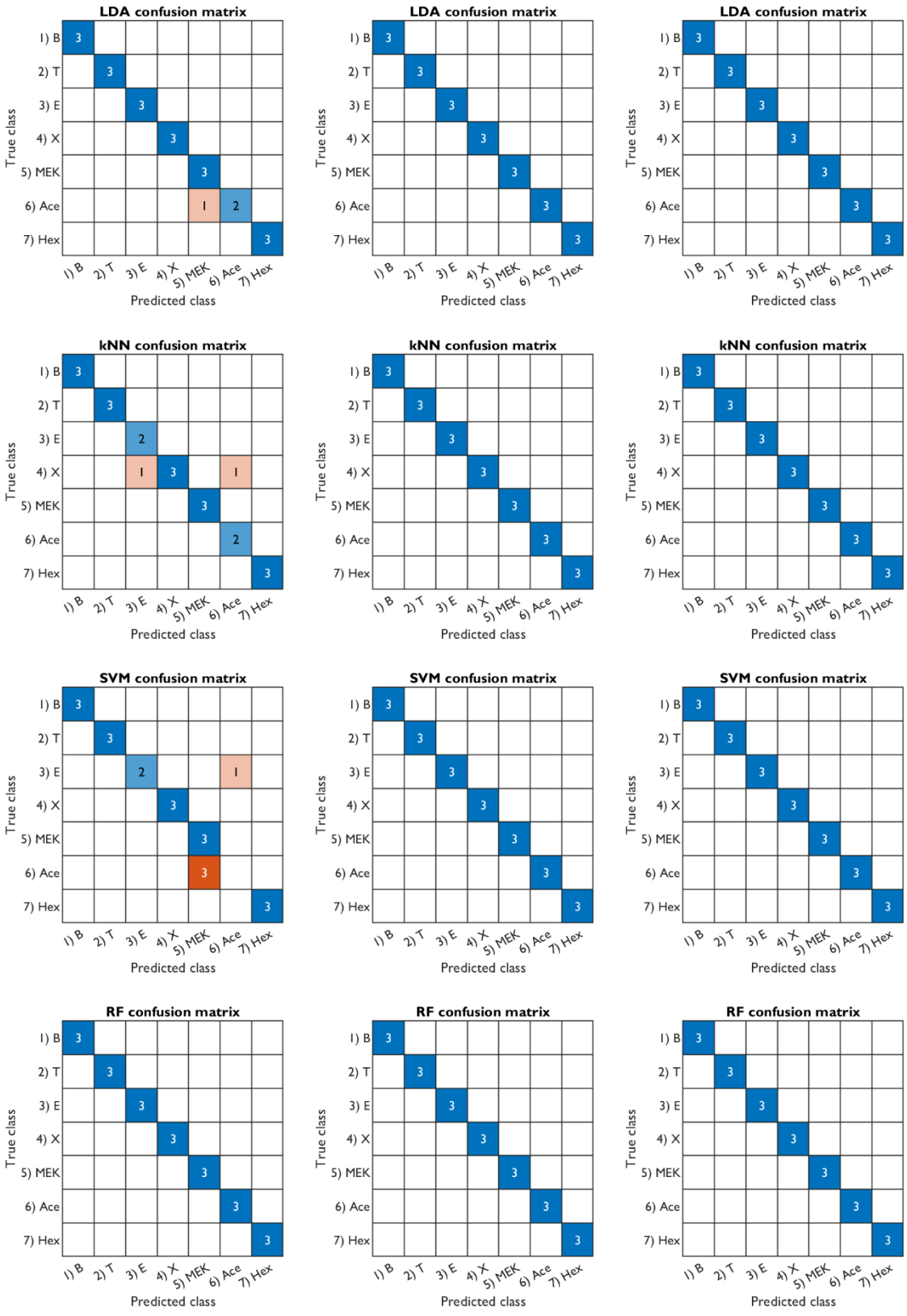

Figure 6.29. Confusion matrices for the application of the classification algorithms applied to feature data from the normalised sensor response (R/R_{ref}) for chlorophenyl (*left*), chloro (*middle*) and alkyl (*right*) silica adsorbents. LDA: linear discriminant analysis; SVM: support vector machine; kNN: k-nearest neighbours (k = 3); RF: random forest (number of trees: 40).

Abbreviations: B, benzene; T, toluene; E ethyl benzene; X, *para*-xylene; MEK, methyl ethyl ketone; Ace, acetone; Hex, n-hexane.

Table 6.11. Classification Accuracy

	LDA	kNN	SVM	RF	Mean
Chlorophenyl	96%	93%	85%	100%	94%
Chloro	100%	100%	100%	100%	100%
Alkyl	100%	100%	100%	100%	100%

These confusion matrixes clearly show that, for these vapours, the signals for mono-component vapours are discriminable. Surprisingly, although these errors derived from similar compounds (e.g. ethyl benzene verses para-xylene or MEK versus acetone), chlorophenyl silica had the lowest accuracy of the three adsorbents. As noted in the PCA plots, the discrimination of benzene and toluene is high, and 100% accurate for all algorithms and all adsorbents. It should be noted that the concentrations of these vapours, although in the ppb-range, were relatively high. Despite this, these results indicate that the Adsorption Device can be used to accurately discriminate a range of VOCs with different functionality. In addition, the discrimination of chemically similar compounds, such MEK and acetone, is possible with high accuracy, so long as appropriate adsorbents and analysis techniques are used. Discrimination accuracy of different vapour fractions is explored in the following section.

6.5.2 Vapour Fraction Discrimination

This section examines the capability of the Adsorption Device to discriminate dual-component mixtures of benzene, toluene and ethyl benzene. The concentrations and corresponding vapour fractions (expressed as percentages) are shown in Table 6.12. The normalised PID responses (R/R_{ref}) during the sampling and desorption phase (3-10 minutes of the test cycle) are shown in Figure 6.30. In general, for all three adsorbents, traces are observed compare well to previous sections. For example, quick desorption of benzene containing samples and late desorption of ethyl benzene containing samples. Comparing between the adsorbents, desorption peaks for benzene-containing vapours are strongest on chlorophenyl silica and weakest on chloro silica, which corresponds to the observations made in Chapter 5. The 100 °C step appears to have successfully desorbed mono-component ethyl benzene for all three adsorbent. Peaks for all ethyl benzene containing samples are shifted to the right (when this step is applied. In addition, vapour breakthrough is more apparent for chloro silica, especially for benzene. The normalised response at four points during the sampling phase (0.5, 1, 1.5 and 2 minutes) and nine points during the desorption phase (0, 0.5, 0.75, 1, 1.25, 1.5, 1.75, 2, 2.25, 2.5 and 3 minutes) were selected as data features (Figure 6.31, Figure 6.32 & Figure 6.33 for chlorophenyl, chloro and alkyl silicas, respectively). Kurtosis and skewness were not measured.

Table 6.12. Concentrations used in this section

	concentration, ppb			vapour fraction		
Sample	B	T	E	B	T	E
B	250	-	-	100%	-	-
BT	450	690	-	39%	61%	-
TB	450	210	-	68%	32%	-
T	-	540	-	-	100%	-
TE	-	710	360	-	66%	34%
ET	-	280	360	-	44%	56%
E	-	-	570	-	-	100%
EB	280	-	360	44%	-	56%
BE	720	-	360	67%	-	33%

Abbreviations: B, benzene; T, toluene, E ethyl benzene.

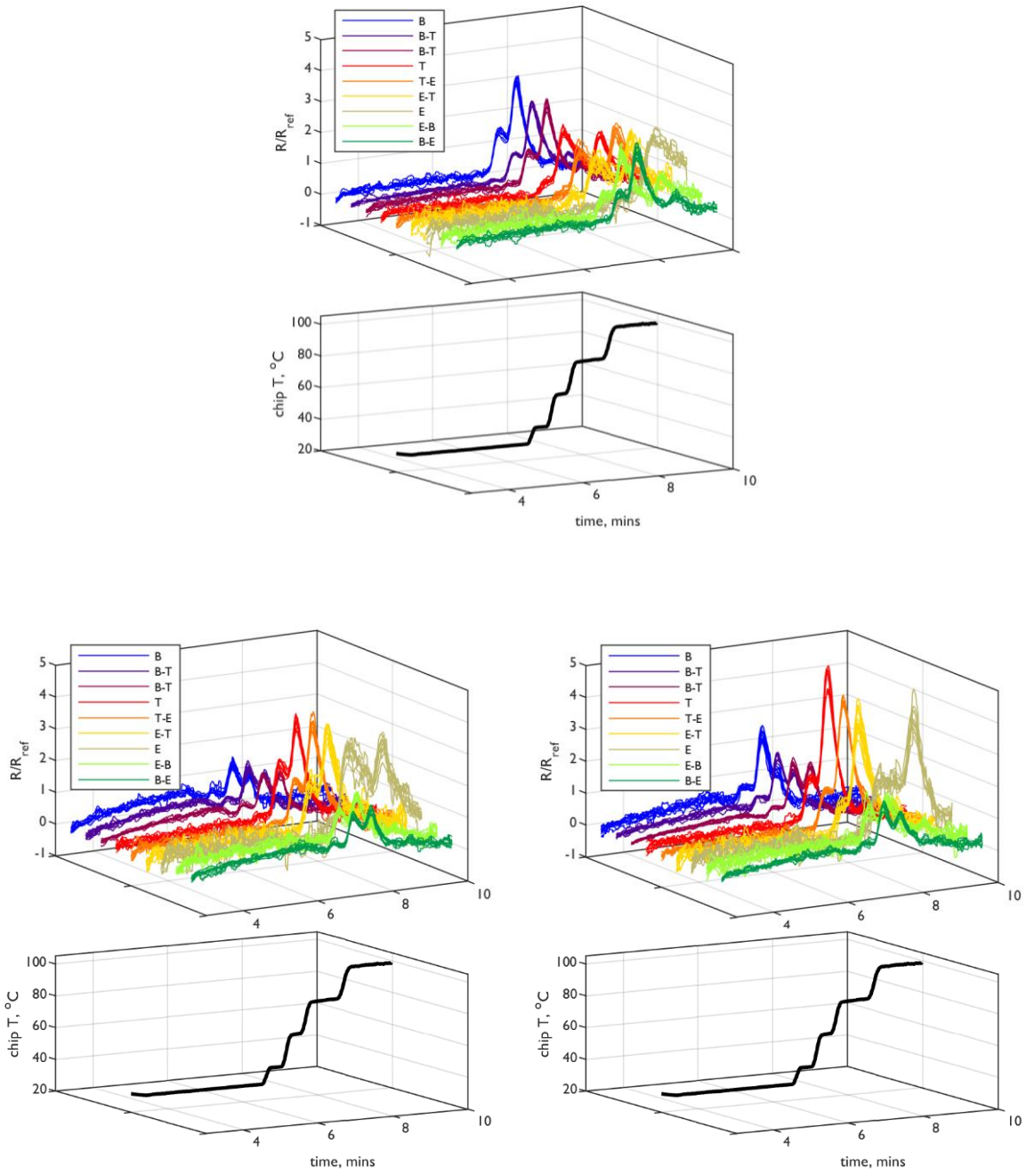

Figure 6.30. Normalised sensor response (R/R_{ref}) for chlorophenyl (*top*), chloro (*bottom left*) and alkyl (*bottom right*) silica adsorbents, for benzene, toluene, ethyl benzene and a range of two-vapour fractions (note the first letter in the legend corresponds to the larger fraction). R is PID response and R_{ref} is the PID response during the sample reference region (1-2 minutes of test cycle). Only sampling and desorption phases are shown. Abbreviations: B, benzene; T, toluene; E ethyl benzene.

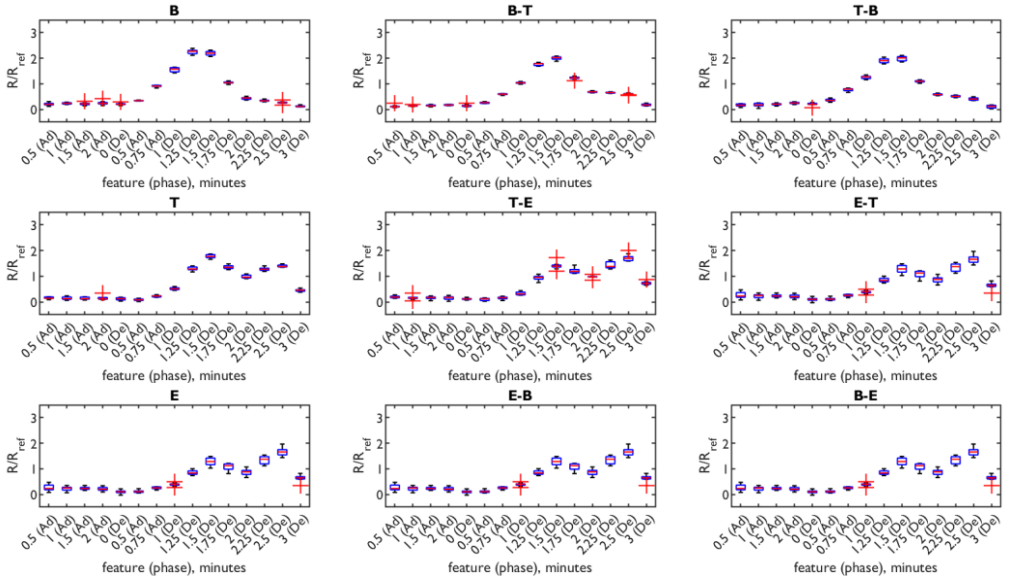

Figure 6.31. Boxplots of feature variables for chlorophenyl silica. The central mark indicates the median, and the bottom and top edges of the box indicate the 25th and 75th percentiles, respectively. The 'whiskers' extend to the most extreme data points not considered outliers, which are plotted using the '+' symbol. Abbreviations: Ad: adsorption (sampling phase), De: desorption (desorption phase), B, benzene; T, toluene, E ethyl benzene.

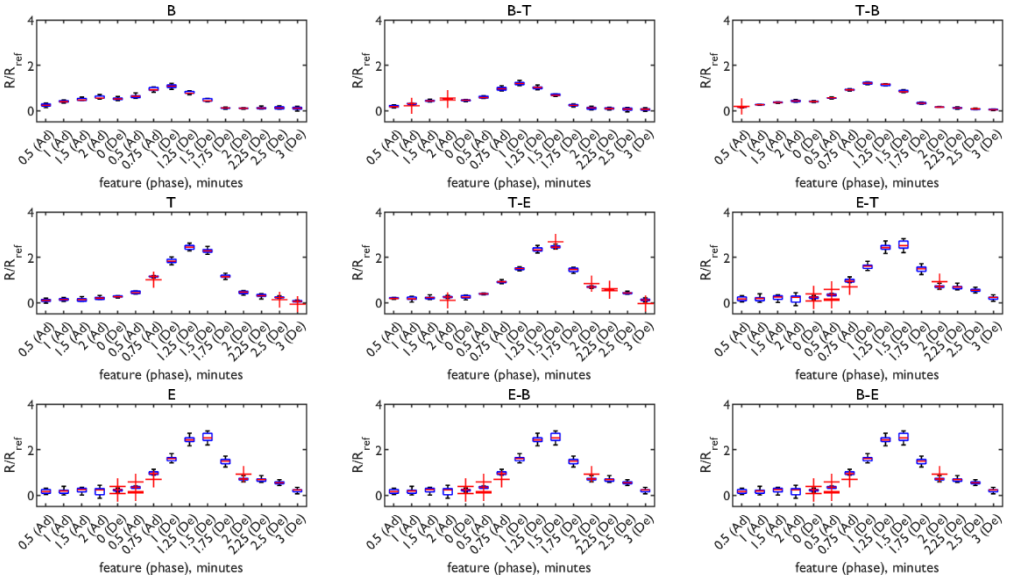

Figure 6.32. Boxplots of feature variables for chloro silica. The central mark indicates the median, and the bottom and top edges of the box indicate the 25th and 75th percentiles, respectively. The 'whiskers' extend to the most extreme data points not considered outliers, which are plotted using the '+' symbol. Abbreviations: Ad: adsorption (sampling phase), De: desorption (desorption phase), B, benzene; T, toluene, E ethyl benzene.

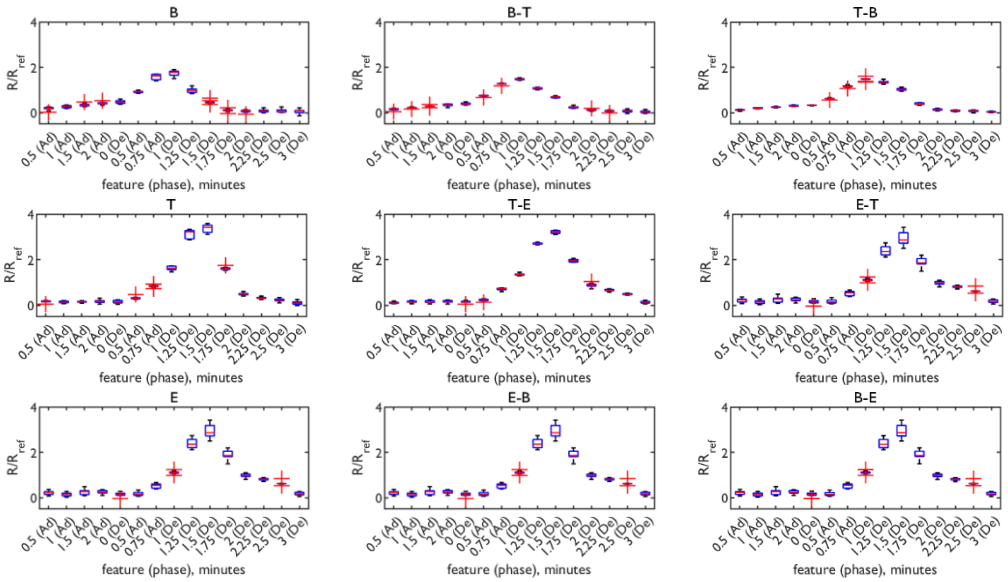

Figure 6.33. Boxplots of feature variables for alkyl silica. The central mark indicates the median, and the bottom and top edges of the box indicate the 25th and 75th percentiles, respectively. The 'whiskers' extend to the most extreme data points not considered outliers, which are plotted using the '+' symbol. Abbreviations: Ad: adsorption (sampling phase), De: desorption (desorption phase), B, benzene; T, toluene, E ethyl benzene.

These features were then used for principle component analysis (Figure 6.34). In general, these analyses suggest that the samples are well grouped and mostly distinct from each other, although there are some samples that are well correlated. For example, the benzene-containing samples on chloro and alkyl silica. For chlorophenyl silica, the benzene containing samples have more variance than for chloro and alkyl silica. All three adsorbents have little variance for the toluene-ethyl benzene mixtures, although alkyl silica appears to perform the best in this instance, having the least overlap of the T-E and E-T samples. Mono-component ethyl benzene correlates the least with other samples for all adsorbents, in accordance with the above observation that most adsorbate is removed at higher temperature steps. As with the earlier sections of this chapter, LDA, kNN, SVM and RF supervised classification algorithms were tested with these features. Feature data were randomly split into training and test data, as shown in Table 6.13. Training data were used to train the classification algorithms, and the accuracy assesed with test data. Confusion (error) matrices for these assessments are shown in Figure 6.35. The classfication accuracy for the algorithms is shown in Table 6.14.

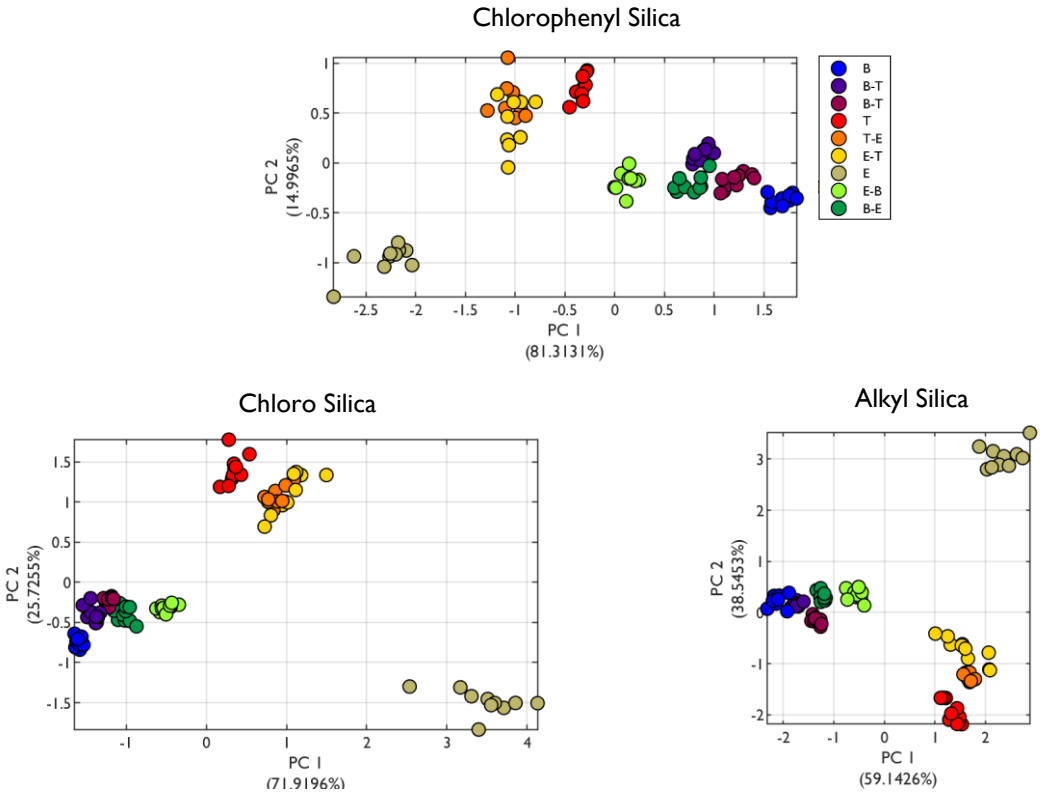

Figure 6.34. Principle Component Analyses (PCA) of the feature data for chlorophenyl (*top*), chloro (*bottom left*) and alkyl (*bottom right*) silica adsorbents, using features selected from normalised sensor responses. Abbreviations: B, benzene; T, toluene, E ethyl benzene

Table 6.13. Split of feature data (training/test)

VOC	chlorophenyl	chloro	alkyl
B	7/3	7/3	7/3
B-T	7/3	7/3	7/3
T-B	7/3	7/3	7/3
T	7/3	7/3	7/3
T-E	7/3	7/3	7/3
E-T	7/3	7/3	7/3
E	7/3	7/3	7/3
E-B	7/3	7/3	7/3
B-E	7/3	7/3	7/3

Abbreviations: B, benzene; T, toluene, E ethyl benzene.

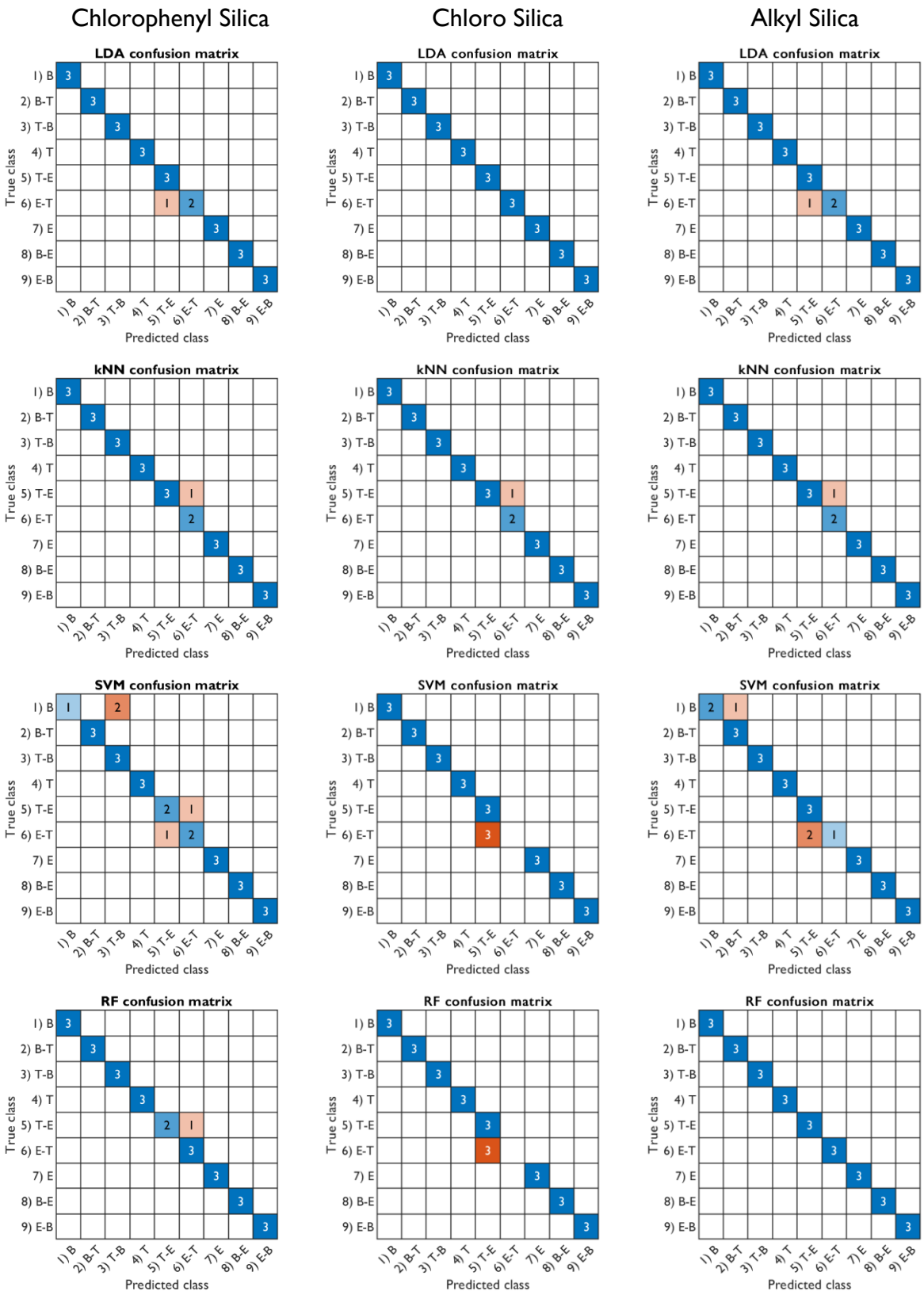

Figure 6.35. Confusion matrices for the application of the classification algorithms applied to feature data from the normalised sensor response (R/R_{ref}) for chlorophenyl (*left*), chloro (*middle*) and alkyl (*right*) silica adsorbents. LDA: linear discriminant analysis; SVM: support vector machine; kNN: k-nearest neighbours (k = 5 for chlorophenyl, 5 for chloro and 3 for alkyl); RF: random forest (number of trees: 39, chlorophenyl; 25 chloro; 25 alkyl). Abbreviations: B, benzene; T, toluene; E ethyl benzene.

Table 6.14. Classification Accuracy

	LDA	kNN	SVM	RF	Mean
Chlorophenyl	96%	96%	85%	96%	93%
Chloro	100%	96%	89%	89%	94%
Alkyl	96%	96%	89%	100%	95%

In general, these confusion matrixes indicate that the used classification algorithms have high accuracy, with an average across all samples of approximately 94%. LDA is especially accurate, with the only incorrect classifications for E-T versus T-E. Interestingly, the quantity adsorbed, as estimated in Chapter 5, had little impact on the different adsorbents accuracy. The largest contribution to inaccuracy came from classifying toluene and ethyl benzene samples. Benzene-toluene discrimination is highly accurate, with the only incorrect classifications occurring for the SVM algorithm. Benzene-ethyl benzene has 100% accuracy across all four algorithms. Based on these accuracies, the Adsorption Device could discriminate a range of vapour fractions for at least these three vapours, and benzene mixtures especially. A key caveat here is the concentrations tested, which are at least an order of magnitude higher than data shown earlier in this chapter. Despite this, selectively well below the ppm-range has been achieved, and it should be possible to carry over the classifications accuracies shown here to much lower concentrations.

6.6 Discussion

The main focus of this chapter was to combine aspects of adsorption and desorption, and use them to examine the potential for sensor selectivity for mixtures of BTEX compounds. Few published sensors that claim selectivity are tested with mixtures of vapours. When gas sensors are used to test VOC mixtures, they are typically included as part of a miniaturised gas chromatography (GC) system.[45,99] While such systems are able to separate mixtures, the systems themselves are often impractical for use as a sensor for automated monitoring air quality (AQ) across a network. The results of this chapter build upon reported sensors that have shown unique signals for individual VOCs, by examining the signals produced by mixtures of benzene, toluene and ethyl benzene.

The three heating profiles introduced in the previous chapter – pulsed, gradual and stepwise – were tested with mixtures of benzene (at concentrations between 5 and 100 ppb) and toluene (at 220 ppb). These concentrations were selected because they represent values that are typical of air quality environments. The results indicate that it is possible to produce sensor responses that can be discriminated from each other in concentrations in the double and triple figure parts-per-billion (ppb) range, for single- and double-component benzene and toluene vapours. Most published sensors that focus on selective detection of VOCs operate in the ppm range. For example, the graphene sensor by Nallon et al was tested using saturated headspace vapour,[137] Tonezzer's tin oxide sensor was tested with vapours at 1-50 ppm,[158] and Agbroko and Covington's PID sensor was tested down to 2 ppm.[109] A notable exception is the molecular receptor sensor developed by Trzciński et al, which was able to detect 10 ppb of benzene (with 10 minute sampling time) and 1.25 ppb (with 50 minutes sampling time), but as previously noted, such receptors are challenging to synthesize.[150] This work has sought to build on these sensors and focus on sensitivity and selectivity simultaneously, while aiming to produce a system that could be feasibly built and readily deployed for AQ applications.

Initial tests of with 40 minute test cycles (section 6.3), confirmed that the Adsorption Device was able to distinguish between mono-component benzene and toluene vapours, as well as differences between different dual-component mixtures. An area where the Adsorption Device struggled for repeatability was at low concentration of benzene (i.e. 10 and 15 ppb), which is likely due to being well below the PID detection limit for benzene. Despite this, these results demonstrated that the Adsorption Device could reliably produce signals in the double digit and higher ppb range. Of the three heating profiles, the stepwise heating profile was found to produce the 'best' PID responses, in terms of the higher consistency and accuracy of the responses, as well as being the quickest profile of the three.

Consequently, this profile was carried forward for experiments that sought to examine performance at practical cycle times.

A key aspect of measuring pollutants for AQ networks is the speed of measurement. It is common for hourly pollutant concentrations to be measured. As demonstrated in section 6.3, the Adsorption Device could produce repeatable signals over a 40 minute period. However, producing readings multiple times per hour would add robustness to hourly readings, and provide some resilience against fluctuations of pollutant concentration over an hourly (or daily etc.) measurement period. Using a ten minute cycle time, the Adsorption Device was successfully able to differentiate between benzene, toluene, ethyl benzene, *para*-xylene and methyl ethyl ketone using both unmodified silica and phenyl silica (section 6.4.1). Classification algorithms were used to validate this observation, and k-nearest-neighbours (kNN) was 100% accurate for both adsorbents tested. All algorithms (kNN, LDA: Linear Discriminant Analysis, SVM: Support Vector Machines and RF: Random Forest) had an accuracy of 96% for this experiment. Although these are high values, it should be noted that they are based on only 5 VOCs, and, as emphasised above, are only tested on mono-component vapours. Despite this, the detection of sub-ppm vapours within 10 minutes is a promising result that competes with the sensor systems mentioned above and in Chapter 1.

The same test conditions were then applied to mixtures of benzene and toluene vapour (section 6.4.2). These results indicated that it is possible to produce distinct sample responses and maintain accuracy using 10 minute cycle times (Table 6.5). The main source of inaccuracy here was differentiating between the 5 ppb and 10 ppb benzene(-toluene) mixtures. Considering just these samples, the classification accuracy was 89% and 66% for unmodified and phenyl silica, respectively. Excluding those samples, the average accuracy of all classification algorithms was 97% and 100% for unmodified and phenyl silica, respectively. These results demonstrate that it is possible to differentiate certain mixtures of benzene and toluene, and at high accuracy when the concentration of benzene is above 10 ppb. Based on the principles observed with the benzene/toluene mixtures, the discrimination of benzene from other aromatic vapours should be possible with similar accuracy (based on the signals observed in the results of the previous chapter).

This hypothesis was tested using three other adsorbents – chlorophenyl, chloro and alkyl silica – and mixtures of benzene, toluene and ethyl benzene (section 6.5). Some small modifications to the phase times and temperatures were also made, while also keeping the test cycle at 10 minutes in length. Some sampling time was sacrificed to allow for a longer thermal desorption/conditioning phase, and to allow the device to reach 100 °C during this phase. This was found to better desorb vapours, such as ethyl benzene, and regenerate the adsorbent between cycles. Investigating a range of compounds – aromatics,

ketones and alkanes – indicated that the Adsorption Device could accurately select between functional groups, although this was only tested with single-component vapours. Testing with different vapour fractions of BTE, it was found that the Adsorption Device could produce discriminable signals for all vapour samples, which was verified using PCA and four classification algorithms (LDA, kNN, SVM and RF). Results were especially accurate for discrimination of benzene, even with mixture of toluene and ethyl benzene. In order to get a more thorough assessment of accuracy, it would be necessary to repeat the test cycles many more times, but the results shown here demonstrate promise for the found accuracies to be repeatable. Of the classification algorithms used, LDA, kNN and RF were found to be the most accurate. The generalizability of these results is limited by having only tested (dual-component mixtures of) three aromatic VOCs, so further studies with other cross-contaminants would need to be done in order to verify accuracies in field conditions. Despite this, this chapter has shown that his method offers an inexpensive, quick and potentially very accurate means of achieving VOC selectivity in the sub-ppm range.

Chapter 7 Conclusion and Further Work

7.1 Conclusion

There is a need for a practical method of selectively measuring VOCs across air quality networks. Many VOCs are toxic, and organisations including the World Health Organisation recommend exposure limits for certain compounds, including benzene – a proven carcinogen. Given the typically low concentrations of volatile pollutants in ambient environments, a selective and sensitive detection method is desirable. Gas chromatography has been considered the gold standard for selective VOC measurement,[27,53–55] but its use for practical applications is limited due to high cost, large size and complexity of operation. Sensors could offer a promising means of addressing practicality issues, as they tend to be small, low-power and automatable. Many VOC sensors and sensor systems have been proposed as selective to certain pollutants, but few have demonstrated robust selectivity. This thesis presents a VOC sensing system for selective detection, achieved through control of the phase equilibrium between gaseous compounds and species adsorbed on the adsorbent. Selection of particular surface chemistries, in combination with temperature control, allows the control of VOC adsorption and desorption to and from modified silica adsorbents.

Many reported VOC adsorbents, such as many MOF materials, only achieve high capacity at high partial pressures and also require high temperatures to regenerate the adsorbent.[178] Therefore, silica was selected as an adsorbent for its high surface area, the reversibility of adsorption and a relatively simple means of modification (silanisation). Modified adsorbents were packed into an aluminium channel mounted onto a peltier device, which controlled the heat of, and therefore desorption from, the adsorbents. This system, here called the Adsorption Device, was designed such that its operation would be automated and practical, and its construction inexpensive. The Adsorption Device fulfilled these

conditions, and operated without the need for the application of high pressure and/or external carrier gases.

Adsorption may be physical (physisorption) or chemical (chemisorption), depending on the strength of interactions between the adsorbent and adsorbate. In pursuing reversible adsorption, lower energy physisorption enables desorption at relatively low temperatures – i.e. up to approximately 100 °C with the Adsorption Device. This thesis presented seven silica adsorbents, each with different chemical functionality: unmodified (silanol group), amino, chloro, alkyl, fluoroalkyl, phenyl and chlorophenyl. Silica was modified via silanisation reactions, which had varying effects on adsorbent surface area and pore volume, in addition to surface functionality. Contact angle measurement indicated that unmodified and amino silicas were hydrophilic, whereas chloro, alkyl, fluoroalkyl, phenyl and chlorophenyl silicas were hydrophobic. All materials were found to be thermostable in the operational temperature range of the Adsorption Device (20-105 °C). Nitrogen isotherms for all adsorbents were Type IV. Further analysis of the isotherms with the Freundlich adsorption model indicated that the silica materials are 'poor' adsorbents, but this categorisation is typically reserved for pollutant trap applications, rather than as sensing materials.

As common pollutants with proven toxicity, benzene, toluene, ethyl benzene and *para*-xylene (BTEX) were chosen as primary VOCs of interest for this work. Analysis of BTEX adsorption with the seven adsorbents revealed that different functionality influenced adsorbent capacity. Groups containing aromatic groups – phenyl and chlorophenyl silicas – were shown to have high capacity, which is most likely due to the additional energy stabilisation available through pi-pi stacking interactions. The estimated enthalpies of adsorption for BTEX with all adsorbents indicate that adsorption was physical rather than chemical, although the strength of this interaction varied depending on the adsorbent surface functionality. The introduction of aromatic functionality – phenyl and chlorophenyl groups – appears to increase BTEX enthalpy of adsorption. Characterisation data of fluoroalkyl silica indicated that the functionalisation may have formed a thick silane layer over the silica particle, covering, or perhaps filling, the pores and significantly reducing the surface area and accessible pore volume. This had subsequent effects for BTEX adsorption on fluoroalkyl silica, despite the introduction of potentially BTEX-favourable apolar fluoroalkyl moiety. Therefore, adding functionality needs to be carefully considered alongside physical features (i.e. pore size and surface area).

A useful feature of the Adsorption Device is the capability to track adsorption in real time, as the detection component (photoionisation detector, PID) is downstream of the adsorbent channel. Principle Component Analysis (PCA) demonstrated that the signals produced during adsorption varied sufficiently between vapours (and adsorbents) that they could be distinguished from each other. The

estimated quantity of adsorbate broadly corresponded with the boiling points (and inversely with vapour pressures) of BTEX – for example, benzene, the compound with the lowest boiling point (and highest vapour pressure), adsorbed the least on all adsorbents tested. Adsorbents that could form favourable interactions with BTEX were able to increase the amount of adsorption, including phenyl, chlorophenyl and alkyl silica.

This thesis proposed that desorption of adsorbate could be influenced by applying different heating profiles. Adsorbent surface chemistry also influences the phase equilibrium between gaseous compound and solid adsorbent. The reversible nature of BTEX adsorption on silica meant that adsorbate was found to desorb spontaneously in the absence of a sample flow, even at ambient temperatures. Desorption rate is influenced by the temperature of the adsorbent, and three different heating profiles were developed for use with the Adsorption Device: pulsed (on-off heating steps of increasing temperature), gradual (exponential increase in chip temperature) and stepwise (gradual three step increase). These were found to modulate the PID response, and in turn presented partially unique signals for BTEX compounds on different adsorbents. The primary motivation of applying different heating profiles was to elucidate the identity of the sample vapour, or vapours. For this reason the photoionisation detector (PID) response data was normalised to the reference reading taken of the direct sample vapour. This was found to make the vapour largely independent of sample concentration, at least in the concentration range tested (approximately 0-100 ppb). As was the case for sampling phase (i.e. adsorption) data, PCA for desorption phase data demonstrated that the response signals varied sufficiently between vapours that they could be distinguished from each other. Responses for TEX vapours were strong for all adsorbents except fluoroalkyl. Signals for benzene were less pronounced, largely due to less adsorption as described above. Phenyl and chlorophenyl silicas demonstrated the strongest responses for benzene, followed by alkyl and unmodified silica.

This work evaluated the accuracy of four classification algorithms – LDA, kNN, SVM and RF – to identify individual BTEX and methyl ethyl ketone vapours using unmodified and phenyl silica in the adsorption device. Operating with a stepwise heating profile and a 10 minute test cycle time, vapour classification accuracy was 98% and 99% for unmodified and phenyl silica, respectively. This work also evaluated the capability of the Adsorption Device to discriminate mixtures of benzene and toluene. Discrimination accuracy between the six different samples (benzene only, toluene only and four toluene-benzene mixtures), was lower than the values found for individual vapours, but at 94% and 86% are of similar precision to previously reported sensors that claim VOC selectivity.[137,158] Further studies with chlorophenyl, chloro and alkyl silicas indicated that the Adsorption Device could produce discriminable signals for a range of vapour fractions of benzene, toluene and ethyl benzene at high accuracy.

This work has demonstrated the operation of a VOC discrimination platform that uses temperature modulation to control the adsorption and desorption of BTEX pollutants in the ppb range. Although at a prototype stage, the Adsorption Device could be a precursor to a deployable device for use in air quality monitoring applications. The small size and low cost of its components would enable many sensors of this type to be readily installed across a network to collect data autonomously. PCA has shown that the signals produced by the adsorption device are sufficiently unique that discrimination between samples is possible with high accuracy in the sub-ppm range. Methodological limitations of this project mean that testing the device for multiple pollutants across wide concentration ranges was not possible. Despite this, this work has established a methodology that could be developed into a sensitive, practical and selective sensor. In particular, the responses for benzene are promising and further work should focus development of a device that can measure benzene in multi-component mixtures in the single and double ppb range.

7.2 Further Work

7.2.1 Hardware Development

The Adsorption Device shown in this thesis was a lab prototype. Further work should focus on developing this setup towards a portable and deployable system that can be used to collect in-field data. For this to be possible, a pump unit with flow control and air scrubber would need to be integrated. Solenoid valves would be replaced with compact versions, and together with the other electrical components, integrated onto a printed circuit board. An additional feature that could increase the performance of the Adsorption Device would be the inclusion of an H-bridge, which could reverse the current flow through the peltier module, allowing the adsorbent channel to be cooled. Based on the thermodynamic experiments from this work, lower temperature sampling would increase adsorption and capacity.

7.2.2 Testing and Analysis

To increase the robustness of results produced with the Adsorption Device, it would be necessary to test it with samples that have multiple cross contaminants. This work was limited to testing two-to-three gases simultaneously due to the size limitations of the Owlstone calibration gas ovens. More gases could be included by obtaining additional calibration gas ovens, using gas cylinders or heating multiple volatiles inside Teflon sampling bags. Analysing the Adsorption Device exhaust with GC-MS would allow a direct and quantitative comparison to be made. In terms of analysis and 'output' of the Adsorption Device, building upon binary or multi-class algorithms is important. This may be possible to achieve with a classification-regression analysis pipeline. For instance, classifying an analyte as a benzene-toluene mixture, then using regression algorithms to estimate the vapour fraction of each component.

7.2.3 Multi-Channel System

A potentially worthwhile addition to the Adsorption Device would be another channel. As shown in this thesis, different VOC-adsorbent combinations produce different signals in response to the same heating profile and vapour sample. If a sensor had two, or more, channels with varying adsorbent functionality, such as opposing functional group polarity, this would have the effect of adding an

additional dimension to the sensor output. Simulating a two-channel system using feature data for chlorophenyl and chloro silica from section 6.5 shows that classification accuracy can be increased (Figure 7.1). The single channel data misclassified the toluene and ethyl benzene mixtures (samples 5 and 6) 5 and 7 times respectively. The simulated data suggests a misclassification reduction of 50%. This proposal would involve having mutiple adsorbents in channels in parallel, but it would also be possible to arrange the adsorbents in series, such that certain adsorbents effectively filter out certain compounds.

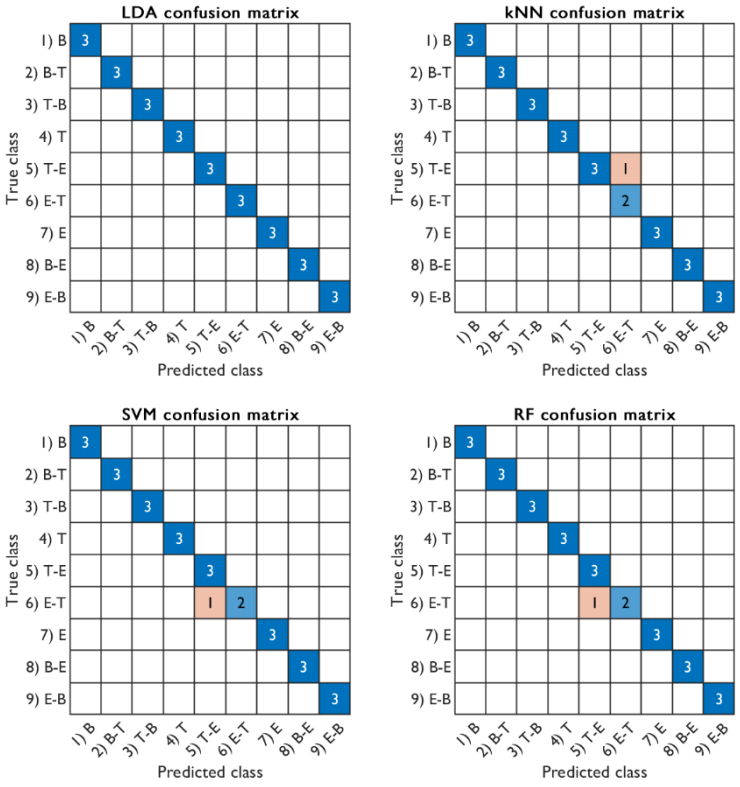

Figure 7.1. Confusion matrices for the application of the classification algorithms applied to feature data from the combined normalised sensor response (R/R_{ref}) for chlorophenyl and chloro silica adsorbents. LDA: linear discriminant analysis; SVM: support vector machine; kNN: k-nearest neighbours (k = 5); RF: random forest (number of trees: 23). Abbreviations: B, benzene; T, toluene, E ethyl benzene.

In summary, combining multiple channels and hardware improvements would almost certainly lead to improvements of sensitivity and selectivity. Based on the results shown in this work, this could lead to the development of a highly accurate, deployable and selective BTEX sensor for air quality applications.

Chapter 8 Appendices

Appendix 1: Example C++ Script

Below is an example C++ script used to control the Adsorption Device, and measure the PID response. This example script was used to collect the VOC isotherms shown in Chapter 4.

```
  /*
  VOC Sensing Project
  Andrew Stretton

*/

char scriptname[] = "Kinetics02_variableConc_singleStep";  //scriptname and version here

//*********************************************************************************
//*********************************************************************************
//*********************************************************************************

//  p-i-d CONSTANTS
#include <PID_v1.h>
double Setpoint, Input, Output;
double aggKp=50, aggKi=1, aggKd=2;        //aggressive PID parameters
double consKp=5, consKi=0.2, consKd=1;    //conservative PID parameters
PID myPID(&Input, &Output, &Setpoint,2,5,1, DIRECT);
unsigned long previousMillis = 0;
unsigned long startMillis;
unsigned long nowMillis;
const unsigned long period = 1000;

//  THERMISTOR INFO and T CALCULATION:
int ThermistorPin = 0;
int Vo;
float R1 = 10000;
float logR2, R2, T;
float c1 = 9.198701e-04, c2 = 2.5542625e-04, c3 = 1.059149506e-07;
const int T_sampling = 25;

//  TIMING
int count5minEXP = 0;       //expo 5 min - run 1
int count10minEXP = 0;      //expo 10 min - run 1
int COUNT = 0;
int CYCLE = 1;

//  Flow Control - TRANSISTOR GATE PINS
const int sol_0 = 7;      // config: normal sideways
const int sol_1 = 8;      // config: normal
```

```
41. const int sol_2 = 9;      // config: normal
42. const int sol_3 = 10;     // config: reverse
43. const int fan_1 = 13;     // transistor to control fan
44.
45. //  Flow Control - VARIABLES
46. const int pause = 1000;         // in milliseconds!
47. const int mins_SAMP = 900;     // in seconds! 600 for 10, 300 for 5 etc
48. const int mins_5  = 300;
49. const int mins_1  = 60;
50. //const int mins_SAMP = 10;       // TEST PARAMETERS!!!
51. //const int mins_5  = 5;          // TEST PARAMETERS!!!
52. //const int mins_1  = 1;          // TEST PARAMETERS!!!
53.
54. //  PID (sensor) Measure
55. const int PIDpin = 5;
56. float PIDvalue;
57.
58.
59. //#############################################################################
60. //#############################################################################
61.
62.
63. //  PHASE #2 ***************************************************************
64. const long temp1_K01_2 = 80;
65. const long time_start_K01_2 = 0;
66. const long time_cond_K01_2 = time_start_K01_2 + mins_5;
67. const long time_ref_K01_2  = time_cond_K01_2 + mins_5;
68. const long time_BG_K01_2   = time_ref_K01_2  + mins_5;
69. const long time_samp_K01_2 = time_BG_K01_2   + mins_SAMP;
70. const long time_anal_off1_K01_2 = time_samp_K01_2 + (mins_1 * 1);
71. const long time_anal_on1_K01_2  = time_anal_off1_K01_2 + mins_5;
72. const long time_anal_off2_K01_2 = time_anal_on1_K01_2  + mins_1;
73. const long time_anal1_K01_2 = time_anal_off2_K01_2 + mins_1;
74. const long time_end_K01_2  = time_anal1_K01_2 + mins_1;
75.
76.
77. //#############################################################################
78. //#############################################################################
79. //#############################################################################
80. //#############################################################################
81. //#############################################################################
82.
83.
84. void setup() {
85.   Input = analogRead(0);           //initialize variables
86.   Setpoint = 100;                   //temperature set point
87.   myPID.SetMode(AUTOMATIC);        //turns PID on
88.   startMillis = millis();
89.
90.   pinMode(sol_0, OUTPUT);
91.   pinMode(sol_1, OUTPUT);
92.   pinMode(sol_2, OUTPUT);
93.   pinMode(sol_3, OUTPUT);
94.   pinMode(fan_1, OUTPUT);
95.
96.   // headers
97.   Serial.begin(9600);
98.   Serial.print("runtime");
99.   Serial.print('\t');
100.         Serial.print("cycle");
101.         Serial.print('\t');
102.         Serial.print("mins");
103.         Serial.print('\t');
104.         Serial.print("chip T");
105.         Serial.print('\t');
106.         Serial.print("PID adc");
```

```
107.          Serial.print('\t');
108.          Serial.print("output");
109.          Serial.print('\t');
110.          Serial.print("setpoint");
111.          Serial.print('\t');
112.          Serial.print("inputStream");
113.          Serial.print('\t');
114.          Serial.print("route");
115.          Serial.print('\t');
116.          Serial.print("phase");
117.          Serial.print('\t');
118.          Serial.print(scriptname);
119.          Serial.print('\n');
120.        }
121.
122.        //*********************************************************************
123.        //*********************************************************************
124.
125.        void loop() {
126.          unsigned long currentMillis = millis();
127.          if (currentMillis - previousMillis >= pause){
128.            previousMillis = currentMillis;
129.            unsigned long seconds = millis()/1000;
130.            float minutes =  millis()/60000.00;
131.            Serial.print(minutes);                    // runtime of the script
132.            Serial.print("\t");
133.            Serial.print(CYCLE);                      // cycle
134.            Serial.print("\t");
135.        //    float countMins = (COUNT/60.00) - (time_start_K01_1/60);
136.            float countMins = (COUNT/60.00);
137.            Serial.print(countMins);                  // time (mins) of the phase
138.            Serial.print("\t");
139.            COUNT = COUNT + 1;
140.
141.            thermistor_T();
142.            Serial.print("\t");
143.            pid_read();
144.            Serial.print("\t");
145.
146.            switch(COUNT){
147.              case time_end_K01_2:                // end of the final phase
148.              COUNT = time_start_K01_2;           // start of first ANALYSIS phase
149.              CYCLE = CYCLE + 1;
150.            }
151.
152.            // set p-i-d parameters
153.            double gap = abs(Setpoint-T); //distance away from setpoint
154.            if(gap<0.25){
155.              myPID.SetTunings(consKp, consKi, consKd);
156.            } else {
157.              myPID.SetTunings(aggKp, aggKi, aggKd);
158.            }
159.            myPID.Compute();
160.            analogWrite(3,Output);
161.            Serial.print(Output);
162.            Serial.print("\t");
163.            Serial.print(Setpoint);
164.            Serial.print("\t");
165.
166.
167.        //  PHASE ***************************************************************
168.            if ((COUNT >= time_start_K01_2) && (COUNT < (time_cond_K01_2))){
169.                conditioning();
170.                Serial.println("delay_1: conditioning");
171.            } else if (COUNT >= (time_cond_K01_2) && COUNT < (time_ref_K01_2)) {
172.                reference();
```

```
173.           } else if (COUNT >= (time_ref_K01_2) && COUNT < (time_BG_K01_2)) {
174.               background();
175.           } else if (COUNT >= (time_BG_K01_2) && COUNT < (time_samp_K01_2)) {
176.               sampling();
177.           } else if (COUNT >= (time_samp_K01_2) && COUNT < (time_anal1_K01_2)) {
178.             // ANALYSIS - triple step
179.             if(COUNT >= (time_samp_K01_2) && COUNT < (time_anal_off1_K01_2)){

180.             digitalWrite(fan_1, HIGH);
181.             Setpoint = T_sampling;
182.             } else if(COUNT >= (time_anal_off1_K01_2) && COUNT < (time_anal_on1_K01
    _2)){
183.               digitalWrite(fan_1, LOW);
184.               Setpoint = temp1_K01_2;
185.             } else if(COUNT >= (time_anal_on1_K01_2) && COUNT < (time_anal_off2_K01
    _2)){
186.               digitalWrite(fan_1, HIGH);
187.               Setpoint = T_sampling;
188.             }
189.             zeroairCHIP();
190.             Serial.print("delay_1: heating period");
191.             Serial.print('\n');
192.           } else if (COUNT >= (time_anal_off2_K01_2) && COUNT < (time_end_K01_2)) {

193.               analysisEnd();
194.               Serial.println("delay_1: analysis end");
195.
196.
197.           } else {
198.             // ANALYSIS - run over
199.             analysisEnd();
200.             Serial.println("END analysis continued");
201.           }                                                    //  END OF CODE
202.         }
203.       }
204.
205.       //*************************************************************************
206.       //***** FUNCTIONS *********************************************************
207.       //*************************************************************************
208.
209.       void thermistor_T(){
210.         Vo = analogRead(ThermistorPin);
211.         R2 = R1 * (1023.0 / (float)Vo - 1.0);
212.         logR2 = log(R2);
213.         T = ((1.0 / (c1 + c2*logR2 + c3*logR2*logR2*logR2)) - 273.15);
214.         Input = T;
215.         Serial.print(T);
216.         //Serial.print('\n');
217.       }
218.       void pid_read(){
219.         PIDvalue = analogRead(PIDpin);
220.         Serial.print(PIDvalue);
221.       }
222.       void zeroairCHIP(){
223.         digitalWrite(sol_0, LOW);
224.         digitalWrite(sol_1, LOW);
225.         digitalWrite(sol_2, HIGH);
226.         digitalWrite(sol_3, HIGH);
227.         Serial.print("zero_air");
228.         Serial.print('\t');
229.         Serial.print("CHIP");
230.         Serial.print('\t');
231.       }
232.       void zeroairBYPASS(){
233.         digitalWrite(sol_0, LOW);
234.         digitalWrite(sol_1, LOW);
```

```
235.          digitalWrite(sol_2, LOW);
236.          digitalWrite(sol_3, LOW);
237.          Serial.print("zero_air");
238.          Serial.print('\t');
239.          Serial.print("BYPASS");
240.          Serial.print('\t');
241.          Serial.print("background");
242.          Serial.print('\n');
243.        }
244.        void sampleCHIP(){
245.          digitalWrite(sol_0, HIGH);
246.          digitalWrite(sol_1, HIGH);
247.          digitalWrite(sol_2, HIGH);
248.          digitalWrite(sol_3, HIGH);
249.          Serial.print("sample");
250.          Serial.print('\t');
251.          Serial.print("CHIP");
252.          Serial.print('\t');
253.          Serial.print("sampling");
254.          Serial.print('\n');
255.        }
256.        void sampleBYPASS(){
257.          digitalWrite(sol_0, HIGH);
258.          digitalWrite(sol_1, HIGH);
259.          digitalWrite(sol_2, LOW);
260.          digitalWrite(sol_3, LOW);
261.          Serial.print("sample");
262.          Serial.print('\t');
263.          Serial.print("BYPASS");
264.          Serial.print('\t');
265.          Serial.print("reference");
266.          Serial.print('\n');
267.        }
268.
269.        void conditioning() {
270.          Setpoint = 80;
271.          zeroairCHIP();
272.          digitalWrite(fan_1, LOW);
273.        }
274.        void reference() {
275.          Setpoint = T_sampling;
276.          sampleBYPASS();
277.          digitalWrite(fan_1, HIGH);
278.        }
279.        void background() {
280.          Setpoint = T_sampling;
281.          zeroairBYPASS();
282.          digitalWrite(fan_1, HIGH);
283.        }
284.        void sampling() {
285.          Setpoint = T_sampling;
286.          sampleCHIP();
287.          digitalWrite(fan_1, HIGH);
288.        }
289.        void analysisEnd() {
290.          Setpoint = T_sampling;
291.          zeroairCHIP();
292.          digitalWrite(fan_1, HIGH);
293.        }
```

Appendix 2: VOC Langmuir Fit

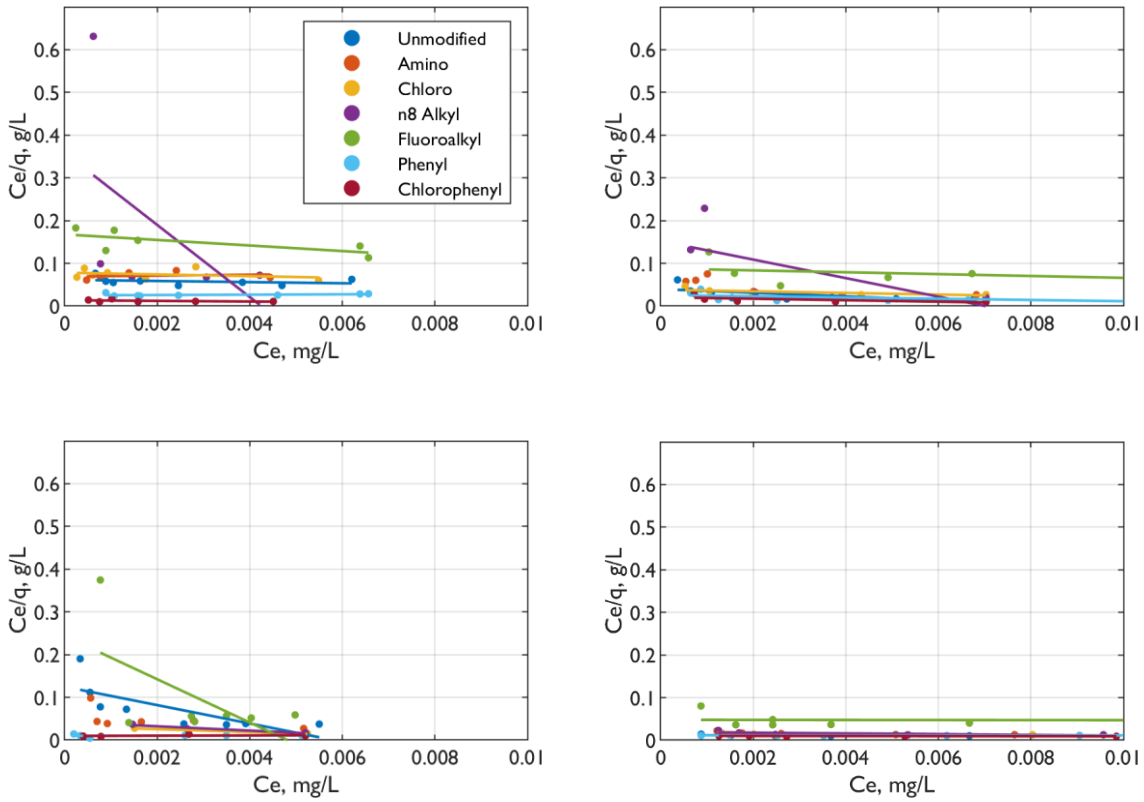

Figure 8.1. Langmuir model fitting to VOC Isotherms for benzene (top left), toluene (top right), ethylbenzene (bottom left) and toluene (bottom right).

Appendix 3: Classification Algorithm Optimisation

From 6.4.1 BTEX and MEK Discrimination

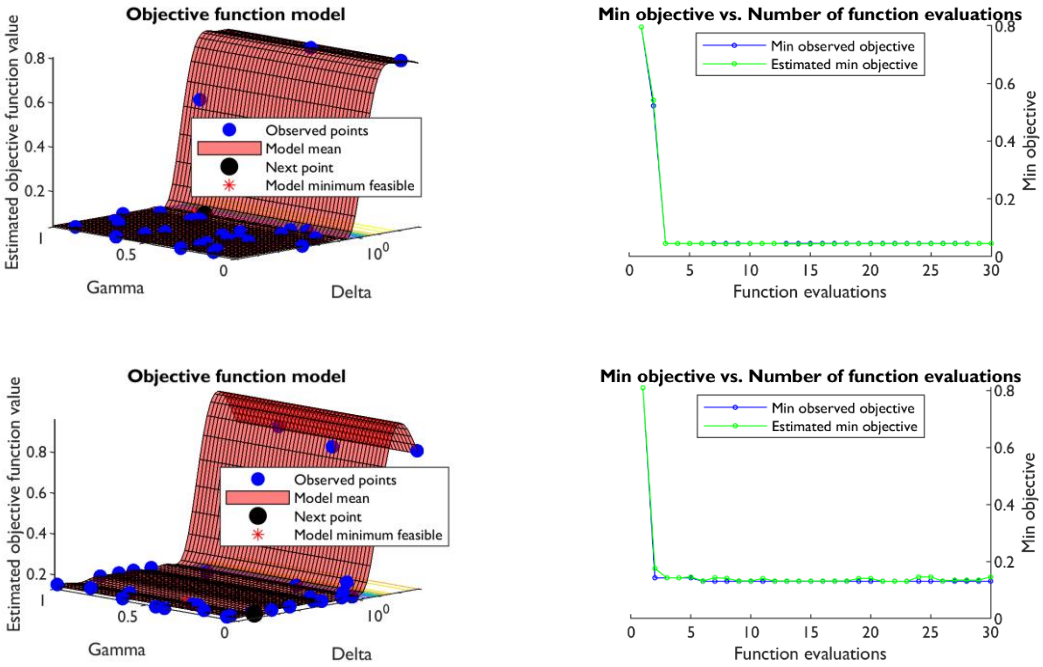

Figure 8.2. LDA Optimisation Parameters for short cycle time classification problem to discriminate BTEX and MEK. Top - unmodified silica. Bottom – phenyl silica.

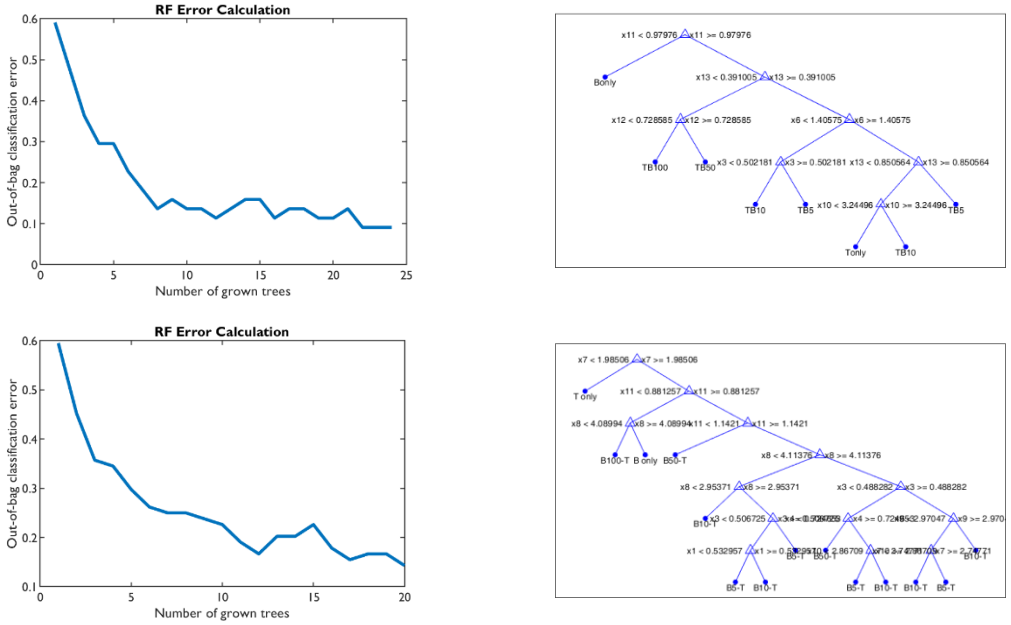

Figure 8.3. RF error calculation (*left*) and decision tree (*right*) for 10 minute cycle time classification problem to discriminate BTEX and MEK. *Right* – decision tree. Top - unmodified silica. Bottom – phenyl silica.

From 6.4.2 Benzene-Toluene Discrimination (10 Minutes)

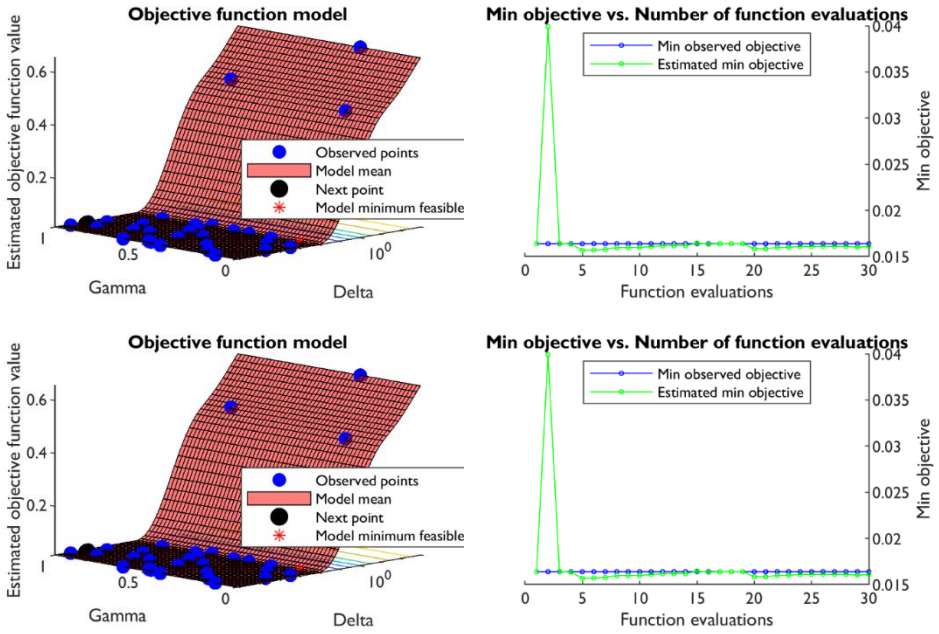

Figure 8.4. LDA Optimisation Parameters for 10 minute cycle time classification problem to discriminate Benzene and Toluene. Top - unmodified silica. Bottom – phenyl silica.

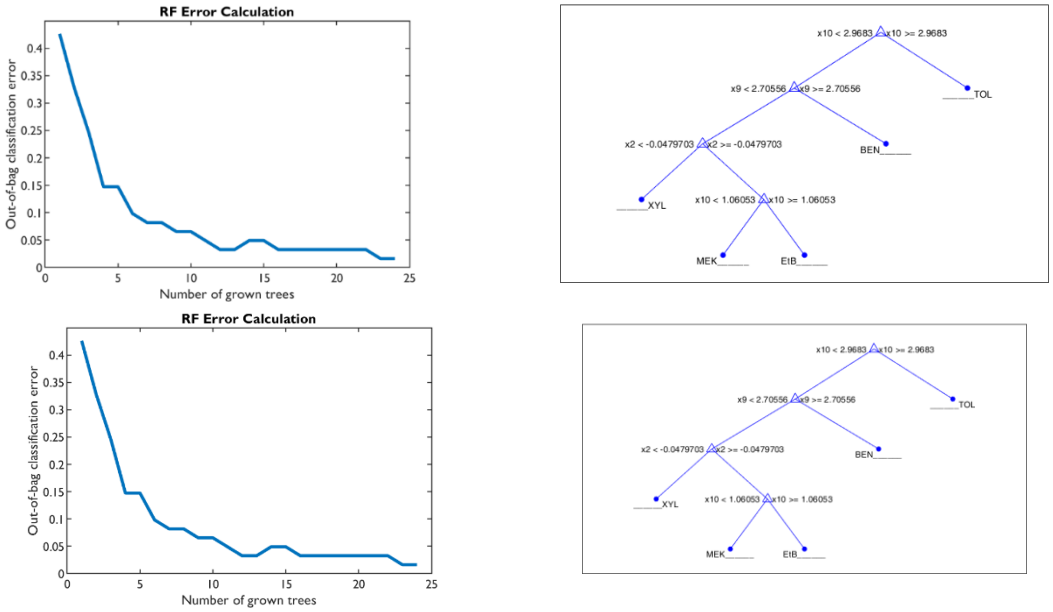

Figure 8.5. RF error calculation (*left*) and decision tree (*right*) for 10 minute cycle time classification problem to discriminate Benzene and Toluene. *Right* – decision tree. Top - unmodified silica. Bottom – phenyl silica.

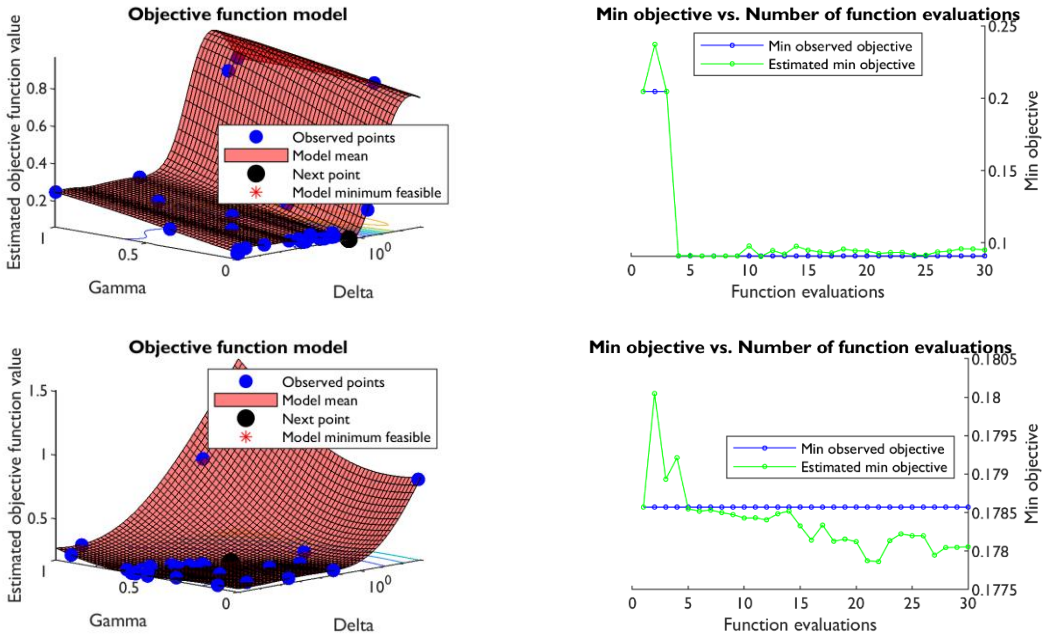

Figure 8.6. LDA Optimisation Parameters for 5 minute cycle time classification problem to discriminate benzene and toluene. Top - unmodified silica. Bottom – phenyl silica.

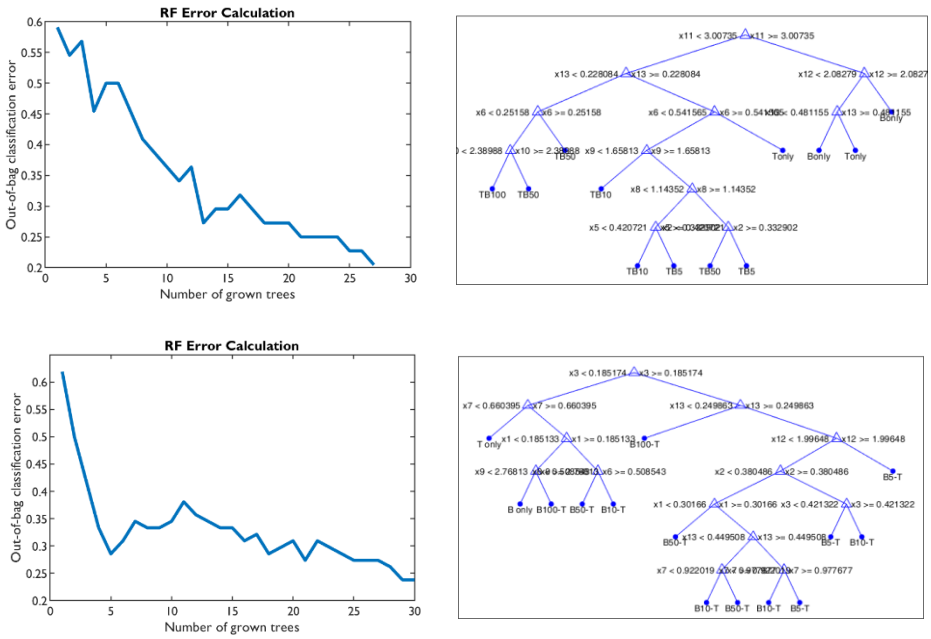

Figure 8.7. RF error calculation (*left*) and decision tree (*right*) for 5 minute cycle time classification problem to discriminate Benzene and Toluene. *Right* – decision tree. Top - unmodified silica. Bottom – phenyl silica.

From 6.5.1 BTEX, MEK, Acetone and n-Hexane Discrimination

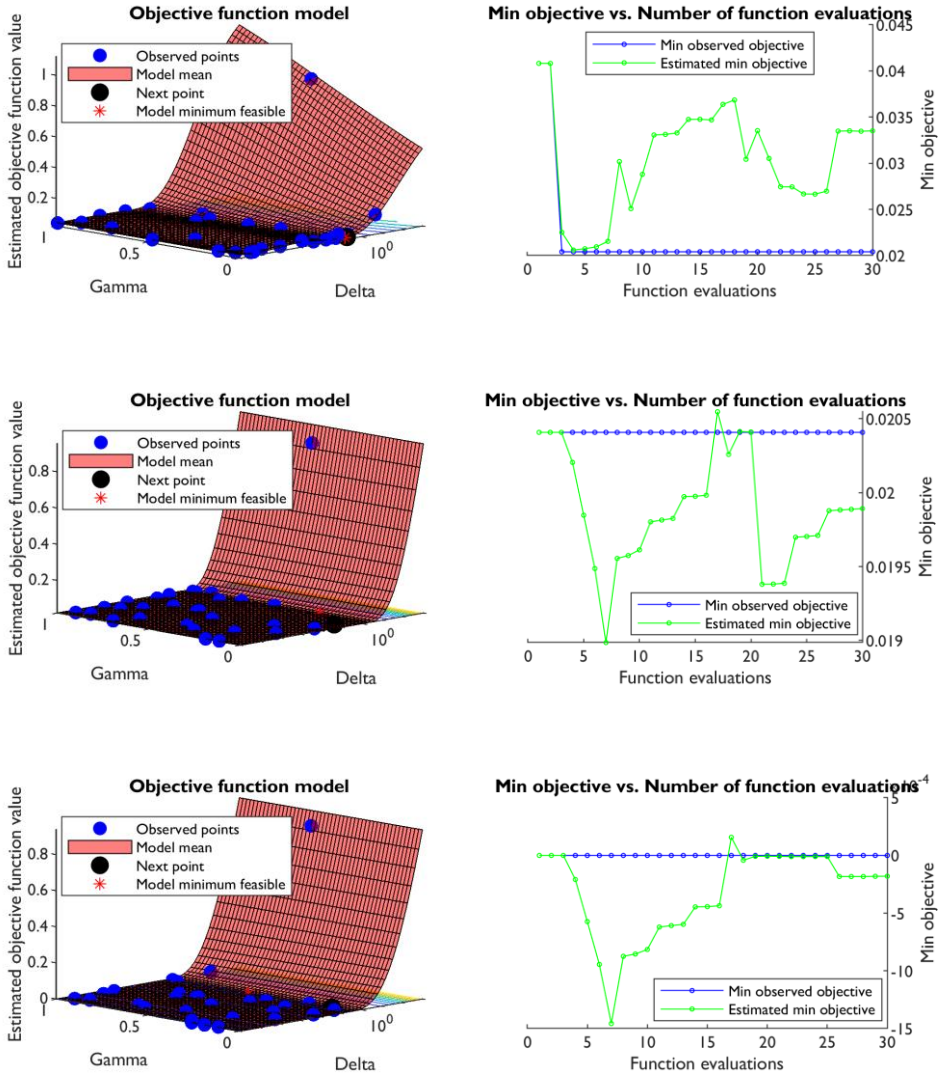

Figure 8.8. LDA Optimisation Parameters for 10 minute cycle time classification problem to discriminate benzene, toluene, ethyl benzene, para-xylene, methyl ethyl ketone (MEK), acetone and n-hexane. Top - chlorophenyl silica, middle – chloro silica, bottom – alkyl silica.

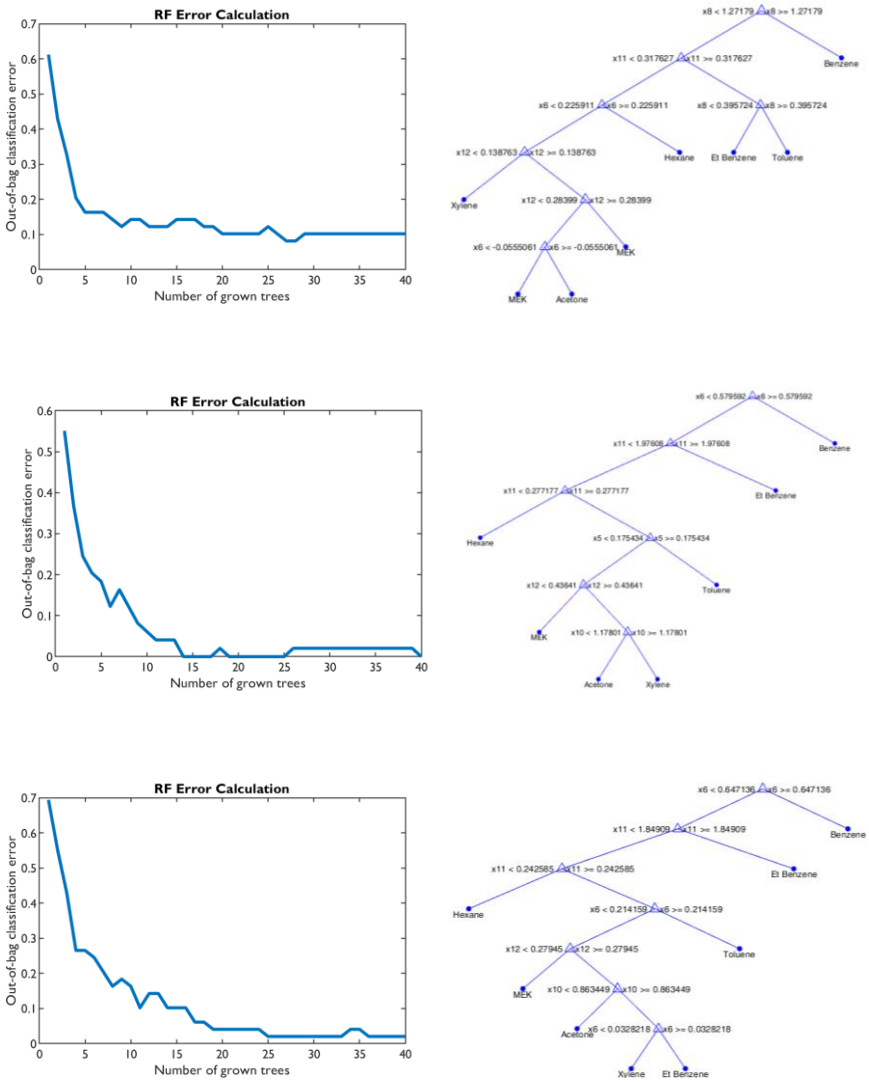

Figure 8.9. RF error calculation (*left*) and decision tree (*right*) for 5 minute cycle time classification problem to discriminate benzene, toluene, ethyl benzene, para-xylene, methyl ethyl ketone (MEK), acetone and n-hexane. *Right* – decision tree. Top - chlorophenyl silica, middle – chloro silica, bottom – alkyl silica.

From 6.5.2 Benzene-Toluene-Ethyl Benzene Vapour Fractions

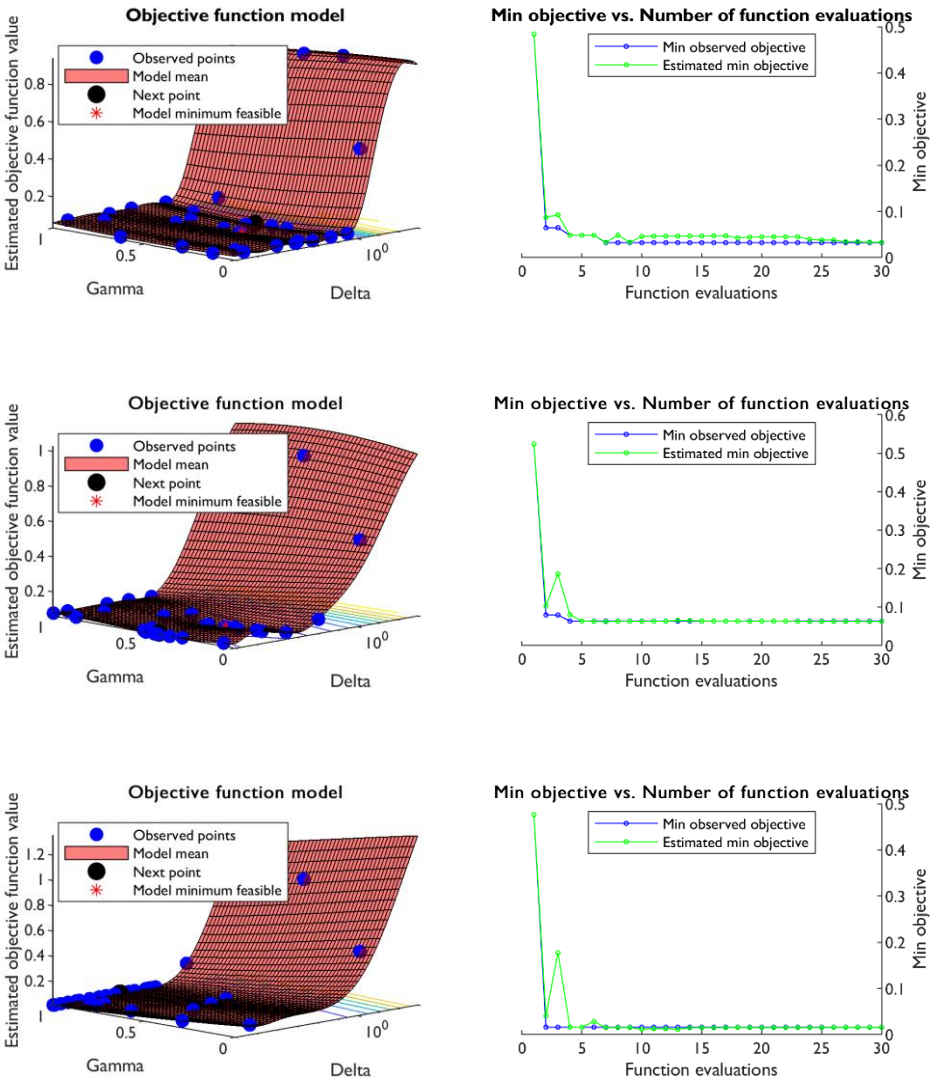

Figure 8.10. LDA Optimisation Parameters for 10 minute cycle time classification problem to discriminate benzene, toluene, ethyl benzene and their fractions. Top - chlorophenyl silica, middle – chloro silica, bottom – alkyl silica.

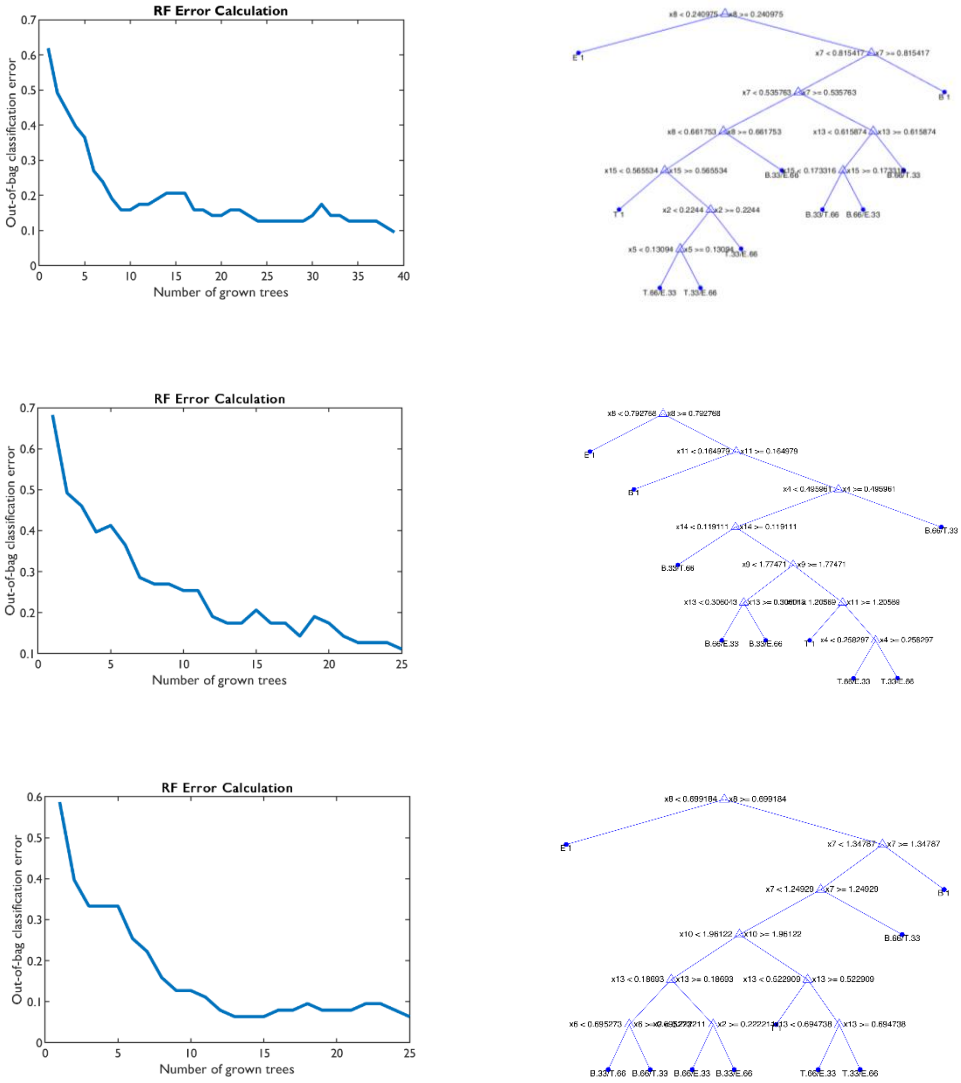

Figure 8.11. RF error calculation (*left*) and decision tree (*right*) for 5 minute cycle time classification problem to discriminate Benzene and Toluene. *Right* – decision tree. Top - chlorophenyl silica, middle – chloro silica, bottom – alkyl silica.

References

1. The European Parliament and the Council of the European Union. Directive 2004/42/CE of the European Parliament and of the Council of 21 April 2004 on the limitation of emissions of volatile organic compounds due to the use of organic solvents in certain paints and varnishes and vehicle refinishing products and amendi. *Off. J. Eur. Unio* 87–96 (2004) doi:http://eur-lex.europa.eu/LexUriServ/LexUriServ.do?uri=OJ:L:2004:143:0087:0096:EN:PDF.

2. US Code of Federal Regulations, 40: Chapter 1, Subchapter C, Part 51, Subpart F, 51100.

3. Chiu, K. H., Wu, B. Z., Chang, C. C., Sree, U. & Lo, J. G. Distribution of volatile organic compounds over a semiconductor industrial park in Taiwan. *Environ. Sci. Technol.* **39**, 973–983 (2005).

4. Zhang, Z. & Li, G. A review of advances and new developments in the analysis of biological volatile organic compounds. *Microchemical Journal* vol. 95 127–139 (2010).

5. Goldstein, A. H. & Galbally, I. E. Known and unexplored organic constituents in the earth's atmosphere. *Environmental Science and Technology* vol. 41 1514–1521 (2007).

6. Guenther, A. *et al. Estimates of global terrestrial isoprene emissions using MEGAN*. *European Geosciences Union* vol. 6 www.atmos-chem-phys.net/6/3181/2006/ (2006).

7. Sharkey, T. D., Wiberley, A. E. & Donohue, A. R. Isoprene emission from plants: Why and how. *Annals of Botany* vol. 101 5–18 (2008).

8. He, C. *et al.* Recent Advances in the Catalytic Oxidation of Volatile Organic Compounds: A Review Based on Pollutant Sorts and Sources. *Chem. Rev.* **119**, 4471–4568 (2019).

9. Sexton, K. & Westberg, H. Ambient Air Measurements of Petroleum Refinery Emissions. *J. Air Pollut. Control Assoc.* **29**, 1149–1152 (1979).

10. Cai, C., Geng, F., Tie, X., Yu, Q. & An, J. Characteristics and source apportionment of VOCs measured in Shanghai, China. *Atmos. Environ.* **44**, 5005–5014 (2010).

11. De Gouw, J. & Warneke, C. Measurements of volatile organic compounds in the earth's atmosphere using proton-transfer-reaction mass spectrometry. *Mass Spectrometry Reviews* vol. 26 223–257 (2007).

12. Weschler, C. J. Changes in indoor pollutants since the 1950s. *Atmos. Environ.* **43**, 153–169 (2009).

13. McDonald, B. C. *et al.* Volatile chemical products emerging as largest petrochemical source of urban organic emissions. *Science (80-.).* **359**, 760–764 (2018).

14. UK Government. *Clean Air Strategy 2019: executive summary*. https://www.gov.uk/government/publications/clean-air-strategy-2019 (2019).

15. Steinfeld, J. I. Atmospheric Chemistry and Physics: From Air Pollution to Climate Change. *Environ. Sci. Policy Sustain. Dev.* **40**, 26–26 (1998).

16. Bridlescombe, P, Air Pollution Episodes in *Encyclopedia of environamental health, 2nd Edition* (ed. Nriagu, J. O.), 41-48 (Elsevier Science, 2019).

17. Arashiro, M. *et al.* Effect of secondary organic aerosol from isoprene-derived hydroxyhydroperoxides on the expression of oxidative stress response genes in human bronchial epithelial cells. *Environ. Sci. Process. Impacts* **20**, 332–339 (2018).

18. Gittins, M. J. *et al. Volatile Organic Compounds in the Atmosphere*. vol. 4 (Royal Society of Chemistry, 1995).

19. de Lacy Costello, B. *et al.* A review of the volatiles from the healthy human body. *J. Breath Res.* **8**, (2014).

20. Pleil, J. D., Stiegel, M. a & Risby, T. H. Clinical breath analysis: discriminating between human endogenous compounds and exogenous (environmental) chemical confounders. *J. Breath Res.* **7**, 017107 (2013).

21. Saalberg, Y. & Wolff, M. VOC breath biomarkers in lung cancer. *Clin. Chim. Acta* **459**, 5–9 (2016).

22. Jalal, A. H. *et al.* Prospects and Challenges of Volatile Organic Compound Sensors in Human Healthcare. *ACS Sensors* vol. 3 1246–1263 (2018).

23. Adiguzel, Y. & Kulah, H. Breath sensors for lung cancer diagnosis. *Biosens. Bioelectron.* (2015) doi:10.1016/j.bios.2014.10.023.

24. Horváth, I., Lázár, Z., Gyulai, N., Kollai, M. & Losonczy, G. Exhaled biomarkers in lung cancer. *European Respiratory Journal* vol. 34 261–275 (2009).

25. Chan, H. P., Lewis, C. & Thomas, P. S. Exhaled breath analysis: Novel approach for early detection of lung cancer. *Lung Cancer* vol. 63 164–168 (2009).

26. Prabhakar, B., Shende, P. & Augustine, S. Current trends and emerging diagnostic techniques for lung cancer. *Biomedicine and Pharmacotherapy* vol. 106 1586–1599 (2018).

27. Oakley-Girvan, I. & Davis, S. W. Breath based volatile organic compounds in the detection of breast, lung, and colorectal cancers: A systematic review. *Cancer Biomarkers* vol. 21 29–39 (2017).

28. Altomare, D. F. *et al.* Exhaled volatile organic compounds identify patients with colorectal cancer. *Br. J. Surg.* **100**, 144–150 (2013).

29. Prabhakar, A. *et al.* Acetone as biomarker for ketosis buildup capability--a study in healthy individuals under combined high fat and starvation diets. *Nutr. J.* **14**, 41 (2015).

30. Zhou, M., Liu, Y. & Duan, Y. Breath biomarkers in diagnosis of pulmonary diseases. *Clinica Chimica Acta* (2012) doi:10.1016/j.cca.2012.07.006.

31. Phillips, M. *et al.* Point-of-care breath test for biomarkers of active pulmonary tuberculosis. *Tuberculosis* **92**, 314–320 (2012).

32. Caro, J. & Gallego, M. Environmental and biological monitoring of volatile organic compounds in the workplace. *Chemosphere* **77**, 426–433 (2009).

33. Ramírez, N., Cuadras, A., Rovira, E., Borrull, F. & Marcé, R. M. Chronic risk assessment of exposure to volatile organic compounds in the atmosphere near the largest Mediterranean industrial site. *Environ. Int.* **39**, 200–209 (2012).

34. Rumchev, K., Brown, H. & Spickett, J. Volatile organic compounds: Do they present a risk to our health? *Reviews on Environmental Health* vol. 22 39–55 (2007).

35. Moriarty, F. *Air quality guidelines for Europe*. *Environmental Pollution* vol. 55 http://wedocs.unep.org/handle/20.500.11822/8681 (2003).

36. Schwartz, J. Air pollution and children's health. *Pediatrics* **113**, 1037–1043 (2004).

37. International Agency for Research on Cancer. *Agents Classified by the IARC Monographs, Volumes 1–123 – IARC*. https://monographs.iarc.fr/agents-classified-by-the-iarc/ (2019).

38. Mentel, T. F. The formation, properties and impact of secondary organic aerosol: Current and emerging issues. *Atmos. Chem. Phys.* **9**, 5155–5236 (2009).

39. Beloff, B. R., Beaver, E. R. & Massin, H. Assessing societal costs associated with environmental impacts. *Environ. Qual. Manag.* **10**, 67–82 (2000).

40. Esplugues, A. *et al.* Indoor and outdoor air concentrations of BTEX and determinants in a cohort of one-year old children in Valencia, Spain. *Sci. Total Environ.* **409**, 63–69 (2010).

41. Bari, M. A., Kindzierski, W. B., Wheeler, A. J., Héroux, M. È. & Wallace, L. A. Source apportionment of indoor and outdoor volatile organic compounds at homes in Edmonton, Canada. *Build. Environ.* **90**, 114–124 (2015).

42. Council, E. P. and of the. Council Directive 1999/13/EC of 11 March 1999 on the limitation of emissions of volatile organic compounds due to the use of organic solvents in certain activities and installations. *Off. J. Eur. Comm.* L85/1-L85/22 (1999) doi:http://eur-lex.europa.eu/LexUriServ/LexUriServ.do?uri=OJ:L:1999:085:0001:0022:EN:PDF.

43. Department of Environment Food and Rural Affairs. Environmental Permitting Guidance, The Solvent Emissions Directive. 100 (2010).

44. European Commission (EC). Directive 2008/50/EC of the European Parliament and of the Council of 21 May 2008 on ambient air quality and cleaner air for Europe. EC - European Commission. Official Journal of the European Union L152, pp. 1-44. (2008).

45. Garg, A. *et al.* Zebra GC: A mini gas chromatography system for trace-level determination of hazardous air pollutants. *Sensors Actuators B Chem.* **212**, 145–154 (2015).

46. Sun, J. H. *et al.* A micro gas chromatography column with a micro thermal conductivity detector for volatile organic compound analysis. *Rev. Sci. Instrum.* **84**, 025001 (2013).

47. Supelco Solutions. GC Column Selection Guide - Achieve Optimal Method Performance. 1–28 (2010).

48. Rahman, M. M. *et al.* Basic Overview on Gas Chromatography Columns. in *Analytical Separation Science* 823–834 (Wiley-VCH Verlag GmbH & Co. KGaA, 2015). doi:10.1002/9783527678129.assep024.

49. De Blas, M., Navazo, M., Alonso, L., Durana, N. & Iza, J. Automatic on-line monitoring of atmospheric volatile organic compounds: Gas chromatography-mass spectrometry and gas chromatography-flame ionization detection as complementary systems. *Sci. Total Environ.* **409**, 5459–5469 (2011).

50. Liaud, C., Nguyen, N. T., Nasreddine, R. & Le Calvé, S. Experimental performances study of a transportable GC-PID and two thermo-desorption based methods coupled to FID and MS detection to assess BTEX exposure at sub-ppb level in air. *Talanta* **127**, 33–42 (2014).

51. Gallego, E., Roca, F. J., Perales, J. F., Sánchez, G. & Esplugas, P. Characterization and determination of the odorous charge in the indoor air of a waste treatment facility through the evaluation of volatile organic compounds (VOCs) using TD-GC/MS. *Waste Manag.* **32**, 2469–2481 (2012).

52. Larin, A., Womble, P. C. & Dobrokhotov, V. Novel highly-integrated mems based solid state detectors for analytical gas chromatography. *Sensors Actuators, B Chem.* **256**, 1057–1068 (2018).

53. Boots, A. W., Bos, L. D., van der Schee, M. P., van Schooten, F. J. & Sterk, P. J. *Exhaled Molecular Fingerprinting in Diagnosis and Monitoring: Validating Volatile Promises*. *Trends in Molecular Medicine* vol. 21 http://linkinghub.elsevier.com/retrieve/pii/S1471491415001574 (2015).

54. Wang, X. R., Cassells, J. & Berna, A. Z. Stability control for breath analysis using GC-MS. *J. Chromatogr. B Anal. Technol. Biomed. Life Sci.* **1097–1098**, 27–34 (2018).

55. Langford, V. S., Graves, I. & McEwan, M. J. Rapid monitoring of volatile organic compounds: A comparison between gas chromatography/mass spectrometry and selected ion flow tube mass spectrometry. *Rapid Commun. Mass Spectrom.* **28**, 10–18 (2014).

56. Lara-Lbeas, I. *et al.* Sub-ppb level detection of BTEX Gaseous mixtures with a compact prototype GC equipped with a preconcentration unit. *Micromachines* **10**, 187 (2019).

57. Berruex, L. G. & Freitag, R. Separation and Purification of Biochemicals. in *Encyclopedia of Physical Science and Technology* 651–673 (2003). doi:10.1016/b0-12-227410-5/00683-9.

58. Heeter, G. A. & Liapis, A. I. Frontal chromatography of proteins. Effect of axial dispersion on column performance. in *Journal of Chromatography A* vol. 796 157–164 (1998).

59. Vogg, S., Müller-Späth, T. & Morbidelli, M. Design space and robustness analysis of batch and counter-current frontal chromatography processes for the removal of antibody aggregates. *J. Chromatogr. A* **1619**, (2020).

60. Stone, M. T., Cotoni, K. A. & Stoner, J. L. Cation exchange frontal chromatography for the removal of monoclonal antibody aggregates. *J. Chromatogr. A* **1599**, 152–160 (2019).

61. Gonzalvez, A., Garrigues, S., De La Guardia, M. & Armenta, S. The ways to the trace level analysis in infrared spectroscopy. *Analytical Methods* vol. 3 43–52 (2011).

62. Huang, G. G., Wang, C., Tang, H., Huang, Y. & Yang, J. ZnO Nanoparticle-Modified Infrared Internal Reflection Elements for Selective Detection of Volatile Organic Compounds functional groups were observed . The conditions for were optimized by varying such factors as the volume of. *Anal. Chem.* **78**, 2397–2404 (2006).

63. Sung, L. Y., Shie, R. H. & Lu, C. J. Locating sources of hazardous gas emissions using dual pollution rose plots and open path Fourier transform infrared spectroscopy. *J. Hazard. Mater.* **265**, 30–40 (2014).

64. Fateley, W. G. *et al.* Observing industrial atmospheric environments by FT-IR. *J. Mol. Struct.* **347**, 153–168 (1995).

65. Volkamer, R., Etzkorn, T., Geyer, A. & Platt, U. Correction of the oxygen interference with UV spectroscopic (DOAS) measurements of monocyclic aromatic hydrocarbons in the atmosphere. *Atmos. Environ.* **32**, 3731–3747 (1998).

66. Parsons, M. T. *et al.* Real-time monitoring of benzene, toluene, and p-xylene in a photoreaction chamber with a tunable mid-infrared laser and ultraviolet differential optical absorption spectroscopy. *Appl. Opt.* **50**, A90 (2011).

67. Badjagbo, K., Sauvé, S. & Moore, S. Real-time continuous monitoring methods for airborne VOCs. *TrAC - Trends Anal. Chem.* **26**, 931–940 (2007).

68. Iglesias, R. A., Tsow, F., Wang, R., Forzani, E. S. & Tao, N. Hybrid Separation and Detection Device for Analysis of Benzene, Toluene, Ethylbenzene, and Xylenes in Complex Samples. *Anal. Chem.* **81**, 8930–8935 (2010).

69. Nasreddine, R., Person, V., Serra, C. A. & Le Calvé, S. Development of a novel portable miniaturized GC for near real-time low level detection of BTEX. *Sensors Actuators, B Chem.* **224**, 159–169 (2016).

70. Jian, R. S., Huang, Y. S., Lai, S. L., Sung, L. Y. & Lu, C. J. Compact instrumentation of a μGC for real time analysis of sub-ppb VOC mixtures. *Microchem. J.* **108**, 161–167 (2013).

71. Zhou, M. *et al.* A fully automated portable gas chromatography system for sensitive and rapid quantification of volatile organic compounds in water. *RSC Adv.* (2016) doi:10.1039/c6ra09131h.

72. Meciarova, L., Vilcekova, S. & Balintova, M. *Measurement of VOCs with a portable GC/SAW detector*. *Chemical Engineering Transactions* vol. 40 (2014).

73. Lu, C., Whiting, J., Sacks, R. D. & Zellers, E. T. Portable Gas Chromatograph with Tunable Retention and Sensor Array Detection for Determination of Complex Vapor Mixtures multiadsorbent preconcentrator / focuser , a tandem-col- retention window approach is combined with Monte Carlo. *Anal. Chem.* **75**, 1400–1409 (2003).

74. INFICON HAPSITE® ER Chemical Identification System. https://products.inficon.com/en-us/nav-products/product/detail/hapsite-er-identification-system/?path=Products%2Fpg-ChemicalDetection%2F.

75. Defiant Technologies. http://www.defiant-tech.com/.

76. Chromatotec AirTOXIC BTX PID | Thomson Environmental Systems. https://www.thomsongroup.com.au/product/chromatec-airtoxic-btx/.

77. Series 9100 Gas Chromatograph, MOCON Inc. http://products.baseline-mocon.com/item/ronmental-monitoring-series-9100-gas-chromatograph/omatograph-series-9100-gas-chromatograph-1/item-1025.

78. PerkinElmer Torion T-9 Portable GC/MS. https://www.perkinelmer.co.uk/product/torion-t-9-portable-gc-ms-instrument-ntsst090500.

79. Electronic Sensor Technology Inc. https://www.estcal.com/.

80. PetroPro Portable Gas Chromatograph, INFICON. https://products.inficon.com/en-us/nav-products/product/detail/petropro-portable-gas-chromatograph/.

81. INFICON Micro GC Fusion® Gas Analyzer. https://products.inficon.com/en-us/nav-products/product/detail/micro-gc-fusion-gas-analyzer/.

82. Seer Technology. https://seertechnology.com/.

83. Zimmermann, S., Wischhusen, S. & Müller, J. Micro flame ionization detector and micro flame spectrometer. *Sensors Actuators B Chem.* **63**, 159–166 (2000).

84. Benz, M., Benz, L. & Patel, S. V. High Temperature Mass Detection Using a Carbon Nanotube Bilayer Modified Quartz Crystal Microbalance as a GC Detector. *Anal. Chem.* **87**, 2779–2787 (2015).

85. Staples, E. J., Matsuda, T. & Viswanathan, S. Real Time Environmental Screening of Air , Water and Soil Matrices Using a novel Field Portable GC / SAW System. *Management* 8–10 (1998).

86. Lin, Z. *et al.* A zone-heated gas chromatographic microcolumn: Energy efficiency. *Sensors Actuators, B Chem.* **254**, 561–572 (2018).

87. Sun, J. *et al.* Fabrication and characterization of microelectromechanical systems-based gas chromatography column with embedded micro-posts for separation of environmental carcinogens. *J. Chromatogr. A* **1291**, 122–128 (2013).

88. Chen, B.-X., Hung, T.-Y., Jian, R.-S. & Lu, C.-J. A multidimensional micro gas chromatograph employing a parallel separation multi-column chip and stop-flow [small mu]GC [times] [small mu]GCs configuration. *Lab Chip* **13**, 1333–1341 (2013).

89. Ali, S., Ashraf-Khorassani, M., Taylor, L. T. & Agah, M. MEMS-based semi-packed gas chromatography columns. *Sensors Actuators, B Chem.* **141**, 309–315 (2009).

90. Zampolli, S. *et al.* Selectivity enhancement of metal oxide gas sensors using a micromachined gas chromatographic column. *Sensors Actuators, B Chem.* **105**, 400–406 (2005).

91. Zampolli, S. *et al.* Real-time monitoring of sub-ppb concentrations of aromatic volatiles with a MEMS-enabled miniaturized gas-chromatograph. *Sensors Actuators, B Chem.* **141**, 322–328 (2009).

92. Collin, W. R., Bondy, A., Paul, D., Kurabayashi, K. & Zellers, E. T. μGC × μGC: comprehensive two-dimensional gas chromatographic separations with microfabricated components. *Anal. Chem.* **87**, 1630–7 (2015).

93. Stadermann, M. *et al.* Ultrafast gas chromatography on single-wall carbon nanotube stationary phases in microfabricated channels. *Anal. Chem.* **78**, 5639–44 (2006).

94. Regmi, B. P., Chan, R., Atta, A. & Agah, M. Ionic liquid-coated alumina-pretreated micro gas chromatography columns for high-efficient separations. *J. Chromatogr. A* **1566**, 124–134 (2018).

95. Liu, J. *et al.* Smart multi-channel two-dimensional micro-gas chromatography for rapid workplace hazardous volatile organic compounds measurement. *Lab Chip* **13**, 818–25 (2013).

96. Wang, J. *et al.* Belt-Mounted Micro-Gas-Chromatograph Prototype for Determining Personal Exposures to Volatile-Organic-Compound Mixture Components. *Anal. Chem.* **91**, 4747–4754 (2019).

97. Gaddes, D., Westland, J., Dorman, F. L. & Tadigadapa, S. Improved micromachined column design and fluidic interconnects for programmed high-temperature gas chromatography separations. *J. Chromatogr. A* **1349**, 96–104 (2014).

98. Sklorz, A., Janßen, S. & Lang, W. Application of a miniaturised packed gas chromatography column and a SnO2 gas detector for analysis of low molecular weight hydrocarbons with focus on ethylene detection. *Sensors and Actuators, B: Chemical* vol. 180 43–49 (2012).

99. Zampolli, S. *et al.* Real-time monitoring of sub-ppb concentrations of aromatic volatiles with a MEMS-enabled miniaturized gas-chromatograph. *Sensors Actuators B Chem.* **141**, 322–328 (2009).

100. Brilli, F. *et al.* Proton Transfer Reaction Time-of-Flight Mass Spectrometric (PTR-TOF-MS) determination of volatile organic compounds (VOCs) emitted from a biomass fire developed under stable nocturnal conditions. *Atmos. Environ.* **97**, 54–67 (2014).

101. Shaw, M. D. *et al.* Airborne determination of the temporo-spatial distribution of benzene, toluene, nitrogen oxides and ozone in the boundary layer across Greater London, UK. *Atmos. Chem. Phys.* **15**, 5083–5097 (2015).

102. Blake, R. S., Monks, P. S. & Ellis, A. M. Proton-transfer reaction mass spectrometry. *Chemical Reviews* vol. 109 861–896 (2009).

103. Batterman, S., Chambliss, S. & Isakov, V. Spatial resolution requirements for traffic-related air pollutant exposure evaluations. *Atmos. Environ.* **94**, 518–528 (2014).

104. Moriarty, F. *Air quality guidelines for Europe, 2nd Edition*. *WHO regional publications. European series ; No. 91* http://wedocs.unep.org/handle/20.500.11822/8681 (2000) doi:10.1016/0269-7491(88)90163-7.

105. Spinelle, L., Gerboles, M., Kok, G., Persijn, S. & Sauerwald, T. Review of portable and low-cost sensors for the ambient air monitoring of benzene and other volatile organic compounds. *Sensors (Switzerland)* vol. 17 1520 (2017).

106. EU. Directive 2007/2/EC of the European Parliament and of the council of 14 March 2007 establishing an Infrastructure for Spatial Information in the European Community (INSPIRE). *Off. J. Eur. Union* **50**, 1–14 (2007).

107. Marchi, I., Rudaz, S. & Veuthey, J.-L. Atmospheric pressure photoionization for coupling liquid-chromatography to mass spectrometry: A review. *Talanta* **78**, 1–18 (2009).

108. Jian, R.-S., Huang, Y.-S., Lai, S.-L., Sung, L.-Y. & Lu, C.-J. Compact instrumentation of a μ-GC for real time analysis of sub-ppb VOC mixtures. *Microchem. J.* **108**, 161–167 (2013).

109. Agbroko, S. O. & Covington, J. A novel, low-cost, portable PID sensor for the detection of volatile organic compounds. *Sensors Actuators, B Chem.* **275**, 10–15 (2018).

110. Pyo, S., Lee, K., Noh, T., Jo, E. & Kim, J. Sensitivity enhancement in photoionization detector using microelectrodes with integrated 1D nanostructures. *Sensors Actuators, B Chem.* **288**, 618–624 (2019).

111. Skoog, D. A., Holler, F. J. & Crouch, S. R. *Principles of instrumental analysis*.

112. Jacquinot, P., Hodgson, A. W. E., Müller, B., Wehrli, B. & Hauser, P. C. Amperometric detection of gaseous ethanol and acetaldehyde at low concentrations on an Au-Nafion electrode. *Analyst* **124**, 871–876 (1999).

113. Knake, R. & Hauser, P. C. Sensitive electrochemical detection of ozone. *Anal. Chim. Acta* **459**, 199–207 (2002).

114. Nagai, T., Tamura, S. & Imanaka, N. Solid electrolyte type ammonia gas sensor based on trivalent aluminum ion conducting solids. *Sensors Actuators B Chem.* **147**, 735–740 (2010).

115. Ono, M., Shimanoe, K., Miura, N. & Yamazoe, N. Reaction analysis on sensing electrode of amperometric NO2 sensor based on sodium ion conductor by using chronopotentiometry. *Sensors Actuators B Chem.* **77**, 78–83 (2001).

116. Ono, M., Shimanoe, K., Miura, N. & Yamazoe, N. Amperometric sensor based on NASICON and NO oxidation catalysts for detection of total NOx in atmospheric environment. *Solid State Ionics* **136–137**, 583–588 (2000).

117. Sadaoka, Y. & Mori, M. Detection of VOC in air with a planar-type potentiometric gas sensor based on YSZ with a Pt electrode modified with TiO2. *Sensors Actuators, B Chem.* **248**, 878–885 (2017).

118. Gębicki, J., Kloskowski, A. & Chrzanowski, W. Prototype of electrochemical sensor for measurements of volatile organic compounds in gases. *Sensors Actuators, B Chem.* **177**, 1173–1179 (2013).

119. Sato, T., Plashnitsa, V. V, Utiyama, M. & Miura, N. YSZ-based sensor using NiO sensing electrode for detection of volatile organic compounds in ppb level. *J. Electrochem. Soc.* **158**, J175–J178 (2011).

120. Han, F., Li, F., Liu, S. & Niu, L. Sub-stoichiometric WO2.9 as co-catalyst with platinum for formaldehyde gas sensor with high sensitivity. *Sensors Actuators B Chem.* **263**, 369–376 (2018).

121. Sekhar, P. K. & Subramaniyam, K. Detection of Harmful Benzene, Toluene, Ethylbenzene, Xylenes (BTEX) Vapors Using Electrochemical Gas Sensors. *ECS Electrochem. Lett.* **3**, B1–B4 (2013).

122. Mori, M. & Sadaoka, Y. Potentiometric VOC detection at sub-ppm levels based on YSZ electrolyte and platinum electrode covered with gold. *Sensors Actuators, B Chem.* **146**, 46–52 (2010).

123. Mori, M., Itagaki, Y. & Sadaoka, Y. VOC detection by potentiometric oxygen sensor based on YSZ and modified Pt electrodes. *Sensors Actuators, B Chem.* **161**, 471–479 (2012).

124. Jin, H. *et al.* Further enhancement of the light-regulated mixed-potential signal with ZnO-based electrodes. *Sensors Actuators B Chem.* **255**, 3516–3522 (2018).

125. Knake, R., Jacquinot, P. & Hauser, P. C. Amperometric detection of gaseous formaldehyde in the ppb range. in *Electroanalysis* vol. 13 631–634 (John Wiley & Sons, Ltd, 2001).

126. Meixner, H. & Lampe, U. Metal oxide sensors. *Sensors Actuators B Chem.* **33**, 198–202 (1996).

127. Wang, C., Yin, L., Zhang, L., Xiang, D. & Gao, R. Metal oxide gas sensors: sensitivity and influencing factors. *Sensors (Basel).* **10**, 2088–106 (2010).

128. Dey, A. Semiconductor metal oxide gas sensors: A review. *Mater. Sci. Eng. B* **229**, 206–217 (2018).

129. Development, O. of R. &. Next Generation Air Monitoring (NGAM) VOC Sensor Evaluation Report.

130. Koo, W. T. *et al.* Heterogeneous Sensitization of Metal-Organic Framework Driven Metal@Metal Oxide Complex Catalysts on an Oxide Nanofiber Scaffold Toward Superior Gas Sensors. *J. Am. Chem. Soc.* **138**, 13431–13437 (2016).

131. Kadosaki, M., Sakai, Y., Tamura, I., Matsubara, I. & Itoh, T. Development of an oxide semiconductor thick film gas sensor for the detection of total volatile organic compounds. *Electron. Commun. Japan* **93**, 34–41 (2010).

132. Ke, M.-T., Lee, M.-T., Lee, C.-Y. & Fu, L.-M. A MEMS-based Benzene Gas Sensor with a Self-heating WO3 Sensing Layer. *Sensors* **9**, 2895–2906 (2009).

133. Kanda, K. & Maekawa, T. Development of a WO3 thick-film-based sensor for the detection of VOC. in *Sensors and Actuators, B: Chemical* vol. 108 97–101 (Elsevier, 2005).

134. Castro-Hurtado, I., Mandayo, G. G. & Castaño, E. Conductometric formaldehyde gas sensors. A review: From conventional films to nanostructured materials. *Thin Solid Films* **548**, 665–676 (2013).

135. Park, H. J. *et al.* A ppb-level formaldehyde gas sensor based on CuO nanocubes prepared using a polyol process. *Sensors Actuators B Chem.* **203**, 282–288 (2014).

136. Chu, X., Chen, T., Zhang, W., Zheng, B. & Shui, H. Investigation on formaldehyde gas sensor with ZnO thick film prepared through microwave heating method. *Sensors Actuators B Chem.* **142**, 49–54 (2009).

137. Nallon, E. C., Schnee, V. P., Bright, C., Polcha, M. P. & Li, Q. Chemical Discrimination with an Unmodified Graphene Chemical Sensor. *ACS Sensors* **1**, 26–31 (2016).

138. Camou, S., Horiuchi, T. & Haga, T. PPB level benzene gas detection by portable BTX sensor based on integrated hollow fiber detection cell. in *Proceedings of IEEE Sensors* 235–238 (IEEE, 2006). doi:10.1109/ICSENS.2007.355765.

139. Camou, S., Tamechika, E. & Horiuchi, T. Portable sensor for determining benzene concentration from airborne/ liquid samples with high accuracy. *NTT Tech. Rev.* **10**, (2012).

140. Horiuchi, T., Ueno, Y., Camou, S., Haga, T. & Tate, A. Portable aromatic VOC gas sensor for onsite continuous air monitoring with 10-ppb benzene detection capability. *NTT Tech. Rev.* **4**, 30–37 (2006).

141. Silva, L. I. B., M-Costa, A., Freitas, A. C., Rocha-Santos, T. A. P. & Duarte, A. C. Polymeric nanofilm-coated optical fibre sensor for speciation of aromatic compounds. *Int. J. Environ. Anal. Chem.* **89**, 183–197 (2009).

142. Bui, D. A. & Hauser, P. C. A deep-UV light-emitting diode-based absorption detector for benzene, toluene, ethylbenzene, and the xylene compounds. *Sensors Actuators, B Chem.* **235**, 622–626 (2016).

143. Pinalli, R., Pedrini, A. & Dalcanale, E. Environmental Gas Sensing with Cavitands. *Chemistry - A European Journal* vol. 24 1010–1019 (2018).

144. Yang, H., Yuan, B., Zhang, X. & Scherman, O. A. Supramolecular chemistry at interfaces: Host-guest interactions for fabricating multifunctional biointerfaces. *Acc. Chem. Res.* **47**, 2106–2115 (2014).

145. Lai, C. S. I. *et al.* Piezoelectric quartz crystal detection of benzene vapour using chemically modified cyclodextrins. *J. Chem. Soc. Perkin Trans. 2* 319–324 (1988) doi:10.1039/P29880000319.

146. Schierbaum, K. D., Gerlach, A., Haug, M. & Göpel, W. Selective detection of organic molecules with polymers and supramolecular compounds: application of capacitance, quartz microbalance and calorimetric transducers. *Sensors Actuators A. Phys.* **31**, 130–137 (1992).

147. Nelli, P., Dalcanale, E., Faglia, G., Sberveglieri, G. & Soncini, P. Cavitands as selective materials for QMB sensors for nitrobenzene and other aromatic vapours. *Sensors Actuators B. Chem.* **13**, 302–304 (1993).

148. Dickert, F. L., Bäumler, U. P. A. & Zwissler, G. K. Supramolecular structures and chemical sensing. *Synth. Met.* **61**, 47–52 (1993).

149. Schierbaum, K. D. *et al.* Molecular recognition by self-assembled monolayers of cavitand receptors. *Science (80-.).* **265**, 1413–1415 (1994).

150. Trzciński, J. W. *et al.* In Search of the Ultimate Benzene Sensor: The EtQxBox Solution. *ACS Sensors* **2**, 590–598 (2017).

151. Gutierrez-Osuna, R. Pattern analysis for machine olfaction: A review. *IEEE Sensors Journal* vol. 2 189–202 (2002).

152. Dobrokhotov, V., Larin, A. & Sowell, D. Vapor trace recognition using a single nonspecific chemiresistor. *Sensors* **13**, 9016–9028 (2013).

153. Jerger, A., Kohler, H., Becker, F., Keller, H. B. & Seifert, R. New applications of tin oxide gas sensors: II. Intelligent sensor system for reliable monitoring of ammonia leakages. *Sensors Actuators, B Chem.* **81**, 301–307 (2002).

154. Zeng, G. *et al.* Detection and Discrimination of Volatile Organic Compounds using a Single Film Bulk Acoustic Wave Resonator with Temperature Modulation as a Multiparameter Virtual Sensor Array. *ACS Sensors* **4**, 1524–1533 (2019).

155. Bordbar, M. M., Tashkhourian, J. & Hemmateenejad, B. Structural Elucidation and Ultrasensitive Analyses of Volatile Organic Compounds by Paper-Based Nano-Optoelectronic Noses. *ACS Sensors* **4**, 1442–1451 (2019).

156. Li, Z. & Suslick, K. S. Portable Optoelectronic Nose for Monitoring Meat Freshness. *ACS Sensors* **1**, 1330–1335 (2016).

157. Seesaard, T., Lorwongtragool, P. & Kerdcharoen, T. Development of fabric-based chemical gas sensors for use as wearable electronic noses. *Sensors (Switzerland)* **15**, 1885–1902 (2015).

158. Tonezzer, M. Selective gas sensor based on one single SnO2 nanowire. *Sensors Actuators, B Chem.* **288**, 53–59 (2019).

159. Thommes, M. *et al.* Physisorption of gases, with special reference to the evaluation of surface area and pore size distribution (IUPAC Technical Report). *Pure Appl. Chem.* **87**, 1051–1069 (2015).

160. Sing, K. S. W. Reporting physisorption data for gas/solid systems with special reference to the determination of surface area and porosity (Recommendations 1984). *Pure Appl. Chem.* **57**, 603–619 (1985).

161. Thommes, M. & Cychosz, K. A. Physical adsorption characterization of nanoporous materials: Progress and challenges. *Adsorption* **20**, 233–250 (2014).

162. Zhang, X., Gao, B., Creamer, A. E., Cao, C. & Li, Y. Adsorption of VOCs onto engineered carbon materials: A review. *Journal of Hazardous Materials* vol. 338 102–123 (2017).

163. Oh, K. J., Park, D. W., Kim, S. S. & Park, S. W. Breakthrough data analysis of adsorption of volatile organic compounds on granular activated carbon. *Korean J. Chem. Eng.* **27**, 632–638 (2010).

164. Brown, J. & Shirey, B. A Tool for Selecting an Adsorbent for Thermal Desorption Applications. *SUPELCO Tech. Rep.* 1–12 (2001).

165. Dragoi, B., Rakic, V., Dumitriu, E. & Auroux, A. Adsorption of organic pollutants over microporous solids investigated by microcalorimetry techniques. *J. Therm. Anal. Calorim.* **99**, 733–740 (2010).

166. Wang, H. *et al.* VOC adsorption and desorption behavior of hydrophobic, functionalized SBA-15. *J. Mater. Res.* **31**, 516–525 (2016).

167. Zhao, X. S., Ma, Q. & Lu, G. Q. VOC removal: Comparison of MCM-41 with hydrophobic zeolites and activated carbon. *Energy and Fuels* **12**, 1051–1054 (1998).

168. Rahimi, M., Singh, J. K. & Müller-Plathe, F. CO2 Adsorption on Charged Carbon Nanotube Arrays: A Possible Functional Material for Electric Swing Adsorption. *J. Phys. Chem. C* **119**, 15232–15239 (2015).

169. Long, R. Q. & Yang, R. T. Carbon nanotubes as a superior sorbent for nitrogen oxides. *Ind. Eng. Chem. Res.* **40**, 4288–4291 (2001).

170. Lamari Darkrim, F., Malbrunot, P. & Tartaglia, G. P. Review of hydrogen storage by adsorption in carbon nanotubes. *International Journal of Hydrogen Energy* vol. 27 193–202 (2002).

171. Yan, T., Li, T. X., Li, H. & Wang, R. Z. Experimental study of the ammonia adsorption characteristics on the composite sorbent of CaCl2 and multi-walled carbon nanotubes. *Int. J. Refrig.* **46**, 165–172 (2014).

172. Rafique, M. M. A. & Iqbal, J. Production of Carbon Nanotubes by Different Routes-A Review. *J. Encapsulation Adsorpt. Sci.* **01**, 29–34 (2011).

173. Kobayashi, N., Izumi, H. & Morimoto, Y. Review of toxicity studies of carbon nanotubes. *Journal of Occupational Health* vol. 59 394–407 (2017).

174. Meek, S. T., Greathouse, J. A. & Allendorf, M. D. Metal-organic frameworks: A rapidly growing

class of versatile nanoporous materials. *Advanced Materials* vol. 23 249–267 (2011).

175. Yang, K., Sun, Q., Xue, F. & Lin, D. Adsorption of volatile organic compounds by metal-organic frameworks MIL-101: Influence of molecular size and shape. *J. Hazard. Mater.* **195**, 124–131 (2011).

176. Xie, L. H., Liu, X. M., He, T. & Li, J. R. Metal-Organic Frameworks for the Capture of Trace Aromatic Volatile Organic Compounds. *Chem* **4**, 1911–1927 (2018).

177. Shafiei, M., Alivand, M. S., Rashidi, A., Samimi, A. & Mohebbi-Kalhori, D. Synthesis and adsorption performance of a modified micro-mesoporous MIL-101(Cr) for VOCs removal at ambient conditions. *Chem. Eng. J.* **341**, 164–174 (2018).

178. Szulejko, J. E. & Kim, K.-H. Is the maximum adsorption capacity obtained at high VOC pressures (>1,000 Pa) really meaningful in real-world applications for the sorptive removal of VOCs under ambient conditions (<1 Pa)? *Sep. Purif. Technol.* **228**, 115729 (2019).

179. Zhang, L. *et al.* Adsorptive and catalytic properties in the removal of volatile organic compounds over zeolite-based materials. *Cuihua Xuebao/Chinese Journal of Catalysis* vol. 37 800–809 (2016).

180. Pellejero, I. *et al.* Nanoporous silicalite-only cantilevers as micromechanical sensors: Fabrication, resonance response and VOCs sensing performance. *Sensors Actuators B Chem.* **168**, 74–82 (2012).

181. A, R. *et al.* Kinetics Study of Gas Pollutant Adsorption and Thermal Desorption on Silica Gel. *Appl. Sci.* **7**, 609 (2017).

182. Ncube, M. & Su, Y. The removal of volatile organic compounds from supply air using a desiccant column – A theoretical study. *Int. J. Sustain. Built Environ.* **1**, 259–268 (2012).

183. Serrano, D. P., Calleja, G., Botas, J. A. & Gutierrez, F. J. Adsorption and Hydrophobic Properties of Mesostructured MCM-41 and SBA-15 Materials for Volatile Organic Compound Removal. *Ind. Eng. Chem. Res.* **43**, 7010–7018 (2004).

184. Hung, C., Bai, H. & Karthik, M. Ordered mesoporous silica particles and Si-MCM-41 for the adsorption of acetone: A comparative study. *Sep. Purif. Technol.* **64**, 265–272 (2009).

185. Liu, S. *et al.* Engineering surface functional groups on mesoporous silica: towards a humidity-resistant hydrophobic adsorbent. *J. Mater. Chem. A* **6**, 13769–13777 (2018).

186. Dean, J. *Lange's Handbook of Chemistry*. (McGraw-Hill Professional, 1999).

187. Platonov, I. A., Rodinkov, O. V, Gorbacheva, A. R., Moskvin, L. N. & Kolesnichenko, I. N. Methods and devices for the preparation of standard gas mixtures. *Journal of Analytical Chemistry* vol. 73 109–127 (2018).

188. Maria, P. C. *et al.* Using thermogravimetry for weight loss monitoring of permeation tubes used for generation of trace concentration gas standards. *Anal. Chem.* **74**, 305–307 (2002).

189. Vertical Owlstone Vapor Generator (V-OVG) from Owlstone Inc. https://www.owlstoneinc.com/products/v-ovg/.

190. OVG-4 Calibration Gas Generator by Owlstone Inc. https://www.owlstoneinc.com/products/ovg-4/.

191. Hermanson, G. T, Chapter 13 Silane Coupling Agents in *Bioconjugate Techniques, 2nd Edition*, 565-567. (Elsevier Science, 2013).

192. ISO 15901-2:2006. Pore size distribution and porosity of solid materials by mercury porosimetry and gas adsorption -- Part 2: Analysis of mesopores and macropores by gas adsorption. 30 (2006).

193. Alphasense Ltd. PID-AH2 Photo Ionisation Detector. 1–2 http://www.alphasense.com/WEB1213/wp-content/uploads/2016/09/PID-AH2.pdf (2016).

194. Shrivastava, A. & Gupta, V. Methods for the determination of limit of detection and limit of quantitation of the analytical methods. *Chronicles Young Sci.* **2**, 21 (2011).

195. Qu, F., Zhu, L. & Yang, K. Adsorption behaviors of volatile organic compounds (VOCs) on porous clay heterostructures (PCH). *J. Hazard. Mater.* **170**, 7–12 (2009).

196. Webster, C. E., Drago, R. S. & Zerner, M. C. Molecular dimensions for adsorptives. *J. Am. Chem. Soc.* **120**, 5509–5516 (1998).

197. Atkins, P. & Paula, J. De. Atkins' Physical chemistry 8th edition. *Chemistry* (2009) doi:10.1021/ed056pA260.1.

198. Esbensen, K. H. & Geladi, P. Principal Component Analysis: Concept, Geometrical Interpretation, Mathematical Background, Algorithms, History, Practice. in *Comprehensive Chemometrics* vol. 2 211–226 (Elsevier, 2009).

199. Arroyo, P., Lozano, J. & Suárez, J. I. Evolution of wireless sensor network for air quality measurements. *Electron.* **7**, (2018).

200. He, W. W. *et al.* Phenyl Groups Result in the Highest Benzene Storage and Most Efficient Desulfurization in a Series of Isostructural Metal-Organic Frameworks. *Chem. - A Eur. J.* **21**, 9784–9789 (2015).

201. Lowell, S. (Seymour) & Lowell, S. (Seymour). Characterization of porous solids and powders: surface area, pore size, and density. *Choice Rev. Online* **42**, 42-5288-42–5288 (2013).

202. H.Freundlich. Uber die adsorption in lunsungen. *J. Phys. Chem.* **57**, 387–470 (1906).

203. Yang, R. T. Gas Separation by Adsorption Processes. *Gas Sep. Purif.* **2**, 41 (1988).

204. Brunauer, S., Emmett, P. H. & Teller, E. Adsorption of Gases in Multimolecular Layers. *J. Am. Chem. Soc.* **60**, 309–319 (1938).

205. Yuan, Y. & Lee, T. R. Contact angle and wetting properties. *Springer Ser. Surf. Sci.* **51**, 3–34 (2013).

206. Ncube, T., Suresh Kumar Reddy, K., Al Shoaibi, A. & Srinivasakannan, C. Benzene, Toluene, m-Xylene Adsorption on Silica-Based Adsorbents. *Energy and Fuels* **31**, 1882–1888 (2017).

207. Biffinger, J. C., Kim, H. W. & DiMagno, S. G. The polar hydrophobicity of fluorinated compounds. *ChemBioChem* vol. 5 622–627 (2004).

208. Silverstein, T. P. The real reason why oil and water don't mix. *J. Chem. Educ.* **75**, 116–118 (1998).

209. Jia, H., Liggins, J. R. & Chow, W. S. Entropy and biological systems: Experimentally-investigated entropy-driven stacking of plant photosynthetic membranes. *Sci. Rep.* **4**, 4142 (2014).

210. Launer, P. J. Infrared analysis of organosilicon compounds: spectra-structure correlations. in *Silicone Compounds Register and Review* 100–103 (1987).

211. Sigma-Aldrich. IR Spectrum Table & Chart | Sigma-Aldrich. *sigmaaldrich* https://www.sigmaaldrich.com/technical-documents/articles/biology/ir-spectrum-table.html (2018).

212. Pazokifard, S., Mirabedini, S. M., Esfandeh, M. & Farrokhpay, S. Fluoroalkylsilane treatment of TiO 2 nanoparticles in difference pH values: Characterization and mechanism. in *Advanced Powder Technology* vol. 23 428–436 (Elsevier, 2012).

213. Seyed Shahabadi, S. M., Rabiee, H., Seyedi, S. M., Mokhtare, A. & Brant, J. A. Superhydrophobic dual layer functionalized titanium dioxide/polyvinylidene fluoride-co-hexafluoropropylene (TiO2/PH) nanofibrous membrane for high flux membrane distillation. *J. Memb. Sci.* **537**, 140–150 (2017).

214. Albert, S., Keppler, K., Lerch, P., Quack, M. & Wokaun, A. Synchrotron-based highest resolution FTIR spectroscopy of chlorobenzene. *J. Mol. Spectrosc.* **315**, 92–101 (2015).

215. Treybal, R. E. *Mass-transfer operations*. (McGraw-Hill, 1980).

216. Fang, L., Zhang, G. & Wisthaler, A. Desiccant wheels as gas-phase absorption (GPA) air cleaners: Evaluation by PTR-MS and sensory assessment. in *Indoor Air* vol. 18 375–385 (John Wiley & Sons, Ltd (10.1111), 2008).

217. Oliveira, R. J. *et al.* CO2/CH4 adsorption at high-pressure using silica-APTES aerogel as adsorbent and near infrared as a monitoring technique. *J. CO2 Util.* **32**, 232–240 (2019).

218. Sinnokrot, M. O. & Sherrill, C. D. Substituent effects in π-π interactions: Sandwich and t-shaped configurations. *J. Am. Chem. Soc.* **126**, 7690–7697 (2004).

219. Sinnokrot, M. O., Valeev, E. F. & Sherrill, C. D. Estimates of the ab initio limit for π-π interactions: The benzene dimer. *J. Am. Chem. Soc.* **124**, 10887–10893 (2002).

220. Liu, S. *et al.* Modified Silica Adsorbents for Toluene Adsorption under Dry and Humid Conditions: Impacts of Pore Size and Surface Chemistry. *Langmuir* **35**, 8927–8934 (2019).

221. Sui, H., An, P., Li, X., Cong, S. & He, L. Removal and recovery of o-xylene by silica gel using vacuum swing adsorption. *Chem. Eng. J.* **316**, 232–242 (2017).

222. Sui, H., Wang, Z., He, L., Han, Z. & Li, X. Piecewise loading bed for reversible adsorption of VOCs on silica gels. *J. Taiwan Inst. Chem. Eng.* **102**, 51–60 (2019).

223. Coasne, B., Alba-Simionesco, C., Audonnet, F., Dosseh, G. & Gubbins, K. E. Adsorption and structure of benzene on silica surfaces and in nanopores. *Langmuir* **25**, 10648–10659 (2009).

224. Russo, P. A., Ribeiro Carrott, M. M. L. & Carrott, P. J. M. Adsorption of toluene, methylcyclohexane and neopentane on silica MCM-41. *Adsorption* **14**, 367–375 (2008).

225. Peng, F., Luoa, T., Yuan, Y. & Qiu, L. Performance of optimized TVOCs sensor. in *Procedia Engineering* vol. 7 392–398 (2010).

226. RAE Systems, I. Technical Note TN-165 Combating Drift In Portable And Fixed PIDs. 1–2 (2000).

Y Diwedd